Exploring the AdS/CFT Correspondence: Non-Relativistic Generalisations & Holographic Multiboundary Wormholes

PEACH, ALEXANDER,MATTHEW

Exploring the AdS/CFT Correspondence: Non-Relativistic Generalisations & Holographic Multiboundary Wormholes

Alexander Matthew Peach

A thesis presented for the degree of
Doctor of Philosophy

Department of Mathematical Sciences

Durham University

United Kingdom

March 2017

Exploring the AdS/CFT Correspondence: Non-Relativistic Generalisations & Holographic Multiboundary Wormholes

Alexander Matthew Peach

Submitted for the degree of Doctor of Philosophy
March 2017

Abstract

In this thesis I explore two pertinent avenues of the AdS/CFT correspondence: the rich, pragmatic context of non-relatavistic holography and the story of holographic multiboundary wormholes and their relation to the profound interplay between bulk geometry and boundary entanglement. In chapter 1, I introduce the AdS/CFT correspondence and review the key ideas that motivate and underlie the work in subsequent chapters. In chapter 2 we consider the development of a holographic dictionary for asymptotically locally Schrödinger spacetimes for $z < 2$ in a massive vector model in various spatial dimensions. We carry out a linearised analysis of bulk perturbations and identify the boundary data as sources and vevs for the dual stress-energy complex. We verify that a sensible asymptotic expansion of bulk perturbations in sub-leading powers of r exists by expanding them in eigenvalues of the boundary dilatation operator. The third chapter extends the work of the Chapter 2 to the case with $z = 2$ in the massive vector model, in various dimensions, where the additional lightlike direction is regarded as internal from the boundary point of view, qualitatively unlike the $z < 2$ case. Chapter 4 considers the entanglement structure of states holographically dual to multiboundary wormholes in the high-temperature limit, in which the thermal scale associated to each boundary is much larger than the AdS scale. We find that the entanglement structure in this limit is almost entirely bipartite in this regime. The fifth chapter investigates the extent to which the results of chapter 4 generalise to regions of small moduli. We utilise heuristic tensor network methods to construct tensor network models of multiboundary wormhole states built by sewing tensors to Coxeter tilings and their quotients. We find in several cases that we can construct holographic states representing multiboundary wormhole geometries for which the entanglement structure is mostly, or almost entirely bipartite.

Contents

Declaration

The work in this thesis is based on research carried out at the Department of Mathematical Sciences at Durham University. The results are based on the following collaborative works:

- T. Andrade, C. Keeler, A. Peach, and S. F. Ross, *Schrdinger holography for z ¡ 2*, *Classical and Quantum Gravity* **32** (2015), no. 3 035015
- T. Andrade, C. Keeler, A. Peach, and S. F. Ross, *Schrdinger holography with z = 2*, *Classical and Quantum Gravity* **32** (2015), no. 8 085006
- D. Marolf, H. Maxfield, A. Peach, and S. Ross, *Hot multiboundary wormholes from bipartite entanglement*, *Classical and Quantum Gravity* **32** (2015), no. 21 215006
- A. Peach and S. F. Ross, *Tensor Network Models of Multiboundary Wormholes*, arXiv:1702.0598

No part of this thesis has been submitted for a degree in this or any other institution.

Acknowledgements

This thesis would not have been possible were it not for a number of people. First and foremost in this regard are Mum, Dad and my fiancé Heidi whose unconditional love, support and encouragement underscore all of my ambitions and successes. I can't possibly thank you enough and you all share in this achievement with me.

I must also particularly thank Dr. Henry Maxfield for being effortlessly inspirational and for taking a great deal of time to explain so many things to me during his time at Durham University. Likewise, I owe all my friends in the Maths Department at Durham thanks for many fascinating discussions and helpful comments!

I'd also like to thank my supervisor Prof. Simon Ross for his patient and thoughtful guidance and supervision throughout this intensely rewarding and challenging journey and for inviting me to work with him and other experts within the field on the exciting topics in this thesis.

I'd like to thank the Snettisham Halls Exhibition Grant Foundation in my beautiful home village of Snettisham, Norfolk. Were it not for their generous financial support throughout my time at University, from my undergraduate days, through my masters and eventually to my PhD, I would not have been able to take this passion so far.

1 Introduction

There are at least a couple of reasons why any physicist should care about the AdS/CFT correspondence. On the one-hand, it entails a fully non-perturbative definition of quantum gravity and is arguably one of our most powerful hints for a framework that successfully marries gravity according to Einstein with the microscopic paradigm of quantum mechanics [5–9]. On the other hand, the AdS/CFT correspondence amounts to an extremely powerful strong/weak duality providing us with a unique window into the behaviour of strongly-coupled quantum systems, including condensed matter systems that we can actually realise experimentally [10, 11]. In this section I present a review of the main ideas underlying the research conducted in this thesis. I introduce black hole thermodynamics and the holographic principle of which the AdS/CFT correspondence is an explicit realisation. I describe the AdS/CFT correspondence, discussing the original result and its natural generalisations, including non-relativistic cases that bring the powerful formalism of AdS/CFT to experimentally pertinent systems in condensed matter physics [10, 40–42, 66]. I then discuss the fascinating interplay between bulk geometry and boundary quantum information that continues to shed light on how the AdS/CFT correspondence is realised holographically [12–16].

1.1 Black Holes & The Holographic Principle

Regarding the question of quantum gravity, one of the most important and remarkable results found in recent times is that black holes are thermal objects; they radiate thermally, and they carry entropy. Initially, Hawking's area theorem demonstrated that the area of the event horizon of a black hole is always increasing, analogous to the second law of thermodynamics [17]. Bekenstein later argued that black holes would violate the second law of thermodynamics, if a thermodynamic system was thrown into a black hole, unless the black hole carried an entropy proportional to the area of its horizon $\mathcal{H}$ [18],

$$S = \frac{1}{4l_p^2} Area(\mathcal{H}) \tag{1.1}$$

where l_p is the Planck length.

This remarkable result (1.1), an inevitable feature of semiclassical gravity in black hole geometries, has profound implications for the amount of information that can be contained in any portion of space in a theory of quantum gravity. Consider, for simplicity, a spherical shell with area A occupied by a collection of matter with total energy M which is collapsed to form a black hole of mass M and horizon area A. According to the second law of thermodynamics, entropy cannot decrease, hence the entropy of the collapsing system cannot exceed (1.1), as illustrated in figure 1. A covariant generalisation of this result is provided by the Bousso-bound [19]. This result strongly suggests that in a quantum theory of gravity, that physical information pertaining to any portion of spacetime is encoded in its boundary[1]. This led Susskind and t'Hooft to propose the holographic principle, according to which quantum gravity is holographic in precisely this sense [20, 21].

The thermodynamic nature of black holes was decisively clarified by Hawking's initially surprising result that black holes evaporate thermally [22]. This result can be obtained most cleanly by considering the fact that the near-horizon geometry of a Schwarzchild black hole is locally Rindler space; the same as for a uniformly accelerating observer in flat space. Consequently, the state of quantum fields observed by a fiducial observer outside the horizon is prepared by the Euclidean path-integral on an infinite strip sliced in Rindler time, which prepares a thermal state in the black hole exterior [10]. As such, the state of quantum fields in the exterior region

[1]Further evidence for includes the fact that boundaries are physical in gravitational systems, since large diffeomorphisms act non-trivially on physical configurations.

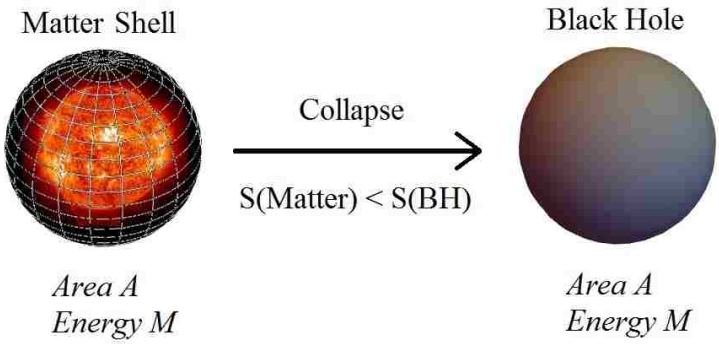

Figure 1: A spherical shell of matter with radius R collapses to form a black hole with event horizon radius R. The second law of thermodynamics means that the final black hole has a greater entropy than the collapsing shell. Consequently, the largest amount of information that can be contained in any spherical shell is bounded by the entropy of a black hole of the same size, which scales with the area (as opposed to the volume) of the collapsing shell.

.

of a black hole, according to a fiducial observer, is thermal; if they carried with them a particle detector they would observe thermal excitations.

In classical thermodynamic systems, the thermodynamic entropy counts the number of microstates in the statistical ensemble. The question arises then as to whether or not the entropy carried by the black hole is similarly a reflection of coarse-graining of an underlying microscopic description. Naively we might think of the black hole entropy as counting classical black hole microstates, but this is ruled out by the no-hair theorem, stating that a black hole (rather like a point particle! [23]) does not have any classical microstates; they are uniquely determined by their mass, angular momentum and charge. The suspicion is therefore that the microstates associated to the black hole entropy must arise from quantum gravity. Remarkably, the result [24] by Strominger and Vafa demonstrated that it's possible to derive the black hole entropy in string theory, where it arises as the degeneracy of D-brane configurations that support an extremal, maximally supersymmetric black hole. Though this result also correctly predicts the black hole entropy for certain non-extremal cases, it's presently unknown if this result can be generalised to Schwarzchild black holes.

The fact that the black hole entropy measures the area of it's horizon in Planck units is perhaps our most poignnant hint that in a quantum theory of gravity, spacetime should fundamentally be quantised at $o(l_p)$ [25] (see figure 2. Most notably, the result (1.1) amounts to a highly non-trivial constraint on any candidate theory of quantum gravity. Specifically, the thermodynamic character of black holes in the IR (according to a fiducial observer in the exterior) must emerge as the

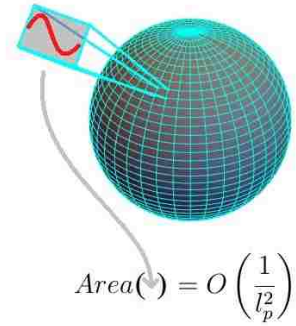

Figure 2: In quantum gravity, the black hole entropy can be thought to derive from microscopic degrees of freedom associated to Planck-scale regions of the black hole horizon, since the Bekenstein-Entropy measures the horizon area according to (1.1).

red-shifted picture of UV physics close to the horizon, so that the black hole entropy amounts to an IR constraint on the UV physics of quantum gravity.

The existence of Hawking radiation leads to a startling puzzle known as the black hole information paradox. Namely, a given infalling pure state is converted to a mixed (thermal) state. When the black hole eventually evaporates it therefore appears that the information pertaining to the infalling stuff has been removed from the universe. Hawking's calculation assumes nothing other than the effectiveness of local quantum field theory at low energies, locality and unitarily evolving states. The black hole information paradox appears to offer the radical suggestion that perhaps Hawking's original calculation was incorrect, and that in particular some of these most basic underlying assumptions may prove false in quantum gravity. In this sense addressing the black hole information paradox might well require the conceptual leap that will utimately lead to the foundations of a prevailing theory of quantum gravity. The general consensus on this matter is not settled, though many suggestions have emerged, ranging from suggestions that information loss in this sense is actually not pathological and even to attempts to modify quantum mechanics itself. A remarkable answer to the question of black hole information loss comes from the AdS/CFT correspondence, which we now describe.

1.2 The AdS/CFT Correspondence

In its original form, the AdS/CFT correspondence entails a conjectured full equivalence between type-IIB string theory with asymptotically $AdS_5 \times S_5$ boundary conditions and $\mathcal{N} = 4$ Super Yang-Mills, being a conformal field theory, living at the boundary of the AdS_5 [5]. This duality is a lucid manifestation of the holographic principle, since the 4-dimensional CFT lives at the

boundary of the 10 dimensional string theory (with 5 dimensions being the compact directions of the S_5). The quintissential relation that captures this duality is an equivalence of the bulk and boundary partition functions,

$$\mathcal{Z}_{CFT}[\phi_0] = \mathcal{Z}_{String}[\phi, \phi_0] \tag{1.2}$$

where the CFT is $\mathcal{N} = 4$ SYM and the bulk fields ϕ have corresponding boundary conditions ϕ_0 realising the asymptotically $AdS_5 \times S_5$ boundary conditions [6]. As an elementary sanity check we can observe that the symmetry group of $AdS_5 \times S_5$, along with supersymmetry, gives the superconformal group in four dimensions, the group of symmetries of $\mathcal{N} = 4$ SYM, so that both sides of the duality have the same symmetries. Whilst the field theory lives at the boundary of the AdS_5, the role of the compactified directions in this sense is that their Kaluza-Klein modes correspond to chiral operators in the CFT [7].

In the terminology of AdS/CFT, the CFT side of the duality is referred to as the boundary theory, since it effectively lives at the boundary of the asymptotically AdS geometry. The corresponding dual gravity side is referred to as the bulk theory.

In general we do not know how to compute $\mathcal{Z}_{String}$ since for example we do not know how to quantise string theory with Ramond-Ramond fluxes. However, the r.h.s of (1.2) is tractable when the string theory is well approximated by semiclassical type IIB supergravity, which is the case in the limit of large-N and large t'Hooft coupling $\lambda = g_{YM}^2 N$ [6]. In this limit the relation (1.2) becomes,

$$\mathcal{Z}_{CFT}[\phi_0] = \sum_i e^{S_{SUGRA}(\phi_i, (\phi_0)_i)} \tag{1.3}$$

Where the summation runs over the set of bulk saddles supported by the bulk field configurations $(\phi_i, (\phi_0)_i)$. Most cases seen in the literature consider a single bulk saddle where subdominant saddle can be neglected, which drops the sum in (1.3).

The regime of large λ means that the CFT is very strongly coupled and the supergravity theory is weakly coupled. The ensuing strong/weak duality is an extremely powerful result of the AdS/CFT correspondence that permits one to study the relatively intractable strong-coupling regime of CFTs from the viewpoint of weakly-coupled, semiclassical gravity. There are many similar AdS/CFT correspondences that can be motivated using the so-called "top-down" approach akin to Maldacena's original method, wherein one motivates the correspondence starting with D-brane configurations in string theory [26, 27]. The more general and ambitious claim is

that the AdS/CFT correspondence is an equivalence between *any* theory of quantum gravity with asymptotically $AdS_{d+1} \times X$ boundary conditions (where X is an arbitrary geometry) and a CFT_d which lives at the boundary of AdS_{d+1}. Thus we assume the relation,

$$\mathcal{Z}_{QG}[\phi, \phi_0] \simeq \sum_i e^{S_{\text{Gravity}}(\phi_i, (\phi_0)_i)} = \mathcal{Z}_{CFT}[\phi_0] \tag{1.4}$$

where the first equality is approximately true in the semi-classical case only. This relation fundamentally represents an equivalence between quantum theories.

But how are observables in each theory related according to (1.4)? There is a natural way to associate, to each bulk mode in (1.4) a corresponding holographic dual observable operator in the CFT. In Maldacena's top-down motivation of the AdS/CFT correspondence, bulk perturbations ϕ couple to the D-branes at spatial infinity on which the CFT lives via the interaction term,

$$H_{\text{int}} = \int d^d x \ \phi_0 \mathcal{O} \tag{1.5}$$

where ϕ_0 is the asymptotic value of the corresponding bulk field ϕ, which acts as a source for the operator $\mathcal{O}$ in the CFT and the coordinates x run along the D-brane worldvolume [5, 6]. This suggests that the asymptotic values of a given bulk field should be interpreted as source for a holographic dual operator in the CFT [6, 28] so that,

$$\mathcal{Z}_{QG}[\phi, \phi_0] = \left\langle \exp\left[\int_{\partial M} \phi_0 \mathcal{O} \right] \right\rangle \tag{1.6}$$

By using (1.6) we see that turning on a bulk scalar gives rise to a boundary dual primary operator. It's easy to see that the scaling dimension of this primary operator is related to the mass of the dual bulk field [6]. Gauge fields naturally couple to conserved currents in (1.6) so these are holographically dual to conserved currents in the CFT. Additionally the fact that boundary stress tensor is the functional derivative of the $\mathcal{Z}_{CFT}$ with respect to the boundary metric, we ascertain that the bulk metric asymptotics are sources for the boundary stress-tensor. As mentioned earlier, it's according to (1.6) that the holographic duals of bulk Kaluza Klein modes wrapping the S_5 in the $AdS_5 \times S_5$ case are the chiral operators of $\mathcal{N} = 4$ SYM.

The complete holographic dictionary that we ascertain from (1.4) is therefore that the asymptotic conditions for the metric, together with the normalisable bulk modes, determine a holographic dual state in the CFT which is prepared by the Euclidean path-integral on the

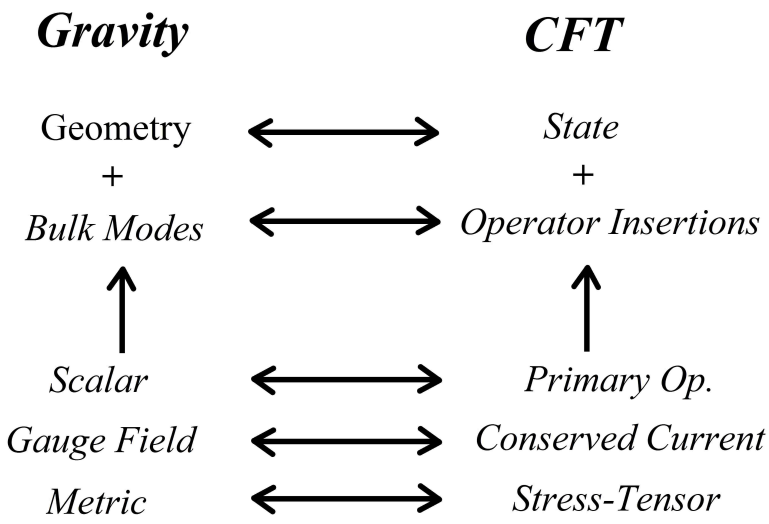

Figure 3: Cartoon of the holographic dictionary for AdS/CFT.

asymptotic geometry along with operator insertions corresponding to operators holographically dual to the bulk modes that are switched on. This general picture of the holographic dictionary in AdS/CFT is depicted in figure 3

In fully quantum gravity we do not know what the physical states are [25, 29], but in the semi-classical regime they are classical gravity configurations, so that a choice of bulk saddle corresponds to a holographically dual state in the CFT according to (1.4). The asymptotic conditions ∂M for the bulk fix the geometry on which the CFT lives so that $\mathcal{Z}[\phi_0, \partial M]_{CFT}$ computes the Euclidean path-integral on ∂M [30]. In this language it's straightforward to show that empty AdS_d is holographically dual, via (1.4) to the ground state in the dual CFT. Empty AdS_d is just global AdS_d which is trivially asymptotically AdS. The geometry of global AdS_d is,

$$ds^2 = l^2(-\cosh^2\rho\, dt^2 + d\rho^2 + \sinh^2\rho\, d\Omega^2_{d-2}) \tag{1.7}$$

The boundary of Euclidean AdS_d (for which we analytically continue $t \to i\tau$) is $\partial M = \mathbb{R}_\tau \times S^{d-2}$, so that the holographic dual state is prepared by the Euclidean path-integral on ∂M which gives the ground state in the CFT, as claimed.

In practice, using the relation (1.6) entails determining CFT correlation function by taking functional derivatives of the bulk gravity action evaluated on an appropriate bulk saddlepoint [6], however this is generically divergent at the boundary at spatial infinity. On the CFT side the correlators contain UV divergences that need to be renormalised with appropriate counter-terms.

We can use the techniques of renormalisation in this case to obtain a finite bulk action principle by introducing a cut-off at some finite value of $r = \epsilon$ and then adding boundary counterterms to the bulk action so as to render it finite in the limit as $\epsilon \to 0$ at the boundary. This is the process of holographic renormalisation [31]. An important upshot of this discussion is that the extra radial direction in AdS/CFT is seen to be holographically related to energy scale in the boundary CFT [32].

We have mentioned the top-down approach to AdS/CFT where one starts from string theory and heuristically derives the corresponding CFT, but we may conversely consider a "bottom-up" approach in which one starts from the CFT and then asks which gravitational theory it might be dual to. CFTs with holographic duals are called holographic CFTs. For a holographic CFT to have a semiclassical holographic dual we require that the CFT has a huge denegeracy of states at high-energies and furthermore that the CFT has a mass-gap or equivalently small degeneracy of low-energy states [33]. We also require that the bulk and boundary central charges coincide[2].

This tantalisingly beautiful correspondence, in a very real sense, entails a fully non-perturbative and background-independent definition of quantum gravity. More remarkably (1.4) implies that gravity's quantum avatar is not fundamentally the formidably geometric creature of Einstein's theory. Indeed (1.4) suggests that in some immediately obscure sense, quantum gravity *is* an ordinary, background-dependent conformal field theory [3]. Though this relation gives us a definition of quantum gravity and tells us exactly what theory is it, we first have to decipher what gravitational dynamics mean to the dual boundary CFT before we can ask interesting questions about the bulk, quantum gravity side of the duality. So far we've seen that at the semiclassical level we have some substantial traction in this direction, but if we want to explore gravity in the genuinely quantum regime via this relation we will have to include loop corrections, or equivalently corrections in $\frac{1}{N}$. Remarkably, AdS/CFT appears to offer a complete (if similarly opaque) resolution of the black hole information paradox: since the bulk gravity dynamics are fundamentally the same thing as a unitary boundary CFT, then the whole process of black hole formation and evaporation must accordingly be described completely by a unitary, information-preserving CFT.

[2]The bulk central charge arises from two copies of the Virasoro algebra which generate the asymptotic symmetries of asymptotically AdS spacetimes [34].

[3]In the present context this makes sense because boundary conditions are not gauge artefacts in gravitational theories

1.3 Non-Relativistic Generalisations

It's extremely tempting to suppose that the correspondence (1.4) can be generalised even further. The most general statement might be to relax the condition that the boundary is asymptotically AdS, or equivalently, that the dual theory is not necessarily conformal. Such generalisations can actually be realised as deformations of a CFT [35–38], where the holographic dictionary for AdS/CFT can be applied perturbatively. From a pragmatic perspective, we might hope to harness the power of the strong/weak coupling duality entailed by the correspondence in order to carry out computations in strongly-coupled quantum systems appearing in nature, which frequently exhibit non-relativistic scaling symmetries [10, 39]. This leads us presently to the story of non-relativistic generalisations of AdS/CFT, which will set the backdrop for chapters 2 and 3 [40]. One hope is that we can formulate a generalisation of AdS/CFT to the context of non-relativistic field theories. This has the added bonus of conferring insight as to the extent to which the formalism of AdS/CFT can be generalised to arbitrary backgrounds, which may in turn lead to valuable hints in our attempts to formulate a quantum theory of gravity.

When we learn about field theory it is often presented as a solely relativistic animal. This is because relativistic quantum field theory is the natural context in which to construct a quantum theory of interacting particles which is local and causal according to relativity. Needless to say a quantum field theory need not be relativistic by construction. Non-relativistic quantum field theories ($NRFT$s) have preferred time and space directions; the synthesis of spatiality and temporality of relativity does not occur and the newtonian intuition prevails. A notably distinct feature is that non-relativistic theories the stress-energy tensor is no longer symmetric; the off-diagonal elements are independent and furnish a so-called stress-energy complex,

$$T_{\mu\nu} = \left\{ \begin{array}{ll} T_{tt} = \mathcal{E} & \text{Energy density} \\ T_{ti} = P_i & \text{Momentum flux density} \\ T_{it} = E_i & \text{Energy flux density} \\ T_{ij} = \Pi_{ij} & \text{Stress density} \end{array} \right\} \tag{1.8}$$

which is conserved [41].

Many of the strongly coupled, non-relativistic systems found in experiments have hyperscaling symmetries such as those that describe fermions at unitarity [42–44]. In this case, schematically

we have a symmetry,

$$x \to \lambda x \qquad t \to \lambda^z t \tag{1.9}$$

where z is the so-called critical scaling exponent [40, 41]. A geometry with this kind of scaling symmetry is the Lifshitz geometry,

$$ds^2 = \left(-r^{2z}dt^2 + r^2 dx_i^2 + l^2\frac{dr^2}{r^2}\right) \tag{1.10}$$

which is invariant under the scaling $x_i \to \lambda x_i, r \to \lambda r, t \to \lambda^z t$ and l sets the scale of curvature. Noteably for $z = 1$, (1.10) is exactly AdS_d. The Lifshitz symmetry group of (1.10) appears at critical points in condensed matter systems describing low-dimensional magnetic materials, liquid crystals and cold atoms [43, 44]. In order to bring the machinery of AdS/CFT to bear in these cases, it is worth considering gravitational theories that are asymptotically of the form (1.10). We can then assume, for that theory, that a relation of the form (1.4) holds, i.e that a form of asymptotically-Lifshitz/Lifshitz-$NRFT$ duality holds and set about establishing an analogue of the standard holographic dictionary that relates observables in each case. With this in hand, we can translate computations in the strong-coupled Lifshitz field theory to calculations in the bulk gravity side. In [45], a holographic dictionary for geometries which may asymptotically be written locally in the form (1.10) was established in precisely this way. Since the non-relativistic scaling preferentially treats the time and space coordinates differently, this motivates us to work with frame-fields instead of the metric. That is, we achieve the required asymptotic conditions for the metric by imposing suitable boundary conditions on the frame fields.

We can write the metric (1.10) with the following choice of frame fields

$$g_{\mu\nu} = e^A_\mu e^B_\nu \eta_{AB} \qquad e^{(r)}_r = lr^{-1} \qquad e^{(0)}_t = r^z \qquad e^{(I)}_i = r dx_i \tag{1.11}$$

where other frame components are set to zero and where η_{AB} is the flat metric and the local frame indices $A = ((0), (i), (r))$. We can partially fix a gauge in which $e^{(r)}_r = lr^{-1}$ and $e^{(r)}_\alpha = 0$ for $\alpha = (t, x_i)$ running over the time and spatial coordinates. The form (1.11) for the frame fields motivates the boundary conditions of [45] in which a metric is called asymptically *locally* Lifshitz if the frame fields have the following asymptotic form at the timelike boundary at $r \to \infty$.

$$e^{(0)}_\alpha = r^z \hat{e}^{(0)}_\alpha(r, x_\alpha), \qquad e^{(I)}_\alpha = r^z \hat{e}^{(I)}_\alpha(r, x_\alpha) \tag{1.12}$$

where the expansion around of the $\hat{e}(r, x_\alpha)$ around $r \to \infty$ contains a finite leading piece, plus sub-leading terms that decay in the limit. This conditions allows the boundary metric to be locally (1.10). So far we've not mentioned which theory we're considering and the conditions (1.12) are appropriately generic since the precise, subleading terms appearing in the metric will be determined by the dynamics of a given theory realising (1.12).

In [45] the asymptotic conditions (1.12) are realised as a particular solution of the massive vector theory coupled to gravity with the action,

$$S = -\frac{1}{16\pi G}\int d^{d_s+3}x\sqrt{-g}\left(R - 2\Lambda - \frac{1}{4}F_{\mu\nu}F^{\mu\nu} - \frac{1}{2}m^2 A_\mu A^\mu\right) - \frac{1}{8\pi G}\int d^{d_s+2}\xi\sqrt{-\gamma}K, \quad (1.13)$$

for which the massive vector field A supports the non-relativistic hyperscaling symmetry. Sources and vevs in the boundary $NRFT$ are identified as the leading terms that appear in a linearised analysis of bulk perturbations to the frame fields compatible with the asymptotic conditions. In accordance with an appropriate generalisation of (1.4), this leads to an identifcation between bulk asymptotics and sources for the boundary stress-energy complex in addition to an irrelevant operator dual to the time-components of the massive vector. In chapters 2 and 3 we will explore in detail how this rich story generalises to geometries with are asymptotically locally Schrödinger, again in the context of gravity coupled to a massive vector. The upshot in these cases is that while we remain agnostic to the existence of the boundary $NRFT$, appropriate holographic dictionaries analogous to (1.4) are shown to exist.

For a generic bulk theory, it is not necessarily possible that boundary conditions such as (1.12) exist, that is that an asymptotic expansion of bulk fields in subleading powers of r consistent with the interpretation (1.6) exists. In chapters 2 we will see that in the generalisation of AdS/CFT to asymptotically locally Sch́odinger backgrounds, the existence of a "good" asymptotic expansion is strongly dependent on the dynamical critical exponent appearing in the metric.

1.4 Entanglement Entropy

In the last subsections we've described the AdS/CFT correspondence and how this formalism can be applied to more generic, specifically non-relativistic backgrounds. In view of understanding what AdS/CFT has to tell us about quantum gravity more generally, an extremely important question is how a relation like (1.4) can possibly work, that is, how are gravitational dynamics

encoded holographically in a non-gravitational context in the CFT? We know so far that fixing the asymptotic conditions in (1.4) for the bulk fixes a choice of state in the boundary CFT, so a pertinent question to ask in the semiclassical case is, how is the geometry in the bulk encoded holographically? Overwhelmingly the answer appears to be that the key aspect of this is the interplay between bulk geometry and boundary quantum information, namely entanglement entropies. This correspondence has led to the inception of the field of holographic entanglement entropy which has led to intensely rich and exciting developments. Before proceeding further we should briefly review the idea of entanglement entropy in quantum systems.

Entanglement entropy diagnoses a kind of correlation between quantum systems which is only possible due to the superposition principle and is therefore a property unique to quantum mechanics.

Suppose there are two rooms A and B and suppose that Alice and Bob, two observers, are placed in seperate rooms A and B respectively. Suppose that the total quantum state is the pure density matrix ρ in a Hilbert space bipartitioned so that $\mathcal{H} = \mathcal{H}_A \otimes \mathcal{H}_B$. Supposing that Alice has no means of measuring B then the quantum state seen by Alice on A the described by the reduced density matrix associated to the factor $\mathcal{H}_A$, obtained by tracing out the degrees of freedom in B,

$$\rho_A = \mathrm{Tr}_B(\rho) \tag{1.14}$$

That is, ρ_A contains all of the information about correlation functions in A measurable by Alice. The density matrix ρ_A is generically a mixed state due to the fact that Alice and Bob's systems may be correlated. Entanglement entropy diagnoses precisely this kind of correlation between subsystems, that manifests in the case of pure states in the way that the state on a given subsystem appears mixed. The Von Neumann entropy of the reduced density matrix A measures the amount of quantum entanglement between A and A^C in the pure state ρ;

$$S(A) = -\mathrm{Tr}(\rho_A \log \rho_A) \tag{1.15}$$

Equivalently, this quantity diagnoses whether or not a given state on the product of factors is seperable, that is whether or not it can be write as a product of states on each seperate factor.

For a generic pure state $\rho = |\psi\rangle\langle\psi|$ it's entanglement entropy is simply $S = -\mathrm{Tr}(\rho \log \rho) = \langle\psi| \log 1 |\psi\rangle = 0$, so the entanglement entropy for pure states vanishes.

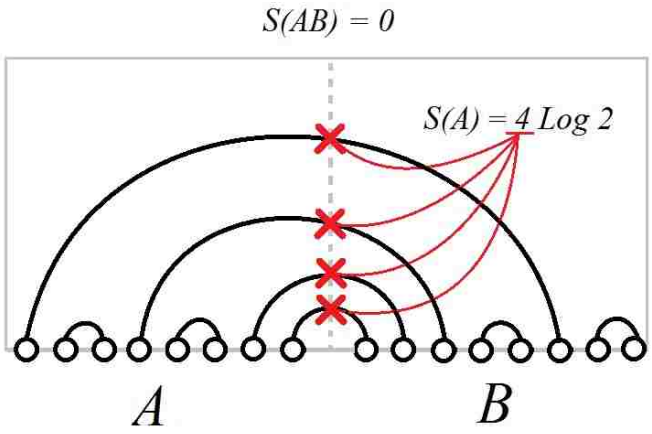

Figure 4: Cartoon illustrating that entanglement between subsystems A and B of qubits counts the number of entangled qubits between A and B. Each node represents a qubit, and the lines connecting nodes depict maximally entangled qubits. In this case, 4 pairs of qubits are maximally entangled, hence $S(A) = 4 \log 2$.

The poster-child for an entanglement in quantum mechanics is the maximally-entangled Bell state of two qubits,

$$|\psi\rangle = \frac{1}{\sqrt{2}}(|0\rangle|0\rangle + |1\rangle|1\rangle) \tag{1.16}$$

The entanglement entropy of a single qubit (the first one, for example) in the state (1.16) is,

$$S(1) = -\operatorname{Tr}(\rho_2 \log \rho_2) = -\frac{1}{2}\sum_{i=0}^{1}\langle i|_2 \log \rho_2 |i\rangle_2 = \frac{1}{2}\sum_{i=0,j=0}^{1}\langle i|_2 \log\left(\frac{1}{2}|j\rangle_2\langle j|_2\right)|i\rangle_2 = \log 2 \tag{1.17}$$

since $\rho_2 = \frac{1}{2}I_2$ is diagonal. The entropy (1.15) is maximal when ρ_A is diagonal, in which case we say that the state ρ_A is maximally mixed, or maximally entangled with ρ_{A^C}. The state (1.16) evidently maximally entangles the two qubits.

Generally a quantum state in $\mathcal{H}_\mathcal{A}$ can be described as a state of N qubits where $dim(\mathcal{H}_\mathcal{A}) = 2^N$. If a state on $\mathcal{H}$ is maximally entangled we have $S(A) = N \log 2 = \log[dim(\mathcal{H}_\mathcal{A})]$ otherwise $S(A)$ is smaller. This means that the entanglement entropy is bounded by $S \leq \log[dim(\mathcal{H}_\mathcal{A})]$.

According to (1.17), one way to interpret entanglement entropy $S(A)$ is that it measures the number of entangled qubits between A and A^C, as depicted in the figure 4. Conversely, given a state ρ_A in a closed system A with entanglement entropy $S(A) \leq N \log 2 = \log[\dim(\mathcal{H}_A)]$, N counts the minimum number of qubits in an auxilliary system B required to be entangled with ρ_A in order that ρ_A can be obtained by tracing out B from a pure state ρ_{AB}. In this case we say that the auxilliary state ρ_B purifies the mixed state ρ_A.

For a pure state $|\psi\rangle \in \mathcal{H} = \mathcal{H}_A \otimes \mathcal{H}_B$ with $(dim[\mathcal{H}_A], dim[\mathcal{H}_B]) = (m, n)$, there exists a basis $\{|a_i\rangle\} \in \mathcal{H}_A$ with $i = 1, ...m$ and $\{|b_j\rangle\} \in \mathcal{H}_B$ with $i = 1, ...n$ so that $|\psi\rangle$ has the following Schmidt decomposition,

$$|\psi\rangle = \sum_i p_i^{1/2} |a_i\rangle \otimes |b_i\rangle \tag{1.18}$$

where p_i are real and positive. One can immediately deduce the reduced density matrices on the factors A and A^C,

$$\rho_A = \sum_{i=1}^{n} p_i |a_i\rangle\langle a_i| \qquad \rho_B = \sum_{i=1}^{n} p_i |b_i\rangle\langle b_i| \tag{1.19}$$

This makes evident that the entanglement entropies associated to each reduced density matrix are equal, since their eigenvalues coincide. This expressed that for pure states we have,

$$S(A) = S(B) \tag{1.20}$$

whis is manifest in figure 4. For a pure state then we have the further constraint that $S(A) \leq \min(\log(n), \log(m))$.

Entanglement entropy in simple quantum mechanical systems, where there are only a finite number of degrees of freedom such as in the familiar case of a 2-qubit system, are easy to compute. In field theories, on the other hand, we have an infinite number of degrees of freedom and computing entanglement entropies is far more difficult. The fact that field theories contain an infinite number of degrees of freedom means that the entanglement entropy associated to any spatial subregion diverges in the UV. One can consider taking a field theory on a lattice and keeping the leading contribution to the entanglement entropy as the lattice spacing goes to zero in the UV. This regularised piece captures physical information about the entanglement entropy of the corresponding subregion [46]. For a useful review of the basic properties of entanglement entropy in quantum mechanics and quantum field theory, see for example [16, 47].

1.5 The Ryu-Takayanagi Conjecture

A remarkable conjecture, relating quantum entanglement and bulk geometry in the context of AdS/CFT was motivated by Ryu & Takayanagi [12, 16, 47]. Their claim is that the entanglement entropy of the reduced density matrix associated to a spatial subregion A of a CFT is equal to the area of a minimal-area codimension-2 spacelike surface γ_A in the bulk which is homologous to A, as depicted in figure 5. Given a subregion A of a holographic CFT, the Ryu-Takayanagi

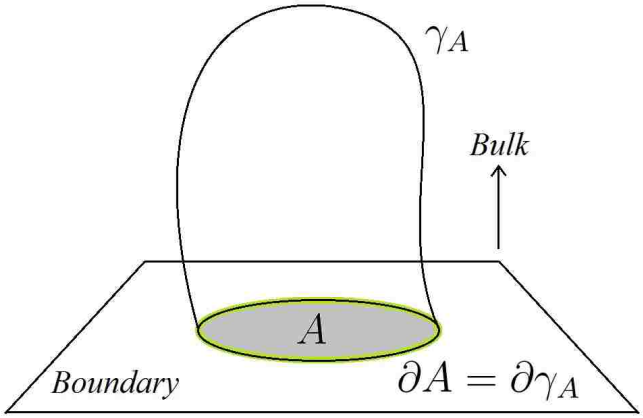

Figure 5: Cartoon of the RT-formula 1.21 for the entanglement entropy of a subregion A (shaded) in the boundary CFT, which is given by the area of an extremal codimension-2 surface in the bulk whose boundary is the boundary of A (shaded green).

conjecture states that,

$$S_A = \frac{1}{4G_n}\text{Area}(\gamma_A) \tag{1.21}$$

This relationship represents perhaps the most striking equivalence between bulk geometry and boundary entanglement entropy and has recently been derived from the AdS/CFT dictionary by Lewkowycz and Maldacena by applying the replica trick to the Euclidean bulk path-integral [15].

There's an immediately striking resemblance between (1.21) and the Bekenstein-Hawking entropy 1.1 of a black hole and in fact the RT formula actually generalises the latter. To see this, consider applying the formula (1.21) in a black hole background to it's entire asymptotic boundary. In this case the appropriate bulk extremal surface γ has no boundary, as illustrated in figure 6. However, the presence of the horizon in the bulk represents a topological obstruction, meaning that the only surfaces permitted by (1.21), due crucially to the homology constraint, are those that wrap the horizon. The minimal area surface in this case is precisely the horizon itself, so that the formula (1.21) gives exactly $S_A = \frac{1}{4G_n}Area(\text{Horizon})$, which is exactly the Bekenstein-Hawking entropy formula (1.1) (in natural units).

A covariant generalisation of (1.21) exists called the HRT prescription, which is applicable to time-dependent cases [48].

The simplest example to check for (1.21) is with the bulk geometry being AdS_3, which is dual to the ground state in the CFT_2. The most trivial exercise is to consider the entanglement entropy of the state on the whole boundary, which we know is the pure ground state. The minimal area surface on a constant-time slice which is homologous to the whole boundary is simply the

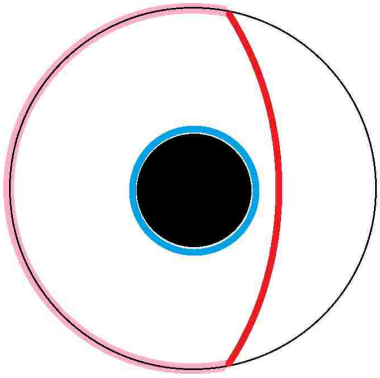

Figure 6: Schematic depiction of the homology contraint in the RT-formula (1.21) applied to black holes. The red surface cannot be continuously deformed to the pink-shaded boundary subregion due to the black hole. However, adding the combination of the red and blue surfaces, the latter being the black hole horizon, gives a candidate RT-surface which is homoglous to the pink-shaded region.

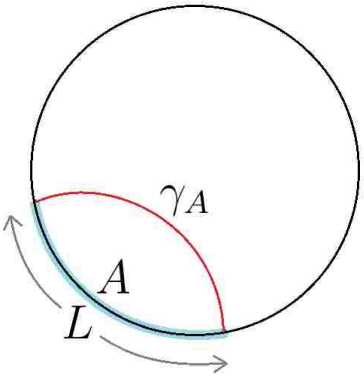

Figure 7: The RT-formula (1.21) equates the entanglement entropy, in the ground state, of the CFT_2 subregion A (blue-shaded) of length L to a length of boundary-anchored geodesic γ_A (red) on a constant time-slice of AdS_3.

empty set, for which the formula (1.21) tells us correctly that the entanglement entropy is zero. A more interesting case to check is the entanglement entropy of a spatial subinterval A of size L in the CFT_2 in the ground state. The conjecture (1.21) implies that the entanglement entropy of this subinterval is given by the length $L(\gamma)$ of a boundary-anchored geodesic on a constant time slice of AdS_3, as depicted in figure 7.

For AdS_3 with the geometry,

$$ds^2 = \frac{l^2}{r^2}(-dt^2 + dx^2 + dr^2) \tag{1.22}$$

The boundary anchored geodesic on the spatial slice with endpoints $(x_0, x_1) = (-\frac{L}{2}, \frac{L}{2})$ is the

semicircle,

$$x(\tau) = \frac{L}{2}\cos\tau, \qquad r(\tau) = \frac{L}{2}\sin\tau, \qquad \tau \in (\frac{\epsilon}{L}, \pi - \frac{\epsilon}{L}) \tag{1.23}$$

where ϵ is introduced to regulate the UV divergence as the geodesic tends to the boundary at spatial infinity as $\epsilon \to 0$ [49]. The formula (1.21) then gives the entropy of A

$$S_A = \frac{L}{2G_N}\log\left(\frac{L}{\epsilon}\right) \tag{1.24}$$

This agrees exactly with the known CFT_2 result,

$$S_A = \frac{c}{3}\log\left(\frac{L}{\epsilon}\right) \tag{1.25}$$

up to the identification

$$c = \frac{3l}{2G_N} \tag{1.26}$$

This is precisely the Brown-Henneaux central charge for the two copies of the Virasoro algebra which furnish the group of asymptotic symmetries for asymptotically AdS_3 spacetimes [34][4].

1.6 Holographic Eternal Black Holes and ER=EPR

We have already talked about the holographic dual of empty AdS_d, which is holographically dual to the ground state in the CFT, but there are many bulk gravity solutions which are asymptotically AdS with interesting holographic dual descriptions. Some of the most interesting are AdS black hole solutions and their multiboundary generalisations which we now describe.

The Schwarzchild-AdS_d black holes have two timelike boundaries at spatial infinity, as depicted in the Penrose diagram 8. The simplest asymptotically AdS black hole is the 3-dimensional case found by Bañados, Teitelbohm and Zanelli appropriately named the BTZ black hole with two asymptotic boundaries [50]. The Euclidean BTZ black hole has the geometry,

$$ds^2 = (r^2-1)d\tau^2 + \frac{dr^2}{r^2-1} + r^2 d\phi^2 \qquad \phi \sim \phi + \frac{4\pi^2}{\beta} \qquad \tau \sim \tau + 2\pi. \tag{1.27}$$

Rescaling by a factor of $\beta/2\pi$ we find that the boundary at spatial infinity is $I_\beta \times S^1$ where $I_\beta = (0, \beta)$ denotes the periodic Euclidean time direction (with period β) which connects the two

[4]Interestingly though this result predates the AdS/CFT correspondence by 11 years, the relation to the conformal group in two dimensions was not apparently acknowledged at the time.

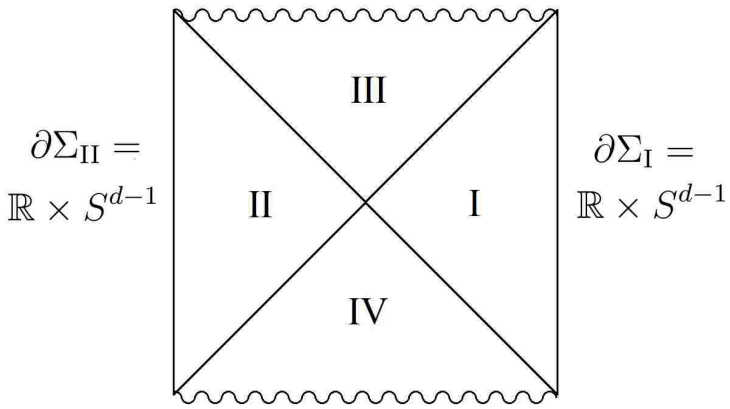

Figure 8: Penrose diagram of the extended Schwarzchild AdS space. Regions I and II are exterior to the black and white hole horizons in regions III and IV respectively, and their timelike boundaries $\partial\Sigma_{\rm I,II}$ lie at spatial infinity in regions I,II. Spacelike singularities are contained behind the horizon in regions III and IV.

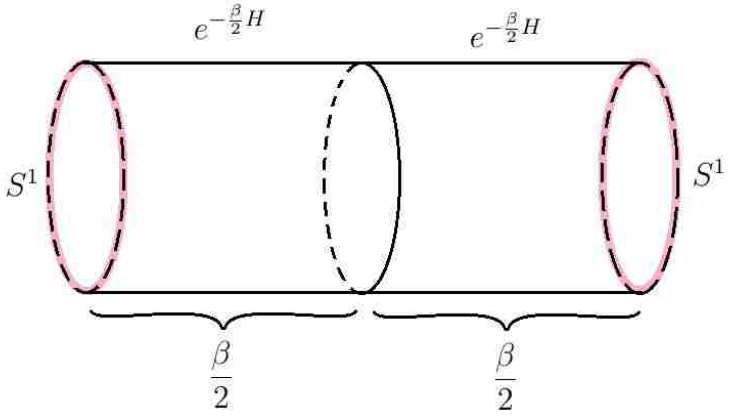

Figure 9: The Euclidean path-integral that prepares the thermofield double (TFD) state on two copies of S^1 (highlighted) on the $t = 0$ slice of the boundary of the BTZ black hole.

circles on the $t = 0$ slice. The path-integral that prepares the holographic dual state on each boundary circle on the $t = 0$ is the the Euclidean path integral on $I_{\beta/2} \times S^1$, two of which are sewn together to give $I_\beta \times S^1$ as depicted in figure 9. This path-integral generates the thermofield double state in the dual CFT,

$$|TFD\rangle = \sum_i e^{-\frac{\beta}{2}H} |E_i\rangle_1 \otimes |E_i\rangle_2 \tag{1.28}$$

This result redounds to a general feature of holographic duality, namely that bulk black holes are dual to thermal states in the CFT. The thermofield-double state has the property that the

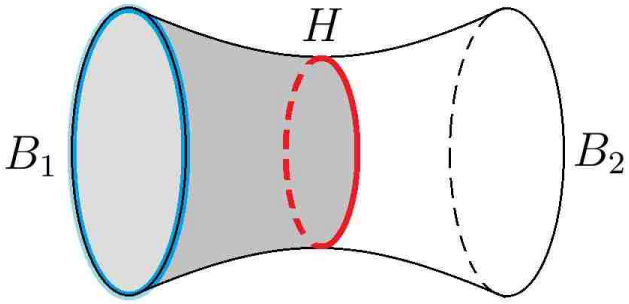

Figure 10: The RT-surface for the single boundary B_1 (shaded blue) on the $t = 0$ slice of BTZ is the horizon H which maximally entangles the two boundaries.

reduced density matrix on either factor is the thermal density matrix,

$$\rho_{\text{Thermal}} = e^{-\beta H} \tag{1.29}$$

with inverse temperature β. This means that on any given boundary the state looks exactly thermal. Since the total state is pure, the thermal character of the state on an single boundary is entirely a consequence of the entanglement between the two-boundaries, that the state on one boundary is purified by the state in the opposite boundary. The entanglement entropy on one boundary on a constant time slice is given by the area of the BTZ horizon which is $\Delta\phi = 4\pi^2/\beta$, as depicted in figure 10.

Maldacena and Susskind argued that the entanglement between the two boundaries for the AdS-Schwarzchild black holes, *is* the wormhole connecting them [14]. Indeed, the boundary CFTs in the TFD state are not coupled to one another, so that in a sense their correlation comes entirely from the wormhole that connects them. This underlies the essence of the $ER = EPR$ conjecture, that the entanglement between a maximally entangled pair of qubits is fundamentally the same thing as a highly quantum wormhole connecting the qubits (see figure 11); in this sense, quantum entanglement and bulk connectivity are fungible [51].

The bipartite BTZ wormhole supports the entangled TFD state in the boundary. The natural generalisations of AdS black holes are the asymptotically AdS multiboundary wormholes geometries that connect multiple asymptotic boudaries [52–55]. The $ER = EPR$ intuition suggests that there may be a sense in which intrinsically multipartite entanglement is necessary in order to support multiboundary wormhole geometries in the bulk (see figure 12). This question is generically very difficult to answer on the one-hand, since unlike for the BTZ case, we know far less about how to do the path-integral that prepares the states holographically dual to multiboundary

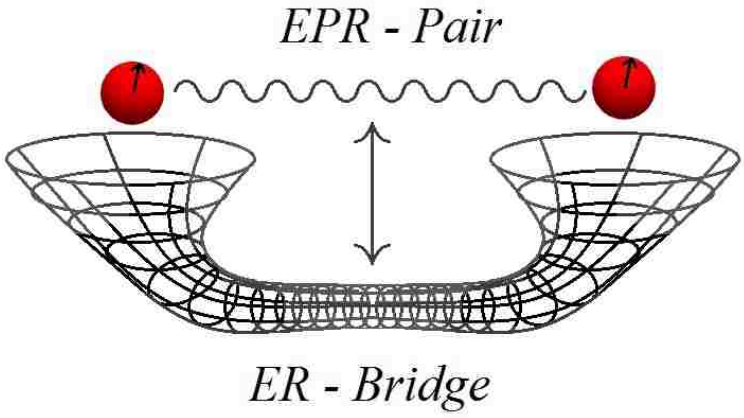

Figure 11: Cartoon depicting the $ER = EPR$ conjecture: an EPR pair is conjectured to be fundamentally equivalent to a highly quantum ER-bridge connecting the locations of the two qubits.

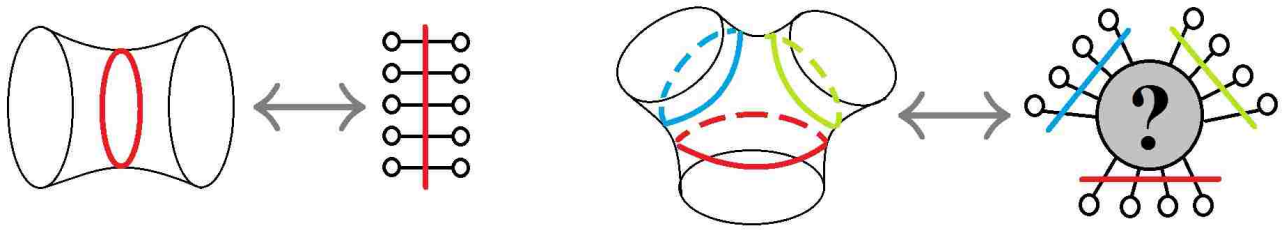

Figure 12: (Left) The entanglement between the two boundaries in BTZ can be distilled to bell pairs crossing the horizon, meaning that the entanglement is entirely bipartite. (Right) for a triply-connected, three-boundary wormhole with three horizons (red, green and blue), we might anticipate that the entanglement structure is in some sense intrisically tripartite.

wormholes. The so-called high-temperature regime, which is the subject of chapter 4, is one such regime where we can understand the path-integral for holographic multiboundary wormholes. An additional complication here is that intrinsically multipartite entanglement is much harder to diagnose than bipartite entanglement, for which many such measures exist. In both chapters 4 and 5 we attempt to understand the entanglement structure of holographic multiboundary wormholes.

1.7 Holographic Bulk Locality & Quantum Error-Correcting Codes

In AdS/CFT, the boundary CFT does not manifestly respect locality in the bulk, except insofar as we've seen at a heuristic level where it is related to energy scale in the CFT. However for certain CFT states to be holographically dual to local bulk geometries then clearly there must be

a sense in which bulk locality is encoded in CFT states. One could thus consider to what extent one's access to bulk information is limited by resticting to access to only a portion of the CFT. One way to gain a handle on this question is via the approach of holographic bulk reconstruction [56, 57], which we now describe.

To motivate this approach begin by considering the usual holographic dictionary, where the restriction of a bulk operator to the boundary defines the source for a corresponding boundary operator

$$\lim_{r\to\infty} r^{\Delta}\phi(x) = \phi_0(x) \tag{1.30}$$

where ϕ_0 is the source for the dual operator of conformal dimension Δ in the CFT. The "inverse" of (1.30) is the fact that one can express the bulk operator as an integral over the whole boundary of the ϕ_0 weighted with the integration kernel K known as the bulk-to-boundary propagator,

$$\phi(X) = \int_{\partial\mathcal{M}} d^d x \; K(X;x)\phi_0(x) \tag{1.31}$$

The role of K is to implement the kinematic constraint (1.30) as well as the dynamics in the form of the bulk wave equation for ϕ. Equation (1.31), it should be stressed, is a statement purely about bulk fields and their asymptotics. The relation (1.31) suggests the following CFT analogue, wherein one can construct an operator in the CFT which is local in the bulk,

$$\mathcal{O}_{\text{Bulk}}(X) = \int_{\partial\mathcal{M}} d^d x \; \mathcal{K}(X;x)\mathcal{O}(x) \tag{1.32}$$

where again the role of $\mathcal{K}$, here called the "smearing function" is to implement the kinematic and dynamical constraints for the bulk local operator $\mathcal{O}_{\text{Bulk}}(X)$. In contrast to (1.31), (1.30) is now a statement about operators in the CFT. The operator $\mathcal{O}_{\text{Bulk}}(X)$ manifestly acts non-locally in the CFT. Here then we have a relation that proxies bulk locality purely in terms of non-local operators in the CFT. We may call $\mathcal{O}_{\text{Bulk}}$ a local bulk operator to the extent that it's a quantity which is local in the bulk, but again this is genuinely an operator in the CFT. Causality requires that $\mathcal{O}_{\text{Bulk}}(X)$ commutes with $\mathcal{O}(y)$ for X and y spacelike seperated. This means that $\mathcal{K}$, which reconstructs $\mathcal{O}_{\text{Bulk}}(X)$ according to (1.32) can be chosen to be supported only on a portion of the CFT which is the set of points spacelike seperated from X. This is the idea of global AdS reconstruction [58].

Naturally we can consider further restrictions of $\mathcal{K}$ to a subregion A of the CFT. The

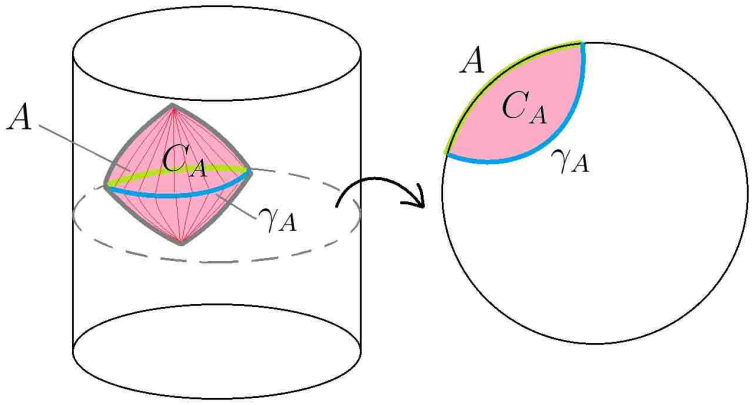

Figure 13: Cartoon of AdS-Rindler wedge reconstruction. The Rindler wedge C_A corresponding to a boundary subinterval A on a constant time slice is the bulk domain of dependence of A, whose boundary on that constant time slice is the minimal spacelike surface γ_A. In AdS-Rindler reconstruction, operators localised in the pink shaded region can be reconstructed as an operator supported entirely within A.

existence of non-existence of $\mathcal{K}_A$ in these cases is then a statement about whether or not A contains information about the support of $\mathcal{O}_{\text{Bulk}}(X)$, which leads to the idea of "subregion-subregion" duality.

A well-established form of bulk reconstruction for boundary subregions is the AdS-Rindler reconstruction [56, 57], which describes how to construct a local bulk operator of the form (1.32) in the Rindler wedge C_A, or bulk domain of dependence of a connected CFT subregion A, as illustrated in figure 13. This is an explicit example of subregion-subregion duality wherein a connected CFT subregion A contains information about C_A. The ensuing encoding of bulk non-local operators 1.32 is highly redundant due to the fact that a given bulk point lies within the Rindler wedge of an infinite number of boundary subregions, as illustrated in figure 14 a). Naively we would claim that reconstruction of a local bulk operator in any wedge (were it possible) gives rise to the same operator, but this leads to issues, namely that if this were true then Schur's lemma forces the operator to be trivially proportional to the identity. The end result is that a local bulk operator $\mathcal{O}_{\text{Bulk}}$ has a different representation in the CFT on each subregion from which it can be constructed. The fact that local bulk operators are encoded in a highly redundant manner in the CFT has motivated some to draw strong parrellels between this feature and the way in which information is redundantly encoded in quantum error correcting codes.

According to the proposals of [59], bulk locality is encoded in a holographic CFT state at the level of a sub-algebra of light bulk observables which realise an operator-algebra quantum-

error-correcting code (QEC). The basic idea, which closely parrellels AdS-Rindler reconstruction, is that bulk information, namely information about operators that are localised in the bulk, is robust up to erasures of the CFT subregions. If for example we erase a CFT subregion A whose causal wedge contains the bulk point X, then operators supported at X cannot be reconstructed on A^C. How sensetive $\mathcal{O}_{\text{Bulk}}$ is to erasures of the boundary depends only on how far X is into the bulk, as illustrated in figure 14 b). Notably, because bulk locality is herein related only to the size of the dual erasure threshold, this proposal supports the idea that one can carry out bulk reconstruction (1.32) outside of the causal wedge, into the entanglement wedge. This latter idea has recently seen explicit realisations [60, 61]. The QEC proposal maintains that local bulk information is encoded as a quantum secret-sharing scheme in the boundary state, where access to information in any particular portion of the bulk requires a sufficiently large share of the boundary in hand, as depicted in figure 14 c). In chapters 4 and 5 we will observe that the key features of this relation are realised in the context of holographic multiboundary wormholes.

The redundant nature of the encoding of bulk information in the QEC proposal has been compared with gauge invariance in the CFT, suggesting that boundary gauge invariance may play a key role in realising the emergence of locality in the radial direction [62, 63]. Remarkably it has been recently proposed that the holographic entanglement entropy formula (1.21) can be derived from the QEC proposals [64] which similarly highlights the role of bulk gauge transformations.

Very recently the notion of causal density matrices in quantum field theories has offered the tantalising suggestion that the QEC proposals are more generic and far-reaching than has previously been thought [65]. This approach may in turn shed light on holography beyond AdS/CFT.

1.8 Outline of the Thesis

In this introduction we've described the AdS/CFT correspondence and outlined many of it's salient results. Additionally we've discussed non-relativistic generalisations of AdS/CFT and also the problem of understanding the entanglement structure of holographic multiboundary wormholes. These ideas will set a backdrop for this thesis. In chapter 2 we consider generalising the formalism of AdS/CFT to the case of asymptotically locally Schödinger backgrounds, where the dynamical critical exponent $z < 2$ boundary conditions analogous to (1.12) are motivated and for the massive vector gravity theory, suitable asymptotic expansion for the bulk fields are found

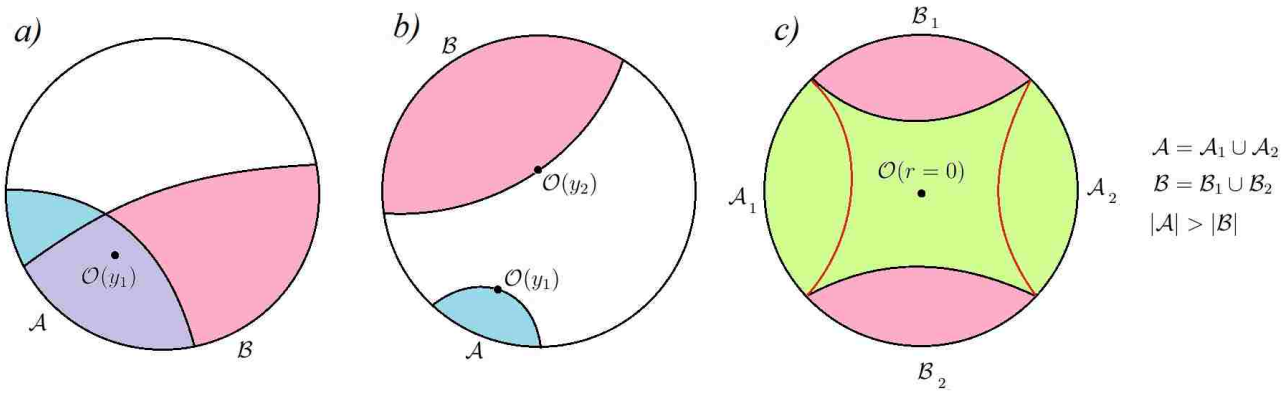

Figure 14: Cartoon of the QEC proposal of [59]. a) The operator $\mathcal{O}(y_1)$ lies within the red and blue causal wedges of the CFT subregions $\mathcal{A}$ and $\mathcal{B}$ respectively, and can be accordingly reconstructed from CFT operators supported entirely on either subregion. As such, the encoding of $\mathcal{O}(y_1)$ is redundant in the CFT. b) Regions $\mathcal{A}$ and $\mathcal{B}$ are chosen so that the points y_1,y_2 lie just within the tips of the causal wedges $C_{\mathcal{A}}$ and $C_{\mathcal{B}}$. If we erase regions $\mathcal{A}$ or $\mathcal{B}$ we can no longer reconstruct operators at y_1,y_2 respectively. Since y_2 is deeper in the bulk than y_1, information about $\mathcal{O}(y_2)$ is less sensitive to boundary erasures of a given size. c) To reconstruct the operator $\mathcal{O}(r=0)$ at the central point requires access to a share that is at least half the size of the boundary [59], the disconnected intervals $\mathcal{A}$ contain the central point within it's entanglement wedge (green), but not inside the causal wedges of $\mathcal{A}_1$ and $\mathcal{A}_2$. This implies that one can reconstruct $\mathcal{O}(r=0)$ within the entanglement wege of $\mathcal{A}$. Since $|\mathcal{A}| > |\mathcal{B}|$, information about $\mathcal{O}(r=0)$ cannot be reconstructed from $\mathcal{B}$. These features furnish a quantum secret-sharing scheme.

with which we associate bulk asymptotics to corresponding sources in the boundary $NRFT$ in cases with different dimensions. In chapter 3 we work in the similar setting but in the qualitatively distinct setting where $z = 2$. In this case the leading asymptotics include contributions from the additional null direction. We argue that in this case the null direction should be regarded as an internal spacefrom the boundary $NRFT$ point of view, by analogy with the similar story that occurs in $AdS_5 \times S^5 = SYM_{\mathcal{N}=4}$ case, where the leading asymptotics similarly contain contributions from the S_5 directions. Here, as for the $z < 2$ case we establish the existence of a good holographic dictionary in this context for the same massive vector theory in cases with different dimensions. In chapter 4 we turn to the question of investigating the entanglement structure of holographic multiboundary wormholes. We explore the entanglement structure in the three-dimensional gravity case wherein we can utilise the powerful quotient formalism to construct multi-boundary geometries. We explore the limit in which the states in each boundary are taken to have infinitely large temperatures, the so-called high-temperature limit, where substantial geometric simplifications occur, culminating in the result that the entanglement structure of the dual state for multiboundary wormholes is almost exclusively bipartite in this limit. In

chapter 5, we address the question of understanding the entanglement structure of holographic multiboundary wormholes at generic values of the moduli by using powerful tensor network methods to proxy the path-integral in this tractable setting. We find, surprisingly, that in many of the cases we consider, we can construct holographic tensor network states modelling the wormhole which are entirely, or almost entirely bipartite, suggesting that the main result of chapter 4 might be more generic than one might have initially supposed. We comment on the fact that these tensor network models reproduce many of the salient features of the QEC ideas.

2 Schrödinger Holography for $z < 2$

The work in this chapter is reproduced from a collaborative paper [1] with Dr. Tomas Andrade, Dr. Cindy Keeler and Prof. Simon Ross. In this work we investigated holography for asymptotically Schrödinger spacetimes, using a frame formalism. Our dictionary is based on the anisotropic scaling symmetry. We consider $z < 2$, where the holographic dictionary is cleaner; we make some comments on $z = 2$, which is subsequently addressed in chapter 2. We propose a definition of asymptotically locally Schrödinger spacetime where the leading components of the frame fields provide suitable geometric boundary data. We show that an asymptotic expansion exists for generic boundary data satisfying our boundary conditions for $z < 2$.

2.1 Introduction

Holography for non-relativistic field theories has been actively studied for several years now. It has the potential to offer us tools to study a broader class of field theories holographically, which may include theories of interest for modelling condensed matter physics [42, 66, 67]. It also offers the possibility to deepen our understanding of holographic relations between field theories and gravity. The non-relativistic theories of interest are characterised by the existence of an anisotropic scaling symmetry which treats the time and space directions differently, $t \to \lambda^z t, \quad x \to \lambda x$, where z is called the dynamical exponent. There are two main cases of interest, Schrödinger and Lifshitz. In the first case the theory has a Galilean boost symmetry; in the latter case there is no such symmetry, so the theory has a preferred rest frame. As a result Schrödinger theories have a conserved particle number which is not present in the Lifshitz case. The case $z = 2$ is special for Schrödinger, in this case the theory has an additional special conformal symmetry. A holographic dual for theories with Schrödinger symmetry was proposed first [42, 66], but the Lifshitz case [67] has been more fully explored, because of its greater simplicity and close resemblance to the well-understood AdS case.

For Lifshitz, the holographic dual has a metric

$$ds^2 = -\frac{dt^2}{r^{2z}} + \frac{d\vec{x}^2 + dr^2}{r^2}, \tag{2.1}$$

with d_s spatial directions $\vec{x}$, which has an isometry $t \to \lambda^z t$, $x \to \lambda x$, $r \to \lambda r$ realizing the anisotropic scaling symmetry. The bulk geometry has a single additional direction, r, related to energy scale in the dual field theory. Points for which $r \to 0$ are identified with the region in which the boundary theory lives, although, due to the anisotropic scaling, there is no conformal boundary properly speaking. Motivated by this, in [41] it was proposed that it is convenient to describe the geometry in terms of frame fields in constructing the holographic dictionary, and this dictionary was worked out in detail in [45]. This has been further developed in [68–72], and an alternative perspective based on a deformation of AdS for z near one developed in [73, 74].

For Schrödinger, the bulk metric is

$$ds^2 = -\frac{dt^2}{r^{2z}} + \frac{2dtd\xi + d\vec{x}^2 + dr^2}{r^2}. \tag{2.2}$$

Here we have once again chosen coordinates for which the boundary corresponds to $r \to 0$ in the

sense explained above. The isometry $t \to \lambda^z t$, $x \to \lambda x$, $\xi \to \lambda^{2-z}\xi$ $r \to \lambda r$ realises the anisotropic scaling symmetry, and there are isometries $\vec{x} \to \vec{x} + \vec{v}t$, $\xi \to \xi - \vec{v}\cdot\vec{x} - \frac{1}{2}v^2 t$, which realise the Galilean boost symmetry. The presence of the additional null direction ξ can be understood in field theory terms as arising from realizing the non-relativistic field theory with Galilean boosts as the light cone reduction of a Lorentz-invariant theory in one higher dimension [42, 75]. For $z = 2$ this reduction is compatible with the anisotropic scaling symmetry. Thus, from the field theory point of view ξ appears to play a kinematical role, as a useful device for realizing the symmetries of a Schrödinger theory in the more familiar framework of relativistic theories; momentum in the ξ direction can be interpreted as a conserved particle number. Its role holographically has however remained somewhat unclear. The scaling symmetry acts non-trivially on ξ for $z \neq 2$, so in this case it is only the higher-dimensional theory that is scale invariant, and it seems natural to assume that the holographic dictionary is formulated in terms of this higher-dimensional theory.

By a coordinate transformation $t \to \sigma t$, $\xi \to \sigma^{-1}\xi$, the metric (2.2) can be rewritten as

$$ds^2 = -\frac{\sigma^2 dt^2}{r^{2z}} + \frac{2dtd\xi + d\vec{x}^2 + dr^2}{r^2}. \tag{2.3}$$

and for small σ the geometry outside of some neighbourhood of $r = 0$ can be viewed as a deformation of AdS. This motivated the programme of [35–38], which studies Schrödinger holographically as the perturbation of a relativistic theory by an irrelevant vector operator, decomposing the linearised fluctuations of bulk fields in terms of sources and vevs of operators of given scaling dimension with respect to the relativistic scaling symmetry. This programme has had some success, but because the deforming operator is irrelevant, the understanding can only be perturbative in σ.

Our aim is instead to formulate a holographic dictionary based on identifying modes in the bulk with sources and vevs of operators of definite scaling dimension with respect to the anisotropic scaling symmetry, by applying the insights gained from the study of the Lifshitz case. Focusing on this non-relativistic perspective will allow us to treat the problem non-perturbatively. We formulate the dictionary in terms of frame fields. Such a formulation was attempted in [76] for $z = 2$, where an appropriate choice of frame fields and boundary conditions was identified, but difficulties were encountered in solving the equations of motion in an asymptotic expansion for general boundary conditions. One of our key insights is that it is easier to treat the case $z < 2$, where the derivatives with respect to the boundary coordinates all come with powers of r,

so dependence on these coordinates is negligible at leading order, and can be incorporated by adding appropriate subleading corrections to bulk fields.

The difference between $z < 2$ and $z = 2$ can be illustrated by considering a scalar field on a fixed Schrodinger background. The massive scalar wave equation $\Box\phi - m^2\phi = 0$ in the background (2.2) is

$$r^2\partial_r^2\phi - (d_s+1)r\partial_r\phi + r^2(2\partial_t\partial_\xi\phi + \partial_{\vec{x}}^2\phi) + r^{4-2z}\partial_\xi^2\phi - m^2\phi = 0. \tag{2.4}$$

For $z < 2$, all of the derivatives along the boundary are suppressed at small r, appearing as $r^z\partial_t$, $r^{2-z}\partial_\xi$ and $r\partial_{\vec{x}}$, and the asymptotic radial falloff of the bulk solution is independent of the dependence on $t, \xi, \vec{x}$. Thus we can solve the equation in a power series in r, allowing the leading term in the series to have an arbitrary dependence on $t, \xi, \vec{x}$, and adding subleading corrections depending on derivatives of the leading term. For $z = 2$ by contrast, the ∂_ξ derivatives are not suppressed, and dependence on ξ cannot be treated in this way.

Physically, this difference in the asymptotic expansion is due to a difference in the holographic dictionary. For $z < 2$, ϕ (with the usual boundary conditions) is holographically dual to a local operator O of dimension $\Delta = \frac{1}{2}(d_s+2) + \sqrt{\frac{1}{4}(d_s+2)^2 + m^2}$ (with respect to the anisotropic scaling symmetry) which lives in a space parametrised by $t, \xi, \vec{x}$.[5] For $z = 2$ by contrast, it is natural to decompose ϕ into Fourier modes, $\phi = \sum_{k_\xi} \phi_{k_\xi}(r,t,\vec{x})e^{ik_\xi\xi}$, and identify each mode ϕ_{k_ξ} with a dual operator O_{k_ξ} of dimension $\Delta = \frac{1}{2}(d_s+2) + \sqrt{\frac{1}{4}(d_s+2)^2 + m^2 + k_\xi^2}$, living in a space parametrised by $t, \vec{x}$. In this $z = 2$ case, the correlation functions of O_{k_ξ} are constrained by the scaling symmetry.[6]

This distinction between $z < 2$ Schrödinger and $z = 2$ Schrödinger is analogous to the distinction between Lifshitz and the $\mathrm{AdS}_2 \times \mathbb{R}^d$ geometry, which is the $z \to \infty$ limit of Lifshitz. For Lifshitz we think of the spatial directions as part of the space the field theory lives in, but for $\mathrm{AdS}_2 \times \mathbb{R}^d$ the $\mathbb{R}^d$ directions are internal directions which are not affected by the scaling symmetry, and we think of the dual as a quantum mechanics living just in the time direction, with operators $O_{\vec{k}}$ labelled by the momentum in the $\mathbb{R}^d$ directions.

[5] Also, for $z < 2$ the anisotropic scaling symmetry acts non-trivially on the ξ direction, so we have a scaling invariance only in this higher dimensional theory. If we restricted to the sector of a given momentum k_ξ, non-zero k_ξ will break the scaling symmetry of expressions in the $t, \vec{x}$ space. So for instance the form of correlation functions in $t, \vec{x}$ is not constrained by the symmetry.

[6] It is also interesting to note that once we restrict to a sector of fixed k_ξ, the scalar wave equation has a non-relativistic structure; the equation is first order in time derivatives.

Thus, if we take the anisotropic scaling symmetry and the corresponding frame decomposition as the central elements in formulating the holographic dictionary, it is easier to work out the correspondence for $z < 2$, where the dual theory naturally lives in all the $t, \xi, \vec{x}$ directions. The heart of our discussion will be a detailed treatment of $1 < z < 2$ in the context of a massive vector theory, showing that it is possible to formulate the holographic dictionary in a familiar fashion, solving the equations of motion for given boundary data depending on $t, \xi, \vec{x}$ in an asymptotic expansion in powers of r, and constructing a well-behaved action by adding local boundary counterterms to the bulk action. As in the discussion of Lifshitz, the leading terms in the frame fields in the bulk will be interpreted as sources for the stress energy complex in the field theory.

Although we do not consider $z < 1$ in this chapter, we expect that our definitions and frame analysis can be equally well applied in that case. For the other end of our range, $z = 2$, our procedure will need modification. For $z = 2$ we would want instead to formulate a dictionary in terms of a non-relativistic theory living in the $t, \vec{x}$ directions, where the different Fourier modes of the bulk fields are each thought of as corresponding to an operator in this field theory with k_ξ-dependent scaling dimension, as discussed above for a scalar field. The ξ direction is at least asymptotically null, so we cannot decompose the metric in a standard Kaluza-Klein reduction. However, in our holographic context it is more natural for us to think in terms of the frame fields, which are one-forms, which we can simply decompose into the component along $d\xi$ and the components along the remaining boundary directions. In this $z = 2$ case, the zero-modes in the leading terms in the frame fields in the bulk will be interpreted as sources for the stress energy complex in the non-relativistic field theory living in the $t, \vec{x}$ directions. In addition, for $z = 2$ there are potential logarithmic terms in the asymptotic expansion which need to be treated carefully. We therefore leave a detailed study of $z = 2$ until the next chapter.

We start in the next section by reviewing the Schrödinger solution in a little more detail, introducing the massive vector theory we will work in for the remainder of this chapter (although it should be easy to extend these ideas to alternative realizations of Schrödinger such as topologically massive gravity). We introduce our frame decomposition of the metric following [76] and discuss how the frame rotation symmetry can be partially fixed by relating the frame fields to the massive vector. We then define our asymptotically locally Schrödinger boundary conditions in terms of these frame fields. In section 2.3, we review the structure of the stress energy complex for non-relativistic theories, and discuss the description in the higher-dimensional theory including the ξ direction. In section 2.4 we give a linearised analysis around the Schrödinger solution for

$z < 2$, and identify the linearised modes with sources and vevs for the stress energy complex and matter operator. In section 2.5, we discuss the asymptotic expansion for $z < 2$, and show that a solution can be obtained in an expansion in powers of r,[7] and that all divergences in the action can be eliminated by adding boundary counterterms which are local functions of the boundary data.

2.2 Asymptotically locally Schrödinger boundary conditions

We consider the metric (2.2) as a solution of the theory with a massive vector introduced in [42]. The action is

$$S = -\frac{1}{16\pi G}\int d^{d_s+3}x\sqrt{-g}\left(R - 2\Lambda - \frac{1}{4}F_{\mu\nu}F^{\mu\nu} - \frac{1}{2}m^2 A_\mu A^\mu\right) - \frac{1}{8\pi G}\int d^{d_s+2}\xi\sqrt{-\gamma}K, \quad (2.5)$$

where γ is the induced metric on the boundary and K is the trace of the extrinsic curvature, with

$$m^2 = z(z+d_s), \quad \Lambda = -\frac{(d_s+2)(d_s+1)}{2}. \quad (2.6)$$

The equations of motion that follow are

$$R_{\mu\nu} - \frac{1}{2}Rg_{\mu\nu} + \Lambda g_{\mu\nu} = \frac{1}{2}\left(F^\alpha{}_\mu F_{\alpha\nu} - \frac{1}{4}F^2 g_{\mu\nu}\right) + \frac{m^2}{2}\left(A_\mu A_\nu - \frac{1}{2}A^2 g_{\mu\nu}\right) \quad (2.7)$$

$$\nabla_\mu F^{\mu\nu} = m^2 A^\nu \quad (2.8)$$

The metric (2.2) is a solution of (2.7), (2.8) supported by the matter field

$$A = \alpha r^{-z}dt, \quad \alpha = \sqrt{\frac{2(z-1)}{z}}. \quad (2.9)$$

The massive vector field A_μ physically singles out the t direction as special.

We want to define a class of asymptotically locally Schrödinger spacetimes which asymptotically approach (2.2) locally as $r \to 0$. Inspired by the analysis in the Lifshitz case, it is natural to do so by introducing an appropriate set of frame fields. We will adopt the frame decomposition

[7] In our analysis, this is traded for an expansion in eigenvalues of a suitable dilatation operator, but the existence of a dilatation expansion implies the existence of an expansion in powers of r, since each term in the dilatation expansion has an expansion in positive powers of r.

proposed in [76] ,

$$ds^2 = g_{AB}e^A e^B = -e^+e^+ + 2e^+e^- + e^I e^I + e^r e^r, \tag{2.10}$$

for some frame fields e^A, $A = +, -, I, r$. We will always adopt the radial gauge choice $e^r = r^{-1}dr$. In the background (2.2) $e^+ = r^{-z}dt$, $e^- = r^{z-2}d\xi$, $e^I = r^{-1}dx^i$, so each of the frame fields has a well-defined scaling with r at large r.[8] Note the main novelty compared to more familiar cases is that to achieve this simple form for the individual frame fields, we take the frame metric g_{AB} to have off-diagonal components.

The decomposition of the metric does not fix the choice of frame fields uniquely; it is invariant under transformations which preserve the metric g_{AB}, so we have the freedom to redefine the e^A infinitesimally by

$$e^+ \to e^+ + \alpha^I e^I, \quad e^- \to e^- + \beta^I e^I, \quad e^I \to e^I - \beta^I e^+ + \alpha^I(e^+ - e^-) \tag{2.11}$$

and

$$e^+ \to e^+ + \gamma e^+, \quad e^- \to e^- + \gamma(e^+ - e^-). \tag{2.12}$$

The decomposition is also invariant under rotations among the spatial frame fields e^I. We could leave this symmetry unfixed in the spirit of the treatment of the Lifshitz case in [71, 72], but we prefer to relate the distinguished frame fields to physical quantities, fixing this symmetry as much as possible. This will simplify the task of identifying the sources for the operators in the stress energy complex.

In our massive vector theory, the symmetries (2.11,2.12) will be restricted by assuming a form for the massive vector field. We can first restrict (2.11) by assuming A has no e^I component, so

$$A = A_+ e^+ + A_- e^- + A_r e^r. \tag{2.13}$$

The transformations which preserve this are those with $A_+\alpha^I + A_-\beta^I = 0$, together with the rotations of the spatial frame fields. The action of (2.12) is

$$A_+ \to A_+ + \gamma(A_+ + A_-), \quad A_- \to A_- - \gamma A_-. \tag{2.14}$$

Since the frame field e^+ is a null vector, it doesn't have a fixed length. The symmetry (2.12)

[8] Note that for this flat background, the frame index I and the coordinate index i are equivalent.

rescales it; we can therefore use this flexibility to fix the value of the projection of A along e^+. A convenient choice is to set $A_+ = \alpha$, its background value.

Thus we choose

$$A = \alpha(e^+ + \psi e^- + s_r e^r), \tag{2.15}$$

where α is the constant background value in (2.9), and ψ is the single scalar degee of freedom in the boundary conditions for the matter field, and we've taken an overall factor of α out for convenience. We will find that the operator dual to ψ is irrelevant, so we always set the source part to zero.

Given any solution of the massive vector theory, we can write the metric and vector field as in (2.10,2.15). The physical degrees of freedom are then the frame fields e^A and the scalar ψ. As in Lifshitz, a part of the degrees of freedom in the massive vector field has been assigned to the frame fields, to make physical some of the components that would have been pure gauge. Unlike in Lifshitz, this does not make all of the components of e^+, e^- physical. The remaining gauge symmetry is

$$e^+ \to e^+ - \psi\beta^I e^I, \quad e^- \to e^- + \beta^I e^I, \quad e^I \to e^I - \beta^I e^+ - \psi\beta^I(e^+ - e^-), \tag{2.16}$$

together with the rotations of the spatial frame fields e^I.

We then say that a spacetime is *asymptotically locally Schrödinger* if the metric and massive vector can be written as in (2.10,2.15) with

$$e^+ = r^{-z}\hat{e}^+, \quad e^- = r^{z-2}\hat{e}^-, \quad e^I = r^{-1}\hat{e}^I, \tag{2.17}$$

and the scalar $\psi = r^{\Delta_-}\hat{\psi}$ for some exponent Δ_-,[9] where the fields $\hat{e}^A, \hat{\psi}$ are arbitrary functions of $t, \xi, \vec{x}, r$ with finite limits as $r \to 0$. The boundary limits of the $\hat{e}^A$ (which with characteristic abuse of notation we will sometimes refer to simply as $\hat{e}^A$) define the boundary geometry for our asymptotically locally Schrödinger spacetime (while the scalar $\hat{\psi}$ is the source for a scalar operator in the dual field theory).

[9] This leading asymptotic falloff of the scalar will be determined later by the linearised analysis, where for $d_s = 2$ we find that $\Delta_- = 2 - 2z$, corresponding to a scalar operator of dimension $2z + 2$ in the dual field theory.

2.3 Stress energy complex and dimensional reduction

We want to view this data as describing the geometry our field theory lives in, so it should provide sources for the stress energy complex. Let us therefore review the structure of this in a non-relativistic theory. Any non-relativistic theory, Lifshitz or Schrödinger, will have an energy density $\mathcal{E}$ and an energy flux $\mathcal{E}^i$, satisfying the conservation equation (in a flat boundary space)

$$\partial_t \mathcal{E} + \partial_i \mathcal{E}^i = 0, \tag{2.18}$$

along with a momentum density $\mathcal{P}_i$ and a spatial stress tensor Π_{ij} satisfying the conservation equation

$$\partial_t \mathcal{P}_i + \partial_j \Pi_i^j = 0. \tag{2.19}$$

The Schrodinger theory additionally has a conserved particle number, so there is a particle number density ρ and a particle number flux ρ^i satisfying

$$\partial_t \rho + \partial_i \rho^i = 0. \tag{2.20}$$

The scale invariance implies $z\mathcal{E} + \Pi_i^i + (2-z)\rho = 0$; the additional term for $z \neq 2$ is associated with the breaking of the scaling symmetry by non-zero particle number. $\mathcal{E}$ has dimension $z + d_s$, which implies $\mathcal{E}^i$ has dimension $2z + d_s - 1$, and $\mathcal{P}_i$ has dimension $1 + d_s$, which implies Π_{ij} has dimension $z + d_s$. The particle number has dimension $2 - z$, so its density ρ has dimension $2 - z + d_s$, so ρ^i has dimension $1 + d_s$. In fact, in a non-relativistic theory $\rho^i = \mathcal{P}_i = \rho v^i$, where v^i is the local velocity of the particles, so these are not independent operators.

In the Lifshitz story the stress energy complex was realised directly in the holographic dual, but in Schrodinger the non-relativistic field theory is constructed as the reduction of a one higher dimensional field theory over a null circle labelled by the coordinate ξ. For $z < 2$, it is the higher-dimensional quantities that we expect to appear in our holographic dictionary. In [77], non-relativistic quantities were obtained by dimensional reduction from the stress tensor of a relativistic theory. In the present chapter, we work in a frame formalism adapted to the anisotropic scaling symmetry, so the description in the higher-dimensional theory is still not relativistic; in particular different components have different scaling dimensions even in the higher-dimensional description.

In the higher-dimensional theory for $z < 2$, we expect to have an energy current whose sources

are in the frame field $\hat{e}^+$, a ξ-momentum current which is physically identified with particle number whose sources are in $\hat{e}^-$, and spatial momentum currents whose sources are in $\hat{e}^I$. The energy current consists of an energy density E, an energy flux E^i in the spatial directions, and an energy flux E^ξ in the null direction. The conservation equation is

$$\partial_t E + \partial_i E^i + \partial_\xi E^\xi = 0. \tag{2.21}$$

The relation between these $d_s + 2$ dimensional operators and the above $d_s + 1$ dimensional theory is that the densities in the $d_s + 1$ dimensional theory are the integral of the higher-dimensional densities over the ξ circle, so $\mathcal{E} = \oint d\xi E$ etc. Thus E has dimension $d_s + 2$, so that integrating over $d\xi$ (which has dimension $z - 2$) gives $\mathcal{E}$ dimension $z + d_s$. This can also be understood directly in the higher-dimensional theory; the densities in this theory are per unit volume in $\vec{x}$ and ξ. The volume element $d\xi\, d^{d_s}x$ has dimension $z - 2 - d_s$, so E has dimension $d_s + 2$ so the total energy obtained by integrating over the volume element has dimension z. The spacetime volume element in $d_s + 2$ dimensions has length dimension $d_s + 2$ with respect to the anisotropic scaling, so this is the dimension of a marginal operator. The conservation equation implies E^i has dimension $z + d_s + 1$ and E^ξ has dimension $2z + d_s$, as ∂_ξ has dimension $2 - z$.

The spatial momentum currents similarly consist of the spatial momentum density P_i, a stress tensor T_{ij} in the spatial directions, and a stress T_i^ξ in the ξ direction, satisfying the conservation equation

$$\partial_t P_i + \partial_j T_i^j + \partial_\xi T_i^\xi = 0. \tag{2.22}$$

P_i has dimension $3 - z + d_s$, so that the total momentum has dimension 1, and the integral over ξ gives $\mathcal{P}_i = \oint d\xi P_i$ dimension $d_s + 1$ as expected in a non-relativistic theory. The conservation equation then implies that T_{ij} has dimension $d_s + 2$ and T_i^ξ has dimension $z + d_s + 1$.

Finally, the ξ-momentum current consists of the momentum density P_ξ in the ξ direction, which will be identified with particle number density. This density comes with a particle number flux P_ξ^i in the spatial directions and P_ξ^ξ in the ξ direction, satisfying

$$\partial_t P_\xi + \partial_j P_\xi^j + \partial_\xi P_\xi^\xi = 0. \tag{2.23}$$

P_ξ has dimension $4 - 2z + d_s$, implying P_ξ^i has dimension $3 - z + d_s$ and P_ξ^ξ has dimension $d_s + 2$.As noted earlier, $P_\xi^i = P_i$, and T_{ij} is a symmetric tensor. The Ward identity from the

scaling symmetry is $zE + T^i_i + (2-z)P^\xi_\xi = 0$.[10]

Apart from these Ward identities the components of the stress complex are independent; note in particular that T^ξ_i and P^i_ξ have different dimensions, so the stresses in the spatial and ξ directions cannot be combined into a symmetric tensor. Note that E^ξ, E^i and T^ξ_i are irrelevant operators.

For $z < 2$, our holographic dictionary will naturally be formulated in terms of this $d_s + 2$ dimensional field theory, and the frame fields $\hat{e}^A$ provide sources for the corresponding currents, which can be arbitrary functions of $t, \xi, \vec{x}$. We can view these currents as the components of the non-symmetric tensor

$$T^\alpha{}_B = \frac{1}{\sqrt{-\gamma}} \frac{\delta}{\delta e^B_\alpha} S. \tag{2.24}$$

The residual gauge symmetry (2.16) corresponds to the fact that there are not independent physical sources for P_i, P^i_ξ, while the symmetry under rotations of the $\hat{e}^I$ corresponds to T_{ij} being a symmetric tensor.

As in the Lifshitz case, there are irrelevant operators in the stress energy complex, and we would expect to need to set their sources to zero. For generic sources, there is no diffeomorphism-invariant part in the source for T^ξ_i, as we can always make a ξ-dependent redefinition of the x^i coordinates to set the $d\xi$ components in e^I to zero.[11] Therefore the only diffeomorphism-invariant sources for irrelevant operators are in e^+, and we can set these to zero by adopting the irrotational condition

$$\hat{e}^+ \wedge d\hat{e}^+ = 0. \tag{2.25}$$

As in Lifshitz, this can be viewed as a condition that the boundary geometry defined by the $\hat{e}^A$ admits a foliation by surfaces of absolute time, as is appropriate for a non-relativistic theory. As in Lifsihtz we will find that there is a range of values of z for which solutions exist in an asymptotic expansion even if we do not impose this condition. Since the energy flux E^i is irrelevant for all $z > 1$, one might expect that we would always need to set its source to zero. But the diffeomorphism symmetry implies that only derivatives of this source actually appear, so there is a range of values for which the asymptotic expansion exists even in the presence of this source, as in Lifshitz. Here the relevant range is $z < 3/2$.

[10] The Ward identities (2.18,2.19,2.20) and $z\mathcal{E} + \Pi^i_i + (2-z)\rho = 0$ are obtained by taking the above identities and integrating over the ξ circle.

[11] The zero-mode of the source of T^ξ_i along the ξ direction is diffeomorphism-invariant, so in the discussion of $z = 2$ we will have to explicitly set this to zero.

For $z = 2$, the story is different. We argued in the introduction that because the anisotropic scaling symmetry doesn't act on ξ and the asymptotic falloffs of bulk modes of different k_ξ are different, the appropriate holographic dictionary is now in terms of a theory that lives in $d_s + 1$ dimensions, with modes of different k_ξ identified with distinct operators in this theory, whose scaling dimensions may be k_ξ dependent. Thus, to identify the boundary data $\hat{e}^A, \psi$ as sources for the dual operators, we should expand them in Fourier modes in ξ. For the frame fields, we should also decompose them as

$$\hat{e}^A = \hat{e}^A_a dx^a + \hat{e}^A_\xi d\xi, \tag{2.26}$$

where a runs over t, x^i. For the zero modes, where $\hat{e}^A$ is independent of ξ, this decomposition is the analogue in our frame language of the Kaluza-Klein decomposition of the metric and massive vector field. With respect to the ξ-independent diffeomorphisms acting in the lower-dimensional boundary coordinates, e^A_a will transform as a one-form and e^A_ξ will transform as a scalar.

As noted above, the operators in the stress complex in the $d_s + 1$ dimensional non-relativistic theory are obtained by integrating the higher-dimensional densities over the ξ circle, $\mathcal{E} = \oint d\xi E$ etc. That is, they are the zero modes of the higher-dimensional fields along this circle direction. The sources for these operators are thus the ξ-independent part of the sources $\hat{e}^A_a$. The conservation equations (2.18 - 2.20) are obtained by integrating (2.21 - 2.23) over the ξ circle; the last terms in the latter equations will drop out on doing the integral as they are a total derivative. Thus, for $z = 2$, we could obtain correlation functions of the non-relativistic stress energy complex just by considering appropriate ξ-independent sources $\hat{e}^A_a$. We can also consider ξ-independent sources $\hat{e}^A_\xi$, which are interpreted for $z = 2$ as providing sources for some particular scalar operators.[12]

2.4 Linearised analysis for $z < 2$

We now turn to a linearised analysis of the equations of motion (2.7,2.8) for $z < 2$. We will see that this analysis confirms that the limits as $r \to 0$ of the rescaled frame fields $\hat{e}^A_\alpha$ can be interpreted as the sources corresponding to the stress energy complex $T^\alpha{}_B$, in that the modes canonically conjugate to the sources in the symplectic flux satisfy the expected Ward identities as a consequence of the linearised equations in the bulk. We will identify ψ as the bulk dual of an operator of dimension $2z + 2$ when $d_s = 2$. We will see that the equations can be solved in a power series in r in the asymptotic region, where the subleading terms are determined locally in

[12] The situation is similar to the Lifshitz theories obtained by dimensional reduction in [70].

terms of the sources.

We will consider the case $d_s = 2$, which is physically the most interesting (the results for other values of d_s will be similar in structure) and $d_s = 0$, which is a special case and was previously analysed in [36], so discussing this case will be useful for comparison purposes.

The linearised version of our frame fields is

$$\hat{e}^+ = (1 + \delta\hat{e}^+_t)dt + \delta\hat{e}^+_\xi d\xi + \delta\hat{e}^+_i dx^i, \tag{2.27}$$

$$\hat{e}^- = (1 + \delta\hat{e}^-_\xi)d\xi + \delta\hat{e}^-_t dt + \delta\hat{e}^-_i dx^i, \tag{2.28}$$

$$\hat{e}^I = (\delta^I_j + \delta\hat{e}^I_j)dx^j + \delta\hat{e}^I_t dt + \delta\hat{e}^I_\xi d\xi. \tag{2.29}$$

The linearised fields are then $\delta\hat{e}^A_\alpha$ and the ψ, s_r in (2.15). The constant modes in $\delta\hat{e}^A_\alpha$ are assumed to represent sources for the corresponding components of $T^\alpha_{\ A}$.

The linearised version of the residual gauge symmetry (2.16) is $\delta\hat{e}^-_i \to \delta\hat{e}^-_i + \hat{\beta}^i$, $\delta\hat{e}^I_t \to \delta\hat{e}^I_t - \hat{\beta}^i$ (where $\beta^I = r^{z-1}\hat{\beta}^i$). This implies that the sources for $T^+{}_I = P_i$ and $T^I{}_\xi = P^i_\xi$ are not independent, as expected. The rotation symmetry of the e^I also implies that only the symmetric part of δe^I_j provide independent sources. The equations of motion are easier to discuss in the metric language, so we will resolve this gauge symmetry by passing back from the frame fields to the metric and vector for this linearised analysis.

In the metric language, the linearised perturbations are $h_{\mu\nu}$, a_μ. The linearised equations in the metric language are as in [41][13]

$$\nabla_\mu f^{\mu\nu} - \nabla_\mu(h^{\mu\lambda}F_\lambda{}^\nu) - \nabla_\mu h^{\beta\nu}F^\mu_{\ \beta} + \frac{1}{2}\nabla_\lambda h F^{\lambda\nu} = m^2 a^\nu \tag{2.30}$$

and

$$\begin{aligned} R^{(1)}_{\mu\nu} = {} & \frac{2}{d-2}\Lambda h_{\mu\nu} + \frac{1}{2}f_{\mu\lambda}F_\nu{}^\lambda + \frac{1}{2}f_{\nu\lambda}F_\mu{}^\lambda - \frac{1}{2}F_{\mu\lambda}F_{\nu\sigma}h^{\lambda\sigma} - \frac{1}{2(d-2)}f_{\lambda\rho}F^{\lambda\rho}g_{\mu\nu} \\ & + \frac{1}{2(d-2)}F_{\lambda\rho}F_\sigma{}^\rho h^{\lambda\sigma}g_{\mu\nu} - \frac{1}{4(d-2)}F_{\lambda\rho}F^{\lambda\rho}h_{\mu\nu} + \frac{1}{2}m^2 a_\mu A_\nu + \frac{1}{2}m^2 a_\nu A_\mu, \end{aligned} \tag{2.31}$$

[13]Note that $h_{\mu\nu}$ denotes the perturbation of the metric, and indices are raised and lowered with the background metric, so $h^{\mu\nu}$ is the perturbation of the metric with the indices raised, not the perturbation of the inverse metric.

where $d = d_s + 3$ is the dimension of the spacetime, $f_{\mu\nu} = \partial_\mu a_\nu - \partial_\nu a_\mu$ and

$$R^{(1)}_{\mu\nu} = \frac{1}{2} g^{\lambda\sigma} [\nabla_\lambda \nabla_\mu h_{\nu\sigma} + \nabla_\lambda \nabla_\nu h_{\mu\sigma} - \nabla_\mu \nabla_\nu h_{\lambda\sigma} - \nabla_\lambda \nabla_\sigma h_{\mu\nu}]. \tag{2.32}$$

It is convenient to write

$$h_{tt} = r^{-2z} H_{tt}, \qquad h_{t\xi} = r^{-2} H_{t\xi}, \qquad h_{\xi\xi} = r^{2(z-2)} H_{\xi\xi}, \tag{2.33}$$

$$h_{ti} = r^{-(z+1)} H_{ti} \qquad h_{\xi i} = r^{z-3} H_{\xi i}, \qquad h_{ij} = r^{-2} H_{ij}, \tag{2.34}$$

$$a_r = \alpha r^{-1} s_r \qquad a_t = \alpha r^{-z} s_t \qquad a_\xi = \alpha r^{z-2} s_\xi \qquad a_i = \alpha r^{-1} s_i. \tag{2.35}$$

Then, a given linearised mode will contribute at the same order in r in all the different fields, and the power of r will correspond to the scaling dimension of the mode. The s_r here is the same as in (2.15), and the other fields are related to the linearised frame fields by

$$H_{tt} = -2\delta\hat{e}^+_t + 2r^{2z-2}\delta\hat{e}^-_t, \quad H_{t\xi} = -r^{2-2z}\delta\hat{e}^+_\xi + \delta\hat{e}^-_\xi + \delta\hat{e}^+_t, \quad H_{\xi\xi} = 2r^{2-2z}\delta\hat{e}^+_\xi, \tag{2.36}$$

$$H_{ti} = -r^{1-z}\delta\hat{e}^+_i + r^{z-1}\delta\hat{e}^-_i + r^{z-1}\delta\hat{e}^I_t, \quad H_{\xi i} = r^{1-z}\delta\hat{e}^+_i + r^{1-z}\delta\hat{e}^I_\xi, \quad H_{ij} = \delta\hat{e}^I_j + \delta\hat{e}^J_i, \tag{2.37}$$

$$s_t = \delta\hat{e}^+_t, \quad s_\xi = r^{2-2z}\delta\hat{e}^+_\xi + \psi, \quad s_i = r^{1-z}\delta\hat{e}^+_i. \tag{2.38}$$

Note that in the expansion about a flat background the I and i indices are equivalent at leading order, so in these equations, $\delta\hat{e}^I_\alpha$ should be understood as $\delta\hat{e}^I_\alpha \delta_{Ii}$.

2.4.1 Linearised solutions for $d_s = 2$

Let us now study the equations for $d_s = 2$. Our interest is in understanding the identification of the solutions of the linearised equations with sources and vevs for the dual operators. We identify the sources with the leading constant parts of the linearised frame fields $\delta\hat{e}^A$, which appear in the linearised fields in the frame language as set out in (2.36 - 2.38). Since we have not yet carried out a holographic renormalization procedure, the vevs will also have divergent contributions from the source modes, but we are interested in identifying the relation between the bulk solutions which are not locally determined by the sources and the finite part of the vevs. In many cases, we can identify the mode corresponding to the vev by its conformal dimension alone, but in general we follow [78] and identify the vev as the linearised solution which is canonically conjugate to the

source with respect to the symplectic inner product defined by calculating the symplectic flux.

Since dependence on the boundary directions introduces only subleading terms for $z < 2$, we can first understand this identification by considering constant modes, which are independent of the boundary directions. We then discuss briefly the linearised equations for non-constant modes and check that the solutions we are identifying with the vevs do indeed satisfy appropriate Ward identities as a result of the asymptotic equations of motion in the non-constant cases.

When the fields are independent of spatial coordinates x^i, the rotation symmetry in these directions will be unbroken, so we can decompose the linearised fields into a tensor, vector and scalar part with respect to this linearised symmetry. Below we will treat these tensor, vector and scalar modes first, initially for constant modes and then including dependence on t, ξ. To make this decomposition we should further decompose H_{ij} into a trace and a trace free part, $H_{ij} = k\delta_{ij} + \bar{H}_{ij}$, where $\bar{H}^i_i = 0$. The tensor mode is $\bar{H}_{ij}$. The vector modes are H_{ti}, $H_{\xi i}$ and s_i. The scalar modes are H_{tt}, $H_{t\xi}$, $H_{\xi\xi}$, k, s_t, s_ξ and s_r (which is determined algebraically in terms of the other modes). We will always assume the t, ξ dependence is harmonic, $e^{i\omega t + ik_\xi \xi}$, so in writing equations we will make the replacements $\partial_t \to i\omega$, $\partial_\xi \to ik_\xi$.

When we include dependence on the x^i, there is a different decomposition, which splits the modes into scalars (which now include scalar-derived vectors and tensors) and vectors (including vector-derived tensors). We set up the equations for this general case in section 2.4.1.4, and comment on the Ward identities.

2.4.1.1 Tensor modes

The tensor equation of motion is

$$r^2 \bar{H}''_{ij} - 3r\bar{H}'_{ij} - (k_\xi^2 r^{2(2-z)} + 2k_\xi \omega r^2)\bar{H}_{ij} = 0. \tag{2.39}$$

The solution for $\omega = k_\xi = 0$ is

$$\bar{H}_{ij} = \bar{H}^{(0)}_{ij} + \bar{H}^{(4)}_{ij} r^4, \tag{2.40}$$

corresponding to the source and vev for the trace free part of the spatial stress tensor T_{ij}. For general (k_ξ, ω), we will have an infinite series of subleading corrections which involve boundary derivatives of these leading terms. As the equation of motion only involves the combinations $k_\xi \omega$

and k_ξ^2, the solution can be written as

$$\bar{H}_{ij} = \sum_{m,n\geq 0} a_{ij(m,n)} (k_\xi \omega r^2)^{2m} (k_\xi r^{2-z})^{2n} + k_\xi^2 \omega^2 r^4 \log r^2 \sum_{m,n\geq 0} b_{ij(m,n)} (k_\xi \omega r^2)^{2m} (k_\xi r^{2-z})^{2n}. \quad (2.41)$$

We can take $a_{ij(0,0)} = \bar{H}_{ij}^{(0)}$ and $a_{ij(2,0)} = \bar{H}_{ij}^{(4)}$ as the independent coefficients. The expansion includes log terms because a subleading term determined by $\bar{H}_{ij}^{(0)}$ and the independent term $\bar{H}_{ij}^{(4)}$ occur at the same power of r. The subleading terms in the expansion are all determined in terms of $\bar{H}_{ij}^{(0)}$ and $\bar{H}_{ij}^{(4)}$ by solving (2.39) in a power series in k_ξ, ω. The explicit factors of k_ξ, ω in (2.41) imply that there will be no factors of k_ξ, ω in the equations for the $a_{ij(m,n)}$, $b_{ij(m,n)}$, so the subleading terms are determined locally in the boundary directions. They are solutions of ODEs in the radial direction.

2.4.1.2 Vector modes

The vector equations of motion are

$$r^2 s_i'' - 3r s_i' - [(z-1)(z+3) + k_\xi^2 r^{4-2z} + 2k_\xi \omega r^2] s_i + z r H_{\xi i}' + z(z-1) H_{\xi i} = 0, \quad (2.42)$$

$$k_\xi [r(H_{\xi i}' + H_{ti}') + (z-1)(H_{\xi i} - H_{ti} - 2s_i)] + \omega r^{2z-2} [r H_{\xi i}' + (z-1) H_{\xi i}] = 0, \quad (2.43)$$

$$r^2 H_{\xi i}'' + (2z-5) r H_{\xi i}' + [(z-1)(z-5) - r^2 k_\xi \omega] H_{\xi i} + k_\xi^2 r^{4-2z} H_{ti} = 0, \quad (2.44)$$

and

$$\begin{aligned} &r^2 H_{ti}'' - r(2z+1) H_{ti}' + [(z-1)(z+3) - k_\xi^2 r^{4-2z} - r^2 k_\xi \omega] H_{ti} \\ &\quad + 2(z-1)[(z+3)s_i - (z-1) H_{\xi i} - r(s_i + H_{\xi i})'] + (r^2 k_\xi \omega + r^{2z} \omega^2) H_{\xi i} = 0. \end{aligned} \quad (2.45)$$

For $k_\xi = \omega = 0$, (2.43) is trivially satisfied, and we solve (2.42,2.44,3.37). For general k_ξ, ω, we solve (2.42,2.43,2.44), which imply (2.45).

For $k_\xi = \omega = 0$, the solution for the vector modes can be written as

$$H_{\xi i} = (s_i^{(-)} + H_{\xi i}^{(-)}) r^{1-z} + H_{\xi i}^{(+)} r^{5-z}, \quad (2.46)$$

$$H_{ti} = -s_i^{(-)} r^{1-z} + H_{ti}^{(-)} r^{z-1} + H_{ti}^{(+)} r^{z+3} + \frac{(z-4)}{2(3-z)} H_{\xi i}^{(+)} r^{5-z}, \quad (2.47)$$

$$s_i = s_i^{(-)} r^{1-z} + \frac{z}{2(z-1)} H_{\xi i}^{(+)} r^{5-z} + s_i^{(+)} r^{z+3}. \quad (2.48)$$

We have chosen to define and normalise the independent modes so that the solutions with a $(-)$ superscript correspond to the sources, coming from the constant modes in the frame fields. From (2.38), we see that $s_i^{(-)}$ corresponds to the constant part in $\delta\hat{e}_i^+$, the source term for the energy flux E^i. From (2.37), $H_{\xi i}^{(-)}$ is then the constant part of $\delta\hat{e}_\xi^I$, the source term for the stress T_i^ξ, and $H_{ti}^{(-)}$ is the source term for the momentum density P_i. The modes with a $(+)$ superscript should then correspond to the vevs of these operators. By dimensions alone we see that $\langle P_i\rangle \sim H_{\xi i}^{(+)}$. The vevs $\langle E^i\rangle$ and $\langle T_i^\xi\rangle$ should be related to $H_{ti}^{(+)}$ and $s_i^{(+)}$.

We can work out the identification by computing the symplectic flux at the boundary $r = 0$, and identifying the modes canonically conjugate to the sources with the vevs, following [78]. Generically, the symplectic flux will have divergent contributions involving just the source modes, corresponding to the divergences in the vevs which need to be removed by holographic renormalization, but we focus on constant perturbations for which the result is finite, enabling us to relate the $(+)$ modes to the finite part of the vevs. The appropriate symplectic current for the Einstein-massive vector theory we are considering was worked out in [79]. It involves combining the usual gravitational symplectic current j_g^μ with an additional component j_a^μ,

$$j^\mu = j_g^\mu + j_a^\mu. \tag{2.49}$$

These are respectively given by

$$j_g^\mu = P^{\mu\nu\alpha\beta\gamma\delta}(h^*_{2\alpha\beta}\nabla_\nu h_{1\gamma\delta} - h_{1\alpha\beta}\nabla_\nu h^*_{2\gamma\delta}), \tag{2.50}$$

$$j_a^\mu = a^*_{2\nu}(f_1^{\mu\nu} - h_1^{\mu\lambda}F_\lambda{}^\nu - h_1^{\beta\nu}F^\mu_{\ \beta} + \frac{1}{2}h_1 F^{\mu\nu}) - (1 \leftrightarrow 2), \tag{2.51}$$

where

$$P^{\mu\nu\alpha\beta\gamma\delta} = \frac{1}{2}(g^{\mu\nu}g^{\gamma(\alpha}g^{\beta)\delta} + g^{\mu(\gamma}g^{\delta)\nu}g^{\alpha\beta} + g^{\mu(\alpha}g^{\beta)\nu}g^{\gamma\delta} - g^{\mu\nu}g^{\alpha\beta}g^{\gamma\delta} - g^{\mu(\gamma}g^{\delta)(\alpha}g^{\beta)\nu} - g^{\mu(\alpha}g^{\beta)(\gamma}g^{\delta)\nu}), \tag{2.52}$$

indices in parentheses are symmetrized, and $*$ indicates complex conjugation.

Given the current found from two linearised solutions, the symplectic flux through the boundary, $\mathcal{F}$, is defined as the pullback of the current to the surface $r = 0$. As usual, this is defined by evaluating the pullback at some cutoff surface $r = r_\epsilon$ and taking the limit $r_\epsilon \to 0$, so

we write

$$\mathcal{F} = \lim_{r_\epsilon \to 0} \frac{i}{2} \int_{r=r_\epsilon} d^{d_s} x d\xi \sqrt{\gamma} n^\mu j_\mu, \tag{2.53}$$

where n_μ the unit outward-pointing normal to the boundary. The overall factor of $i/2$ is purely conventional.

As mentioned above, for constant perturbations the flux turns out to be finite. In the vector sector we find

$$\begin{aligned}\mathcal{F} = -i \int_{r=0} d^{d_s} x d\xi \Big[& H^{(-)}_{\xi i} \wedge (2H^{(+)}_{ti} - (z-1)s^{(+)}_i) + 2H^{(-)}_{ti} \wedge H^{(+)}_{\xi i} \\ & + s^{(-)}_i \wedge (2H^{(+)}_{ti} + \frac{(z-1)(z+2)}{z} s^{(+)}_i) \Big],\end{aligned} \tag{2.54}$$

where $A \wedge B = A_1 B_2 - A_2 B_1$, where $1, 2$ label the two linearised solutions which define the current. This enables us to identify, up to an overall normalization which we neglect for simplicity,

$$\langle P_i \rangle = 2H^{(+)}_{\xi i}, \quad \langle T^\xi_i \rangle = 2H^{(+)}_{ti} - (z-1)s^{(+)}_i, \quad \langle E^i \rangle = 2H^{(+)}_{ti} + \frac{(z-1)(z+2)}{z} s^{(+)}_i. \tag{2.55}$$

For non-zero k_ξ, ω, the solutions of the linearised equations of motion can be given in a power series expansion; since the equations involve only $k_\xi \omega$ and k_ξ^2, this will be of the same form as in (2.41). The interesting new feature here is that because of the different structure of the equations (we now need to solve (2.43)), there is a reduction in the number of independent mode solutions. Solving (2.43) at leading order implies a relation among the coefficients,

$$k_\xi [2H^{(+)}_{ti} - (z-1)s^{(+)}_i] + 2\omega H^{(+)}_{\xi i} = 0, \tag{2.56}$$

which corresponds to the Ward identity

$$\partial_t P_i + \partial_\xi T^\xi_i = 0, \tag{2.57}$$

confirming our identification of the linearised solutions with the vevs.

2.4.1.3 Scalar modes

We consider now the scalar modes H_{tt}, $H_{t\xi}$, $H_{\xi\xi}$, k, s_r, s_t, s_ξ. They are governed by the equations

$$
\begin{aligned}
0 =& \left(\frac{k_\xi z}{2} + \omega z r^{2z-2}\right) H_{\xi\xi} - k_\xi z k + (z-2)\left(k_\xi + \omega r^{2z-2}\right) s_\xi + k_\xi r s_t' - k_\xi z s_t \\
&+ (k_\xi + \omega r^{2z-2}) r s_\xi' - i\left(k_\xi^2 r^{2-z} + 2k_\xi \omega r^z + z(z+2) r^{z-2}\right) s_r, && (2.58)\\
0 =& -\frac{1}{2} r(z+2) H_{\xi\xi}' + \left(\frac{1}{2}\omega^2 r^{2z} - z^2 + z\right) H_{\xi\xi} - 3 r H_{t\xi}' - r^2 k_\xi \omega H_{t\xi} + \frac{1}{2} k_\xi^2 H_{tt} r^{4-2z} \\
&- 3 r k' - \left(k_\xi^2 r^{4-2z} + 2k_\xi \omega r^2\right) k + (z-1)[r s_\xi' + 2z s_\xi - i k_\xi r^{2-z} s_r], && (2.59)\\
0 =& \frac{\omega}{2} r H_{\xi\xi}' + \left(\frac{1}{2} k_\xi (z-1) r^{2-2z} + \frac{3}{2}\omega(z-1)\right) H_{\xi\xi} + \left(\frac{\omega}{2} - \frac{1}{2} k_\xi r^{2-2z}\right) r H_{t\xi}' \\
&- \frac{1}{2} k_\xi r^{2-2z} r H_{tt}' + \omega r k' + (z-1) r^{2-2z} k_\xi [H_{tt} - k + s_t] \\
&- \omega(z-1) s_\xi - i\left(z^2 + z - 2\right) r^{-z} s_r, && (2.60)\\
0 =& -\frac{1}{2}\omega r^{2z-2} r H_{\xi\xi}' - (z-1)\left(\omega r^{2z-2} + \frac{k_\xi}{2}\right) H_{\xi\xi} + \frac{1}{2} k_\xi r H_{t\xi}' + k_\xi r k', && (2.61)\\
0 =& \frac{1}{2} r^2 H_{\xi\xi}'' + r^2 H_{t\xi}'' + \frac{1}{2} r^2 H_{tt}'' + r^2 k'' + r\left(z - \frac{5}{2}\right) H_{\xi\xi}' + 2\left(z^2 - 3z + 2\right) H_{\xi\xi} \\
&- (z+2) r H_{t\xi}' + \frac{1}{2}(1-4z) r H_{tt}' + 2\left(z^2 - 1\right) H_{tt} + (z-4) r k' \\
&- \left(k_\xi^2 r^{4-2z} + 2k_\xi \omega r^2 + \omega^2 r^{2z}\right) k - 2(z-1) r s_t' + 4\left(z^2 - 1\right) s_t \\
&+ (1-z) r s_\xi' + 4(z-1) s_\xi + i(z-1)\left(k_\xi r^{2-z} + 2\omega r^z\right) s_r, && (2.62)\\
0 =& r^2 H_{\xi\xi}'' + (4z-7) r H_{\xi\xi}' + 4\left(z^2 - 4z + 3\right) H_{\xi\xi} - 2k_\xi^2 r^{4-2z} k, && (2.63)\\
0 =& r^2 H_{\xi\xi}'' + 2r^2 H_{t\xi}'' + r^2 k'' + \left(\omega^2 r^{2z} - 4z + 4\right) H_{\xi\xi} - 6 r H_{t\xi}' + k_\xi^2 r^{4-2z} H_{tt} \\
&+ (z-4) r H_{\xi\xi}' - 3 r k' - \left(k_\xi^2 r^{4-2z} + 2k_\xi \omega r^2\right) k \\
&- 2k_\xi \omega r^2 H_{t\xi} + 2(z-1)[i k_\xi r^{2-z} s_r - r s_\xi' + 4 s_\xi]. && (2.64)
\end{aligned}
$$

In addition, we have equations

$$\begin{aligned}0 =& r^2 s_\xi'' + 2(z-1)z H_{\xi\xi} + k_\xi^2 r^{4-2z} s_t + (2z-5) r s_\xi' + z r H_{\xi\xi}' \\ & - \left(k_\xi \omega r^2 + 8z - 8\right) s_\xi + i k_\xi r^{2-z}(2 s_r - r s_r'), \end{aligned} \tag{2.65}$$

$$\begin{aligned}0 =& r^2 s_\xi'' + r^2 s_t'' - k_\xi \omega r^2 s_t + \left(\omega^2 r^{2z} - 2z^2 - 2z + 4\right) s_\xi - 3 r s_\xi' - (2z+1) r s_t' \\ & + \frac{1}{2} z r H_{\xi\xi}' - z r k' + 2i \left(k_\xi z r^{2-z} + \omega r^z\right) s_r - i \left(k_\xi r^{2-z} + \omega r^z\right) r s_r', \end{aligned} \tag{2.66}$$

$$\begin{aligned}0 =& \frac{1}{2} r^2 H_{\xi\xi}'' + \frac{1}{2} r^2 H_{t\xi}'' + r^2 k'' + \frac{3}{2}(z-2) r H_{\xi\xi}' + 2\left(z^2 - 3z + 2\right) H_{\xi\xi} + \\ & - \frac{3}{2} r H_{t\xi}' - 3 r k' - \left(k_\xi^2 r^{4-2z} + k_\xi \omega r^2\right) k. \end{aligned} \tag{2.67}$$

For constant modes, (2.58,2.60,2.61) are automatically satisfied if $s_r = 0$, and (2.65,2.66,2.67) are non-trivial equations. For general k_ξ, ω, we solve (2.58-2.64), which imply (2.65,2.66,2.67).

The solution for constant modes is

$$s_r = 0, \tag{2.68}$$

$$\begin{aligned} H_{tt} =& \frac{(3z-2) s_\xi^{(-)}}{6z} r^{2-2z} - 2 s_t^{(0)} + 2 r^{2z-2} H_{tt}^{(-)} + r^{2z+2} H_{tt}^{(+)} \\ & + \frac{(6-5z) H_{\xi\xi}^{(+)}}{4(z-3)(z-2)} r^{6-2z} + \frac{(6 k^{(4)}(z-4) + 5 s_\xi^{(4)}(z-1)(z+2))}{6(z-3)} r^4, \end{aligned} \tag{2.69}$$

$$H_{t\xi} = -\left(H_{\xi\xi}^{(-)} + \frac{2}{3} s_\xi^{(-)}\right) r^{2-2z} + s_t^{(0)} + H_{t\xi}^{(0)} - \frac{1}{2} H_{\xi\xi}^{(+)} r^{6-2z} + \left(\frac{(z-1)(z+2)}{6} s_\xi^{(4)} - k^{(4)}\right) r^4, \tag{2.70}$$

$$H_{\xi\xi} = 2 H_{\xi\xi}^{(-)} r^{2-2z} + H_{\xi\xi}^{(+)} r^{6-2z}, \tag{2.71}$$

$$k = \frac{1}{3} s_\xi^{(-)} r^{2-2z} + 2 k^{(0)} + \frac{1}{2(3-z)} H_{\xi\xi}^{(+)} r^{6-2z} + k^{(4)} r^4, \tag{2.72}$$

$$s_\xi = (H_{\xi\xi}^{(-)} + s_\xi^{(-)}) r^{2-2z} + s_\xi^{(4)} r^4 + \frac{z}{2(z-1)} H_{\xi\xi}^{(+)} r^{6-2z}, \tag{2.73}$$

$$s_t = -\frac{1}{3} s_\xi^{(-)} r^{2-2z} + s_t^{(0)} + s_t^{(+)} r^{2z+2} + \frac{3z H_{\xi\xi}^{(+)} r^{6-2z}}{4(z-1)(z-3)} - \left(\frac{z k^{(4)}}{2(z-1)} + \frac{(z+2) s_\xi^{(4)}}{4}\right) r^4. \tag{2.74}$$

We have once again chosen the definition and normalization of the modes so that the (0) and $(-)$ modes correspond to constant leading terms in the frame fields. The r-independent modes with a (0) superscript correspond to sources for the diagonal components of the stress energy complex: $s_t^{(0)}$ is the constant part of $\delta\hat{e}_t^+$, so it is the source for the energy density E, $H_{t\xi}^{(0)}$ is the constant part of $\delta\hat{e}_\xi^-$, so it is the source for P_ξ^ξ, and $k^{(0)}$ is the constant part of $\delta\hat{e}_i^I$, so it is the

source for the trace of the spatial stress tensor T_i^i. There is a single mode $H_{tt}^{(-)}$ of dimension $2z-2$, which comes from the constant part of $\delta\hat{e}_t^-$, so it is the source for the particle number density P_ξ. There are two modes of dimension $2-2z$, corresponding to sources for operators of dimension $2z+2$. The first is $H_{\xi\xi}^{(-)}$, which comes from the constant part of $\delta\hat{e}_\xi^+$, and hence corresponds to the source for the energy flux E^ξ. The second must be the source part of ψ, so we learn that this is dual to an operator O of dimension $2z+2$. The source for this should not change $\delta\hat{e}_\xi^+$, so we can identify this source as $s_\xi^{(-)}$. Note that as in the Lifshitz case, the source mode for this matter operator also appears in other fields, unlike the source modes for the stress tensor, whose appearance is constrained by the boundary diffeomorphism invariance.

We would again like to identify the remaining modes with the vevs of these operators. Dimensions alone suffices to fix $\langle P_\xi\rangle \sim H_{\xi\xi}^{(+)}$, to relate $\langle E\rangle$, $\langle T_i^i\rangle$ and $\langle P_\xi^\xi\rangle$ to $k^{(4)}$ and $s_\xi^{(4)}$, and to relate $\langle E^\xi\rangle$ and $\langle O\rangle$ to $H_{tt}^{(+)}$ and $s_t^{(+)}$. To determine the relation we use the symplectic flux, which is calculated as in the vector sector. The symplectic flux is again finite and is given by

$$\begin{aligned}\mathcal{F} = i\int_{r=0} d^{d_s}x d\xi \Bigg[& s_t^{(0)} \wedge \left(2k^{(4)} + \frac{1}{3z}(z-1)(z^2-4z-6)s_\xi^{(4)}\right) \\ & + H_{t\xi}^{(0)} \wedge \left(2k^{(4)} + \frac{1}{3}(z-1)(z+2)s_\xi^{(4)}\right) \\ & + k^{(0)} \wedge \left(-4k^{(4)} + \frac{2}{3}(z-1)(2z+1)s_\xi^{(4)}\right) - 2H_{tt}^{(-)} \wedge H_{\xi\xi}^{(+)} \\ & - H_{\xi\xi}^{(-)} \wedge \left(2H_{tt}^{(+)} + \frac{2(z-1)}{z}s_t^{(+)}\right) - \frac{2(z^2-1)}{z}s_\xi^{(-)} \wedge s_t^{(+)}\Bigg]. \end{aligned} \tag{2.75}$$

This implies the identifications

$$\langle P_\xi\rangle = 2H_{\xi\xi}^{(+)}, \quad \langle P_\xi^\xi\rangle = -2k^{(4)} - \frac{1}{3}(z-1)(z+2)s_\xi^{(4)}, \tag{2.76}$$

$$\langle E\rangle = -2k^{(4)} - \frac{1}{3z}(z-1)(z^2-4z-6)s_\xi^{(4)}, \tag{2.77}$$

and

$$\langle T_i^i\rangle = \langle T_1^1\rangle + \langle T_2^2\rangle = 4k^{(4)} - \frac{2}{3}(z-1)(2z+1)s_\xi^{(4)}. \tag{2.78}$$

The Ward identity from the scaling invariance is $zE + T_i^i + (2-z)P_\xi^\xi = 0$, which is indeed satisfied by these vevs. The other vevs are

$$\langle E^\xi\rangle = 2H_{tt}^{(+)} + \frac{2(z-1)}{z}s_t^{(+)} \tag{2.79}$$

Operator	Source	Expectation value
E	$s_t^{(0)}$	$-2k^{(4)} - \frac{1}{3z}(z-1)(z^2-4z-6)s_\xi^{(4)}$
E^i	$s_i^{(-)}$	$2H_{ti}^{(+)} + \frac{(z+1)(z+2)}{z}s_i^{(+)}$
E^ξ	$H_{\xi\xi}^{(-)}$	$2H_{tt}^{(+)} + \frac{2(z-1)}{z}s_t^{(+)}$
$P_i = P_\xi^i$	$H_{ti}^{(-)}$	$2H_{\xi i}^{(+)}$
$T_1^1 + T_2^2$	$k^{(0)}$	$4k^{(4)} - \frac{2}{3}(z-1)(2z+1)s_\xi^{(4)}$
$T_1^1 - T_2^2$, T_2^1	$\bar{H}_{ij}^{(0)}$	$\bar{H}_{ij}^{(4)}$
T_i^ξ	$H_{\xi i}^{(-)}$	$2H_{ti}^{(+)} - (z-1)s_i^{(+)}$
P_ξ	$H_{tt}^{(-)}$	$2H_{\xi\xi}^{(+)}$
P_ξ^ξ	$H_{t\xi}^{(0)}$	$-2k^{(4)} - \frac{1}{3}(z-1)(z+2)s_\xi^{(4)}$
O	$s_\xi^{(-)}$	$\frac{2(z^2-1)}{z}s_t^{(+)}$

Table 1: The identification of linearised modes with sources and vevs for the operators in the dual field theory.

and

$$\langle O \rangle = \frac{2(z^2-1)}{z} s_t^{(+)}. \tag{2.80}$$

For a solution with non-zero k_ξ, ω, there is a power series expansion of the same form as in (2.41), with an extra factor of k_ξ in s_r. As in the vector case, there is a reduction in the number of independent mode solutions because of the different structure of the equations of motion. There is a linear combination of (2.58,2.60) which is independent of s_r. That and (2.61) imply the relations

$$k_\xi \left(k^{(4)} + \frac{1}{6}(z-1)(z+2)s_\xi^{(4)} \right) - \omega H_{\xi\xi}^{(+)} = 0, \tag{2.81}$$

$$-2k_\xi \left(H_{tt}^{(+)} + \frac{(z-1)}{z}s_t^{(+)} \right) + \omega \left(2k^{(4)} + \frac{1}{3z}(z-1)(z^2-4z-6)s_\xi^{(4)} \right) = 0; \tag{2.82}$$

which correspond to the Ward identities

$$\partial_t P_\xi + \partial_\xi P_\xi^\xi = 0, \tag{2.83}$$

$$\partial_t E + \partial_\xi E^\xi = 0. \tag{2.84}$$

This confirms our identification of the vevs in terms of the linearised modes. The identification of sources and vevs for the different operators is summarized in table 1.

2.4.1.4 Linearised solutions with spatial dependence

The most general linearised solutions include spatial dependence. Considering a single Fourier mode in all boundary directions, we can use the rotation symmetry to orient the spatial coordinates so that the spatial momentum is along the x direction, so the coordinate dependence in all modes is $e^{i\omega t+ik_\xi\xi+ik_x x}$. Then the modes split up into the scalar modes H_{tt}, $H_{t\xi}$, $H_{\xi\xi}$, H_{tx}, $H_{\xi x}$, H_{xx}, H_{yy} s_t, s_x, s_r and the vector modes H_{ty}, $H_{\xi y}$, H_{xy}, s_y. As in the discussion with no spatial dependence, these all have an expansion in powers of $k_\xi\omega r^2$ and $k_x^2 r^2$. The leading terms take the same form as for the constant modes above.

The equations of motion in the vector sector are

$$rk_x[r^z\omega H_{\xi y}+k_\xi r^{2-z}(H_{ty}+H_{\xi y})]-(k_\xi^2 r^{4-2z}+2k_\xi\omega r^2)H_{xy}-3rH'_{xy}+r^2H''_{xy}=0, \tag{2.85}$$

$$z(z-1)H_{\xi y}-k_x^2r^2s_y-(k_\xi^2r^{4-2z}+2k_\xi\omega r^2+(z-1)(z+3))s_y+r(zH'_{\xi y}-3s'_y+rs''_y)=0, \tag{2.86}$$

$$k_\xi[(z-1)(H_{ty}-H_{\xi y}+2s_y)-r(H_{ty}+H_{\xi y})']-\omega r^{2z}[(z-1)H_{\xi y}+rH'_{\xi y}]-k_xr^zH'_{xy}=0, \tag{2.87}$$

$$k_x(k_\xi r^{3-z}H_{xy}-k_xr^2H_{\xi y})+k_\xi^2r^{4-2z}H_{ty}+((z-1)(z-5)-k_\xi\omega r^2)H_{\xi y} +r((2z-5)H'_{\xi y}+rH''_{\xi y})=0, \tag{2.88}$$

$$k_xr(r^z\omega H_{xy}-k_xrH_{ty})+(k_\xi\omega r^2-k_\xi^2r^{4-2z}-(z-1)(z+3))H_{ty}+2(z-1)(z+3)s_y +(k_\xi\omega r^2+\omega^2r^{2z}-2(z-1)^2)H_{\xi y}+r(rH''_{ty}-2(z-1)(H_{\xi y}+s_y)'-(1+2z)H'_{ty})=0. \tag{2.89}$$

We can solve these equations order by order in $k_\xi\omega$ and k_x^2. The subleading components determine the subleading terms in the expansion of the fields. But there are also additional constraints on the leading terms, corresponding to the expected Ward identities. Equation (2.87) gives at leading order

$$k_\xi[2H^{(+)}_{ty}-(z-1)s^{(+)}_y]+2\omega H^{(+)}_{\xi y}+k_x\bar{H}^{(4)}_{xy}=0 \tag{2.90}$$

which corresponds to the Ward identity

$$\partial_tP_y+\partial_\xi T^\xi_y+\partial_xT^x_y=0. \tag{2.91}$$

In the scalar sector, the equations of motion are

$$
\begin{aligned}
0 =& 2k_x r(k_\xi r^{2-z} + \omega r^z)(H_{tx} + H_{\xi x}) + k_x^2 r^2\Big(\frac{1}{2}H_{tt} - \frac{1}{2}H_{\xi\xi} - H_{t\xi} - k\Big) - 2(1-z^2)H_{tt} \\
&+ 2(2-3z+z^2)H_{\xi\xi} - (k_\xi r^{2-z} + \omega r^z)^2 k + i(z-1)(k_\xi r^{2-z} + 2\omega r^z)s_r - 4(1-z^2)s_t \\
&- 4(1-z)s_\xi - (z+2)rH'_{t\xi} + \frac{1}{2}(2z-5)rH'_{\xi\xi} + (z-4)rk' - (z-1)rs'_\xi \\
&+ r[(1-4z)H'_{tt} - 2(z-1)s'_t] + \frac{1}{2}r^2 H''_{tt} + r^2 H''_{t\xi} + \frac{1}{2}r^2 H''_{\xi\xi} + r^2 k'', \qquad (2.92)\\
0 =& k_x r\Big(k_\xi r^{2-z} H_{tx} + (2k_\xi r^{2-z} + \omega r^z)H_{\xi x}\Big) - k_x^2 r^2(H_{t\xi} + H_{\xi\xi} + k) + 4(z^2-3z+2)H_{\xi\xi} \\
&- 2(k_\xi^2 r^{4-2z} + \omega k_\xi r^2)k - 3r\Big(H'_{t\xi} - (z-2)H'_{\xi\xi} + 2k'\Big) + r^2 H''_{t\xi} + r^2 H''_{\xi\xi} + 2r^2 k'', \qquad (2.93)\\
0 =& rk_x[\omega r^z(H_{\xi\xi} + k) - 2i(z-1)s_r - k_\xi H_{tt} + (\omega r^z - k_\xi r^{2-z})H_{t\xi}] \\
&+ (k_\xi^2 r^{4-2z} + k_\xi \omega r^2 - (z-1)(z+3))H_{tx} - (k_\xi \omega r^2 + \omega^2 r^{2z} - 2(z-1)^2)H_{\xi x} \\
&- 2(z-1)(z+3)s_x + (2z+1)rH'_{tx} + 2r(z-1)(H'_{\xi x} + s'_x) - r^2 H''_{tx}, \qquad (2.94)\\
0 =& -2k_x k_\xi r^{3-z} H_{\xi x} + k_x^2 r^2 H_{\xi\xi} - 4(z-1)(z-3)H_{\xi\xi} + 2k_\xi^2 r^{4-2z}k + (7-4z)rH'_{\xi\xi} \\
&- r^2 H''_{\xi\xi}, \qquad (2.95)\\
0 =& k_x r\Big(k_\xi r^{2-z}(H_{t\xi} + k) - \omega r^z H_{\xi\xi}\Big) - k_\xi^2 r^{4-2z} H_{tx} + \Big(k_\xi \omega r^2 - (z-1)(z-5)\Big)H_{\xi x} \\
&+ (5-2z)rH'_{\xi x} - r^2 H''_{\xi x}, \qquad (2.96)\\
0 =& r^2 k'' + r^2 H''_{\xi\xi} + 2r^2 H''_{t\xi} - (z-1)rs'_\xi - 3rk' + (z-4)rH'_{\xi\xi} - 6rH'_{t\xi} + 8(z-1)s_\xi \\
&+ 2i(z-1)k_\xi r^{2-z} s_r - (k_\xi^2 r^{4-2z} + 2\omega k_\xi r^2)k + \Big(4(1-z) + \omega^2 r^{2z}\Big)H_{\xi\xi} - 2k_\xi \omega r^2 H_{t\xi} \\
&+ k_\xi^2 r^{4-2z} H_{tt}, \qquad (2.97)\\
0 =& 2k_x r\Big(k_\xi r^{2-z}(H_{tx} + 2H_{\xi x}) + \omega r^z H_{\xi x}\Big) - r^2 k_x^2(2H_{tx} + H_{\xi\xi}) + r^2 k'' + r^2 H''_{\xi\xi} \\
&- 2(z-1)rs'_\xi - 3rk' + (z-4)rH'_{\xi\xi} - 6rH'_{t\xi} + 8(z-1)s_\xi + 2i(z-1)k_\xi r^{2-z} s_r \\
&- (k_\xi^2 r^{4-2z} + 2\omega k_\xi r^2)k + \Big(4(1-z) + \omega^2 r^{2z}\Big)H_{\xi\xi} - 2k_\xi \omega r^2 H_{t\xi} + k_\xi^2 r^{4-2z} H_{tt}, \qquad (2.98)\\
0 =& k_x k_\xi r^{3-z} s_x - k_x^2 r^2 s_\xi + 2z(z-1)H_{\xi\xi} + 2ik_\xi r^{2-z} s_r + k_\xi^2 r^{4-2z} s_t - \Big(8(z-1) + k_\xi \omega r^2\Big)s_\xi \\
&rzH'_{\xi\xi} - ik_\xi r^{3-z} s'_r + (2z-5)rs'_\xi + r^2 s''_\xi, \qquad (2.99)\\
0 =& sk_x r(k_\xi r^{2-z} + \omega r^z)s_x - 2k_x^2 r^2(s_\xi + s_t) + 4i(zk_\xi r^{2-z} + \omega r^z)s_r \\
&+ \Big(2\omega^2 r^{2z} - 4(z-1)(z+2)\Big)s_\xi + zrH'_{\xi\xi} - 2zrk' - 2i(k_\xi r^{2-z} + \omega r^z)rs'_r - 6rs'_\xi - 2k_\xi \omega r^2 s_t \\
&- 2(1+2z)rs'_t + 2r^2 s''_t + 2r^2 s''_\xi, \qquad (2.100)\\
0 =& k_x r[2is_r + k_\xi r^{2-z} s_t + (k_\xi r^{2-z} + r^z \omega)s_\xi - irs'_r] + z(z-1)H_{\xi x} \\
&- (k_\xi^2 r^{4-2z} + 2k_\xi \omega r^2 + (z-1)(z+3))s_x + zrH'_{\xi x} - 3rs'_x + r^2 s''_x, \qquad (2.101)
\end{aligned}
$$

and additionally,

$$
\begin{aligned}
0 =& k_\xi^2 r^{4-2z} H_{tt} + 2k_\xi k_x r^{3-z} H_{tx} - 2(k_x^2 + k_\xi\omega) r^2 H_{t\xi} + 2rk_x(k_\xi r^{2-z} + \omega r^z) H_{\xi x} \\
& - \Big(k_x^2 r^2 + 2z(z-1) + \omega^2 r^2\Big) H_{\xi\xi} - \Big(2k_\xi^2 r^{4-2z} + r^2(k_x^2 + 4k_\xi\omega)\Big) k \\
& - 2ik_\xi(z-1) r^{2-z} s_r + 4z(z-1) s_\xi - 6rH'_{t\xi} - (2+z) rH'_{\xi\xi} - 6rk' + 2(z-1) rs'_\xi, \qquad (2.102) \\
0 =& k_x r\Big((z-1)(H_{tx} + H_{\xi x}) - rH'_{tx}\Big) + (z-1)(k_\xi r^{2-z} + 3\omega r^z) H_{\xi\xi} - 2k_\xi(z-1) r^{2-z} k \\
& - 2i(z-1)(z+2) s_r - 2(z-1)\omega r^z s_\xi + k_\xi r^{2-z}\Big(2(z-1)(H_{tt} + s_t) - rH'_{tt}\Big) \\
& + (-k_\xi r^{2-z} + \omega r^z) rH'_{t\xi} + \omega r^{z+1}(H'_{\xi\xi} + k'), \qquad (2.103) \\
0 =& -k_x r\Big((z-1) H_{\xi x} + rH'_{\xi x}\Big) - (z-1)(k_\xi r^{2-z} + 2\omega r^z) H_{\xi\xi} + k_\xi r^{3-z} H'_{t\xi} - r\omega r^z H'_{\xi\xi} \\
& + 2k_\xi r^{3-z} k', \qquad (2.104) \\
0 =& k_\xi(z-1) r^{2-z}(H_{tx} - H_{\xi x} + 2s_x) - (z-1)\omega r^z H_{\xi x} - k_\xi r^{3-z} H'_{tx} - (k_\xi r^{2-z} + \omega r^z) rH'_{\xi x} \\
& + k_x r\Big((z-1)(H_{\xi\xi} + 2s_\xi) + 2r(H'_{t\xi} + H'_{\xi\xi} + k')\Big), \qquad (2.105) \\
0 =& k_x r(2zH_{\xi x} + 2s_x + rs'_x) - 2ik_x^2 r^2 s_r + (k_\xi r^{2-z} + 2\omega r^z) zH_{\xi\xi} - 2zk_\xi r^{2-z} k \\
& - 2i\Big(k_\xi^2 r^{4-2z} + z(z+2) + 2k_\xi\omega r^2\Big) s_r + 2(z-2)(k_\xi r^{2-z} + \omega r^z) s_\xi + 2k_\xi r^{2-z}(-zs_t + rs'_t) \\
& + 2(k_\xi r^{2-z} + \omega r^z) s'_\xi. \qquad (2.106)
\end{aligned}
$$

Again, the constraints corresponding to the Ward identities are modified. Equation (2.105) gives

$$
k_\xi[2H^{(+)}_{tx} - (z-1)s^{(+)}_x] + 2\omega H^{(+)}_{\xi x} + k_x[2k^{(4)} - \frac{1}{3}(z-1)(2z+1)] = 0, \qquad (2.107)
$$

which corresponds to the Ward identity

$$
\partial_t P_x + \partial_\xi T^\xi_x + \partial_x T^x_x = 0; \qquad (2.108)
$$

(2.104) gives

$$
k_\xi\Big(k^{(4)} + \frac{1}{6}(z-1)(z+2) s^{(4)}_\xi\Big) - \omega H^{(+)}_{\xi\xi} - k_x H^{(+)}_{\xi x} = 0, \qquad (2.109)
$$

which corresponds to the Ward identity

$$
\partial_t P_\xi + \partial_\xi P^\xi_\xi + \partial_x P^x_\xi = 0; \qquad (2.110)
$$

and there is a linear combination of (2.106) and (2.103) which is independent of s_r which gives

$$k_\xi\left(2H_{tt}^{(+)}+\frac{2(z-1)}{z}s_t^{(+)}\right)-\omega\left(2k^{(4)}+\frac{1}{3z}(z-1)(z^2-4z-6)\right)+k_x\left(2H_{tx}^{(+)}+\frac{1}{z}(z-1)(z+2)s_x^{(+)}\right)=0 \tag{2.111}$$

which corresponds to the Ward identity

$$\partial_t E+\partial_\xi E^\xi+\partial_x E^x=0. \tag{2.112}$$

Thus the full linearised perturbations behave as we expect.

2.4.2 Linearised solutions for $d_s=0$

The solution for other values of d_s is qualitatively similar to the one discussed above, but the three-dimensional bulk is a special case. In this case there are no spatial dimensions. Hence the previous analysis of the spatially independent modes corresponds to the general analysis in this case, and there are no vector or tensor modes, so the structure is similar to the scalar mode analysis in $d_s=2$. There will be no field k in this case, corresponding to the absence of the trace of the spatial stress tensor.

The solution for the constant modes is

$$s_r=0, \tag{2.113}$$

$$H_{tt}=-2s_t^{(0)}+H_{tt}^{(+)}r^{2z}+2H_{tt}^{(-)}r^{2z-2}-\frac{zH_{\xi\xi}^{(+)}r^{4-2z}}{2(z-2)(2z-3)}+\frac{2z(z-1)r^2s_\xi^{(2)}}{(z-2)}, \tag{2.114}$$

$$H_{t\xi}=s_t^{(0)}+H_{t\xi}^{(0)}-H_{\xi\xi}^{(-)}r^{2-2z}-\frac{(z-1)H_{\xi\xi}^{(+)}r^{4-2z}}{2(z-2)}+z(z-1)r^2s_\xi^{(2)}, \tag{2.115}$$

$$H_{\xi\xi}=2H_{\xi\xi}^{(-)}r^{2-2z}+H_{\xi\xi}^{(+)}r^{4-2z}, \tag{2.116}$$

$$s_\xi=(H_{\xi\xi}^{(-)}+s_\xi^{(-)})r^{2-2z}+r^2s_\xi^{(2)}+\frac{zH_{\xi\xi}^{(+)}r^{4-2z}}{2(z-1)}, \tag{2.117}$$

$$s_t=s_t^{(+)}r^{2z}+s_t^{(0)}-\frac{zs_\xi^{(-)}r^{2-2z}}{4z-2}+\frac{zH_{\xi\xi}^{(+)}r^{4-2z}}{4(z-2)(z-1)}-\frac{z}{2}r^2s_\xi^{(2)}. \tag{2.118}$$

As in the previous case, the r-independent modes correspond to sources for the stress energy complex: $s_t^{(0)}$ is the constant part of $\delta\hat{e}_t^+$, so it is the source for the energy density E, and $H_{t\xi}^{(0)}$ is the constant part of $\delta\hat{e}_\xi^-$, so it is the source for P_ξ^ξ. There is a single mode $H_{tt}^{(-)}$ of dimension $2z-2$, which comes from the constant part of $\delta\hat{e}_t^-$, so it is the source for the particle number

density P_ξ. The two modes of dimension $2-2z$ are $H^{(-)}_{\xi\xi}$, which comes from the constant part of $\delta\hat{e}^+_\xi$, and hence corresponds to the source for the energy flux E^ξ, and $s^{(-)}_\xi$, which is the source for an operator O of dimension $2z+2$.

We would again like to identify the remaining modes with the vevs of these operators. Dimensions alone suffice to fix $\langle P_\xi\rangle \sim H^{(+)}_{\xi\xi}$, to relate $\langle E\rangle$ and $\langle P^\xi_\xi\rangle$ to $s^{(2)}_\xi$, and to relate $\langle E^\xi\rangle$ and $\langle O\rangle$ to $H^{(+)}_{tt}$ and $s^{(+)}_t$. The symplectic flux is

$$\begin{aligned}\mathcal{F} = -i\int_{r=0} d^{d_s}x d\xi \Big[& H^{(-)}_{\xi\xi}\wedge H^{(+)}_{tt} + H^{(-)}_{tt}\wedge H^{(+)}_{\xi\xi} \\ & + 2(z-1)s^{(-)}_\xi \wedge s^{(+)}_t - z(z-1)H^{(0)}_{t\xi}\wedge s^{(2)}_\xi - (z-1)(z-2)s^{(0)}_t \wedge s^{(2)}_\xi\Big].\end{aligned} \tag{2.119}$$

This enables us to identify the vevs

$$\langle P_\xi\rangle = H^{(+)}_{\xi\xi}, \quad \langle P^\xi_\xi\rangle = -z(z-1)s^{(2)}_\xi, \tag{2.120}$$

$$\langle E\rangle = -(z-1)(z-2)s^{(2)}_\xi, \tag{2.121}$$

which indeed satisfy the Ward identity from the scaling invariance, which is $zE + (2-z)P^\xi_\xi = 0$,

$$\langle E^\xi\rangle = H^{(+)}_{tt}, \tag{2.122}$$

and

$$\langle O\rangle = 2(z-1)s^{(+)}_t. \tag{2.123}$$

For non-zero k_ξ, ω, there will be Ward identities $\partial_t E + \partial_\xi E^\xi = 0$, $\partial_t P_\xi + \partial_\xi P^\xi_\xi = 0$ and $zE + (2-z)P^\xi_\xi = 0$, which leave us with just one free vev in the stress energy complex.

2.4.2.1 Comparison to previous work

In [36], a full linearised analysis for $z < 2$ and $d_s = 0$ was carried out. They write the Schrödinger metric in a different radial coordinate, $\rho = r^2$, and introduce σ as discussed in the introduction by rescaling the boundary coordinates, $u^2 = -t^2/\sigma^2$, $v^2 = -\sigma^2\xi^2$, so the Schrodinger metric becomes

$$ds^2 = \frac{d\rho^2}{4\rho^2} + \frac{2du\,dv}{\rho} + \frac{\sigma^2 du^2}{\rho^z}. \tag{2.124}$$

Their focus is on $z < 1$, where $\sigma^2 > 0$; for the range $z > 1$ we are interested in we need $\sigma^2 < 0$. We will henceforth set $\sigma^2 = -1$; then their b is identical to our α. The linearised perturbations are written as

$$A^{(1)}_\mu = a_\mu, \quad g^{(1)}_{ab} = \rho^{-1} h_{ab}, \tag{2.125}$$

where $\mu = u, v, r$, $a, b = u, v$. Relative to our definitions above,

$$a_u = \alpha \rho^{-z/2} s_t, \quad a_v = \alpha \rho^{z/2-1} s_\xi, \quad a_r = \alpha \rho^{-1/2} s_r, \tag{2.126}$$

and

$$h_{uu} = \rho^{1-z} H_{tt}, \quad h_{uv} = H_{t\xi}, \quad h_{vv} = \rho^{z-1} H_{\xi\xi}. \tag{2.127}$$

In [36], the perturbation is decomposed into a part which only affects the metric h_{ab} and a V mode which enters in both a_μ and h_{ab} (following the decomposition into T and X modes in [35]).

To relate to our analysis above, we will consider the case where the modes are constant in the boundary directions, so h_{ab}, a_μ are functions only of ρ. As in our analysis, this implies that $a_\rho = 0$. The metric can be written as

$$h_{vv} = h_{(0)vv} + \rho h_{(2)vv}, \quad h_{uv} = h_{(0)uv} + \rho h_{(2)uv} - \frac{1}{2}\rho^{1-z} h_{(0)vv} - \frac{(1-z)}{2(2-z)} \rho^{2-z} h_{(2)vv}, \tag{2.128}$$

$$h_{uu} = h_{(0)uu} + \rho h_{(2)uu} - \frac{z}{4(1-2z)} \rho^{2-2z} h_{(0)vv} - \frac{z}{4(3-2z)} \rho^{3-2z} h_{(2)vv} - \frac{1}{2-z} \rho^{2-z} h_{(2)uv} + h^V_{uu}, \tag{2.129}$$

where

$$\partial^2_\rho h^V_{uu} = \frac{z\alpha}{2} \rho^{1-z} \partial_\rho (\rho^{-z/2} a_v) + z\alpha \partial_\rho (\rho^{-z/2} a_u). \tag{2.130}$$

In solving this equation, we will take h^V_{uu} to have no constant or linear pieces in ρ, so that $h_{(0)uu}$ and $h_{(2)uu}$ represent the whole of the ρ^0 and ρ coefficients. The vector field satisfies

$$\rho^{z/2} \partial_\rho [\rho^{1-z} \partial_\rho (\rho^{z/2} a_v)] = -\frac{z\alpha}{2} \rho^{-z/2} h_{(2)vv}, \tag{2.131}$$

$$\rho^{z/2} \partial_\rho [\rho^{1-z} \partial_\rho (\rho^{z/2} a_u)] = -(1-z)\rho^{1-z} \partial_\rho a_v - \frac{z(1-z)\alpha}{4} \rho^{-3z/2} h_{(0)vv} + \frac{z^2\alpha}{4} \rho^{1-3z/2} h_{(2)vv}; \tag{2.132}$$

and there is a single constraint for constant solutions,

$$-4h_{(2)uv} - 2z\rho^{1-z} h_{(2)vv} + 2z\alpha\rho^{1-z} \partial_\rho (\rho^{z/2} a_v) = 0. \tag{2.133}$$

Solving this system of equations, we find that

$$a_v = \alpha_v \rho^{-z/2} + \beta_v \rho^{z/2} + \frac{z\alpha}{2(z-1)} h_{(2)vv} \rho^{1-z/2}, \tag{2.134}$$

$$a_u = \alpha_u \rho^{-z/2} + \beta_u \rho^{z/2} - \frac{z}{4z-2} \alpha_v \rho^{1-3z/2} - \frac{z}{2} \beta_v \rho^{1-z/2} + \frac{z\alpha}{4(2z-1)} h_{(0)vv} \rho^{1-3z/2} + \frac{z\alpha}{4(z-2)(z-1)} h_{(2)vv} \rho^{2-3z/2}, \tag{2.135}$$

$$h_{uu} = h_{(0)uu} + \rho h_{(2)uu} - \frac{z}{2(z-2)(2z-3)} h_{(2)vv} \rho^{3-2z} - \frac{1}{(2-z)} h_{(2)uv} \rho^{2-z} - \frac{z\alpha}{(z-1)} \alpha_u \rho^{1-z} - \frac{z^2\alpha}{2(2-z)} \beta_v \rho^{2-z}, \tag{2.136}$$

where the constraint (2.133) implies that $h_{(2)uv} = \frac{z^2\alpha}{2} \beta_v$. The constants $\alpha_{u,v}$, $\beta_{u,v}$ correspond to the V mode solutions of [36].

Comparing to our constant solutions, we see that we can identify the sources

$$h_{(0)vv} = 2H^{(-)}_{\xi\xi}, \quad h_{(0)uv} = s^{(0)}_t + H^{(0)}_{t\xi}, \quad h_{(0)uu} = 2H^{(-)}_{tt}, \tag{2.137}$$

$$\alpha_v = \alpha(H^{(-)}_{\xi\xi} + s^{(-)}_\xi), \quad \alpha_u = \alpha s^{(0)}_t; \tag{2.138}$$

and vevs

$$h_{(2)vv} = H^{(+)}_{\xi\xi}, \quad h_{(2)uv} = z(z-1)s^{(2)}_\xi, \quad h_{(2)uu} = H^{(+)}_{tt}, \tag{2.139}$$

$$\beta_v = \alpha s^{(2)}_\xi, \quad \beta_u = \alpha s^{(+)}_t. \tag{2.140}$$

As we might have expected, while the sources for the momentum density and flux appear only in the metric modes, the sources for the energy density and flux appear also in the V modes. The vev mode $s^{(2)}_\xi$ also appears in the V modes. The source and vev for the operator O appear only in the V modes and not in the metric modes. The constraint (2.133) imposes the trace Ward identity.

When we go beyond constant modes, there will be subleading terms in the V modes, determined by solving the equations in [36]. There are also additional constraints; there is a constraint

$$\partial_v h_{(2)uv} = \partial_u h_{(2)uu}, \tag{2.141}$$

which corresponds precisely to the expected Ward identity $\partial_t P_\xi + \partial_\xi P^\xi_\xi = 0$, and a constraint

$$\begin{aligned}\partial_v\partial_\rho h_{uu} = &\partial_u h_{(2)uv} + \frac{z}{2}\alpha\rho^{-z/2}(-2\partial_u a_v + 2z a_\rho - 4\rho\partial_\rho a_\rho - \rho^{1-z}\partial_v a_v) \\ &+ \frac{z\alpha^2}{4}\rho^{-z/2}(4\partial_u h_{(0)vv} + 4\rho\partial_u h_{(2)vv} + \rho^{1-z}(\partial_v h_{(0)vv} + \rho\partial_v h_{(2)vv})).\end{aligned} \tag{2.142}$$

The ρ derivative of this constraint vanishes by virtue of the other equations of motion; the constant part gives

$$\partial_v h_{(2)uu} = \partial_u h_{(2)uv} - z\alpha\partial_u\beta_v, \tag{2.143}$$

which is precisely the expected Ward identity $\partial_t E + \partial_\xi E^\xi = 0$.

Thus our solution is consistent with the one in [36], but our frame perspective offers a different physical interpretation with a new organisation of the sources and vevs. We agree with [36] on the split of the linearised solutions into sources and vevs, but we give a different physical interpretation to these sources and vevs in terms of operators in the field theory.

2.5 Asymptotic expansion for $z < 2$

In this section, we want to go beyond the linearised analysis by showing that solutions of the bulk equations of motion exist for arbitrary boundary data. To do so, we will solve the equations of motion in an asymptotic expansion: that is, we work at large r, and solve the equations in an expansion in powers of r. We will follow closely the treatment of the asymptotic expansion for asymptotically Lifshitz spacetimes in [45, 80, 81], using a radial Hamiltonian framework to analyse the equations. In the course of demonstrating the existence of this asymptotic expansion, we will also see that when the asymptotic expansion exists we can cancel the divergent terms in the action in the usual way by adding appropriate local counterterms determined by the boundary data.

The action we consider is a massive vector theory, which is the same as the theory considered in [45], so the equations are the same. However [45] considered a four-dimensional bulk, whereas our main interest here is a five-dimensional bulk, so some dimension-dependent factors are different. For generality, we write the equations for general d_s. By taking the trace, we can rewrite (2.7) as

$$R_{\mu\nu} = \frac{2}{d-2}\Lambda g_{\mu\nu} + \frac{1}{2}F_{\mu\lambda}F_\nu{}^\lambda - \frac{1}{4(d-2)}F_{\lambda\rho}F^{\lambda\rho}g_{\mu\nu} + \frac{1}{2}m^2 A_\mu A_\nu, \tag{2.144}$$

where $d = d_s + 3$ is the dimension of the bulk spacetime. The Gauss-Codazzi equations on a surface of constant r are then

$$\begin{aligned}\dot{K}_{\alpha\beta} + KK_{\alpha\beta} - 2K_{\alpha\gamma}K^{\gamma}{}_{\beta} =& R_{\alpha\beta} - \frac{2}{d-2}\Lambda h_{\alpha\beta} - \frac{1}{2}F_{\alpha\gamma}F_{\beta}{}^{\gamma} + \frac{2}{8(d-2)}h_{\alpha\beta}F_{\gamma\delta}F^{\gamma\delta} \\ & - \frac{1}{2}\pi_\alpha\pi_\beta + \frac{2}{4(d-2)}h_{\alpha\beta}\pi_\gamma\pi^\gamma - \frac{1}{2}m^2A_\alpha A_\beta, \end{aligned} \tag{2.145}$$

$$\dot{\pi}^\alpha + K\pi^\alpha + \nabla_\beta F^{\beta\alpha} = m^2 A^\alpha \tag{2.146}$$

and the constraints become

$$\nabla_\alpha K^\alpha{}_\beta - \nabla_\beta K^\alpha{}_\alpha = \frac{1}{2}F_{\beta\alpha}\pi^\alpha + \frac{1}{2}m^2 A_\beta A_n, \tag{2.147}$$

$$K^2 - K_{\alpha\beta}K^{\alpha\beta} = R - 2\Lambda + \frac{1}{2}\pi_\alpha\pi^\alpha - \frac{1}{4}F_{\alpha\beta}F^{\alpha\beta} + \frac{1}{2}m^2A_n^2 - \frac{1}{2}m^2A_\alpha A^\alpha. \tag{2.148}$$

and

$$\nabla_\alpha\pi^\alpha = -m^2 A_n. \tag{2.149}$$

In the above equations the Ricci tensor $R_{\alpha\beta}$ and covariant derivatives ∇_β are those determined by the induced metric $h_{\alpha\beta}$ on a surface of constant r. Because we work here in coordinates where the boundary is at $r = 0$, the outward-pointing normal one-form is $n = -dr/r$, and consequently there are some sign differences in radial terms relative to [45]. $K_{\alpha\beta}$ is the extrinsic curvature of the surface of constant r, $\pi_\alpha = n^\mu F_{\mu\alpha} = -rF_{r\alpha}$ is the conjugate momentum for the massive vector, the radial component of the gauge field is $A_n = n^\mu A_\mu = -rA_r$, and $\dot{}$ denotes the derivative in the normal direction, that is $-r\partial_r$.

We want to re-express these equations in terms of frame fields e^A. As in [45], we introduce a frame extrinsic curvature $K^A{}_B = e^\alpha_B \dot{e}^A_\alpha$, which is not a symmetric object, unlike the usual extrinsic curvature. Note that frame indices will be raised and lowered with the metric g_{AB}, which is not diagonal in our case, so it is useful to keep track of the 'natural' index positions in tensor objects.

The equations in frame indices are

$$\begin{aligned}\dot{K}_{(AB)}+KK_{(AB)}+\frac{1}{2}\left(K_{CA}K^{C}{}_{B}-K_{AC}K_{B}{}^{C}\right)+\frac{1}{2}\pi_A\pi_B-\frac{2}{4(d-2)}\eta_{AB}\pi_C\pi^C\\ =R_{AB}-\frac{2}{d-2}\Lambda\eta_{AB}-\frac{1}{2}F_{AC}F_{B}{}^{C}+\frac{2}{8(d-2)}\eta_{AB}F_{CD}F^{CD}-\frac{1}{2}m^2A_AA_B,\end{aligned}\tag{2.150}$$

$$\dot{\pi}^A+K\pi^A-K^{A}{}_{B}\pi^B=-\nabla_BF^{BA}+m^2A^A,\tag{2.151}$$

and the constraints

$$\nabla^AK_{(AB)}-\nabla_BK^{A}{}_{A}=\frac{1}{2}F_{BA}\pi^A+\frac{1}{2}m^2A_BA_n,\tag{2.152}$$

$$K^2-K_{(AB)}K^{AB}-\frac{1}{2}\pi_A\pi^A=R-2\Lambda-\frac{1}{4}F_{AB}F^{AB}+\frac{1}{2}m^2A_n^2-\frac{1}{2}m^2A_AA^A,\tag{2.153}$$

$$\nabla_A\pi^A=-m^2A_n.\tag{2.154}$$

Here $F_{AB}=e^{\alpha}_{A}e^{\beta}_{B}F_{\alpha\beta}$, and $\nabla_A=e^{\alpha}_{A}\nabla_\alpha$, where the covariant derivative ∇_α is a total covariant derivative (covariant with respect to both local Lorentz transformations and diffeomorphisms).

Assuming that the metric is asymptotically locally Schrodinger according to the definition (2.17) then implies that

$$K^{+}{}_{+}=z+\hat{e}_+\dot{\hat{e}}^+,\quad K^{+}{}_{-}=r^{2z-2}\hat{e}_-\dot{\hat{e}}^+,\quad K^{+}{}_{I}=r^{z-1}\hat{e}_I\dot{\hat{e}}^+,\tag{2.155}$$

$$K^{-}{}_{+}=r^{2-2z}\hat{e}_+\dot{\hat{e}}^-,\quad K^{-}{}_{-}=2-z+\hat{e}_-\dot{\hat{e}}^-,\quad K^{-}{}_{I}=r^{1-z}\hat{e}_I\dot{\hat{e}}^-,$$

$$K^{I}{}_{+}=r^{1-z}\hat{e}_+\dot{\hat{e}}^I,\quad K^{I}{}_{-}=r^{z-1}\hat{e}_-\dot{\hat{e}}^I,\quad K^{I}{}_{J}=\delta^I_J+\hat{e}_J\dot{\hat{e}}^I.$$

Since we choose the frame fields so that the massive vector is $A=\alpha(e^++\psi e^-+s_re^r)$ everywhere in the bulk, the canonical momentum π_A has components

$$\begin{aligned}\pi_I=&\alpha(K^{+}{}_{I}+\partial_Is_r),\\ \pi_+=&\alpha(K^{+}{}_{+}+\partial_+s_r),\\ \pi_-=&\alpha(\dot{\psi}+K^{+}{}_{-}+\partial_-s_r).\end{aligned}\tag{2.156}$$

To show that a solution exists in an asymptotic expansion, we want to fix the sources, which will fix the terms appearing on the RHS of these equations, and see that we can satisfy the equations by introducing appropriate subleading terms in r in the expansion which will contribute

to the radial derivative terms on the LHS of the equations. For this to work, the source terms need to involve positive powers of r. Explicit powers of r enter where there are derivatives along the boundary directions: these all come with positive powers of r for $z < 2$. There are also explicit powers in the Ricci rotation coefficients, determined by $de^C = \Omega_{AB}{}^C e^A \wedge e^B$. These are

$$\Omega_{+-}{}^{+} \sim r^{2-z}, \quad \Omega_{+I}{}^{+} \sim r, \quad \Omega_{-I}{}^{+} \sim r^{3-2z}, \quad \Omega_{IJ}{}^{+} \sim r^{2-z}, \tag{2.157}$$

$$\Omega_{+-}{}^{-} \sim r^{z}, \quad \Omega_{+I}{}^{-} \sim r^{2z-1}, \quad \Omega_{-I}{}^{-} \sim r, \quad \Omega_{IJ}{}^{-} \sim r^{z}, \tag{2.158}$$

$$\Omega_{+-}{}^{I} \sim r, \quad \Omega_{+J}{}^{I} \sim r^{z}, \quad \Omega_{-J}{}^{I} \sim r^{2-z}, \quad \Omega_{JK}{}^{I} \sim r. \tag{2.159}$$

Thus, for $z < 2$, the only term that causes problems is $\Omega_{-I}{}^{+}$, which has a power that becomes negative for $z > 3/2$. This is associated with the ∂_I derivative of the source for E^ξ, and the ∂_- derivative of the source for E^i. Hence imposing the geometric condition $\hat{e}^+ \wedge d\hat{e}^+ = 0$, which will set the sources for E^ξ and E^i to zero, eliminates the leading constribution to this one dangerous term (as well as the leading contribution to $\Omega_{IJ}{}^{+}$). Note that because of the diffeomorphism invariance, it is only derivatives of these sources that appear. Thus, even though E^i is irrelevant for all $z > 1$, the asymptotic expansion exists even in the presence of its source for $1 < z < 3/2$. It is only for $z > 3/2$ that we have to set this source to zero to have a good asymptotic expansion. In addition, a source for the operator dual to the matter field would make a contribution $A_- \sim r^{2-2z}$, so we need to set this source to zero for all $z > 1$.

Thus, we expect that an asymptotic expansion will exist for $z < 3/2$ for arbitrary sources in $\hat{e}^A$ so long as we set the source for the irrelevant operator O to zero, and for $3/2 < z < 2$ if the frame fields satisfy the constraint $\hat{e}^+ \wedge d\hat{e}^+ = 0$ and we set the source for the irrelevant operator O to zero.

Explicitly analysing the equations of motion is however somewhat messy because of the off-diagonal structure, so we will demonstrate the existence of the asymptotic expansion using the elegant radial Hamiltonian framework of [80, 81].[14] This involves expanding in eigenvalues of an appropriate bulk dilatation operator. Assuming that we impose some appropriate boundary or regularity condition in the interior of the spacetime, the on-shell solution of the equations of motion will be uniquely determined in terms of the asymptotic boundary data, so the on-shell

[14] An extended version of this formalism for Lifshitz was introduced in [82, 83], but as we work in the frame formalism, we can work simply with an adapted version of the original formalism with a single dilatation operator.

action is a function of the boundary data, which we can write as a boundary term,

$$S = \int d^{d-1}x\sqrt{-\gamma}\lambda(e^{(A)}, \psi). \tag{2.160}$$

We can then think of the canonically conjugate momenta as determined by functional derivatives of this action as in a Hamilton-Jacobi approach, so

$$T^A{}_B = \frac{1}{\sqrt{-\gamma}} e_\alpha^{(A)} \frac{\delta}{\delta e_\alpha^{(B)}} S, \tag{2.161}$$

$$\pi_\psi = \frac{1}{\sqrt{-\gamma}} \frac{\delta}{\delta \psi} S. \tag{2.162}$$

For the action (2.5), this gives $T_{AB} = \pi_{AB} + 2\pi_A A_B$, where $\pi_{AB} = K_{(AB)} - K g_{AB}$. The leading scaling of ψ is r^{Δ_-}, so if we define the dilatation operator

$$\delta_D = -\int d^{d_s+2}x \left(z e_\alpha^{(+)} \frac{\delta}{\delta e_\alpha^{(+)}} + (2-z) e_\alpha^{(-)} \frac{\delta}{\delta e_\alpha^{(-)}} + e_\alpha^{(I)} \frac{\delta}{\delta e_\alpha^{(I)}} - \Delta_- \psi \frac{\delta}{\delta \psi} \right). \tag{2.163}$$

then acting on any function of e^A, ψ, this will agree with the radial derivative at leading order in large r, $\delta_D \sim r\partial_r$. Applying this operator to the action, we have

$$(d_s + 2 - \delta_D)\lambda = z T^+{}_+ + (2-z) T^-{}_- + T^I{}_I - \Delta_- \psi \pi_\psi. \tag{2.164}$$

Now we look for a solution in an expansion in dilatation eigenvalues Δ. Any function of the boundary data will be by construction an eigenfunction of this dilatation operator, so it will contribute only at one order in the expansion in dilatation eigenvalues. We would then want to expand the action, and hence $T^A{}_B$, π_ψ, in an expansion in eigenfunctions of the dilatation operator. Because of the coincidences in the powers noted in our linearised analysis, there will be some degenerate eigenvalues, and λ does not actually have an expansion in terms of eigenfunctions; the dilatation operator δ_D is not diagonalisable, but can only be written in a Jordan normal form. This corresponds to the appearance of the logs in the expansion in powers of r in e.g. (2.41).[15]. However, the first such degenerate eigenvalue occurs at $\Delta = d_s + 2$, where the dilatation eigenvalue expansion first makes a finite contribution to the action. Thus, for the purposes of

[15]Similar logarithms appear in the Lifshitz case for z=2 [84, 85]; for Schrödinger they occur for arbitrary z

considering the terms that contribute to divergences in the on-shell action, we can expand

$$\lambda = \sum_{d_s+2>\Delta\geq 0} \lambda^{(\Delta)} + \ldots, \qquad \delta_D \lambda^{(\Delta)} = \Delta \lambda^{(\Delta)}. \tag{2.165}$$

where $\ldots$ represents terms of higher order which will include logarithms.

Let us now set the source for the irrelevant operator $\psi = 0$. Expanding in dilatation eigenvalues, (2.164) then becomes

$$\begin{aligned}(d_s + 2 - \Delta)\lambda^{(\Delta)} =& z T^{+}{}_{+}{}^{(\Delta)} + (2-z) T^{-}{}_{-}{}^{(\Delta)} + T^{I}{}_{I}{}^{(\Delta)} \\ =& (4-2z)\pi^{(\Delta)}_{--} + 4\pi^{(\Delta)}_{+-} + 2\pi^{I}{}_{I}{}^{(\Delta)} + z\alpha\pi^{(\Delta)}_{-}\end{aligned} \tag{2.166}$$

Expanding the constraint equation (2.153) in dilatation eigenvalues will enable us to evaluate the RHS of (2.166) in terms of the sources and terms at lower orders in the dilatation expansion. The expansion of (2.153) gives

$$\begin{aligned}&\sum_{s<\Delta/2}\left[2K^{(s)}K^{(\Delta-s)} - 2K^{(s)}_{(AB)}K^{AB(\Delta-s)} - \pi^{(s)}_{A}\pi^{A(\Delta-s)} - \frac{1}{m^2}(\nabla_A\pi^A)^{(s)}(\nabla_B\pi^B)^{(\Delta-s)}\right] \\ &+\left[K^{(\Delta/2)2} - K^{(\Delta/2)}_{(AB)}K^{AB(\Delta/2)} - \frac{1}{2}\pi^{(\Delta/2)}_{A}\pi^{A(\Delta/2)} - \frac{1}{2m^2}(\nabla_A\pi^A)^{(\Delta/2)}(\nabla_B\pi^B)^{(\Delta/2)}\right] = src^{(\Delta)},\end{aligned} \tag{2.167}$$

where $src^{(\Delta)}$ is the source contribution from the RHS of (2.153) which is calculated below in (2.172) and following. The terms in the sum at $s = 0$, together with one term at $s = \Delta_-$, will give us the RHS of (2.166). To see this, we need the values of the leading terms in the expansion in dilatation eigenvalues. These are determined by the assumed leading asymptotics of the bulk fields (2.17). We have

$$K^{+}{}_{+}{}^{(0)} = z, \quad K^{-}{}_{-}{}^{(0)} = 2 - z, \quad K^{I}{}_{J}{}^{(0)} = \delta^{I}{}_{J}. \tag{2.168}$$

For the vector momentum we have

$$\pi^{(0)}_{+} = \alpha K^{+}{}_{+}{}^{(0)} = z\alpha, \quad \pi^{(0)}_{-} = 0. \tag{2.169}$$

From this we can calculate that

$$T^{A}{}_{B}{}^{(0)} = -(d_s + 4)\delta^{A}{}_{B}, \tag{2.170}$$

which is encouraging, as it indicates that this can arise as the functional derivative of a simple constant term, $\lambda^{(0)} = -(d_s + 4)$. More importantly, (2.166) can now be combined with (2.167) to give

$$\begin{aligned}(d_s + 2 - \Delta)\lambda^{(\Delta)} = &- src^{(\Delta)} \\ &+ \sum_{s<\Delta/2, s\neq 0} \left[-2K^{(s)}_{(AB)} \pi^{AB(\Delta-s)} - \pi^{(s)}_A \pi^{A(\Delta-s)} - \frac{1}{m^2} (\nabla_A \pi^A)^{(s)} (\nabla_B \pi^B)^{(\Delta-s)} \right] \\ &+ \left[-K^{(\Delta/2)}_{(AB)} \pi^{AB(\Delta/2)} - \frac{1}{2} \pi^{(\Delta/2)}_A \pi^{A(\Delta/2)} - \frac{1}{2m^2} (\nabla_A \pi^A)^{(\Delta/2)} (\nabla_B \pi^B)^{(\Delta/2)} \right]\end{aligned} \tag{2.171}$$

Now let's consider the $src^{(\Delta)}$. We have

$$src = R - 2\Lambda - \frac{1}{4} F_{AB} F^{AB} - \frac{m^2}{2} A_A A^A. \tag{2.172}$$

Since we are going to turn ψ off, $A_A A^A = 0$, and F_{AB} becomes

$$F_{AB} = 2\Omega_{AB}{}^{+} A_{+}. \tag{2.173}$$

The Ricci scalar is

$$R = -4\partial_A \Omega_C{}^{AC} + \Omega_{CAD}\Omega^{CAD} + 2\Omega_{CAD}\Omega^{DAC} + 4\Omega_{AD}{}^{A}\Omega_C{}^{DC}, \tag{2.174}$$

which has contributions at $\Delta = 2, 4 - 2z, 6 - 4z$, while F^2 contributes at just $4 - 2z$ and $6 - 4z$. Thus only -2Λ contributes to $src^{(0)}$. At $\Delta = 2$ we have

$$\begin{aligned}src^{(2)} = &- 4\partial_+ \Omega_{A-}{}^{A} - 4\partial_- \Omega_{A+}{}^{A} - 4\partial_I \Omega_A{}^{IA} + 2\Omega_{IJ}{}^{+}\Omega^{IJ-} + \Omega_{IJK}\Omega^{IJK} \\ &+ 4\Omega_{+IJ}\Omega_-{}^{IJ} + 4\Omega_{-I}{}^{+}\Omega_+{}^{I-} + 4\Omega_{+I}{}^{+}\Omega_-{}^{I-} + 2\Omega_{+-I}\Omega_{-+}{}^{I} + 4\Omega_{+-}{}^{+}\Omega_{-+}{}^{-} \\ &+ 4\Omega_{A+}{}^{B}\Omega_{B-}{}^{A} + 2\Omega_{AI}{}^{B}\Omega_B{}^{IA} + 8\Omega_{A+}{}^{A}\Omega_{B-}{}^{B} + 4\Omega_{AI}{}^{A}\Omega_B{}^{IB},\end{aligned} \tag{2.175}$$

where A, B are taken to run over $+, -$ and all of the I directions. And for $4 - 2z$ we find

$$\begin{aligned}src^{(4-2z)} = &- 4\partial_- \Omega_{A-}{}^{A} - \Omega_{IJ}{}^{+}\Omega^{IJ+} - 4\Omega_{+I}{}^{+}\Omega_-{}^{I+} - 2\Omega_{+-}{}^{+}\Omega_{-+}{}^{+} \\ &+ 4\Omega_{-I}{}^{+}\Omega_-{}^{I-} + 2\Omega_{-IJ}\Omega_-{}^{IJ} + 2\Omega_{A-}{}^{B}\Omega_{B-}{}^{A} + 4\Omega_{A-}{}^{A}\Omega_{B-}{}^{B} \\ &- \alpha^2 \left(-2(\Omega_{+-}{}^{+})^2 + 4\Omega_{+I}{}^{+}\Omega_-{}^{I+} + \Omega_{IJ}{}^{+}\Omega^{IJ+} \right).\end{aligned} \tag{2.176}$$

Lastly for $6-4z$ we have

$$src^{(6-4z)} = \left(-2-2\alpha^2\right)\Omega_{-I}{}^{+}\Omega_{-}{}^{I+}. \tag{2.177}$$

For $z<3/2$ this is a positive eigenvalue and we can allow this term, but for $z>3/2$ it is negative, so we need to restrict the sources so that $\hat{e}^+\wedge d\hat{e}^+=0$, so that $src^{(6-4z)}=0$.

Thus, the source terms will produce contributions to $\lambda^{(\Delta)}$ at $\Delta=2,4-2z$ and for $z<3/2$ at $\Delta=6-4z$. These in turn generate terms in $T^A{}_B$, which we should substitute in the quadratic terms in (2.171) to obtain further contributions to λ. There are two issues to note here.

The first is that some of the expressions for $K^A{}_B$ in terms of $\hat{e}^A$ involve explicit positive powers of r, so in attempting to solve in a power series in r, one might be concerned that having a solution for $K^A{}_B$ in positive powers of r might not necessarily imply that the solution for $\hat{e}^A$ only involved positive powers of r. But by solving first for λ and then determining $T^A{}_B$ from it, we avoid this issue. When we functionally differentiate λ, we pick up a contribution to the dilatation eigenvalue from the different scalings of the different e^A, so

$$\begin{aligned}\lambda^{(\Delta)} \to & T^{+}{}_{+}{}^{(\Delta)},\quad T^{-}{}_{-}{}^{(\Delta)},\quad T^{I}{}_{J}{}^{(\Delta)},\quad T^{+}{}_{I}{}^{(\Delta+1-z)},\quad T^{-}{}_{I}{}^{(\Delta+z-1)},\\ & T^{I}{}_{+}{}^{(\Delta+z-1)},\quad T^{I}{}_{-}{}^{(\Delta+1-z)},\quad T^{+}{}_{-}{}^{(\Delta+2-2z)},\quad T^{-}{}_{+}{}^{(\Delta+2z-2)}.\end{aligned} \tag{2.178}$$

The terms where $K^A{}_B$ in terms of $\hat{e}^A$ involve explicit positive powers of r correspond to those where the functional derivative increases the dilatation eigenvalue. So if we have an expansion in positive powers of r for λ, it will imply that there is a solution for $\hat{e}^A$ only involving positive powers of r.

Contrariwise, one might be concerned that the functional derivative can also lower the dilatation eigenvalue in (2.178), for $T^{+}{}_{-}$, $T^{+}{}_{I}$ and $T^{I}{}_{-}$. This could lead to contributions to these $T^A{}_B$ with negative dilatation eigenvalues appearing from terms in λ with positive dilatation eigenvalues. This could lead to contributions in the sum over quadratic terms in (2.171) with negative eigenvalues, invalidating our assumption that the sum in λ involves only positive eigenvalues. For example, differentiating $src^{(6-4z)}$ looks like it could lead to a contribution in $T^{+}{}_{-}$ of eigenvalue $8-6z$, which is negative for $z>4/3$. There is an elegant argument that such a term cannot arise: the stress tensor contribution obtained by this functional derivative is a function of the boundary data, and is a scalar under boundary diffeomorphisms. Any scalar function of the

e^A_α can be expressed in terms of the Ricci rotation coefficients $\Omega_{AB}{}^C$, and there is no combination of these coefficients that has this dilatation eigenvalue. Hence the functional derivatives that would give these terms must actually vanish.

It is nice to see this more explicitly however, so we will give the calculation in a couple of cases. We find $T^A{}_B$ from varying with respect to the frame field as in (2.161), with S as in (2.160). Since the integrand of S contains a factor of $\sqrt{-\gamma}$ we first compute the frame field variation of this term, finding

$$e^{(A)}_\alpha \int \frac{\delta}{\delta e^{(B)}_\alpha}\sqrt{-\gamma} = -\sqrt{-\gamma}\delta^A{}_B. \tag{2.179}$$

Next, since src terms consist of factors of $\Omega_{AB}{}^C$ or $e^\alpha_{(A)}\partial_\alpha$, we work out their variations; functions f are included in these generic expressions to keep track of derivatives in integration by parts. For ∂_C we have

$$e^{(A)}_\alpha \int \frac{\delta}{\delta e^{(B)}_\alpha} f_1 e^\beta_{(C)}\partial_\beta f_2 = -f_1 e^{(A)}_\alpha e^\alpha_{(C)} e^\beta_{(B)}\partial_\beta f_2 = -f_1\delta^A_C\partial_B f_2. \tag{2.180}$$

For variations of Ω we find

$$e^{(D)}_\gamma \int \frac{\delta\Omega_{AB}{}^C}{\delta e^{(E)}_\gamma} f = 2\Omega_{E[A}{}^C\delta^D_{B]}f + \delta^C_E\delta^D_{[A}\partial_{B]}f + \delta^C_E\delta^D_{[A}(\partial_\alpha e^\alpha_{B]})f + f\delta^C_E\Omega_{AB}{}^D, \tag{2.181}$$

where $[AB] = \frac{1}{2}(AB - BA)$.

Using these results we can now quickly compute the contribution to $T^A{}_B$ coming from $src^{(6-4z)}$. We find that all of the potentially negative contributions ($T^+{}_-$, $T^+{}_I$ and $T^I{}_-$) actually vanish identically. Considering then the $src^{(4-2z)}$ term, we find this leads to

$$T^{+(6-4z)}_- \propto -4\left(1+\alpha^2\right)\left(\delta\Omega_{+I}{}^+\right)\Omega_-{}^{I+} + 4\Omega_-{}^{I+}\left(\delta\Omega_{-I}{}^-\right) \propto -4\alpha^2\Omega_-{}^{I+}\Omega_{-I}{}^+. \tag{2.182}$$

As predicted by the general argument, the only possible term is quadratic in $\Omega_{-I}{}^+$. So if $z > 3/2$, where we set this term to zero, no contributions are left. For $z < 3/2$, $T^+{}_-$ does indeed receive this contribution at $\Delta = 6 - 4z$; the contribution is however unproblematic there because it is still at a positive Δ.

The story for $T^+{}_I$ is similar; all terms remaining after the variation have a factor of $\Omega_{-I}{}^+$.

We have

$$T_I^{+(5-3z)} \propto -4\frac{\partial_-\sqrt{-\gamma}}{\sqrt{-\gamma}}\left(\delta\Omega_{+-}{}^{+}+\delta\Omega_{J-}{}^{J}\right)-4(1+A_+^2)\Omega_-{}^{J+}\delta\Omega_{+J}{}^{+}-4(1+A_+^2)\Omega_{+-}{}^{+}\delta\Omega_{-+}{}^{+}$$
$$+4\Omega_-{}^{K}{}_{J}\delta\Omega_{-K}{}^{J}+4\Omega_{+-}{}^{+}\delta\Omega_{+-}{}^{+}+4\Omega_{J-}{}^{+}\delta\Omega_{+-}{}^{J}+4\Omega_{K-}{}^{J}\delta\Omega_{J-}{}^{K} \tag{2.183}$$
$$+8\Omega_{A-}{}^{A}\delta\Omega_{+-}{}^{+}+8\Omega_{A-}{}^{A}\delta\Omega_{J-}{}^{J}.$$

Many of the terms here are already multiplied by an $\Omega_{-I}{}^{+}$. We need only compute two explicitly:

$$\delta\Omega_{+-}{}^{+}=-\Omega_{I-}{}^{+}, \tag{2.184}$$
$$\delta\Omega_{K-}{}^{J}=\delta_I^J\Omega_{K-}{}^{+}. \tag{2.185}$$

All terms in $T_I^{+(5-3z)}$ coming from $src^{(4-2z)}$ have a factor of $\Omega_{-I}{}^{+}$. As in the previous case, for $z>3/2$ this vanishes. For $z<3/2$, $5-3z>0$, and so all of these contributions are at positive Δ and thus not a concern.

For $T^I{}_-$ we find similarly

$$T_-^{I(5-3z)} \propto -2(1+A_+^2)\Omega^{JK+}\delta\Omega_{JK}{}^{+}-4(1+A_+^2)\Omega_-{}^{J+}\delta\Omega_{+J}{}^{+}+4\Omega_-{}^{J+}\delta\Omega_{-J}{}^{-}. \tag{2.186}$$

Using

$$\delta\Omega_{JK}{}^{+}=2\Omega_{-[J}{}^{+}\delta^I_{K]}, \tag{2.187}$$

we again find that every term in $T_-^{I(5-3z)}$ coming from $src^{(4-2z)}$ has a factor of $\Omega_{-I}{}^{+}$.

Thus, to summarise, there is a solution for λ in a series of positive dilatation eigenvalues Δ. Taking functional derivatives of this solution gives the expression for T^A_B in an expansion in dilatation eigenvalues, which can be used to reconstruct e^A_α in an expansion in positive powers of r which satisfies the equations of motion (with logarithmic terms appearing in the expansion from order r^{d_s+2} onwards, corresponding to the degenerate eigenvalues in the Δ expansion). The terms in the Δ expansion of λ with $\Delta<d_s+2$ are the divergent contributions to the bare action so we also see that we can cancel these terms by adding local functions of the boundary data as boundary counterterms to the action. We can explicitly check that the required counterterms are local functions of the boundary data by solving for the dilatation expansion coefficients $\lambda^{(\Delta)}$ explicitly. To do this one can insert covariant dilatation expansions of the canonical momenta into the equations of motion (2.150) and the constraints (2.152) [80]. Solving for the dilatation

coefficients this way is much more difficult in our case owing to the off-diagonal structure of the metric in our chosen frame basis. To verify that the boundary counterterms are local thus requires a more complete analysis than that we have carried out here. We leave this interesting question for future work.

2.6 Discussion

We have shown that one can construct a holographic dictionary for $z < 2$ Schrödinger along very similar lines to the one constructed for Lifshitz in [45]. This dictionary is based on classifying fields in terms of the anisotropic scaling symmetry of the Schrödinger background, unlike some previous explorations of holography for Schrödinger which have interpreted it as a deformation of AdS and focused on the relativistic scaling symmetry of the AdS solution. We have shown that in this formalism there is an asymptotic expansion for arbitrary boundary data (assuming we set the sources for irrelevant operators to zero) and the subleading terms in this expansion are all determined locally in terms of the sources.

The most important direction for future work is to extend this analysis to $z = 2$, and we address this in the following chapter. As stressed in the introduction, in our frame formalism it is clear that the structure of the dictionary for $z = 2$ will be qualitatively different from $z < 2$. As already noted in [35], the dimensions of operators for $z = 2$ depend on the momentum k_ξ. We interpret this as meaning that the dual theory will live just in the $t, \vec{x}$ directions, and modes of different k_ξ correspond to different operators in this theory. This will imply a different structure for the dictionary; but we expect the frame formalism will still be useful for organising the bulk modes naturally in terms of the sources for the boundary geometry seen by the field theory, and we expect it will be possible to give an asymptotic expansion at least for arbitrary sources for the $k_\xi = 0$ operators.

3 Schrödinger Holography with $z = 2$

The work in this chapter is reproduced from a collaborative paper [2] with Dr. Tomas Andrade, Dr. Cindy Keeler and Prof. Simon Ross. We investigated holography for asymptotically Schrödinger spacetimes, using a frame formalism based on the anisotropic scaling symmetry. We build on the results of the previous chapter for $z < 2$ to propose a dictionary for $z = 2$ case. For $z = 2$, the scaling symmetry does not act on the additional null direction, which implies that in our dictionary it does not correspond to one of the field theory directions. This is significantly different from previous analyses based on viewing Schrödinger as a deformation of AdS. We study this dictionary in the linearised theory and in an asymptotic expansion. We show that a solution exists in an asymptotic expansion for arbitrary sources for the relevant operators in the stress energy complex.

3.1 Introduction

In this chapter we consider constructing a holographic dictionary for asymptotically locally Schrödinger spacetimes with $z = 2$, thus extending the work of the previous chapter beyond the $z < 2$ regime considered there. The analysis in this chapter thus follows very closely that undertaken in chapter 2; we consider the same massive vector model and impose the same gauge choices that we made there. Consequently the requisite review material for this chapter is already presented in chapter 2. However, for completeness, we briefly recall the key points of this review below.

Recalling from the previous chapter, the metric for a $(d_s + 3)$-dimensional Schrödinger spacetime is,

$$ds^2 = -\frac{dt^2}{r^{2z}} + \frac{2dtd\xi + d\vec{x}_{d_s}^2 + dr^2}{r^2}, \tag{3.1}$$

where the boundary lies at $r \to 0$ and the number of spatial boundary dimensions is d_s. The isometry $t \to \lambda^z t$, $x \to \lambda x$, $\xi \to \lambda^{2-z}\xi$, $r \to \lambda r$ realises the anisotropic scaling symmetry, and there are isometries $\vec{x} \to \vec{x} + \vec{v}t$, $\xi \to \xi - \vec{v} \cdot \vec{x} - \frac{1}{2}v^2 t$, which realise the Galilean boost symmetry. Notably in this chapter, where we consider $z = 2$, we see that the scaling symmetry does not act on ξ.

As in the previous chapter, our aim is to formulate a holographic dictionary for asymptotically locally Schroedinger spacetimes with $z = 2$, based on the anisotropic scaling symmetry, using a frame formalism as in the Lifshitz case [41, 45]. For $z = 2$, focusing on the anisotropic scaling symmetry gives a qualitatively different dictionary to the dictionary constructed in the previous chapter. In the relativistic theory, the usual scaling symmetry acts non-trivially on all the boundary coordinates, so one thinks of the dual as living in the $(t, \xi, \vec{x})$ space. Bulk fields are dual to local operators $\mathcal{O}(t, \xi, \vec{x})$. The anisotropic scaling, by contrast, does not act on the ξ direction. Furthermore, as has been known since [42], the asymptotic behaviour of bulk fields, and hence the scaling dimension of dual operators, depends on k_ξ. (Some of these will be irrelevant operators, whose sources we must either set to zero, or deal with perturbatively) Hence if we want to focus on the anisotropic scaling symmetry, the natural dual is a field theory living in the $(t, \vec{x})$ space, with local operators $\mathcal{O}_{k_\xi}(t, \vec{x})$. To relate bulk fields holographically to these operators, we need to expand the bulk fields in Fourier modes in the ξ direction.[16] The situation

[16]For scalar fields, this is a straightforward Fourier expansion. For tensor fields, we also need to perform a decomposition into components along ξ and in the transverse space. This is complicated by the null nature of ξ in the background (3.1), as we discuss below.

is analogous to $AdS_2 \times \mathbb{R}^d$ backgrounds, where the dual is a theory with local operators $\mathcal{O}_k(t)$ whose dimensions depending on momentum in the spatial directions [86]. The limit as $z \to 2$ from below is analogous to the $z \to \infty$ limit of Lifshitz, which gives the $\mathrm{AdS}_2 \times \mathbb{R}^d$ geometry.

As we remarked in the previous chapter, the ξ direction is at least asymptotically null, so we cannot decompose the metric in a standard Kaluza-Klein reduction. However, since our boundary conditions are naturally formulated in terms of frame fields, we can decompose these into their component along $d\xi$ and their components along the remaining boundary directions. The key distinction between the holographic dictionary for $z = 2$ will be then that the zero-modes (under ∂_ξ) in the leading terms in the frame fields in the bulk will be interpreted as sources for the stress energy complex in the non-relativistic field theory living in just the $(t, \vec{x})$ directions, and not the ξ directions. We will therefore primarily focus on understanding holography for $z = 2$ for the sector with $k_\xi = 0$, that is, for ξ-independent sources. This class includes arbitrary sources for the stress energy complex in the non-relativistic field theory.

As in chapter 2 we consider the metric (3.1) as a solution of the massive vector theory introduced in [42], whose action we recall is given by

$$S = -\frac{1}{16\pi G}\int d^{d_s+3}x\sqrt{-g}\left(R - 2\Lambda - \frac{1}{4}F_{\mu\nu}F^{\mu\nu} - \frac{1}{2}m^2 A_\mu A^\mu\right) - \frac{1}{8\pi G}\int d^{d_s+2}x\sqrt{-h}K, \quad (3.2)$$

with

$$m^2 = z(z + d_s), \quad \Lambda = -\frac{(d_s+2)(d_s+1)}{2}. \quad (3.3)$$

Again, d_s labels the number of boundary spatial directions. The equations of motion that follow are

$$R_{\mu\nu} - \frac{1}{2}Rg_{\mu\nu} + \Lambda g_{\mu\nu} = \frac{1}{2}\left(F^\rho{}_\mu F_{\rho\nu} - \frac{1}{4}F^2 g_{\mu\nu}\right) + \frac{m^2}{2}\left(A_\mu A_\nu - \frac{1}{2}A^2 g_{\mu\nu}\right), \quad (3.4)$$

$$\nabla_\mu F^{\mu\nu} = m^2 A^\nu. \quad (3.5)$$

The metric (3.1) is a solution of (3.4), (3.5) supported by the matter field

$$A = \alpha r^{-z}dt, \quad \alpha = \sqrt{\frac{2(z-1)}{z}}. \quad (3.6)$$

We will henceforth set $z = 2$, which implies $\alpha = 1$.

Once again we choose a set of frame fields e^A, $A = +, -, I, r$ such that the metric is

$$ds^2 = g_{AB}e^A e^B = -e^+e^+ + 2e^+e^- + e^I e^I + e^r e^r. \tag{3.7}$$

In the background (3.1) at $z = 2$, $e^+ = r^{-2}dt$, $e^- = d\xi$, $e^I = r^{-1}dx^i$, so that each of the frame fields has a well-defined scaling with r at small r, near the boundary. We adopt exactly the same choice of gauge for the frame fields and the matter field as seen in the previous chapter. These comprise a radial gauge choice $e^r = r^{-1}dr$, and the further restriction that the vector field can be written as,

$$A = e^+ + \psi e^- + s_r e^r, \tag{3.8}$$

where ψ is the single scalar degree of freedom in the boundary conditions for the matter field and s_r labels the radial component of the field which is left arbitrary here. Again, we will find that the operator dual to ψ is irrelevant, so we always set the source part to zero.

In the previous chapter, a spacetime was defined to be asymptotically locally Schrödinger if the metric and massive vector can be written as in (3.7, 3.8) with

$$e^+ = r^{-z}\hat{e}^+, \quad e^- = r^{z-2}\hat{e}^-, \quad e^I = r^{-1}\hat{e}^I, \tag{3.9}$$

and the scalar $\psi = r^{\Delta_-}\hat{\psi}$ for some exponent Δ_-, where the fields $\hat{e}^A, \hat{\psi}$ are arbitrary functions of $t, \xi, \vec{x}, r$ with finite limits as $r \to 0$. Note we do not directly impose a boundary condition on s_r, since it does not represent an independent degree of freedom; it is determined algebraically by the other components.

This definition requires modification for the case of $z = 2$. As we argued above, we think of the dual field theory as living in just the $t, \vec{x}$ directions. As a result, it is just the Fourier zero modes of the frame fields that we expect to provide geometrical boundary data, that is the sources for the dual stress tensor complex living in the $t, \vec{x}$ directions. We therefore say that a spacetime is *asymptotically locally Schrödinger* for $z = 2$ if the Fourier zero modes of the frame fields satisfy

$$e^+_{k_\xi=0} = r^{-2}\hat{e}^+, \quad e^-_{k_\xi=0} = \hat{e}^-, \quad e^I_{k_\xi=0} = r^{-1}\hat{e}^I. \tag{3.10}$$

The non-zero modes of the frame fields will have fall-offs that depend on the momentum k_ξ in the ξ direction (we will see this explicitly in the linearised analysis in section 3.2). These will be dual to some additional tensor operators in the field theory. We do not make any assumption

about the boundary conditions for these fields in defining our asymptotically locally Schrödinger boundary conditions, but clearly some of them will be irrelevant operators, and to satisfy our boundary condition (3.10) we will need to set the sources for the irrelevant operators to zero.

In section 3.1.1, we discuss the analogue of Kaluza-Klein reduction in our frame formalism. In section 3.1.2, we review the structure of the stress energy complex for non-relativistic theories. In section 3.2 we set up the linearised analysis around the Schrödinger solution for $z = 2$ in general dimensions. Section 3.3 discusses the case of two boundary spatial dimensions, $d_s = 2$, identifying the linearised modes with sources and vevs for the stress energy complex. Section 3.4 discusses the special case $d_s = 0$, including its degenerate Ward identities, and compares it to previous work. In section 3.5, we discuss the asymptotic expansion for $z = 2$, and show that a solution can be obtained in an expansion in powers of r,[17] and that all divergences in the action can be eliminated by adding boundary counterterms which are local functions of the boundary data. We summarise and discuss future directions in section 3.6.

3.1.1 Kaluza-Klein decomposition

Since we want to relate the bulk theory to a boundary theory living just in the $t, \vec{x}$ directions, it is useful to set up a decomposition of the bulk fields in the analogue of Kaluza-Klein reduction on the ξ direction. It is natural to decompose the frame fields as

$$\hat{e}^A = \hat{e}^A_a dx^a + \hat{e}^A_\xi d\xi, \tag{3.11}$$

where a runs over t, x^i. This decomposition is the analogue in our frame language of the Kaluza-Klein decomposition of the metric. Each of these components should then be expanded in Fourier components with respect to ξ.

In the bulk, there are diffeomorphisms which preserve our choice of radial gauge, generated by the vector field

$$\chi = \chi^\alpha \partial_\alpha + \sigma r \partial_r - \frac{1}{2} r^2 \partial_i \sigma \partial_i - \frac{1}{2} r^2 \partial_\xi \sigma \partial_t - \frac{1}{2}(r^2 \partial_t \sigma + \ln r \partial_\xi \sigma)\partial_\xi, \tag{3.12}$$

where χ^α, σ are functions of the boundary coordinates $t, \vec{x}, \xi$. We use α to denote all nonradial

[17] In our analysis, this is traded for an expansion in eigenvalues of a suitable dilatation operator, but the existence of a dilatation expansion implies the existence of an expansion in powers of r, since each term in the dilatation expansion has an expansion in positive powers of r.

spacetime coordinates; thus α runs over t, x^i, ξ. These generate the diffeomorphisms χ^α of the boundary coordinates, which act on the boundary frame fields by the Lie derivative $\delta\hat{e}^A = \mathcal{L}_\chi \hat{e}^A$, and an anisotropic Weyl transformation σ on the boundary, which acts as $\delta\hat{e}^+ = 2\sigma\hat{e}^+, \delta\hat{e}^- = 0, \delta\hat{e}^I = \sigma\hat{e}^I$. In the context of our Kaluza-Klein decomposition, it is natural to decompose χ^α and σ in Fourier modes in ξ. The zero modes in the Fourier decomposition of χ^a, σ correspond to diffeomorphisms and a Weyl transformation of the field theory background, while that of χ^ξ is naturally interpreted as a gauge transformation of the vector $\hat{e}_a^-$, ensuring that the dual operator is indeed a conserved current.

For the non-zero modes, in a Kaluza-Klein reduction the usual approach is to gauge-fix them. That is, since we are singling out a direction to reduce along, it is natural to use a formalism which is covariant in the lower dimensional space, but where we fix symmetries which depend on the additional direction. In the usual Kaluza-Klein reduction, where we split the metric into a lower-dimensional metric, vector field and scalar, the usual gauge fixing is to set the non-zero modes of the vector and scalar to zero, so that the physical content is a massive tensor field. Analogously, in our frame based description, we will gauge fix the diffeomorphisms χ^α by setting the non-zero modes of $\hat{e}_\xi^A$ to zero. That is, we use the diffeomorphism symmetry to make the components along the extra dimension constant in ξ. We also have non-zero modes in the Weyl scaling σ, but we will not gauge fix this as the scaling symmetry may develop an anomaly.

The zero modes of $\hat{e}_a^A$ for $A = +, I$ then define the boundary geometry, which provides a background for the dual field theory living in the $t, \vec{x}$ directions, and will correspond to the sources for the stress complex in the field theory, which will be reviewed in the next subsection. The zero mode of $\hat{e}_a^-$ is a one-form vector field which provides the source for the conserved current associated to particle number. The zero modes of $\hat{e}_\xi^A$, which were interpreted as geometrical in the relativistic context, and in our previous discussion for $z < 2$, are in this decomposition instead just sources for additional scalar operators, as is $\hat{\psi}$.[18] After the gauge-fixing above, the non-vanishing components for the ξ-dependent modes are the $\hat{e}_a^A$, which are sources for additional massive vector operators in the dual field theory, with k_ξ-dependent dimensions. Our analysis will focus mainly on the zero-modes, as in the usual Kaluza-Klein decomposition.

[18]The $\hat{e}_\xi^I$ are sources for operators which are scalars under coordinate transformations, but vectors under frame rotations.

3.1.2 Stress energy complex

We reviewed the structure of the stress energy complex in a non-relativistic theory in chapter 2.[19] We present the important observations again here. In a non-relativistic theory the components of the stress energy complex satisfy the conservation equations,

$$\partial_t \mathcal{E} + \partial_i \mathcal{E}^i = 0, \tag{3.13}$$

$$\partial_t \mathcal{P}_i + \partial_j \Pi_i^j = 0. \tag{3.14}$$

$$\partial_t \rho + \partial_i \rho^i = 0. \tag{3.15}$$

Where we recall that $\mathcal{E}$ is the energy density, $\mathcal{E}^i$ is the energy flux, $\mathcal{P}_i$ is momentum density, Π_{ij} is the spatial stress tensor, ρ is particle number and finally ρ^i is particle number flux (we recall that the particle number is conseved in a Schrödinger theory). The scale invariance for $z = 2$ implies $2\mathcal{E} + \Pi_i^i = 0$. $\mathcal{E}$ has dimension $2 + d_s$, which implies $\mathcal{E}^i$ has dimension $3 + d_s$, and $\mathcal{P}_i$ has dimension $1 + d_s$, which implies Π_{ij} has dimension $2 + d_s$. The particle number has dimension zero, so its density ρ has dimension d_s, so ρ^i has dimension $1 + d_s$. In fact, in a non-relativistic theory $\rho^i = \mathcal{P}_i = \rho v^i$, where v^i is the local velocity of the particles, so ρ^i and $\mathcal{P}_i$ are not independent operators.

The sources for these operators are then the zero-mode components of the frame fields, $\hat{e}_a^A$: the components of $\hat{e}^+$ provide the sources for $\mathcal{E}, \mathcal{E}^i$; the components of $\hat{e}^-$ provide the sources for ρ, ρ^i; and the components of $\hat{e}^I$ provide the sources for $\mathcal{P}_i$, Π_i^j. We can think of $\mathcal{E}, \mathcal{E}^i$, $\mathcal{P}_i$, Π_i^j, as components of the non-symmetric tensor

$$T^a{}_B = \frac{1}{\sqrt{-h}} \frac{\delta}{\delta e_a^B} S. \tag{3.16}$$

The residual gauge symmetry (2.16) corresponds to the fact that there are not independent physical sources for $\mathcal{P}_i$ and ρ^i, while the symmetry under rotations of the $\hat{e}^I$ corresponds to the symmetricity of Π_{ij}.

There are scalar operators whose sources are $\hat{e}_\xi^A$. Because of the relation to the higher dimensional stress complex, it is natural to refer to these as $\mathcal{E}^\xi$, ρ^ξ, and $\mathcal{P}_i^\xi$ for $A = +, -, I$

[19] In the $z < 2$ discussion in the previous chapter, we were interested in the stress complex in a higher-dimensional spacetime with $t, \xi, \vec{x}$ coordinates, but here we are interested in a dual living just in $t, \vec{x}$, so the relevant stress tensor complex operators are those appearing in (3.13), (3.14), and (3.15) below.

respectively, but we stress again that these are not components of the stress complex in the dual field theory; they are just some scalar operators (with respect to coordinate transformations; $\mathcal{P}_i^\xi$ is a vector with respect to frame rotations). They have dimensions $4+d_s$, $2+d_s$, and $3+d_s$ respectively. The marginal dimension is $2+d_s$, so $\mathcal{E}^i$, $\mathcal{E}^\xi$ and $\mathcal{P}_i^\xi$ are irrelevant operators, and as we will see in the linearised analysis in the next subsection, so is the operator O_ψ dual to the scalar source ψ. For $z=2$ the asymptotic expansion only exists if we set the sources for all these operators to zero. For the scalar operators O_ψ, $\mathcal{E}^\xi$ and $\mathcal{P}_i^\xi$ we need to set the sources to zero by hand. This implies that of the frame fields, only e^- is allowed to have a leading component along $d\xi$. The only irrelevant operator in the stress tensor complex is $\mathcal{E}^i$. We can set its source to zero by adopting the irrotational condition we encountered in the previous chapter,

$$\hat{e}^+ \wedge d\hat{e}^+ = 0. \tag{3.17}$$

3.2 Linearised analysis: generalities

We now turn to a linearised analysis of the equations of motion (3.4,3.5) for $z=2$. This will enable us to confirm several of the features we have asserted in our discussion so far: we will see how the scaling behaviour of bulk fields depends on the momentum k_ξ, and we will see that the set of solutions for $k_\xi = 0$ has the expected structure to correspond to the stress tensor complex and its sources. In this section, we set up the general formalism. In the following two sections we will discuss $d_s = 2$ and $d_s = 0$ in detail.

The linearised version of our frame fields are, as before, given by (2.27),(2.28) and (2.29).

The linearised fields are then $\delta\hat{e}_\alpha^A$ and the ψ, s_r in (3.8). The zero modes in $\delta\hat{e}_a^A$ are assumed to represent sources for the corresponding components of the stress tensor complex. The zero modes in $\delta\hat{e}_\xi^A$ are sources for scalar operators.

The linearised version of the residual gauge symmetry (2.16) is $\delta\hat{e}_i^- \to \delta\hat{e}_i^- + \hat{\beta}^i$, $\delta\hat{e}_t^I \to \delta\hat{e}_t^I - \hat{\beta}^i$ (where $\beta^I = r\hat{\beta}^i$). This implies that the sources for $\mathcal{P}_i$ and ρ^i are not independent, as expected. The rotation symmetry of the e^I also implies that only the symmetric part of δe_j^I provide independent sources. The equations of motion are easier to discuss in the metric language, so we will resolve this gauge symmetry by passing back from the frame fields to the metric and vector for this linearised analysis.

In the metric language, the linearised perturbations are $h_{\mu\nu}$, a_μ. The linearised equations in

the metric language are as in [41][20]

$$\nabla_\mu f^{\mu\nu} - \nabla_\mu(h^{\mu\lambda}F_\lambda{}^\nu) - \nabla_\mu h^{\beta\nu}F^\mu_{\ \beta} + \frac{1}{2}\nabla_\lambda h F^{\lambda\nu} = m^2 a^\nu \tag{3.18}$$

and

$$\begin{aligned} R^{(1)}_{\mu\nu} = {} & \frac{2}{d-2}\Lambda h_{\mu\nu} + \frac{1}{2}f_{\mu\lambda}F_\nu{}^\lambda + \frac{1}{2}f_{\nu\lambda}F_\mu{}^\lambda - \frac{1}{2}F_{\mu\lambda}F_{\nu\sigma}h^{\lambda\sigma} - \frac{1}{2(d-2)}f_{\lambda\rho}F^{\lambda\rho}g_{\mu\nu} \\ & + \frac{1}{2(d-2)}F_{\lambda\rho}F_\sigma{}^\rho h^{\lambda\sigma}g_{\mu\nu} - \frac{1}{4(d-2)}F_{\lambda\rho}F^{\lambda\rho}h_{\mu\nu} + \frac{1}{2}m^2 a_\mu A_\nu + \frac{1}{2}m^2 a_\nu A_\mu, \end{aligned} \tag{3.19}$$

where $d = d_s + 3$ is the dimension of the spacetime, $f_{\mu\nu} = \partial_\mu a_\nu - \partial_\nu a_\mu$ and

$$R^{(1)}_{\mu\nu} = \frac{1}{2}g^{\lambda\sigma}[\nabla_\lambda\nabla_\mu h_{\nu\sigma} + \nabla_\lambda\nabla_\nu h_{\mu\sigma} - \nabla_\mu\nabla_\nu h_{\lambda\sigma} - \nabla_\lambda\nabla_\sigma h_{\mu\nu}]. \tag{3.20}$$

It is convenient to write

$$h_{tt} = r^{-4}H_{tt}, \qquad h_{t\xi} = r^{-2}H_{t\xi}, \qquad h_{\xi\xi} = H_{\xi\xi}, \tag{3.21}$$

$$h_{ti} = r^{-3}H_{ti} \qquad h_{\xi i} = r^{-1}H_{\xi i}, \qquad h_{ij} = r^{-2}H_{ij}, \tag{3.22}$$

$$a_r = r^{-1}s_r \qquad a_t = r^{-2}s_t \qquad a_\xi = s_\xi \qquad a_i = r^{-1}s_i. \tag{3.23}$$

Then a given linearised mode will contribute at the same order in r in all the different fields, and the power of r will correspond to the scaling dimension of the mode. The s_r here is the same as in (3.8), and the other fields are related to the linearised frame fields by

$$H_{tt} = -2\delta\hat{e}^+_t + 2r^2\delta\hat{e}^-_t, \quad H_{t\xi} = -r^{-2}\delta\hat{e}^+_\xi + \delta\hat{e}^-_\xi + \delta\hat{e}^+_t, \quad H_{\xi\xi} = 2r^{-2}\delta\hat{e}^+_\xi, \tag{3.24}$$

$$H_{ti} = -r^{-1}\delta\hat{e}^+_i + r\delta\hat{e}^-_i + r\delta\hat{e}^I_t, \quad H_{\xi i} = r^{-1}\delta\hat{e}^+_i + r^{-1}\delta\hat{e}^I_\xi, \quad H_{ij} = \delta\hat{e}^I_j + \delta\hat{e}^J_i, \tag{3.25}$$

$$s_t = \delta\hat{e}^+_t, \quad s_\xi = r^{-2}\delta\hat{e}^+_\xi + \psi, \quad s_i = r^{-1}\delta\hat{e}^+_i. \tag{3.26}$$

In (3.25) and where appropriate subsequently, the reader should understand $\delta\hat{e}^I_t$ in H_{ti} to stand for $\delta\hat{e}^I_t\delta_{Ii}$, where δ_{Ii} is the Kronecker delta, and similarly for other components with an i index.

[20]Note that $h_{\mu\nu}$ denotes the perturbation of the metric, and indices are raised and lowered with the background metric, so $h^{\mu\nu}$ is the perturbation of the metric with the indices raised, not the perturbation of the inverse metric.

3.2.1 Flux and inner product

We will identify the modes corresponding to components of the stress tensor by adopting the approach of [78], computing the symplectic flux at the boundary $r = 0$, and identifying the modes canonically conjugate to the sources with the vevs. The appropriate symplectic current for the Einstein-massive vector theory we are considering was worked out in [79]. It involves combining the usual gravitational symplectic current j^μ_g with an additional component from the massive vector field, j^μ_a:

$$j^\mu = j^\mu_g + j^\mu_a. \tag{3.27}$$

These are respectively given, as before, by (2.50), (2.51). Given the current, the symplectic flux through the boundary, $\mathcal{F}$, is by definition the pullback of the current to the surface $r = 0$. As usual, this is defined by evaluating the pullback at some cutoff surface $r = r_\epsilon$ and taking the limit $r_\epsilon \to 0$, so we write

$$\mathcal{F} = \lim_{r_\epsilon \to 0} \frac{i}{2} \int_{r=r_\epsilon} dt\, d^{d_s}x\, d\xi \sqrt{\gamma} n^\mu j_\mu, \tag{3.28}$$

where n_μ is the unit outward-pointing normal to the boundary.

We will also be interested in determining which linearised modes are normalizable, to determine which can be allowed to fluctuate in quantising the bulk theory. This requires us to define a suitable inner product. The inner product is usually defined in terms of the symplectic current by considering

$$(\{h_{\mathbf{1}}, a_{\mathbf{1}}\}, \{h_{\mathbf{2}}, a_{\mathbf{2}}\}) = \frac{i}{2} \int_\Sigma \star j(\{h_{\mathbf{1}}, a_{\mathbf{1}}\}, \{h_{\mathbf{2}}, a_{\mathbf{2}}\}), \tag{3.29}$$

where j is the symplectic current defined above, $\star$ is the Hodge dual and Σ is a spacelike surface. However, in the Schrödinger background, there is no natural spacelike surface to consider; Schrödinger is not stably causal and therefore has no global time function. (The level sets of a time function would have supplied a natural choice of Σ.)

We will take Σ to be a surface of constant t. We want to argue that this is a natural choice, as close as we can get to the usual construction in this case. The irrotational condition (3.17) ensures that even the perturbed spacetime has a foliation, and asymptotically this foliation will be described by a constant t surface. Also, although this surface is null in the background spacetime, linear perturbations satisfying our boundary conditions will generically render it timelike.[21] From

[21] The norm of the normal $n = dt$ is $n \cdot n = -r^4 H_{\xi\xi}$. The leading contribution to $H_{\xi\xi}$ comes from the source $\delta\hat{e}^+_\xi$ for $\mathcal{E}^\xi$, but this is set to zero by the boundary conditions. We will find in the linearised analysis below that the leading vev term is the particle number density, which is physically non-negative, so the normal becomes timelike

an initial condition perspective, the fact that constant t surfaces will continue to foliate the spacetime under perturbations makes them appealing. Given that they are null in the background, our remaining concern would be information which propagates 'parallel' to the constant t surfaces; that is, along the ξ direction. However, we work in Fourier modes with constant k_ξ, and moreover focus on the sector with $k_\xi = 0$ (even setting some $k_\xi \neq 0$ components to vanish via gauge choice). For the crude question we want to ask (for a given mode, is this inner product finite?) this seems sufficient.

On surfaces of constant t, the expression (3.29) simplifies to

$$(\{h_{\mathbf{1}}, a_{\mathbf{1}}\}, \{h_{\mathbf{2}}, a_{\mathbf{2}}\}) = \frac{i}{2} \int_{\Sigma_t} dr d^{d_s} x d\xi \sqrt{g} j^t (\{h_{\mathbf{1}}, a_{\mathbf{1}}\}, \{h_{\mathbf{2}}, a_{\mathbf{2}}\}). \tag{3.30}$$

3.3 Linearised analysis with spatial directions

We now specialise to the case with $d_s = 2$. (We will make some comments on differences for other values.) In this case, the analysis closely parallels the discussion for $z < 2$ in the previous chapter. The main difference is that dependence on the null direction ξ affects the linearised solutions at leading order, so that we need an independent discussion for the zero modes and the modes with non-zero k_ξ. The discussion of the zero modes is most interesting, both because this sector contains the stress energy complex of the dual field theory and because subtleties such as anomalies appear only in this sector.

As in the previous chapter, we are interested in identifying the modes corresponding to sources and vevs of dual operators. In many cases, this identification can be made simply using the scaling dimensions of the modes. Otherwise we use the flux to identify the vev as the mode canonically conjugate to the source following [78]. We consider first constant modes, independent of the boundary directions, to identify all sources and vevs, and then verify that they satisfy appropriate Ward identities in the non-constant cases.

We will discuss the case where the fields are independent of spatial coordinates x^i. The rotation symmetry in these directions is then unbroken, so we can decompose the linearised fields into a tensor, vector and scalar part with respect to this linearised symmetry. Below we will treat these initially for constant modes and then including dependence on t, ξ. To make this decomposition we should further decompose H_{ij} into a trace and a trace free part, $H_{ij} = k\delta_{ij} + \bar{H}_{ij}$,

unless the particle number density vanishes.

where $\bar{H}^i_i = 0$. The tensor mode is $\bar{H}_{ij}$. The vector modes are H_{ti}, $H_{\xi i}$ and s_i. The scalar modes are H_{tt}, $H_{t\xi}$, $H_{\xi\xi}$, k, s_t, s_ξ and s_r (the last is determined algebraically in terms of the other modes). We will always assume the t, ξ dependence is harmonic, $e^{i\omega t + ik_\xi \xi}$, so in writing equations we will make the replacements $\partial_t \to i\omega$, $\partial_\xi \to ik_\xi$.

The extension to include dependence on the x^i is a straightforward extension of the calculation for $z < 2$ carried out in chapter 2, so it is postponed to appendix A.

3.3.1 Tensor modes

The tensor equation of motion is

$$r^2 \bar{H}''_{ij} - 3r\bar{H}'_{ij} - (k_\xi^2 + 2k_\xi \omega r^2)\bar{H}_{ij} = 0. \tag{3.31}$$

This is simpler than the equation in the $z < 2$ case, so it can be solved in closed form for arbitrary k_ξ, ω. For $k_\xi = 0$, the solution is simply

$$\bar{H}_{ij} = \bar{H}^{(0)}_{ij} + \bar{H}^{(4)}_{ij} r^4, \tag{3.32}$$

corresponding to the source and vev for the trace free part of the spatial stress tensor Π_{ij}. For non-zero k_ξ, the solution is

$$\bar{H}_{ij} = \bar{H}^{(-)}_{ij} r^2 J_\nu(-i\sqrt{2k_\xi \omega} r) + \bar{H}^{(+)}_{ij} r^2 Y_\nu(-i\sqrt{2k_\xi \omega} r), \tag{3.33}$$

where J_ν and Y_ν are Bessel functions of the first and second kind and $\nu = \sqrt{4 + k_\xi^2}$. These modes are the source and vev for some tensor operator; the asymptotics $r^{2\pm\nu}$ tell us that this is an operator of dimension $2 + \nu$. This is an irrelevant operator for all $k_\xi > 0$.

3.3.2 Vector modes

The vector equations of motion are

$$r^2 s_i'' - 3r s_i' - [5 + k_\xi^2 + 2k_\xi \omega r^2] s_i + 2r H'_{\xi i} + 2H_{\xi i} = 0, \tag{3.34}$$

$$k_\xi [r(H'_{\xi i} + H'_{ti}) + (H_{\xi i} - H_{ti} - 2s_i)] + \omega r^2 [r H'_{\xi i} + H_{\xi i}] = 0, \tag{3.35}$$

$$r^2 H''_{\xi i} - r H'_{\xi i} - (3 + r^2 k_\xi \omega) H_{\xi i} + k_\xi^2 H_{ti} = 0, \tag{3.36}$$

and

$$r^2 H_{ti}'' - 5r H_{ti}' + [5 - k_\xi^2 - r^2 k_\xi \omega] H_{ti} \\ + 2[5 s_i - H_{\xi i} - r(s_i + H_{\xi i})'] + (r^2 k_\xi \omega + r^4 \omega^2) H_{\xi i} = 0. \tag{3.37}$$

3.3.2.1 Zero modes

For $k_\xi = \omega = 0$, (3.35) is trivially satisfied, and we solve (3.34,3.36,3.37). The solutions are obtained as the limit as $z \to 2$ of the solutions in chapter 2:

$$s_i = s_i^{(-)} r^{-1} + H_{\xi i}^{(+)} r^3 + s_i^{(+)} r^5, \tag{3.38}$$

$$H_{ti} = -s_i^{(-)} r^{-1} + H_{ti}^{(-)} r - H_{\xi i}^{(+)} r^3 + H_{ti}^{(+)} r^5, \tag{3.39}$$

$$H_{\xi i} = (H_{\xi i}^{(-)} + s_i^{(-)}) r^{-1} + H_{\xi i}^{(+)} r^3. \tag{3.40}$$

We have chosen to define and normalise the independent modes so that the solutions with a $(-)$ superscript correspond to the sources, coming from the constant modes in the frame fields: $s_i^{(-)}$ is the source term for the energy flux $\mathcal{E}^i$, $H_{\xi i}^{(-)}$ is the source term for the extra vector operator $\mathcal{P}_i^\xi$, and $H_{ti}^{(-)}$ is the source term for the momentum density $\mathcal{P}_i = \rho^i$. The modes with a $(+)$ superscript should then correspond to the vevs of these operators. By dimensions alone we see that $\langle \mathcal{P}_i \rangle \sim H_{\xi i}^{(+)}$. The vevs $\langle \mathcal{E}^i \rangle$ and $\langle \mathcal{P}_i^\xi \rangle$ should be related to $H_{ti}^{(+)}$ and $s_i^{(+)}$.

For $k_\xi = 0$, the flux can also be smoothly obtained as the limit $z \to 2$ of the results in the previous chapter:

$$\mathcal{F} = -i \int_{r=0} dt\, d^2x\, d\xi \Big[H_{\xi i}^{(-)} \wedge (2H_{ti}^{(+)} - s_i^{(+)}) + 2H_{ti}^{(-)} \wedge H_{\xi i}^{(+)} \\ + s_i^{(-)} \wedge (2H_{ti}^{(+)} + 2s_i^{(+)}) \Big], \tag{3.41}$$

where $A \wedge B = A_{\mathbf{1}} B_{\mathbf{2}} - A_{\mathbf{2}} B_{\mathbf{1}}$, with $\mathbf{1}, \mathbf{2}$ labelling the two linearised solutions which define the current. This enables us to identify, up to an overall normalization which we neglect for simplicity,

$$\langle \mathcal{P}_i \rangle = 2H_{\xi i}^{(+)}, \quad \langle \mathcal{P}_i^\xi \rangle = 2H_{ti}^{(+)} - s_i^{(+)}, \quad \langle \mathcal{E}^i \rangle = 2H_{ti}^{(+)} + 2s_i^{(+)}. \tag{3.42}$$

For non-zero ω, the solution is modified first in that (3.35) is no longer trivially satisfied; it sets $H_{\xi i}^{(+)} = 0$, corresponding to the expected Ward identity $\partial_t \mathcal{P}_i = 0$. Secondly, there is an ω^2

term in (3.37), which implies the solution is modified by subleading contributions. In this case there is a single subleading contribution. The solution is

$$s_i = s_i^{(-)} r^{-1} + s_i^{(+)} r^5, \tag{3.43}$$

$$H_{ti} = -s_i^{(-)} r^{-1} + H_{ti}^{(-)} r + \frac{1}{4}\omega^2 H_{\xi i}^{(-)} r^3 + H_{ti}^{(+)} r^5, \tag{3.44}$$

$$H_{\xi i} = H_{\xi i}^{(-)} r^{-1}. \tag{3.45}$$

3.3.2.2 Non-zero k_ξ

For non-zero k_ξ, the leading-order solution with $\omega = 0$ can be written as

$$H_{\xi i} = H_{\xi i}^{(diff)} r^{-1} + r^{1-\nu} H_{\xi i}^{(-)} + r^{1+\nu} H_{\xi i}^{(+)} + (\nu-2) k_\xi^2 H_{\xi i}^{(3-)} r^{3-\nu} + (\nu+2) k_\xi^2 H_{\xi i}^{(3+)} r^{3+\nu}, \tag{3.46}$$

$$\begin{aligned} s_i = {} & r^{1-\nu} H_{\xi i}^{(-)} + r^{1+\nu} H_{\xi i}^{(+)} \\ & - r^{3-\nu} H_{\xi i}^{(3-)} [24(\nu-2) + k_\xi^2(\nu-8)] - r^{3+\nu} H_{\xi i}^{(3+)} [24(\nu+2) + k_\xi^2(\nu+8)], \end{aligned} \tag{3.47}$$

$$\begin{aligned} H_{ti} = {} & -r^{1-\nu} H_{\xi i}^{(-)} - r^{1+\nu} H_{\xi i}^{(+)} \\ & - r^{3-\nu} H_{\xi i}^{(3-)} [12(\nu-2) + k_\xi^2(\nu-6)] - r^{3+\nu} H_{\xi i}^{(3+)} [12(\nu+2) + k_\xi^2(\nu+6)], \end{aligned} \tag{3.48}$$

where ν is as before. We see that we have a source and a vev for an operator of dimension $1+\nu$, and an operator of dimension $3+\nu$. The latter is irrelevant for all $k_\xi > 0$, the former is relevant for $k_\xi^2 < 5$. The mode $H_{\xi i}^{(diff)}$ whose dimension is independent of k_ξ is a pure diffeomorphism. We see that this mode corresponds to a non-zero mode of $\delta\hat{e}_\xi^I$, as expected. As argued in section 3.1.1, the natural approach is to gauge-fix these ξ-dependent diffeomorphisms by setting this mode to zero. The physical content in this non-zero mode sector is thus a pair of vector operators of dimensions $1+\nu$, $3+\nu$. Including non-zero ω will lead to an infinite series of subleading corrections in powers of $k_\xi \omega r^2$.

3.3.3 Scalar modes

We consider now the scalar modes H_{tt}, $H_{t\xi}$, $H_{\xi\xi}$, k, s_r, s_t, s_ξ. They are governed by the equations

$$0 = \left(k_\xi + 2\omega r^2\right) H_{\xi\xi} - 2k_\xi k + k_\xi r s_t' - 2k_\xi s_t + (k_\xi + \omega r^2) r s_\xi' - i\left(k_\xi^2 + 2k_\xi \omega r^2 + 8\right) s_r, \tag{3.49}$$

$$\begin{aligned} 0 = & -2rH_{\xi\xi}' + \left(\frac{1}{2}\omega^2 r^4 - 2\right) H_{\xi\xi} - 3rH_{t\xi}' - r^2 k_\xi \omega H_{t\xi} + \frac{1}{2}k_\xi^2 H_{tt} \\ & - 3rk' - \left(k_\xi^2 + 2k_\xi \omega r^2\right) k + [r s_\xi' + 4s_\xi - i k_\xi s_r], \end{aligned} \tag{3.50}$$

$$\begin{aligned} 0 = & \frac{\omega}{2} r H_{\xi\xi}' + \left(\frac{1}{2}k_\xi r^{-2} + \frac{3}{2}\omega\right) H_{\xi\xi} + \left(\frac{\omega}{2} - \frac{1}{2}k_\xi r^{-2}\right) r H_{t\xi}' \\ & - \frac{1}{2}k_\xi r^{-2} r H_{tt}' + \omega r k' + r^{-2} k_\xi [H_{tt} - k + s_t] - \omega s_\xi - 4i r^{-2} s_r, \end{aligned} \tag{3.51}$$

$$0 = -\frac{1}{2}\omega r^2 r H_{\xi\xi}' - \left(\omega r^2 + \frac{k_\xi}{2}\right) H_{\xi\xi} + \frac{1}{2}k_\xi r H_{t\xi}' + k_\xi r k', \tag{3.52}$$

$$\begin{aligned} 0 = & \frac{1}{2}r^2 H_{\xi\xi}'' + r^2 H_{t\xi}'' + \frac{1}{2}r^2 H_{tt}'' + r^2 k'' - \frac{1}{2}r H_{\xi\xi}' - 4r H_{t\xi}' - \frac{7}{2}r H_{tt}' + 6H_{tt} - 2rk' \\ & - \left(k_\xi^2 + 2k_\xi \omega r^2 + \omega^2 r^4\right) k - 2r s_t' + 12 s_t - r s_\xi' + 4 s_\xi + i\left(k_\xi + 2\omega r^2\right) s_r, \end{aligned} \tag{3.53}$$

$$0 = r^2 H_{\xi\xi}'' + r H_{\xi\xi}' - 4H_{\xi\xi} - 2k_\xi^2 k, \tag{3.54}$$

$$\begin{aligned} 0 = & r^2 H_{\xi\xi}'' + 2r^2 H_{t\xi}'' + r^2 k'' + \left(\omega^2 r^4 - 4\right) H_{\xi\xi} - 6r H_{t\xi}' + k_\xi^2 H_{tt} \\ & - 2r H_{\xi\xi}' - 3rk' - \left(k_\xi^2 + 2k_\xi \omega r^2\right) k - 2k_\xi \omega r^2 H_{t\xi} + 2[i k_\xi s_r - r s_\xi' + 4 s_\xi]. \end{aligned} \tag{3.55}$$

In addition, we have the radial-component gravitational constraint equations:

$$0 = r^2 s_\xi'' + 4H_{\xi\xi} + k_\xi^2 s_t + 3r s_\xi' + 2r H_{\xi\xi}' - \left(k_\xi \omega r^2 + 8\right) s_\xi + i k_\xi (2 s_r - r s_r'), \tag{3.56}$$

$$\begin{aligned} 0 = & r^2 s_\xi'' + r^2 s_t'' - k_\xi \omega r^2 s_t + \left(\omega^2 r^4 - 8\right) s_\xi - 3r s_\xi' - 5r s_t' \\ & + r H_{\xi\xi}' - 2rk' + 2i\left(2k_\xi + \omega r^2\right) s_r - i\left(k_\xi + \omega r^2\right) r s_r', \end{aligned} \tag{3.57}$$

$$0 = \frac{1}{2}r^2 H_{\xi\xi}'' + \frac{1}{2}r^2 H_{t\xi}'' + r^2 k'' - \frac{3}{2}r H_{t\xi}' - 3rk' - \left(k_\xi^2 + k_\xi \omega r^2\right) k. \tag{3.58}$$

3.3.3.1 Zero modes

For $k_\xi = \omega = 0$, (3.49,3.51,3.52) are automatically satisfied if $s_r = 0$, and (3.56,3.57,3.58) are non-trivial equations. The solution for the scalar modes is not a smooth limit of the solution in chapter 2, as that solution involved factors of $(z-2)^{-1}$, so it does not have a smooth limit. This arises because some powers of r in the mode solution which are distinct for $z \neq 2$ coincide for

$z = 2$. As a result the solution involves logarithms. The solution is

$$s_r = 0, \tag{3.59}$$

$$H_{\xi\xi} = 2H^{(-)}_{\xi\xi} r^{-2} + H^{(+)}_{\xi\xi} r^2, \tag{3.60}$$

$$s_\xi = r^{-2}(s^{(-)}_\xi + H^{(-)}_{\xi\xi}) + H^{(+)}_{\xi\xi} r^2 + s^{(4)}_\xi r^4, \tag{3.61}$$

$$k = \frac{1}{3} s^{(-)}_\xi r^{-2} + 2k^{(0)} + \frac{1}{2} H^{(+)}_{\xi\xi} r^2 + k^{(4)} r^4, \tag{3.62}$$

$$H_{t\xi} = -r^{-2}(H^{(-)}_{\xi\xi} + \frac{2}{3} s^{(-)}_\xi) + s^{(0)}_t + H^{(0)}_{t\xi} - \frac{1}{2} H^{(+)}_{\xi\xi} r^2 + (\frac{2}{3} s^{(4)}_\xi - k^{(4)}) r^4, \tag{3.63}$$

$$s_t = -\frac{1}{3} s^{(-)}_\xi r^{-2} + s^{(0)}_t - \frac{3}{2} H^{(+)}_{\xi\xi} r^2 - (k^{(4)} + s^{(4)}_\xi) r^4 + s^{(+)}_t r^6, \tag{3.64}$$

$$\begin{aligned} H_{tt} = {} & \frac{1}{3} s^{(-)}_\xi r^{-2} - 2s^{(0)}_t - H^{(+)}_{\xi\xi} r^2 (1 + 4 \log r) + 2H^{(-)}_{tt} r^2 \\ & + \left(2k^{(4)} - \frac{10}{3} s^{(4)}_\xi \right) r^4 + H^{(+)}_{tt} r^6. \end{aligned} \tag{3.65}$$

In the familiar AdS case, there are logarithmic terms in the Fefferman-Graham expansion for even boundary dimension, which are related to the anomaly in the scaling symmetry [87].[22] One might expect that the logarithm appearing in (3.65) would similarly contribute to an anomaly in the anisotropic scaling symmetry here. However, the anomaly is determined by the variation of the action under the scaling symmetry $\delta_\sigma S$, and because the background metric has $g^{tt} = 0$, H_{tt} cannot contribute to the action at linear order. Thus there is no anomaly term coming from (3.65). The logarithmic term will however have implications for boundary conditions, as in the case of a scalar field at the BF bound, see e.g. [89]. The appearance of the logarithm implies that the only scale-invariant boundary condition is one which fixes the coefficient of the logarithm $H^{(+)}_{\xi\xi}$. If we impose a boundary condition fixing $H^{(-)}_{tt}$ at some scale, this evolves into a mixed boundary condition under scale transformations: $r \to \lambda r$ maps $H^{(-)}_{tt} \to \lambda^{-2}(H^{(-)}_{tt} + 2 \log \lambda H^{(+)}_{\xi\xi})$. This is surprising because $H^{(+)}_{\xi\xi}$ corresponds to a component of the stress energy complex, whereas we had been assuming that our boundary conditions would fix the boundary geometry, encoded in the $(-)$ modes. We will discuss these issues below after considering the flux and inner product.

We calculate the flux to identify the canonically conjugate pairs of modes and hence identify the components of the stress tensor complex. The flux is a smooth limit of the expression for

[22] As noted in [88], the log terms in the FG expansion are proportional to the variation of the integrated anomaly.

$z < 2$ in the previous chapter,

$$\mathcal{F} = i \int_{r=0} dt\, d^{d_s}x\, d\xi \left[s_t^{(0)} \wedge \left(2k^{(4)} - \frac{5}{3} s_\xi^{(4)} \right) + H_{t\xi}^{(0)} \wedge \left(2k^{(4)} + \frac{4}{3} s_\xi^{(4)} \right) + k^{(0)} \wedge \left(-4k^{(4)} + \frac{10}{3} s_\xi^{(4)} \right) - 2H_{tt}^{(-)} \wedge H_{\xi\xi}^{(+)} - H_{\xi\xi}^{(-)} \wedge \left(2H_{tt}^{(+)} + s_t^{(+)} \right) - 3 s_\xi^{(-)} \wedge s_t^{(+)} \right]. \tag{3.66}$$

This implies the identifications

$$\langle \mathcal{E} \rangle = -2k^{(4)} + \frac{5}{3} s_\xi^{(4)}, \tag{3.67}$$

and

$$\langle \Pi_i^i \rangle = \langle \Pi_1^1 \rangle + \langle \Pi_2^2 \rangle = 4k^{(4)} - \frac{10}{3} s_\xi^{(4)}. \tag{3.68}$$

The Ward identity from the scaling invariance is

$$2\mathcal{E} + \Pi_i^i = 0 \tag{3.69}$$

which is indeed satisfied by these vevs. This confirms that, as argued above, the scale anomaly vanishes for these modes despite the presence of logarithms in the radial profiles. The other vevs are

$$\langle \mathcal{E}^\xi \rangle = 2H_{tt}^{(+)} + s_t^{(+)}, \tag{3.70}$$

$$\langle \rho \rangle = 2H_{\xi\xi}^{(+)}, \quad \langle \rho^\xi \rangle = -2k^{(4)} - \frac{4}{3} s_\xi^{(4)}, \tag{3.71}$$

and

$$\langle O \rangle = 3 s_t^{(+)}. \tag{3.72}$$

We would now like to consider the possible boundary conditions. To make the flux through the boundary vanish, boundary conditions should fix one of each conjugate pair in (3.66). In addition, we want to fix the non-normalizable modes for which the inner product (3.29) diverges. For $k_\xi = 0$, the inner product is finite in the UV provided we set $H_{\xi\xi}^{(-)} = s_\xi^{(-)} = 0$. If we allow for non-zero k_ξ, to cancel subleading divergences we must set also $k^{(0)} = 0$. With the conditions $H_{\xi\xi}^{(-)} = s_\xi^{(-)} = k^{(0)} = 0$, the only divergence that is left is proportional to $k_\xi r^{-1}(H_{\xi\xi}^{(+)} H_{t\xi}^{(0)})$, so we need at least one of $H_{t\xi}^{(0)} = 0$ or $H_{\xi\xi}^{(+)} = 0$. A consistent choice is then to set $H_{\xi\xi}^{(-)} = s_\xi^{(-)} = s_t^{(0)} = k^{(0)} = H_{t\xi}^{(0)} = 0$; then both $H_{tt}^{(-)}$ and $H_{\xi\xi}^{(+)}$ are normalizable, and we can choose to fix either of them. We would originally have thought we wanted to fix $H_{tt}^{(-)}$,

Operator	Source	Expectation value
$\mathcal{E}$	$\delta\hat{e}_t^+ = s_t^{(0)}$	$-2k^{(4)} + \frac{5}{3}s_\xi^{(4)}$
$\mathcal{E}^i$	$\delta\hat{e}_i^+ = s_i^{(-)}$	$2H_{ti}^{(+)} + 2s_i^{(+)}$
$\mathcal{E}^\xi$	$\delta\hat{e}_\xi^+ = H_{\xi\xi}^{(-)}$	$2H_{tt}^{(+)} + s_t^{(+)}$
ρ	$\delta\hat{e}_t^- = H_{tt}^{(-)}$	$2H_{\xi\xi}^{(+)}$
$\mathcal{P}_i = \rho^i$	$\delta\hat{e}_i^- = H_{ti}^{(-)}$	$2H_{\xi i}^{(+)}$
ρ^ξ	$\delta\hat{e}_\xi^- = H_{t\xi}^{(0)}$	$-2k^{(4)} - \frac{4}{3}s_\xi^{(4)}$
$\Pi_1^1 + \Pi_2^2$	$\delta\hat{e}_i^I = k^{(0)}$	$4k^{(4)} - \frac{10}{3}s_\xi^{(4)}$
$\Pi_1^1 - \Pi_2^2$, Π_2^1	$\delta\hat{e}_j^I = \bar{H}_{ij}^{(0)}$	$\bar{H}_{ij}^{(4)}$
$\mathcal{P}_i^\xi$	$\delta\hat{e}_\xi^I = H_{\xi i}^{(-)}$	$2H_{ti}^{(+)} - s_i^{(+)}$
O	$s_\xi^{(-)}$	$3s_t^{(+)}$

Table 2: The identification of linearised modes with sources and vevs for the operators in the dual field theory. Note that the sources are the zero modes of the indicated frame field component.

corresponding to fixing the boundary geometry, but as noted above, this is not a scale invariant boundary condition; the only scale invariant boundary condition is to fix instead $H_{\xi\xi}^{(+)} = 0$. In the field theory, this is fixing the particle number density to zero, rather than its source.

For non-zero ω, (3.49,3.51,3.52) become non-trivial. One of these fixes s_r; the other two linear combinations give the expected Ward identities $\partial_t\mathcal{E} = 0$ and $\partial_t\rho = 0$, setting $H_{\xi\xi}^{(+)} = 0$ and $k^{(4)} = \frac{5}{6}s_\xi^{(4)}$. This confirms the identification of the modes corresponding to components of the stress tensor, which is summarised in table 1.

For $\omega = 0$, fixing the particle number to zero was a natural choice of boundary condition, as it preserved scale invariance, but other possibilities exist. The particle number at non-zero ω vanishes as a result of the Ward identity, so we no longer have any freedom in choosing it.

There are also subleading terms in ω^2 in solving the other equations. As in the vector case,

there are a finite number of subleading terms, and the full solution for non-zero ω is

$$s_r = -i\frac{\omega}{2}\left(\frac{1}{2}(H^{(-)}_{\xi\xi} - s^{(-)}_{\xi}) + s^{(4)}_{\xi} r^6\right), \tag{3.73}$$

$$H_{\xi\xi} = 2H^{(-)}_{\xi\xi} r^{-2}, \tag{3.74}$$

$$s_\xi = r^{-2}(s^{(-)}_{\xi} + H^{(-)}_{\xi\xi}) + s^{(4)}_{\xi} r^4, \tag{3.75}$$

$$k = \frac{1}{3}s^{(-)}_{\xi} r^{-2} + 2k^{(0)} - \frac{1}{6}H^{(-)}_{\xi\xi}\omega^2 r^2 + \frac{5}{6}s^{(4)}_{\xi} r^4, \tag{3.76}$$

$$H_{t\xi} = -r^{-2}(H^{(-)}_{\xi\xi} + \frac{2}{3}s^{(-)}_{\xi}) + s^{(0)}_t + H^{(0)}_{t\xi} - \frac{1}{6}s^{(+)}_{\xi} r^4 + \frac{1}{3}H^{(-)}_{\xi\xi}\omega^2 r^2, \tag{3.77}$$

$$s_t = -\frac{1}{3}s^{(-)}_{\xi} r^{-2} + s^{(0)}_t - \frac{11}{6}s^{(4)}_{\xi} r^4 + s^{(+)}_t r^6 + \frac{1}{48}(5H^{(-)}_{\xi\xi} + 3s^{(-)}_{\xi})\omega^2 r^2 + \frac{3}{48}\omega^2 r^8 s^{(+)}_{\xi}, \tag{3.78}$$

$$\begin{aligned} H_{tt} = {} & \frac{1}{3}s^{(-)}_{\xi} r^{-2} - 2s^{(0)}_t + 2H^{(-)}_{tt} r^2 - \frac{5}{3}s^{(4)}_{\xi} r^4 + H^{(+)}_{tt} r^6 + \frac{1}{24}(2H^{(-)}_{\xi\xi} - s^{(-)}_{\xi})\omega^2(1 + 4\log r) r^2 \\ & - \frac{1}{2}k^{(0)}\omega^2 r^4 + \frac{1}{96}H^{(-)}_{\xi\xi}\omega^4(1 - 4\log r) r^6 + \frac{1}{72}\omega^2 s^{(+)}_{\xi} r^8. \end{aligned} \tag{3.79}$$

We see that since the Ward identity sets $H^{(+)}_{\xi\xi} = 0$, the previous logarithmic term is absent for non-zero ω, but there are new derivative terms with logarithms. As before, they will not give an anomaly for the scaling symmetry, as H_{tt} cannot contribute to the action. These now involve the $(-)$ modes, which we are used to thinking of as sources, so it is not worrying that the scale invariant boundary condition is to fix these modes.

If we study the scalar system for $d_s = 1$ or $d_s = 3$, the logarithmic term involving $H^{(+)}_{\xi\xi}$ in the constant modes is absent, but this logarithmic term in the ω-dependent modes persists.

3.3.3.2 Non-zero k_ξ

For non-zero k_ξ, the leading-order solution with $\omega = 0$ has three independent bulk diffeomorphism modes with dimensions which are independent of k_ξ, and six modes whose dimensions depend on k_ξ. The bulk diffeomorphism modes are generated by

$$\chi = r\chi^r_0\partial_r + \left(\chi^t_0 - \frac{i}{2}k_\xi r^2\chi^r_0\right)\partial_t + (\chi^\xi - ik_\xi\chi^r_0\log r)\partial_\xi. \tag{3.80}$$

The resulting modes are

$$s_r = -ik_\xi \chi_0^r, \tag{3.81}$$

$$s_t = -2\chi_0^r, \tag{3.82}$$

$$s_\xi = ik_\xi \chi_0^t r^{-2} + \frac{1}{2}k_\xi^2 \chi_0^r, \tag{3.83}$$

$$H_{tt} = 4\chi_0^r, \tag{3.84}$$

$$H_{t\xi} = -ik_\xi \chi_0^t r^{-2} - \frac{1}{2}(4 + k_\xi^2)\chi_0^r + ik_\xi \chi_0^\xi + k_\xi^2 \log r \chi_0^r, \tag{3.85}$$

$$H_{\xi\xi} = 2ik_\xi \chi_0^t r^{-2} + k_\xi^2 \chi_0^r, \tag{3.86}$$

$$k = -\chi_0^r. \tag{3.87}$$

As argued in section 3.1.1, we can gauge-fix the boundary diffeomorphism symmetry by setting $\delta\hat{e}_\xi^+$ and $\delta\hat{e}_\xi^-$ to zero; this corresponds to setting χ_0^t and χ_0^ξ to zero. We see that there is a logarithmic term involving χ_0^r; as this is now in $H_{t\xi}$, it may contribute to the anomaly. However, we see from (3.69), (3.68) (3.67) than only contributions to $k^{(4)}$ and $s_\xi^{(4)}$ participate in the corresponding Ward identity, and, because these coefficients are zero in the solution (3.81)-(3.87), the anomaly must vanish.

The physical degrees of freedom in the non-zero momentum sector are in the other six modes. The scaling of the fields for these modes is r^Δ where Δ satisfies a sixth-order equation

$$\begin{aligned} &3\Delta^6 - 36\Delta^5 + (120 - 9k_\xi^2)\Delta^4 + 72k_\xi^2\Delta^3 + \\ &(9k_\xi^4 - 112k_\xi^2 - 528)\Delta^2 - 4(9k_\xi^4 + 32k_\xi^2 - 144) - (3k_\xi^6 + 8k_\xi^4 - 272k_\xi^2) = 0. \end{aligned} \tag{3.88}$$

The solutions to (3.88) can be found in closed from, although the explicit expressions are not very illuminating. They are plotted in figure 15. The solutions come in pairs which sum to 4, so we can identify them as the sources and vevs for three scalar operators. Two of these operators are irrelevant for all $k_\xi > 0$, and the third becomes irrelevant at some critical value of k_ξ, as we can see from figure 15.

3.4 Linearised solutions for $d_s = 0$

We now consider the linearised solutions for $d_s = 0$. This case will clearly have a different behaviour from our present perspective: the absence of spatial directions modifies the structure

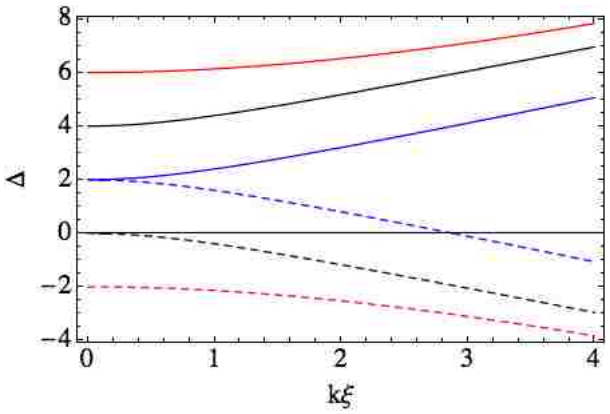

Figure 15: Scaling dimensions of the non-diffeo modes in the scalar sector for $d_s = 2$, $z = 2$ as a function of k_ξ. Pairs of dimensions that add to four are plotted in the same color, using solid and dashed lines.

of the linearised equations, and implies that the stress energy complex simplifies, as there are now no spatial fluxes. This case has also been extensively studied in previous work [35–38], under the name of null warped AdS_3, so we consider it in detail to make contact between our analysis and previous work. In this case, we only have the analogue of the scalar modes in the above discussion. However, the Ward identities in this case become degenerate, so new behavior arises which was not present in the $d_s = 2$ case.

The equations of motion read

$$0 = (k_\xi + 2r^2\omega)H_{\xi\xi} - 2k_\xi s_t - i(4 + k_\xi^2 + 2\omega k_\xi r^2)s_r + (k_\xi + r^2\omega)rs'_\xi + k_\xi rs'_t, \tag{3.89}$$

$$\begin{aligned} 0 = {} & 2k_\xi H_{tt} + 2k_\xi s_t - 2r^2\omega s_\xi - 4is_r + (k_\xi + 3r^2\omega)H_{\xi\xi} \\ & + \omega r^3 H'_{\xi\xi} + (r^2\omega - k_\xi)rH'_{t\xi} - k_\xi rH'_{tt}, \end{aligned} \tag{3.90}$$

$$0 = \omega r^3 H'_{\xi\xi} + (k_\xi + 2r^2\omega)H_{\xi\xi} - k_\xi rH'_{t\xi}, \tag{3.91}$$

$$0 = 4s_\xi + H_{\xi\xi}(r^4\omega^2 - 2) - 2k_\xi r^2\omega H_{t\xi} + k_\xi^2 H_{tt} - 2ik_\xi s_r - 2rH'_{\xi\xi} - 2rH'_{t\xi} + 2rs'_\xi, \tag{3.92}$$

$$\begin{aligned} 0 = {} & 16s_t + 2H_{\xi\xi} + 4s_\xi + rH'_{\xi\xi} - 4rH'_{t\xi} - 5rH'_{tt} + 8H_{tt} + 2is_r(k_\xi + 2r^2\omega) \\ & - 2rs'_\xi - 4rs'_t + 2r^2 H''_{t\xi} + r^2 H''_{\xi\xi} + r^2 H''_{tt}, \end{aligned} \tag{3.93}$$

$$0 = 3rH'_{\xi\xi} + r^2 H''_{\xi\xi}, \tag{3.94}$$

$$0 = 4H_{\xi\xi} + k_\xi^2 s_t - (4 + \omega k_\xi r^2)s_\xi + 2rH'_{\xi\xi} - ik_\xi rs'_r + rs'_\xi + r^2 s''_\xi, \tag{3.95}$$

$$\begin{aligned} 0 = {} & 2ik_\xi s_r - k_\xi r^2\omega s_t + (r^4\omega^2 - 4)s_\xi + rH'_{\xi\xi} - i(k_\xi + r^2\omega)rs'_r \\ & - rs'_\xi - 3rs'_t + r^2 s''_\xi + r^2 s''_t. \end{aligned} \tag{3.96}$$

For constant modes, (3.89), (3.90), (3.91) trivialise, becoming simply $s_r = 0$. A full solution can be found by solving (3.92)-(3.96). For general k_ξ, ω, a complete set of equations is given by (3.89)-(3.94), and we can easily check that (3.95) and (3.96) follow as a consequence of them.

3.4.1 Zero modes

The solution for constant modes is again not a smooth limit of the one in the previous chapter because of the appearance of factors of $(z-2)^{-1}$, which are replaced by logarithmic terms. The solution is

$$H_{\xi\xi} = 2H^{(-)}_{\xi\xi} r^{-2} + H^{(+)}_{\xi\xi}, \tag{3.97}$$

$$H_{t\xi} = -H^{(-)}_{\xi\xi} r^{-2} + s^{(0)}_t + H^{(0)}_{t\xi} + H^{(+)}_{\xi\xi}(1+\log r) + 2s^{(+)}_\xi r^2, \tag{3.98}$$

$$H_{tt} = -2s^{(0)}_t + H^{(+)}_{\xi\xi}(1+2\log r) + 2H^{(-)}_{tt} r^2 - 4s^{(+)}_\xi (1+2\log r) r^2 + H^{(+)}_{tt} r^4, \tag{3.99}$$

$$s_r = 0, \tag{3.100}$$

$$s_t = -\frac{1}{3} s^{(-)}_\xi r^{-2} + s^{(0)}_t - H^{(+)}_{\xi\xi} \log r - s^{(+)}_\xi r^2 + s^{(+)}_t r^4, \tag{3.101}$$

$$s_\xi = (s^{(-)}_\xi + H^{(-)}_{\xi\xi}) r^{-2} + H^{(+)}_{\xi\xi} + s^{(+)}_\xi r^2. \tag{3.102}$$

As in the higher-dimensional case, we have logarithms. The logarithms in H_{tt} and s_t cannot contribute to the anomaly at linear order for the same reason as above: since the background has $g^{tt} = 0$, we cannot build a scalar out of H_{tt} or s_t. The logarithm in $H_{t\xi}$ could in principle contribute to the anomaly, but this is not the case as we shall see below. The logarithms lead to inhomogeneous transformations under scaling, as in $d_s = 2$. When $r \to \lambda r$, $s^{(0)}_t \to s^{(0)}_t - H^{(+)}_{\xi\xi} \log\lambda$, and $H^{(-)}_{tt} \to H^{(-)}_{tt} + 4s^{(+)}_\xi \log\lambda$. These again have the surprising feature that modes that correspond to the components of the boundary geometry have an inhomogeneous transformation depending on vev modes, implying that we cannot have a scale invariant boundary condition that fixes the boundary geometry.

To determine the identification of the components of the stress energy complex, we calculate the flux for these constant modes. This is again the $z \to 2$ limit of the previous expression (for the appropriate definition of the modes),

$$\mathcal{F} = -i \int_{r=0} dt\, d\xi \left[H^{(-)}_{\xi\xi} \wedge H^{(+)}_{tt} + H^{(-)}_{tt} \wedge H^{(+)}_{\xi\xi} + 2s^{(-)}_\xi \wedge s^{(+)}_t - 2H^{(0)}_{t\xi} \wedge s^{(+)}_\xi \right]. \tag{3.103}$$

Note we have redefined the modes here relative to the $z < 2$ case in order to cleanly separate the vevs from the sources. This enables us to identify the vevs

$$\langle \rho \rangle = H^{(+)}_{\xi\xi}, \quad \langle \rho^{\xi} \rangle = -2 s^{(+)}_{\xi}, \tag{3.104}$$

$$\langle E^{\xi} \rangle = H^{(+)}_{tt}, \tag{3.105}$$

and

$$\langle O \rangle = 2 s^{(+)}_{t}. \tag{3.106}$$

Since there is no term in the flux involving $s^{(0)}_t$, we conclude that the vev of $\mathcal{E}$ vanishes. Moreover, this allows us to conclude that the Ward identity for the scaling symmetry is non-anomalous for constant modes. In fact, in the absence of any spatial directions and with $z = 2$, this Ward identity is just $2\mathcal{E} = \mathcal{A}$, where $\mathcal{A}$ is the anomaly. Our flux calculation shows that $\mathcal{E} = 0$, so it must be the case that $\mathcal{A} = 0$.

The calculation of the flux also enables us to identify possible boundary conditions consistent with flux conservation. An analysis of the inner product (3.30) reveals that the leading divergence in (3.30) is of order r^{-5} and it involves the modes parametrised by$H^{(-)}_{\xi\xi}$ and $s^{(-)}_{\xi}$. In addition, there are subleading divergences at order r^{-3}, r^{-1} and $r^{-1}\log r$ with are proportional to $H^{(+)}_{\xi\xi}$. We conclude then that the modes parametrised by $H^{(-)}_{\xi\xi}$, $H^{(+)}_{\xi\xi}$ and $s^{(-)}_{\xi}$ are non-normalizable. The boundary conditions should fix these modes, and allow the conjugate modes $H^{(+)}_{tt}$, $H^{(-)}_{tt}$ and $s^{(+)}_{t}$ to vary. Both $H^{(0)}_{t\xi}$ and $s^{(+)}_{\xi}$ are normalizable, so we can fix either. If we fix $H^{(+)}_{\xi\xi} = 0$, we can also fix $s^{(0)}_t$ in a scale invariant way.

3.4.1.1 Non-zero ω

When we generalise to non-zero ω for $k_\xi = 0$, the structure of the linearised solutions is different from what we might expect. This is because for non-zero ω, the structure of the Ward identities is qualitatively different from the higher-dimensional case. The Ward identities are

$$\partial_t \mathcal{E} = 0, \quad \partial_t \rho = 0, \quad 2\mathcal{E} = \mathcal{A}, \tag{3.107}$$

where we allow for a non-zero anomaly in the trace Ward identity. Note that because of the absence of spatial directions, $\mathcal{E}$ and ρ are now just the energy and particle number, rather than

densities. The first equation says $\mathcal{E}$ is a constant. The trace Ward identity will then imply a restriction on the sources: the term appearing in the anomaly for the trace Ward identity must also be a constant.[23] Any non-zero ω modes in $\mathcal{A}$ must vanish for us to be able to consistently quantise the theory on a given background. The point is that the Ward identities viewed as a system of linear equations for the non-zero ω modes of the vevs are degenerate, and so they have no solutions in the inhomogeneous case (with an anomaly source on the right-hand side).

This might seem a remarkably novel feature, but actually the same degeneracy happens for 1+1 dimensional relativistic field theories. There the Ward identities are in general

$$\partial_t T^t_t + \partial_x T^x_t = 0, \quad \partial_t T^t_x + \partial_x T^x_x = 0, \quad T^t_t + T^x_x = \mathcal{A} \sim R^{(0)}, \tag{3.108}$$

where we have noted that the anomaly in this case is proportional to the Ricci scalar of the background geometry. These equations are not generically degenerate, but if we consider the special kinematics where $\omega = \pm k$, that is $\partial_t = \pm\partial_x$, then we have $T^t_t = \mp T^x_t = \pm T^t_x = -T^x_x$, so the left-hand side of the last equation vanishes, and the anomaly contribution must vanish.

This implies that the metric component h_{uu} cannot have a contribution which is just a function of v and independent of u, and h_{vv} cannot have a component which is just a function of u and independent of v, where $u, v = t \pm x$ are light-like boundary coordinates. Physically, this is setting some potential non-gauge components of the boundary geometry to zero. In general, the boundary metric in the relativistic 1+1 CFT is pure gauge; by a diffeomorphism and a Weyl transformation one can set the boundary metric to be flat. Working about a background $ds^2 = -2dudv$, the diffeomorphisms and conformal transformation generate a linearised perturbation $h_{uu} = 2\partial_u \xi_u$, $h_{vv} = 2\partial_v \xi_v$, $h_{uv} = \partial_{(u}\xi_{v)} + \sigma$. But a component h_{uu} which is independent of u cannot arise from differentiating ξ_u, and similarly a component h_{vv} which is independent of v cannot arise from differentiating ξ_v, so these modes are not diffeomorphism modes (assuming x is periodically identified, so we do not allow linear functions in ξ). But it is precisely these modes that are set to zero by the above anomaly argument, so the theory can only be studied consistently on a background which is in fact diffeomorphic to the flat metric.[24]

[23] Our analysis of the constant modes above found that $\langle \mathcal{E} \rangle = 0$, indicating that the constant part of $\mathcal{A}$ also vanishes, but this statement is (at least potentially) special to the specific holographic theory we are considering, while the vanishing of the non-constant modes of $\mathcal{A}$ is a consequence of the general structure of the Ward identities and must be true for any such theory.

[24] Modulo components which are independent of both u and v; these are also not diffeomorphisms, but are not ruled out by the anomaly.

Returning to the non-relativistic case, this analysis of the Ward identities predicts that for ω non-zero, we will have $H^{(+)}_{\xi\xi} = 0$, one restriction on the source modes, and some set of subleading terms involving ω^2. This is precisely what we find. The solution for non-zero ω is

$$H_{\xi\xi} = 0, \tag{3.109}$$

$$H_{t\xi} = s^{(0)}_t + H^{(0)}_{t\xi} + 2s^{(+)}_\xi r^2, \tag{3.110}$$

$$H_{tt} = -2s^{(0)}_t + 2H^{(-)}_{tt} r^2 - 4s^{(+)}_\xi (1 + 2\log r) r^2 + H^{(+)}_{tt} r^4 - \frac{1}{6} r^6 \omega^2 s^{(+)}_\xi, \tag{3.111}$$

$$s_r = \frac{i}{2}(s^{(-)}_\xi + s^{(+)}_\xi r^4), \tag{3.112}$$

$$s_t = -\frac{1}{3} s^{(-)}_\xi r^{-2} + s^{(0)}_t - s^{(+)}_\xi r^2 + s^{(+)}_t r^4 + \frac{1}{4}\omega^2 r^2 s^{(-)}_\xi + \frac{1}{12}\omega^2 r^6 s^{(+)}_\xi, \tag{3.113}$$

$$s_\xi = s^{(-)}_\xi r^{-2} + s^{(+)}_\xi r^2. \tag{3.114}$$

It turns out that the restriction on the sources is to set $H^{(-)}_{\xi\xi} = 0$. This is the source for $\mathcal{E}^\xi$, which is the extra component in the stress energy complex which is left undetermined because of the degeneration of the Ward identities. It is a non-diffeomorphism mode, as in the above discussion of the relativistic case.

We can learn more about the structure of the scale Ward identity by looking at the (first order) radial components of the equations of motion. More concretely, when we have not yet imposed these first order equations, the r^2 term in (3.110) appears as an independent constant, which we denote by $H^{(+)}_{t\xi}$. This will of course propagate to the other functions, but we do not need the details here. Plugging the solution of the second order equations into the first order equations we learn that

$$\omega H^{(+)}_{\xi\xi} = 0 \tag{3.115}$$

$$\omega(H^{(+)}_{t\xi} - 2s^{(+)}_\xi) = 0 \tag{3.116}$$

$$2(H^{(+)}_{t\xi} - 2s^{(+)}_\xi) = \frac{1}{2}\omega^2 H^{(-)}_{\xi\xi} \tag{3.117}$$

Equations (3.115)-(3.117) correspond to the Ward identities (3.107) provided we identify

$$\rho \sim H^{(+)}_{\xi\xi} \qquad \mathcal{E} \sim H^{(+)}_{t\xi} - 2s^{(+)}_\xi \qquad \mathcal{A} \sim \omega^2 H^{(-)}_{\xi\xi} \tag{3.118}$$

where the $\sim$ indicates equality up to an ω-independent constant. Hence, the anomaly is proportional to $\omega^2 H^{(-)}_{\xi\xi}$, and is set to zero due to the conservation equation $\omega\mathcal{E} = 0$.

It is also useful to note that the relativistic and Schrödinger restrictions are related. If we take the $b \to 0$ limit of the Schrödinger solution, we recover AdS, and the null coordinate ξ becomes a null coordinate in AdS, so considering zero modes $k_\xi = 0$ corresponds in this limit precisely to the special kinematics $\omega = \pm k$ where the AdS Ward identities degenerate, and $H^{(-)}_{\xi\xi} = 0$ reduces to the restriction coming from the Ricci scalar noted above.

3.4.2 Non-zero k_ξ

We now consider the sector of non-zero k_ξ. For our purposes, this sector is less interesting, as the bulk modes are just dual to some higher dimension operators in the field theory. However, in previous work on Schrödinger as a deformation of AdS, attention has naturally focused on this discussion, as this is the generic kinematics. We will therefore give the full results for purposes of comparison.

For non-zero k_ξ, we generally expect the scaling dimensions to depend on k_ξ. However, just as in the higher-dimensional case, there are some modes which can be generated by acting with an appropriate ξ-dependent diffeomorphism.

For $\omega = 0$, the full solution is

$$H_{\xi\xi} = H^{(-)}_{\xi\xi} r^{-2} - \frac{1}{2} k_\xi^2 s_t^{(0)}, \tag{3.119}$$

$$H_{t\xi} = -\frac{1}{2} H^{(-)}_{\xi\xi} r^{-2} + H^{(0)}_{t\xi} - \frac{1}{2} \log r k_\xi^2 s_t^{(0)}, \tag{3.120}$$

$$H_{tt} = -2 s_t^{(0)} + 4(1-\delta_1) s_t^{(1-)} r^{1-\delta_1} + 4(1+\delta_1) s_t^{(1+)} r^{1+\delta_1}, \tag{3.121}$$

$$s_t = s_t^{(0)} + s_t^{(1-)} r^{1-\delta_1} + s_t^{(1+)} r^{1+\delta_1} + s_t^{(3-)} r^{1-\delta_3} + s_t^{(3+)} r^{1+\delta_3}, \tag{3.122}$$

$$s_r = \frac{i}{2} k_\xi \left(s_t^{(0)} + k_\xi^2 s_t^{(1-)} r^{1-\delta_1} + k_\xi^2 s_t^{(1+)} r^{1+\delta_1} - s_t^{(3-)} r^{1-\delta_3} - s_t^{(3+)} r^{1+\delta_3} \right), \tag{3.123}$$

$$\begin{aligned} s_\xi = {} & \frac{1}{4}(H^{(-)}_{\xi\xi} r^{-2} - k_\xi^2 s_t^{(0)}) - \frac{1}{2}(3+\delta_3) r^{1-\delta_3} s_t^{(3-)} - \frac{1}{2}(3-\delta_3) r^{1+\delta_3} s_t^{(3+)} \\ & - \frac{1}{2}(1-\delta_1) r^{1-\delta_-} k_\xi^2 s_t^{(1-)} - \frac{1}{2}(1+\delta_1) k_\xi^2 r^{1+\delta_1} s_t^{(1+)}, \end{aligned} \tag{3.124}$$

where $\delta_1 = \sqrt{1+k_\xi^2}$, $\delta_3 = \sqrt{9+k_\xi^2}$. The bulk diffeomorphism modes are $H^{(-)}_{\xi\xi}$, $H^{(0)}_{t\xi}$ and $s_t^{(0)}$, which correspond to $\delta\hat{e}^+_\xi$, $\delta\hat{e}^-_\xi$ and $\delta\hat{e}^+_t$. As discussed in section 3.1.1, we can set the first two to zero by gauge-fixing the ξ-dependent boundary diffeomorphisms. The logarithmic term does not contribute to the anomaly, as it does not enter at $O(r^2)$, which is the right order to modify the vevs and participate in the Ward identity.

The other four modes correspond to sources and vevs for scalar operators of dimension

$$\Delta = 1 + \sqrt{1 + k_\xi^2}, \qquad \Delta = 1 + \sqrt{9 + k_\xi^2}. \tag{3.125}$$

These are both irrelevant for all $k_\xi > 0$. For general ω, if we set the diffeomorphism modes to zero, we can find the solution for these modes in the same way as in [35]. We find that we can set $H_{t\xi} = H_{\xi\xi} = 0$ without loss of generality (they only carry diffeo modes), and eliminate H_{tt} and s_r algebraically. One is left with two coupled second order equations for s_t and s_ξ, which can be decoupled by increasing the number of derivatives. The diff-invariant dynamics are then captured by the following fourth order equation

$$\begin{aligned} &r^4 s_\xi'''' + 2r^3 s_\xi''' - (9 + 2k_\xi^2 + 4k_\xi \omega r^2) r^2 s_\xi'' + (9 + 2k_\xi^2 - 4k_\xi \omega r^2) r s_\xi' \\ &+ [k_\xi^2(8 + k_\xi^2) + 4k_\xi \omega (4 + k_\xi^2) r^2 + 4k_\xi \omega^2 r^4] s_\xi = 0. \end{aligned} \tag{3.126}$$

The solutions to this equation have the form

$$s_\xi = r^\Delta \sum_{i=0} s_{\xi(i)} r^{2i}, \tag{3.127}$$

where the $s_{\xi(i)}$ are constants and the values of Δ are those found in the $\omega = 0$ case, corresponding to the source and vev for two operators of dimensions (3.125).

3.4.3 Comparison to previous work

We now consider the comparison of our results to previous work on null warped AdS_3. We focus on the linearised analysis in [35, 38] and the analysis of boundary conditions in [90].

Our analysis of the linearised solutions for $k_\xi \neq 0$ is the same as in [35]. The diffeomorphism modes are what they call the T modes, and the operators of dimension (3.125) correspond to their X modes. The significant difference between our analysis and theirs is our emphasis on the role of the zero modes. For [35], the zero modes are not especially interesting: T modes are the source for the relativistic stress energy complex, and the zero modes are a special subsector of non-generic kinematics, which they do not consider explicitly. But in our non-relativistic description, the dual field theory lives in one lower dimension, and the zero modes are accordingly the most important sector to understand. We have also seen that the analysis of the zero modes has novel features

which do not appear in the discussion for $k_\xi \neq 0$.

The importance of this sector can be stated in a different way that is more independent of our interpretation: Apart from terms determined by the anomalies, the stress tensor only has non-zero components with $k_\xi = 0$. Our perspective focuses in a natural way on this part, and at the price of not being fully covariant in both the t and ξ directions, simplifies the duality by only introducing sources for the potentially non-zero part of the stress tensor at $k_\xi = 0$. The $k_\xi \neq 0$ part of the T mode sources considered in [35] are simply set to zero by gauge-fixing in our approach.

In [38], it was proposed that the appropriate sources for the relativistic stress tensor at $k_\xi \neq 0$ involve a combination of the T and X modes. This does not arise in our analysis. Such a mixing was possible only because the analysis is perturbative in b; in our analysis at finite b, the diffeomorphism modes and the other modes have different dimensions, so it is not possible for them to mix.

In [90], a notion of asymptotically Schrödinger boundary conditions was proposed, and it was found that the asymptotic symmetry group for these boundary conditions was an infinite extension of the isometry group. Their boundary condition is different from ours, and does not appear to be satisfied bty our linearised solutions. Their analysis was for asymptotically Schrödinger rather than asymptotically locally Schrödinger boundary conditions, so one might think it should be recovered by setting the boundary geometry modes in our analysis to zero. However, it is easy to see that our zero mode solutions do not satisfy their boundary conditions in this case. In the constant modes (3.97), a non-zero $H^{(+)}_{\xi\xi}$ generates a constant metric perturbation $h_{\xi\xi}$. This perturbation violates their boundary conditions, which require that $h_{\xi\xi} \sim \mathcal{O}(r^2)$ in our notation. In addition, turning on $s^{(+)}_\xi$ will generate a term $h_{tt} \sim s^{(+)}_\xi r^{-2} \log r$, violating their boundary condition $h_{tt} \sim \mathcal{O}(r^{-2})$.

What if we consider other boundary conditions? In fact $H^{(+)}_{\xi\xi}$ is a non-normalizable mode, so we should take a boundary condition where it is fixed. If we take $H^{(+)}_{\xi\xi} = 0$, this is consistent with the boundary conditions of [90]. However, this is fixing the particle number to zero, which seems a strong restriction on the dual field theory. Both $s^{(+)}_\xi$ and its conjugate mode $H^{(0)}_{t\xi}$ are normalizable, so we can choose a boundary condition where $s^{(+)}_\xi = 0$ and $H^{(0)}_{t\xi}$ fluctuates. This has two drawbacks: it's setting the field theory energy to zero, and while we get rid of the problem with $s^{(+)}_\xi$, allowing $H^{(0)}_{t\xi}$ to fluctuate generates $h_{t\xi} \sim H^{(0)}_{t\xi} r^{-2}$, which is again inconsistent with

their boundary conditions, which require $h_{t\xi} \sim \mathcal{O}(r^0)$.

Thus, there is no obvious choice of boundary conditions for our zero modes which will satisfy the assumptions of [90]. It would clearly be interesting to analyse the asymptotic symmetries for our boundary conditions defined in section 3.1, but we leave this for future work.

3.5 Asymptotic expansion

In this section, we want to go beyond the linearised analysis by showing that solutions of the bulk equations of motion exist for arbitrary boundary data in precisely the same way as we did in section 2.5 in the previous chapter, for the $z < 2$ case. Again, we will solve the equations of motion in an asymptotic expansion: that is, we work at large r, and solve the equations in an expansion in powers of r. Here we restrict ourselves to considering the Fourier zero modes, which include the sources for the stress energy complex, and we will of course be setting sources for irrelevant operators to zero. In the course of demonstrating the existence of this asymptotic expansion, we will also see that when the asymptotic expansion exists we can cancel the divergent terms in the action in the usual way by adding appropriate local counterterms determined by the boundary data.

The general formalism was discussed in the previous chapter, but we review it here. We work in terms of the frame fields, and adopt a radial Hamiltonian formalism. The momentum conjugate to A_α is $\pi_\alpha = n^\mu F_{\mu\alpha} = rF_{r\alpha}$. The conjugate to the frame fields is written in terms of a frame extrinsic curvature $K^A{}_B = e^\alpha_B \dot{e}^A_\alpha$, which is not a symmetric object. The equations in frame indices are

$$\begin{aligned}\dot{K}_{(AB)} + KK_{(AB)} + \frac{1}{2}\left(K_{CA}K^C{}_B - K_{AC}K_B{}^C\right) + \frac{1}{2}\pi_A\pi_B - \frac{2}{4(d-2)}\eta_{AB}\pi_C\pi^C \\ = R_{AB} - \frac{2}{d-2}\Lambda\eta_{AB} - \frac{1}{2}F_{AC}F_B{}^C + \frac{2}{8(d-2)}\eta_{AB}F_{CD}F^{CD} - \frac{1}{2}m^2A_AA_B, \qquad (3.128)\end{aligned}$$

$$\dot{\pi}^A + K\pi^A - K^A{}_B\pi^B = -\nabla_B F^{BA} + m^2A^A, \qquad (3.129)$$

and the constraints

$$\nabla^A K_{(AB)} - \nabla_B K^A{}_A = \frac{1}{2} F_{BA}\pi^A + \frac{1}{2} m^2 A_B r A_r, \tag{3.130}$$

$$K^2 - K_{(AB)}K^{AB} - \frac{1}{2}\pi_A\pi^A = R - 2\Lambda - \frac{1}{4}F_{AB}F^{AB} + \frac{1}{2}m^2(rA_r)^2 - \frac{1}{2}m^2 A_A A^A, \tag{3.131}$$

$$\nabla_A \pi^A = -m^2 r A_r. \tag{3.132}$$

Here $F_{AB} = e^\alpha_A e^\beta_B F_{\alpha\beta}$, and $\nabla_A = e^\alpha_A \nabla_\alpha$, where the covariant derivative ∇_α is a total covariant derivative (covariant with respect to both local Lorentz transformations and diffeomorphisms), and $\dot{}$ denotes the derivative in the normal direction, which is $-r\partial_r$.

To show that a solution exists in an asymptotic expansion, we want to fix the sources, which will fix the terms appearing on the RHS of these equations, and see that we can satisfy the equations by introducing appropriate subleading terms in r in the expansion which will contribute to the radial derivative terms on the LHS of the equations. For this to work, the source terms need to involve positive powers of r. Explicit powers of r enter where there are derivatives along the boundary directions. There are also explicit powers in the Ricci rotation coefficients, determined by $de^C = \Omega_{AB}{}^C e^A \wedge e^B$.

We restrict ourselves to considering sources which are independent of the ξ coordinate; that is, we assume that the boundary data has a Killing symmetry ∂_ξ. Note that we do not assume that ∂_ξ is either null or Killing in the bulk; it is only the boundary sources that are required to have this symmetry, and we can allow the vev modes to be arbitrary functions of ξ, this will not affect the derivation of the asymptotic expansion.[25] This is thus slightly different from a similar case considered in [76], where ∂_ξ was taken to be a Killing vector in the bulk.

We need to set to zero the sources for the irrelevant operators. We set the scalar sources ψ, $\hat{e}^+_\xi$ and $\hat{e}^I_\xi$ to zero by hand. Thus, we assume that

$$\hat{e}^+ = \hat{e}^+_a dx^a, \quad \hat{e}^I = \hat{e}^I_a dx^a, \quad \hat{e}^- = \hat{e}^-_\xi (d\xi + \tilde{e}^-_a dx^a). \tag{3.133}$$

The one-forms $\hat{e}^+_a$, $\hat{e}^I_a$ will then define the boundary geometry the dual field theory lives in, while $\tilde{e}^-_a$ is a one-form gauge potential (as usual infinitesimal x^a dependent transformations of the ξ

[25] We would not expect it to be possible to extend the construction of an asymptotic expansion to include sources with arbitrary dependence on ξ; since the dimensions of the dual operators increase as we increase k_ξ, sources with large enough k_ξ are sourcing irrelevant operators, which should cause the expansion to break down. It may be possible to extend the analysis to include sources with sufficiently small k_ξ, but as it is not clear what the interesting values might be, we have not attempted to pursue this.

coordinate induce gauge transformations of $\tilde{e}_a^-$), dual to the conserved particle number. Note that because we chose to set the $d\xi$ components of the other frame fields to zero, non-degeneracy implies $\hat{e}_\xi^- \neq 0$. We will set the source for the irrelevant operator $\mathcal{E}^i$ to zero without choosing a coordinate system by setting

$$\hat{e}^+ \wedge d\hat{e}^+ = 0, \tag{3.134}$$

so that the boundary geometry admits a foliation by surfaces of absolute time. For $z = 2$, all these restrictions are necessary to ensure the existence of the asymptotic expansion.

These restrictions on the frame fields imply that the Ricci rotation coefficients

$$\Omega_{+-}{}^{+} = 0, \quad \Omega_{-I}{}^{+} = 0, \quad \Omega_{IJ}{}^{+} = 0, \quad \Omega_{-J}{}^{I} = 0, \quad \Omega_{+-}{}^{I} = 0. \tag{3.135}$$

Thus, the non-zero Ricci rotation coefficients are

$$\Omega_{+I}{}^{+} \sim r, \quad \Omega_{+J}{}^{I} \sim r^2, \quad \Omega_{JK}{}^{I} \sim r, \tag{3.136}$$

$$\Omega_{+-}{}^{-} \sim r^2, \quad \Omega_{+I}{}^{-} \sim r^3, \quad \Omega_{-I}{}^{-} \sim r, \quad \Omega_{IJ}{}^{-} \sim r. \tag{3.137}$$

The structure of the one-forms implies e_- has only a ∂_ξ component, so ∂_- vanishes. Thus, the only derivatives appearing are ∂_+, which comes with a factor of r^2, and ∂_I, which comes with a factor of r. Thus, we expect an asymptotic expansion to exist for any such boundary data, with arbitrary dependence on t, x^i subject to $\hat{e}^+ \wedge d\hat{e}^+ = 0$.

This can be checked by analysing the theory in the radial Hamiltonian framework of [80, 81], as in chapter 2. This involves expanding in eigenvalues of an appropriate bulk dilatation operator. Assuming that we impose some appropriate boundary or regularity condition in the interior of the spacetime, the on-shell solution of the equations of motion will be uniquely determined in terms of the asymptotic boundary data, so the on-shell action is a function of the boundary data, which we can write as a boundary term,

$$S = \int d^{d-1}x\sqrt{-\gamma}\lambda(e^{(A)}, \psi). \tag{3.138}$$

We can then think of the canonically conjugate momenta as determined by functional derivatives

of this action as in a Hamilton-Jacobi approach, so

$$T^A{}_B = \frac{1}{\sqrt{-\gamma}} e^{(A)}_\alpha \frac{\delta}{\delta e^{(B)}_\alpha} S, \tag{3.139}$$

$$\pi_\psi = \frac{1}{\sqrt{-\gamma}} \frac{\delta}{\delta \psi} S. \tag{3.140}$$

The leading scaling of ψ is r^{Δ_-}, so if we define the dilatation operator

$$\delta_D = -\int d^4x \left(2e^{(+)}_\alpha \frac{\delta}{\delta e^{(+)}_\alpha} + e^{(I)}_\alpha \frac{\delta}{\delta e^{(I)}_\alpha} - \Delta_- \psi \frac{\delta}{\delta \psi} \right), \tag{3.141}$$

then acting on any function of e^A, ψ, this will agree with the radial derivative at leading order in large r, $\delta_D \sim r\partial_r$. Applying this operator to the action, we have

$$(d_s + 2 - \delta_D)\lambda = 2T^+{}_+ + T^I{}_I - \Delta_- \psi \pi_\psi. \tag{3.142}$$

Compared to the $z < 2$ case, we note that (3.141) does not involve $e^{(-)}$, and (3.142) does not involve $T^-{}_-$, as this component does not enter into the trace Ward identity. We determine λ by expanding in dilatation eigenvalues and using (3.142) and (3.131) to determine the contribution at each order in terms of the contributions at earlier orders and the sources.[26] The expansion is

$$\lambda = \sum_{d_s+2>\Delta\geq 0} \lambda^{(\Delta)} + \ldots, \qquad \delta_D \lambda^{(\Delta)} = \Delta \lambda^{(\Delta)}. \tag{3.143}$$

where $\ldots$ represents terms of higher order which will include logarithms. The dilatation eigenfunctions $\lambda^{(\Delta)}$ are determined by

$$\begin{aligned}(d_s + 2 - \Delta)\lambda^{(\Delta)} = &- src^{(\Delta)} \\ &+ \sum_{s<\Delta/2, s\neq 0} \left[-2K^{(s)}_{(AB)} \pi^{AB(\Delta-s)} - \pi^{(s)}_A \pi^{A(\Delta-s)} - \frac{1}{m^2} (\nabla_A \pi^A)^{(s)} (\nabla_B \pi^B)^{(\Delta-s)} \right] \\ &+ \left[-K^{(\Delta/2)}_{(AB)} \pi^{AB(\Delta/2)} - \frac{1}{2} \pi^{(\Delta/2)}_A \pi^{A(\Delta/2)} - \frac{1}{2m^2} (\nabla_A \pi^A)^{(\Delta/2)} (\nabla_B \pi^B)^{(\Delta/2)} \right].\end{aligned} \tag{3.144}$$

The quadratic terms in this expression involve lower orders in δ, which are determined from the

[26] As for $z < 2$, there is not actually a complete expansion in dilatation eigenvalues, as the logarithms in our linearised solutions indicate that the action of the dilatation operator is not completely diagonalizable. The linearised solution indicates that $\Delta = 2$ would be the first order of concern, so these terms contribute at positive powers and thus do not impede the existence of an expansion.

action by the variations (3.139,3.140). We want to focus on the sources:

$$src = R - 2\Lambda - \frac{1}{4}F_{AB}F^{AB} - \frac{m^2}{2}A_A A^A. \tag{3.145}$$

Since we are going to turn ψ off, $A_A A^A = 0$, and F_{AB} becomes

$$F_{AB} = 2\Omega_{AB}{}^{+}A_{+}. \tag{3.146}$$

Because of the constraints on the Ricci rotation coefficients, the only non-zero term is F_{+I}, so F^2 has no non-zero contributions (as $g^{++} = 0$). The Ricci scalar is

$$R = -4\partial_A \Omega_C{}^{AC} + \Omega_{CAD}\Omega^{CAD} + 2\Omega_{CAD}\Omega^{DAC} + 4\Omega_{AD}{}^{A}\Omega_C{}^{DC}. \tag{3.147}$$

Because of the constraints on the sources, particularly the irrotational condition (3.17), the Ricci scalar has contributions only at $\Delta = 2$. Thus only -2Λ contributes to $src^{(0)}$. At $\Delta = 2$ we have

$$\begin{aligned} src^{(2)} = &- 4\partial_+ \Omega_{A-}{}^{A} - 4\partial_- \Omega_{A+}{}^{A} - 4\partial_I \Omega_A{}^{IA} + \Omega_{IJK}\Omega^{IJK} \\ &+ 4\Omega_{+IJ}\Omega_-{}^{IJ} + 4\Omega_{+I}{}^{+}\Omega_-{}^{I-} \\ &+ 4\Omega_{A+}{}^{B}\Omega_{B-}{}^{A} + 2\Omega_{AI}{}^{B}\Omega_B{}^{IA} + 8\Omega_{A+}{}^{A}\Omega_{B-}{}^{B} + 4\Omega_{AI}{}^{A}\Omega_B{}^{IB}, \end{aligned} \tag{3.148}$$

where A, B are taken to run over $+, -$ and all of the I directions. Since the Ω's only contribute to sources with positive eigenvalues, we now know a solution for λ involving only positive eigenvalues of δ_D will exist. As in the previous chapter, we could additionally be concerned that $T^{+}{}_{-}$, $T^{+}{}_{I}$, and $T^{I}{}_{-}$ might pick up contributions at negative dilatation eigenvalue from the derivatives of λ as in (3.139). However, as discussed in the previous chapter, any such contribution would be a boundary scalar, writable entirely in terms of the Ω; as the only nonzero Ω have positive powers of r, the $T^{A}{}_{B}$ cannot pick up a contribution at negative eigenvalue. Consequently, the desired asymptotic expansion must exist. As we noted in the previous chapter, we could check whether or not the counterterms for the on-shell action are local by explicitly plugging in covariant dilatation expansions of the bulk on-shell momenta and solving for the divergent contrubitions in the dilatation expansion of the on-shell action. The essential difficulty in this case, exactly as for the $z < 2$ case considered in the previous chapter, is that the off-diagonal structure of the frame metric makes inverting the covariant expansions very difficult, and so again we leave this question for future work.

3.6 Discussion

In this chapter, we have constructed the holographic dictionary for Schrödinger spacetimes with dynamical exponent $z = 2$ based on a frame field formalism. We have proposed a notion of asymptotically locally Schrödinger boundary conditions, identified the sources and vevs for the stress tensor complex, and demonstrated that solutions satisfying our boundary conditions exist in an asymptotic expansion. We worked in a theory with a massive vector action in 3 and 5 bulk dimensions. Our method is readily generalizable to other dimensions, and in principle to other supporting matter.

The main difference from our previous analysis of the Schrödinger $z < 2$ case in chapter 2 is that in the $z = 2$ case the ξ direction becomes auxiliary; it is invariant under radial rescalings. We argued that consequently, as in $\mathrm{AdS}_n \times \mathbb{R}^d$ holography, the appropriate dictionary is formulated by expanding the bulk fields in Fourier modes in ξ and identifying each Fourier mode with the source and vev of a boundary operator $\mathcal{O}_{k_\xi}$ whose conformal dimension depends on k_ξ. This is also different from previous work starting with [35] which treated $z = 2$ Schrödinger spacetime as a perturbation of AdS.

In addition, as in the Lifshitz $z = 2$ case studied in [70, 84], there are logarithmic terms in our linearised analysis. In the AdS and Lifshitz cases, the logarithmic terms corresponded to anomalies in the scaling symmetry. However, we find that because of the null structure of the background, some of the logarithms that arise in our case do not contribute to the anomaly at linear order. It would be interesting to understand this from the field theory point of view, or to explore it in the full non-linear theory. We also found a curious feature in the $d_s = 0$ case: there is a degeneracy in the Ward identity for the zero modes in ξ that forces us to set source modes that contribute to the scaling anomaly to zero. We noted that a similar feature also appears in the relativistic case for lightlike modes.

Our analysis followed the philosophy of the work in [41, 45] on Lifshitz and chapter 2 on Schrödinger. We therefore gauge fixed the frame transformation symmetries as much as possible. It would be interesting to explore the analogue of the discussion of Lifshitz in [71, 72, 91, 92] instead, where this symmetry is left unfixed. This has been argued to give a more general perspective on the boundary geometry.

4 Hot Multiboundary Wormholes from Bipartite Entanglement

The work in this chapter is reproduced from a collaborative paper [3] with Prof. Don Marolf, Dr. Henry Maxfield and Prof. Simon Ross. In this chapter we analyze the 1+1 CFT states dual to hot (time-symmetric) 2+1 multiboundary AdS wormholes. These are black hole geometries with high local temperature, $n \geq 1$ asymptotically-AdS_3 regions, and arbitrary internal topology. The dual state at $t = 0$ is defined on n circles. We show these to be well-described by sewing together tensor networks corresponding to thermofield double states. As a result, the entanglement is spatially localized and bipartite: away from particular boundary points ("vertices") any small connected region A of the boundary CFT is entangled only with another small connected region B, where B may lie on a different circle or may be a different part of the same circle. We focus on the pair-of-pants case, from which more general cases may be constructed. We also discuss finite-temperature corrections, where we note that the states involve a code subspace in each circle.

4.1 Introduction

The thermofield double (TFD) state

$$|TFD\rangle = \sum_E e^{-E/2T}|E\rangle|E\rangle \tag{4.1}$$

on two copies of a quantum field theory serves as the poster child for many ideas [12–15, 30, 48, 93] relating the emergence of bulk geometry to entanglement in some dual theory. As explained in [30], although a single copy of a CFT can be naturally dual to bulk quantum gravity with a single asymptotically AdS boundary, the particular entanglements between the two copies described by (4.1) allow it to be dual to a two-sided eternal black hole in which two distinct asymptotic regions are connected by an Einstein-Rosen bridge[27]. The state also typifies relations between the area of codimension-2 surfaces and CFT entanglement encapsulated in the Ryu-Takayangi conjecture [12] and the covariant generalization by Hubeny, Rangamani, and Takayanagi (HRT) [48]. Here and below we work in the regime where the bulk planck scale ℓ_p is small in comparison with the bulk AdS scale ℓ_{AdS} (which we generally set to 1), or equivalently where $N \gg 1$ in the CFT (i.e., large central charge c for a $1+1$ CFT).

In discussing $|TFD\rangle$, it is natural to focus on the bipartite entanglement between the associated two copies of the CFT. This entanglement has a special structure: as shown in [95], the entanglement is both local and bipartite in the sense that, when studying regions of the CFT of size greater than the thermal scale, a given region can be said to be entangled *only* with the corresponding spatial region in the second CFT. In particular, when we consider regions A, B (in the same or opposite CFTs) separated by more than this scale, the mutual information

$$I(A:B) = S(A) + S(B) - S(AB), \tag{4.2}$$

vanishes at leading order in large N. This result can easily be understood from a CFT path integral point of view. In general, the thermofield double state is calculated by a CFT path integral over a cylinder, linking the two copies of the spatial section the state (4.1) is defined on. In the high temperature limit, this cylinder becomes short compared to its circumference, so when we consider regions larger than the length of the cylinder, the resulting state naturally only entangles regions on one boundary with the corresponding region on the other boundary.

[27] Though there may be interesting subtleties; see e.g. [94].

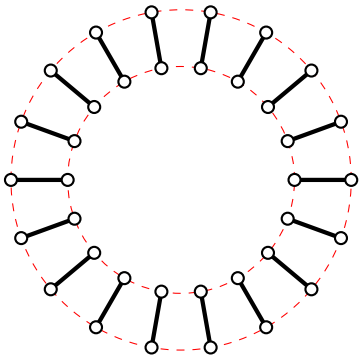

Figure 16: A simple tensor network displaying the localized purely-bipartite entanglement characteristic of holographic $|TFD\rangle$ states at large N on scales longer than the thermal scale. Each node represents a region in the CFT of scale longer than the thermal scale. We focus mainly on CFT states on $S^1 \times \mathbb{R}$ where one takes a high-temperature limit in order to fit many such long-distance regions onto the circle, though one may equally-well consider the planar case. The solid links are the entangling tensors implied by (4.1). The dashed lines guide the eye by linking neighbouring regions in each of the two CFTs.

It will be useful below to visualize this result in the language of tensor networks; see e.g. [96]. The rather trivial nature of the above entanglement then translates into a similarly-trivial coarse-grained tensor network description of $|TFD\rangle$ as shown in figure 16.

While the thermofield double state is a useful simple example, it is important to find further examples where we can understand the relation of bulk geometry to CFT entanglement structures. We are also interested in exploring the role played by multi-party entanglement in connections between 3 or more subsystems and what form it takes in the associated CFT states, see e.g. [97–99].

The vast literature on holographic entanglement has focused primarily on bipartite relations between a given subsystem in the CFT and its complement, so that relatively little is known about multiparty issues. One general result is the monogamy of holographic entanglement established in [100]. But a more detailed investigation of multipartite entanglement was recently initiated in [98] using a class of 2+1-dimensional black hole spacetimes [52–55] describing a collapsing wormhole that connects n regions each asymptotic to (global) AdS_3. When the corresponding Euclidean geometries define the dominant saddle of a natural path integral, such geometries are dual to entangled states on n copies of a 1+1 dimensional CFT on $S^1 \times \mathbb{R}$ defined by a path integral on a Riemann surface Σ with n circular boundaries [30, 101–103]. The corresponding entanglement was found to display a rich dependence on the moduli, including regimes of purely bipartite entanglement, and others of strong multipartite entanglement. Interestingly, the strongly

multipartite regions identified in [98] corresponded to bulk black holes with temperature less than the AdS scale[28]. The recent work [104] describes an infinite family of generalizations of results from both [100] and [98].

We focus below on the opposite limit in which all bulk black holes have high temperature. The length of their horizons is then very large with respect to the AdS scale. We will show that these geometries are dual to states constructed by sewing together copies of $|TFD\rangle$, as shown in figure 17. The entanglement is thus both local and bipartite away from small regions containing certain "vertices" where the sewing involves three or more copies of $|TFD\rangle$. From the CFT path integral point of view, this arises because the boundary circles are large compared to the distance between them; in a conformal frame where the boundaries are finite size, there are thin strips joining them, corresponding to the short tensor networks in figure 17. In section 4.4 we will justify this picture more quantitatively by showing that local pieces of the surface Σ are described by regions of BTZ up to exponential corrections. As a result, as in [105] tripartite entanglement appears to localise in isolated AdS-scale regions of the bulk. Away from these vertices, the construction of the state involves only the sewing together $|TFD\rangle$'s of inverse temperature β_1 and β_2, giving a local version of the $|TFD\rangle$ of inverse temperature $\beta_1 + \beta_2$. Since we focus on 1+1 CFTs, we henceforth refer to the limit of large central charge c rather than large N.

Note that nothing prevents sewing operations that link together disjoint regions in the same CFT as shown in figure 17 (bottom). As we will see, this also provides an interesting picture in our limit of CFT states dual to single-boundary black holes with internal topology. The reader should thus be aware that, while we use term "multiboundary" below, this explicitly includes the very interesting case $n = 1$ as well as $n \geq 2$.

One may expect each local piece of $|TFD\rangle$ in figure 17 (right) to correspond to a bulk region whose geometry near $t = 0$ is well-approximated by a corresponding piece of BTZ. We show in section 4.5 that this is indeed the case, and thus that bulk Ryu-Takayanagi (or, more precisely, HRT) calculations are consistent with the entanglements shown.

We begin by reviewing aspects of general multiboundary wormholes and their relation to CFT states in section 4.2. Section 4.3 then studies the high temperature (equivalently, large horizon length L) limit of the geometry of Σ. We show that the region between the horizons in Σ becomes

[28] It remains an open question whether such phases ever dominate the path integrals described above. But even if not, one presumes them to be dual to some other class of CFT states whose entanglement must be correspondingly multipartite.

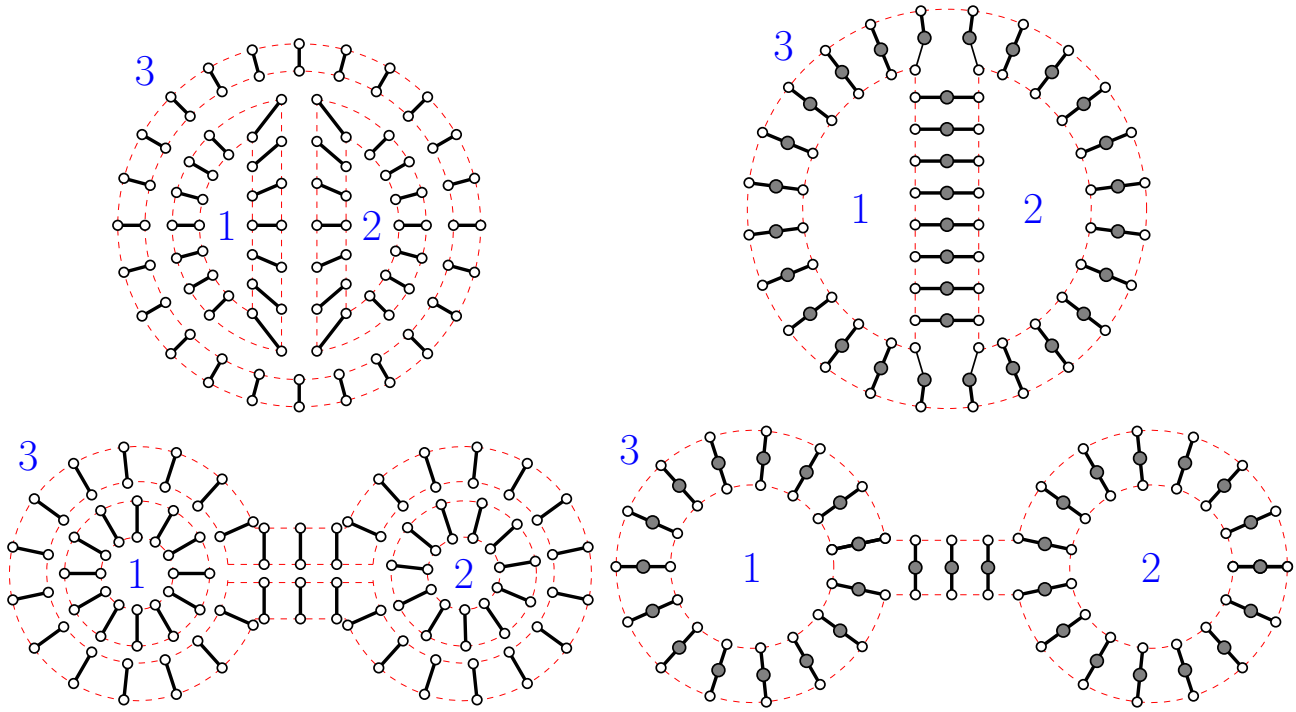

Figure 17: Two topologically-distinct ways in which three copies of the tensor network in figure 16 can be sewn together (left figures) into a single tensor network (right figures) defining a state on 3 copies of the system. The dashed lines (red in color version) internal to the left diagrams guide the eye toward recognising the 3 constituent copies of the network in figure 16. The gray nodes depict identifications between nodes which are identified by sewing together copies of the network in figure 16. Links that meet across adjoining pairs of dashed lines are contracted, establishing entanglement between the remaining boundaries (marked 1, 2, and 3). In the bottom-left figure, two parts of the outermost tensor network are contracted with each other, resulting in two well-separated regions of boundary 1 becoming entangled with each other as shown in the bottom-right figure. As discussed below, all 3-boundary time-symmetric vacuum wormholes with pair-of-pants topology (orientable with no handles) and large horizons correspond at the moment of time-symmetry to one of the cases shown, or to the degenerate case that interpolates between them, when described in the "round" conformal frame in which the energy density is taken to be constant along each of the 3 boundaries. Although we show only a simplified cartoon of the full tensor network, we argue below that sewing the actual $|TFD\rangle$ tensor networks together in this way describes the corresponding CFT states with exponential accuracy away from the two 'vertices' in each diagram where 3 $|TFD\rangle$'s meet.

unimportant in this limit. This allows us to argue in section 4.4 that the CFT path integral produces the structure described by figure 17. Section 4.5 then describes how this same result is seen in the bulk HRT calculation and argues that the desired bulk wormhole does indeed dominate the corresponding bulk path integral. Section 4.6 briefly addresses finite temperature corrections and we conclude in section 4.7 with discussions of the general n-boundary case, internal topology,

higher dimensions, and future directions. In particular we comment explicitly on examples with $n = 1$.

4.2 Path integrals, states, and bulk geometries

We now commence our review. As is well known, the thermofield double state of inverse temperature β is computed by the CFT path integral on the cylinder of circumference 2π and height $\beta/2$. Here one regards each of the two circular boundaries as the (say) $t = 0$ slice of a corresponding CFT. The path integral between field configurations ϕ_1, ϕ_2 on the two boundaries then gives the wavefunction $\Psi(\phi_1, \phi_2)$ of the joint state of the two CFTs.[29] At sufficiently high temperatures, the corresponding bulk path integral is dominated by a saddle point associated with the Euclidean BTZ black hole. In this case we may say that, to good approximation, the corresponding Lorentz-signature bulk black hole is dual to $|TFD\rangle$.

The cylinder of circumference 2π and height $\beta/2$ plays two important roles in the BTZ geometry. First, it is conformally equivalent to (half of) the boundary of Euclidean BTZ. This is what allows Euclidean BTZ to be a saddle for the desired bulk path integral. But this same cylinder is also conformal to the BTZ geometry at $t = 0$, which may be equally-well considered as a slice of either the Euclidean or the Lorentzian black hole. This may be seen by recalling [106] that Euclidean BTZ can be constructed as a quotient of global Euclidean AdS_3 (i.e., of the hyperbolic three-space H^3) by an isometry. The simplest statement requires two steps. One first writes Euclidean AdS_3 in terms of its slicing by hyperbolic planes H^2 (equivalently, by copies of Euclidean AdS_2) as

$$\frac{ds^2}{\ell_{AdS}^2} = dt_E^2 + \cosh^2 t_E d\Sigma^2, \tag{4.3}$$

where $d\Sigma^2$ is the metric on the unit-radius H^2. One then quotients each H^2 slice by a discrete group $\Gamma = \{g^n : n \in \mathbb{Z}\}$ generated by some hyperbolic element g of its $SL(2, \mathbb{R})$ group.[30] The action of g and its fundamental domain in H^2 are indicated in figure 18. Since the different H^2 slices in (4.3) differ only by the overall scale factor $\cosh^2 t_E$, the same is true of their quotients. The spatial slice at $t = 0$ (equivalently, $t_E = 0$) is thus conformal to the geometry at $t_E = -\infty$. This is half of the Euclidean boundary, with the other half being $t_E = +\infty$. We may therefore

[29] In this discussion we assume for simplicity that the CFTs admit (anti-unitary) time-reversal symmetries T which can be used to map bra-vectors to ket-vectors and vice versa, and which can therefore be used to construct (4.1) from the thermal operator $e^{-\frac{1}{2}\beta H}$.

[30] In other words, thinking of $SL(2, \mathbb{R})$ as the Lorentz group $SO(2, 1)$ of 2+1 Minkowski space this g must be a boost preserving some spacelike direction.

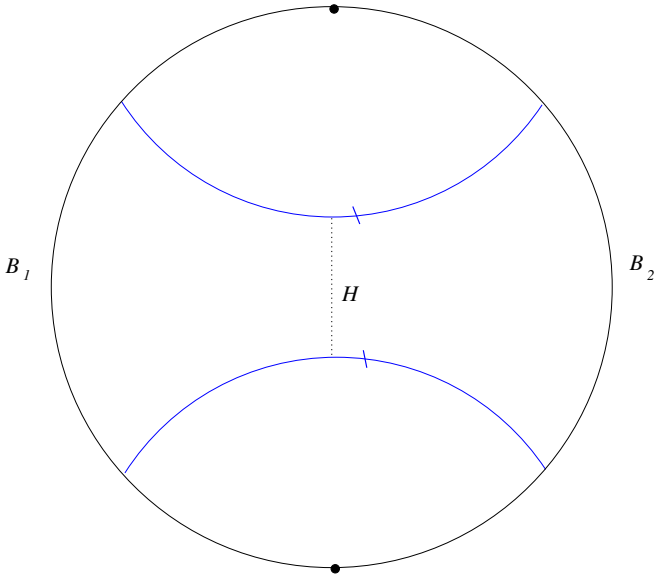

Figure 18: The quotient of the hyperbolic plane H^2 by Γ. The pair of labeled geodesics are identified by g, so the region between them forms a fundamental domain for the quotient. The minimal closed geodesic H is the horizon for the resulting BTZ geometry.

write $|TFD\rangle$ as given by the CFT path integral over the Riemann surface defined by the $t = 0$ slice of the corresponding BTZ geometry.

This final conclusion can be extended to a much larger class of states. Any Riemann surface Σ with n boundaries can be written as a quotient of H^2 by some discrete subgroup Γ_Σ of $SL(2, \mathbb{R})$. We may use (4.3) to construct a corresponding quotient of Euclidean AdS_3, with Σ conformal to both the slices at $t = 0$ and $t_E = -\infty$. So long as this saddle point dominates the bulk path integral with boundary conditions defined by the $t_E = -\infty$ slice, to good approximation the corresponding Lorentz-signature bulk solution – given by substituting $t_E = -it$ into (4.3) – is dual to the CFT state defined by the path integral over the slice at $t = 0$. For notational simplicity we identify Σ with this slice below and write the CFT state as $|\Sigma\rangle$. These quotients of AdS_3 were first considered in [53], and the holographic relation to $|\Sigma\rangle$ was introduced in [101–103]. An exploration of the entanglement properties of these states was initiated in [98].

The Lorentz-signature solutions describe wormholes connecting n asymptotically-AdS_3 boundaries. By topological censorship [107, 108], each boundary is associated with a distinct event horizon. A special property of AdS_3 vacuum solutions is that the geometry outside each event horizon is precisely that external to some BTZ black hole. This allows us to define a useful "round" conformal frame, in which the usual rotational symmetry of this BTZ region is a symmetry of the boundary. That is, for each of these exterior regions there is a coordinate ϕ_i such that

∂_{ϕ_i} is an exact rotational Killing field in the region outside the horizon (and in fact in an open neighbourhood in the interior of the horizon as well). The round conformal frame is the one in which the CFT lives on a spacetime with standard cylinder metric

$$ds^2 = -dt^2 + d\phi_i^2 \tag{4.4}$$

with $\phi \sim \phi + 2\pi$. In addition, the BTZ exterior implies that the bifurcation surface of each horizon – where the future and past horizons meet – is a geodesic in the $t = 0$ surface. The key novelty in the $n > 2$ cases is the existence of a "causal shadow" region in between these horizons.

Our ideas will apply to a codimension one limit in the moduli space of such Riemann surfaces for any n, but for simplicity we will focus our discussion on the case where Σ is an orientable surface with three boundaries and no handles. Such surfaces are topologically the same as a pair of pants. This is the simplest non-trivial example, and is also a primitive building block for constructing other cases, since a general orientable Riemann surface can be constructed by sewing together pairs of pants. The relevant quotient of H^2 is depicted in figure 19. The moduli space of pair-of-pants Riemann surfaces can be parametrized by the lengths L_a $(a = 1, 2, 3)$ of the three horizons, which as usual we take to be measured in units with $\ell_{AdS} = 1$. Without loss of generality we take $L_3 \geq L_1, L_2$. The causal shadow is the region in between these geodesics.

Properties of such states were explored in [98], with most emphasis on the so-called puncture limit $L_a \ll 1$. In particular, [98] showed that in this limit Σ is conformal to the Riemann sphere with small holes removed around n points, and hence $|\Sigma\rangle$ can be related to an n-point function in the CFT. For the three-boundary case, the state was determined up to some constant factors to be, in the round conformal frame,

$$|\Sigma\rangle = \sum_{ijk} C_{ijk} e^{-\frac{1}{2}\tilde{\beta}_1 H_1} e^{-\frac{1}{2}\tilde{\beta}_2 H_2} e^{-\frac{1}{2}\tilde{\beta}_3 H_3} |i\rangle_1 |j\rangle_2 |k\rangle_3, \tag{4.5}$$

where

$$\tilde{\beta}_a = \beta_a - 2\ln r_d - 2\ln 3, \tag{4.6}$$

and C_{ijk} are the three-point OPE coefficients, $\beta_a = \frac{4\pi^2}{L_a}$ is the inverse temperature of the BTZ geometry associated with the region near the a'th boundary, and r_d is an undetermined constant independent of the moduli. The rather explicit expression (4.5) exhibits both dependence on the structure of the CFT and Boltzmann-like suppression factors similar to the thermofield double

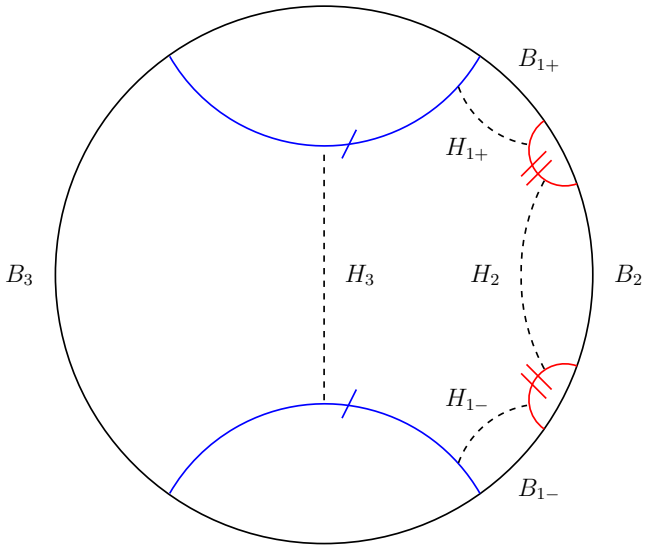

Figure 19: The surface Σ as a quotient of the Poincaré disc for $n = 3$. The pairs of labeled geodesics (blue and red in colour version) are identified by the action of Γ. The region of the Poincaré disc bounded by these geodesics provides a fundamental domain for the quotient. B_3, B_2 and $B_1 = B_{1+} \cup B_{1-}$ become the desired three circular boundaries. There are corresponding minimal closed geodesics H_3, H_2 and $H_1 = H_{1+} \cup H_{1-}$. The lengths L_a of these geodesics fully characterize the geometry of Σ.

state.

4.3 Geometry of Σ in the high temperature limit

Our current aim is to elucidate the structure of $|\Sigma\rangle$ in the limit $L_a \to \infty$ with fixed ratios L_a/L_b. This is the opposite of the limit emphasized in [98, 105]. We assume $L_3 \geq L_1, L_2$, so the ratios $L_1/L_3, L_2/L_3$ take values in $(0, 1]$. In this limit, the geometry of Σ again simplifies. The essential point is that the causal shadow region will play a relatively unimportant role. We will focus on the pair of pants case, but the discussion is easily extended to arbitrary Riemann surfaces. We comment on this extension in section 4.7.

Our limit can be characterised as a high temperature limit, in the sense that the BTZ horizon in each of the exterior regions becomes large compared to the AdS scale (as for a high T BTZ black hole). But we note that the restriction of the state $|\Sigma\rangle$ to a single boundary is not necessarily even approximately thermal: as discussed in [98], when one L_a is larger than the sum of the other ones, reduced density matrix in that exterior region has much less entropy than the thermal value at the same energy.

To understand the geometry of Σ in our limit, it is useful to introduce a different presentation

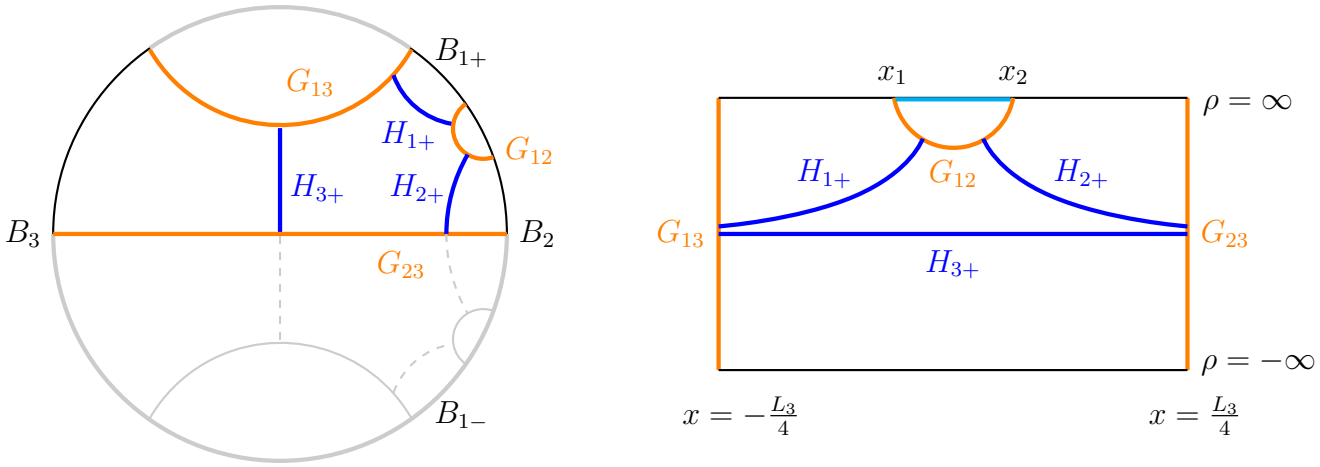

Figure 20: The region Σ_+ bounded by the geodesics G_{ab}, half each of B_2, B_3, and B_{1+} shown in the Poincaré disc (left) and the BTZ frame strip (right). The BTZ presentation is chosen to place the half-horizon H_{3+} along the BTZ horizon. The geodesics G_{13}, G_{23} are respectively the lines $x = -\frac{L_3}{4}$, $x = \frac{L_3}{4}$. In contrast, G_{12} lies in the upper half of the strip; its endpoints have $x = x_1, x_2$ with $\rho = +\infty$. Half each of B_1, B_2 is mapped respectively to the line segments $x \in [-\frac{L_3}{4}, x_1]$, $x \in [x_2, \frac{L_3}{4}]$ at $\rho = \infty$ respectively, whilst half of B_3 is mapped to $\rho = -\infty$. The corresponding Σ_- is the symmetric region below G_{23} in the Poinaré disk (left) and has an identical representation in the BTZ strip.

using two patches with BTZ coordinates on each[31]. We split figure 19 in half along the horizontal geodesic (not drawn explicitly) joining boundaries B_1 and B_2. This divides Σ into two identical regions $\Sigma_\pm$, each containing half of each horizon H_a. The surface Σ is then recovered by gluing together $\Sigma_\pm$ along three geodesics, the two identified geodesics in figure 19 and the new split. We label these geodesics $G_{ab} = G_{ba}$ with $a \neq b$ labelling the boundaries they run between; see figure 20 (left). They can be described more formally as the fixed points of a $\mathbb{Z}_2$ isometry of Σ, which acts as a reflection $\phi \to 2\pi - \phi$ in the round conformal frame on each of the boundaries (with appropriate choices of the origin $\phi = 0$ on each boundary). The event horizon H_a of boundary a is the unique geodesic that runs orthogonally between the two geodesics G_{ab}, G_{ac} $(b \neq c)$ that end on boundary a. Our partition of Σ into $\Sigma_\pm$ also breaks each horizon H_a into two pieces $H_{a\pm}$.

It is useful to describe $\Sigma_\pm$ in planar BTZ coordinates.[32] Consider for definiteness Σ_+. We

[31] In the actual history of our project, this description was also inspired by computing mutual information on pairs of pants with large L_a using the technology of [109].

[32] By planar BTZ we mean the usual BTZ coordinates with no identification on the spatial coordinate on the boundary; this provides a coordinate system on the whole of H^2, thought of as the $t = 0$ surface in AdS_3. Since our $\Sigma_\pm$ are subregions of H^2, they can be conveniently described in these coordinates.

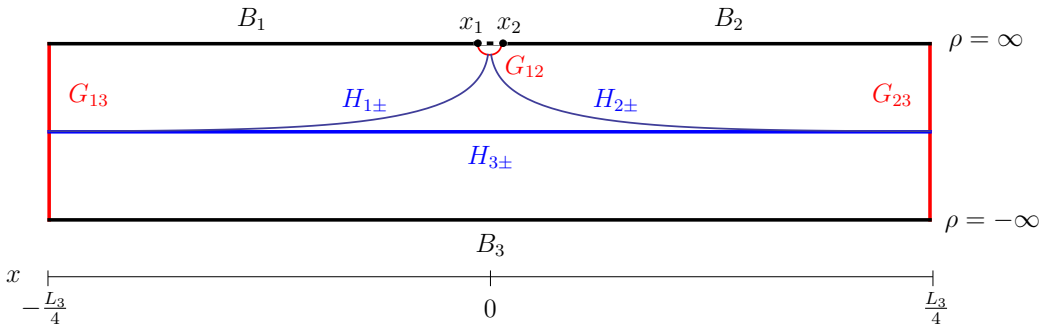

(a) $L_1 + L_2 > L_3$

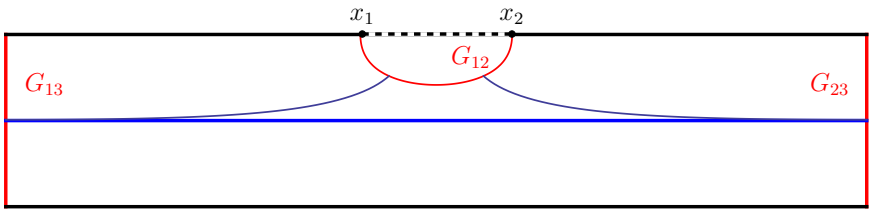

(b) $L_1 + L_2 \sim L_3$

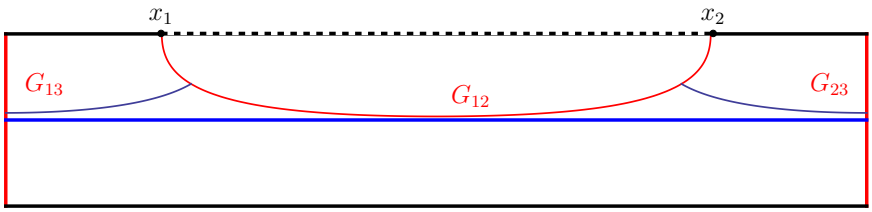

(c) $L_3 > L_1 + L_2$

Figure 21: Half of the pair-of-pants (either Σ_+ or Σ_-) described as a region in planar BTZ. Three examples are shown representing distinct regions of moduli space: $L_1 + L_2 > L_3$ (top), $L_1 + L_2 \sim L_3$ (middle), $L_3 > L_1 + L_2$ (bottom).

choose the BTZ coordinates to be

$$\frac{ds^2_{BTZ}}{\ell^2_{AdS}} = \frac{d\rho^2}{\rho^2 + 1} + (\rho^2 + 1)dx^2, \tag{4.7}$$

with $\rho \in (-\infty, \infty)$. Thus our reference BTZ solution has inverse temperature 2π. Without loss of generality, we take $L_3 \geq L_2 \geq L_1$ and orient Σ_+ such that the portion of H_3 in Σ_+ lies along the horizon at $\rho = 0$, and the boundary B_3 lies at $\rho = -\infty$, in both cases for $x \in [-L_3/4, L_3/4]$. Since the geodesics G_{13} and G_{23} intersect H_3 orthogonally, they will lie at $x = -L_3/4$ and $x = L_3/4$ in these coordinates. The other two boundaries B_1 and B_2 lie at $\rho = \infty$, for $x \in [-L_3/4, x_1]$ and $x \in [x_2, L_3/4]$ (with $x_1 < x_2$), and the remaining geodesic G_{12} runs between these points x_1, x_2. The portions of H_1, H_2 in $\Sigma_\pm$ are the geodesics running from the edges of the strip to meet G_{12} orthogonally. These coordinates are illustrated in figure 20.

The half-surface Σ_+ is thus a strip $x \in [-L_3/4, L_3/4]$ in the planar BTZ coordinates, with a bite cut out of the middle above G_{12}. It is important to emphasize that the boundaries at $-L_3/4, L_3/4$ are not identified with each other; instead they and G_{12} are identified with the corresponding boundaries in a second copy of this region.

In general we could check that a subregion of planar BTZ in the coordinates (4.7) we consider covers half of the pair-of-pants geometry by taking the explicit forms of the metric in the inner and outer charts for the pair-of-pants wormhole found in [103]. There, maps from the outer and inner charts of the pair-of-pants to portions of the Poincare patch of AdS_3 are given. Relating these coordinates to our BTZ coordinates would allow us to determine an explicit map from half of the corresponding $t = 0$ slice to the region of planar BTZ illustrated in figure 20 (right). We do not do this calculation here.

As we verify in appendix B, varying the endpoints x_1, x_2 of B_1, B_2 generates all possible lengths L_1, L_2 for the remaining horizons H_1, H_2 and the map $(x_1, x_2) \mapsto (L_1, L_2)$ is both smooth and one-to-one. When we take the limit of large L_a (at fixed ratios), the results simplify, with a form that depends on the relative lengths. For $L_3 - (L_1 + L_2) \gg 1$,

$$x_1 \sim \frac{L_1}{2} - \frac{L_3}{4} - \log 2, \; x_2 \sim \frac{L_3}{4} - \frac{L_2}{2} + \log 2, \tag{4.8}$$

where the tildes ($\sim$) represent agreement up to exponentially small corrections. Note that up to a fixed order-one offset, the endpoints are respectively $L_1/2$ and $L_2/2$ from the ends of the strip. In the complementary case $L_3 - (L_1 + L_2) \ll 1$, we find instead

$$\frac{x_1 + x_2}{2} \sim \frac{L_1 - L_2}{4}, \quad \frac{x_2 - x_1}{2} = \exp\left(-\frac{L_1 + L_2 - L_3}{4}\right). \tag{4.9}$$

In our BTZ presentation, the long length of H_3 corresponds directly to the large width of the strip. The horizons H_1, H_2 are also long as a result of extending over a large coordinate distance in the x direction and possibly also from extending out towards the boundary of the strip at large ρ. If both of them together are shorter than H_3 ($L_1 + L_2 \leq L_3$), they terminate on G_{12} in the interior of the strip, staying within an order one distance from the horizon H_3 at $\rho = 0$ along their whole length, as in the last panel of figure 21. When the sum is larger (which includes the case where the three lengths are equal), the length of the interval $x_2 - x_1$ is exponentially short, hence H_1, H_2 meet G_{12} at large ρ, as in the first panel of figure 21. In both cases, H_1 and H_2

approach H_3 exponentially for $|x - x_{1,2}| \gg 1$.

The contributions to L_1, L_2 from the width of the strip or from H_1 and H_2 running to large ρ look different, but we should remember that Σ_+ treats the three horizons symmetrically, so this is just an artifact of our choice of coordinates. The symmetry can be made manifest in an appropriate Poincaré disk representation; see e.g. figure 8 of [98]. The relationship between any pair of horizons is thus much the same; consider for example H_1 and H_3. We can see explicitly from the calculation in appendix B that the minimal distance between them is exponentially small, and that they remain exponentially close over a large region. Thus, the area of the causal shadow region remains finite even as their length becomes large.

In fact, since the boundaries of the causal shadow are closed geodesics (and thus have vanishing extrinsic curvature), the Gauss-Bonnet theorem requires this area A_{CS} to be independent of the moduli L_a (for any fixed genus g and number of boundaries n). For the pair of pants we find $A_{CS} = 2\pi$; more generally $A_{CS} = 2(n - 2 + 2g)\pi$. As we will see in the next section, this implies that the causal shadow region plays little role in the path integral construction of the CFT state $|\Sigma\rangle$ at high-T.

In the case where $L_3 - (L_1 + L_2) \gg 1$, the endpoints of the geodesic G_{12} are far apart in coordinate distance, and it will also be exponentially close to H_3 over most of its length. When we glue Σ_+ and Σ_- to form Σ, the section of H_3 that is close to G_{12} will lie close to the corresponding section of H_3 in Σ_-, as in figure 17 (right). All remaining cases with $L_3 \geq L_2 \geq L_1$ are intermediate between the two just described.

4.4 The CFT state at large L_a

Let us now consider the implications of the above results on the structure of Σ for the CFT state $|\Sigma\rangle$. In this section we will argue for large L_a that $|\Sigma\rangle$ will be described to exponential accuracy by figure 17 (right). In particular, when restricted to appropriate regions it agrees to exponential accuracy with the corresponding restriction of a thermofield double state $|TFD\rangle$. We also show, under the assumption that non-handlebody contributions can be ignored, that the Euclidean bulk geometry (4.3) dominates the bulk path integral defined by using Σ as the conformal boundary. It follows that, to exponential accuracy, our bulk pair-of-pants wormhole is dual to the state described by figure 17 (right).

Recall that $|\Sigma\rangle$ is defined by the CFT path integral over Σ. We will use the BTZ representation

of $\Sigma_\pm$ associated with figure 21 to break Σ into three pieces $\Sigma_{1,2,3}$ that are topologically cylinders, corresponding to figure 17 (left). Each piece Σ_a will contain the entire pair-of-pants boundary B_a, but no portion of the boundaries B_b for $b \neq a$. The decomposition is defined by drawing a graph in Σ as shown in figure 22. As noted in the figure caption, far from the vertices the piece Σ_a nearly coincides with the region E_a of Σ exterior to H_a (i.e., lying between H_a and boundary a). The geometry in this latter region is just that of the appropriate BTZ solution outside the horizon and is conformal to a round (rotationally-invariant) cylinder.

We wish to regard both E_a and Σ_a as path integrals constructing states $|E_a\rangle$, $|\Sigma_a\rangle$, each of which is defined on two copies of our CFT (on the outer and inner boundaries of E_a or Σ_a respectively). Indeed, we may write $|\Sigma_a\rangle = \hat{S}_a|E_a\rangle$ where $\hat{S}_a$ is the operator defined by the path integral over the causal shadow region $S_a = \Sigma_a/E_a$ in Σ_a beyond the horizon H_a. We specify the conformal frames of all states by again taking ϕ_a to define the standard angle on the CFT cylinder; this involves a natural extension of ϕ_a through the causal shadow S_a. The region S_a is topologically an annulus and so can be conformally transformed to a cylinder. But S_a is exponentially thin over most of its circumference; indeed, setting $a = 3$ (so that we may replace ϕ_3 by $2\pi/L_3$ times the BTZ x) and multiplying the BTZ metric (4.7) by $\ell_{AdS}^{-2}(1+\rho^2)^{-1}$ gives a metric

$$ds^2_{S_3} = dx^2 + dy^2, \tag{4.10}$$

where $y = \tan^{-1}\rho$ ranges over $[0, f(x)]$ with $f(x)$ is exponentially small far from the vertices of our graph. Introducing $\tilde{y} = y/f$ along with $\tilde{x}$ such that $d\tilde{x} = dx/f$, and multiplying (4.10) by f^{-2} gives a metric

$$f^{-2}ds^2_{S_3} = d\tilde{x}^2 + (d\tilde{y} + f'\tilde{y}d\tilde{x})^2, \tag{4.11}$$

where $f' = df/dx$, on cylinder of unit height $\tilde{y} \in [0,1]$ but with exponentially large circumference. The metric is not flat, though it differs from the standard cartesian flat metric $d\tilde{x}^2 + d\tilde{y}^2$ only by exponentially small corrections proportional to powers of f'. It follows that there is a further conformal transformation to a metric cylinder of unit height – and with exponentially small difference in circumference from the range of $\tilde{x}$ – whose action on the region far from the vertices is exponentially close to the identity map[33].

Rescaling this cylinder to one of circumference 2π allows us to write the path integral over S_a

[33]Here we use the fact that conformal transformations satisfy an elliptic equation with a Green's function that decays exponentially along a strip. We expect that similar arguments are common in the literature, but for a specific example the interested reader interested in details may consult for comparison e.g. section 3.1.1 of [98].

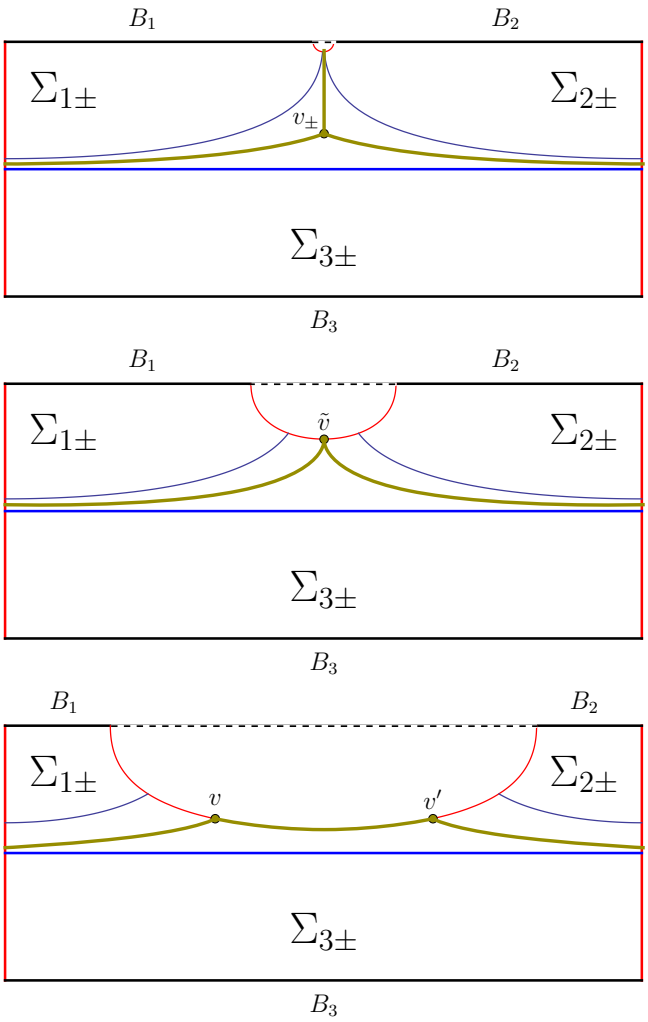

Figure 22: The decomposition of $\Sigma_\pm$ into pieces $\Sigma_{1\pm}, \Sigma_{2\pm}, \Sigma_{3\pm}$. We then glue Σ_{a+} to Σ_{a-} along the relevant G_{ab} to make pieces Σ_a conformal to cylinders with Σ_a containing all of boundary a. The decomposition is determined by a graph. In cases (a) and (c), the graph has two trivalent vertices. In case (a) each piece $\Sigma_\pm$ contains one vertex $v_\pm$. The 3 edges of the graph each connect v_+ to v_- running between two distinct horizons H_a, H_b for $a \neq b$. In case (c) both vertices v, v' lie on the cut along G_{12}, as does the edge that connects them. The other two edges are loops connecting v to v or v' to v'. One lies between H_1 and H_3 while the other lies between H_2 and H_3. Case (b) represents a degenerate limit interpolating between the two in which we choose to fuse the two vertices into a single 4-valent vertex lying on G_{12}. The graph has two edges, each of which are loops. One lies between H_1 and H_3 while the other lies between H_2 and H_3. In the regions far from the vertices the pieces $\Sigma_{1,2,3}$ defined by cutting Σ along the edges of the appropriate graph differ from the cylinders defined by the regions outside horizons $H_{1,2,3}$ only by exponentially small amounts.

in terms of the operator $e^{-\beta H}$ with exponentially small β. Up to exponentially small corrections, this operator acts as the identity with respect to degrees of freedom associated with spatial regions of order-one size as measured by the original spatial coordinate ϕ_a. So far from the vertices we

may identify $|E_a\rangle$ and $|\Sigma_a\rangle$ with exponential accuracy.

On the other hand, the exterior region E_a is half of the BTZ $t = 0$ surface, so $|E_a\rangle$ is given by a path integral over a cylinder of length $\beta/4$, so it is a copy $|TFD\rangle_a$ of (4.1) at twice the temperature of the associated bulk horizon. Thus $|\Sigma_a\rangle$ is, up to exponentially small corrections, a thermofield double state. Recall that for large L_a such $|TFD\rangle_a$ are described by a tensor network of the form shown in fig. 16.

It remains only to sew the $|\Sigma_a\rangle = |TFD\rangle_a$ together into $|\Sigma\rangle$. The sewing procedure is defined by the way the path integrals $\Sigma_{1,2,3}$ combine to form Σ. Away from the vertices of the graph, this identifies the horizons in $E_{1,2,3}$: for $L_1 + L_2 > L_3$, parts of H_3 are identified with each of H_1 and H_2, and the remaining parts of H_1 and H_2 are identified with each other. For $L_1 + L_2 < L_3$, H_1 and H_2 are each entirely identified with corresponding parts of H_3, and the remaining regions of H_3 along G_{12} are identified with each other. Since the sewing operation on path integrals coincides with the sewing operation on tensor networks – one simply sets all arguments equal along the seam and integrates over allowed values[34]– this implies that the state $|\Sigma\rangle$ is given to exponential accuracy by fig. 17 (right), with the top picture relevant for $L_1 + L_2 > L_3$ and the bottom picture relevant for $L_1 + L_2 < L_3$.

Finally, we also wanted to see that $|\Sigma\rangle$ is dual to our bulk geometry with moment of time symmetry Σ. As in [98] we assume that the dominant saddle of the associated bulk integral is a handlebody. The other possible bulk saddles discussed in [98] correspond to disconnected Lorentzian geometries. It is natural to expect this saddle to dominate at large temperatures, by analogy to the familiar result for $|TFD\rangle$ that disconnected solutions dominate only at low temperatures. But one can now make a further argument based on entanglement. If the HRT proposal is correct, and in particular if entanglement is associated with extremal surfaces in the real Lorentz-signature geometry, the disconnected geometries cannot reproduce the entanglement structure of figure 17 (right), which involves entanglement between the different boundaries at leading order in the central charge. It would be interesting to verify this conclusion by direct computation of the Euclidean actions, as it would serve as a check on HRT.

[34]Here for simplicity we again make use of the time-reversal symmetry mentioned in section 4.2 to turn bra-vectors into ket-vectors.

4.5 Holographic entanglement calculations

The previous section used the CFT path integral to show that the CFT state $|\Sigma\rangle$ is given by figure 17 (right), so that the state has local bipartite entanglement with the same local structure as the thermofield double state. In this section we will buttress that argument by showing that our picture of the geometry of Σ, now thought of as the $t = 0$ surface in the bulk spacetime, gives consistent results for entanglement from holographic Ryu-Takayanagi calculations. Indeed, in the history of our project we originally discovered that the state had this simple bipartite structure by performing these holographic calculations explicitly. We consider the entanglement for a region in boundary 3, since our coordinates are adapted to this boundary, but by symmetry similar results apply in the other cases.

Consider first a region in boundary 3 where the horizon H_3 is exponentially close to either H_1 or H_2, that is $x_1 - x \gg 1$ or $x - x_2 \gg 1$. In the exterior region E_3, the planar BTZ coordinate x is identical (up to a scale and a shift of origin) to the round conformal frame coordinate ϕ_3 defined in section 4.2: $\phi_3 = \frac{2\pi}{L_3}x$. In the other exterior region, at similar x but outside H_1, H_2, because the horizon $H_{1,2}$ is exponentially close to H_3, the planar BTZ coordinate x agrees with $\phi_{1,2}$ (up to a scale and a shift of origin) up to exponentially small corrections. We can take for example $\phi_1 = \frac{2\pi}{L_1}x$. This is manifestly true near $\rho = 0$ (see (4.7)) and continues to hold at large ρ due to the properties of geodesics in hyperbolic geometry[35]. So for $x_1 - x \gg 1$, $x - x_2 \gg 1$ we may take x to define the round conformal frame on all three boundaries up to exponentially small corrections.

The above relations allow us to easily map those geodesics involved in any HRT calculation of the mutual information between subregions of boundaries 1 and 3 (or 2 and 3) that lie far from x_1, x_2 to geodesics in BTZ. The BTZ calculation was studied in [95], who found that for regions much larger than the thermal scale, the mutual information is simply proportional to the size of the overlap between the two regions. The overlap is maximal when the two regions are directly opposite each other, in which case the high-temperature result (3.27) of [95] becomes

$$I(A:B) = S(A) + S(B) - S(A \cup B) = \frac{L}{4G}\frac{(\Delta\phi + 2\pi - (2\pi - \Delta\phi))}{2\pi} = \frac{L}{2G}\frac{\Delta\phi}{2\pi} + \mathcal{O}(L^0). \quad (4.12)$$

[35] Two geodesics on H^2 fired at slightly different angles from the same point will diverge exponentially as measured by the proper distance separating them as the curves approach the boundary. So curves of constant $\phi_{1,2}$ and x that meet at the horizon also diverge in a similar manner near the boundary. But two geodesics fired orthogonally from different points x', x'' of the horizon again diverge exponentially at precisely the same rate. So a curve of constant $\phi_{1,2}$ that meets the horizon at x' with $|x' - x_{1,2}| \gg 1$ will meet the boundary at some x'' with $|x'' - x'|$ still exponentially small.

Applying appropriate scalings to (4.12), the mutual information between corresponding regions of boundaries 1 and 3 with $x_1 - x \gg 1$ is

$$I(A:B) = \frac{1}{2G}\Delta x + O(1) = \frac{L_1}{2G}\frac{\Delta\phi_1}{2\pi} + O(1) = \frac{L_3}{2G}\frac{\Delta\phi_3}{2\pi} + O(1). \tag{4.13}$$

In addition, since the region of boundary 1 with $x_1 - x \gg 1$ is well-separated in the bulk from the region of boundary 2 with $x - x_2 \gg 1$, it also follows that these two regions share no mutual information. The situation is exactly similar for the region in boundary 3 with $x - x_2 \gg 1$, which has a mutual information of the same form with a region in boundary 2.

If $|x_2 - x_1| \ll 1$, there are large parts of H_1, H_2 that are far from H_3, and so have yet to be described. This indicates that there are large intervals of $\phi_{1,2}$ along boundaries 1 and 2 with x-values close to the endpoints x_1, x_2. But it also implies a large conformal transformation between the round conformal frame for B_1, B_2 and the planar BTZ coordinate x. As a result, the renormalized length of any geodesic connecting boundary 3 to these regions of boundaries $1, 2$ is very long and HRT calculations give no mutual information between boundary 3 and these regions.

For $|x_2 - x_1| \ll 1$, the above results describe the entanglement properties of boundary 3, with the exception of a region with length of order the thermal length scale (which in the planar BTZ coordinates is of order the AdS scale) near x_1, x_2. So away from the vertices the entanglement structure obtained from bulk calculations corresponds precisely with that predicted by the state pictured in the top panel of figure 17, given by sewing together thermofield double states.

We now turn to the complementary case $|x_2 - x_1| \gg 1$. There is then a large region of boundary 3 not covered by the regions $x_1 - x \gg 1$, $x - x_2 \gg 1$ studied above. But across the region satisfying both $x - x_1 \gg 1$ and $x_2 - x \gg 1$, the geodesic G_{12} lies exponentially close to H_3. So sewing together Σ_+ and Σ_- in this region is well-approximated by simply gluing to each other the boundaries of E_3 (the region outside H_3; the lower half of each diagram in figure 21) along $H_{3\pm}$; i.e., the result is well approximated by the region of the two-sided BTZ geometry with $x_1 < x < x_2$.

Note that the two asymptotic boundaries of this new BTZ geometry are identified with different regions of boundary 3 coming respectively from Σ_+ and Σ_-. In particular, since our slicing of the pair of pants into $\Sigma_\pm$ was performed using the $\mathbb{Z}_2$ reflection symmetry, we see that a given value of x with $x_1 < x < x_2$ corresponds both to some point ϕ_3 and also to $2\pi - \phi_3$ in

terms of the usual coordinate on boundary 3 that defines the round conformal frame. Thus, in this case the mutual information of a region in boundary 3 with the corresponding region on the opposite side in boundary 3 will be as given in (4.13), supporting the local thermofield-double like entanglement between the two pieces of this boundary as indicated in the bottom panel of fig. 17.

4.6 Finite size corrections

We have shown that $|\Sigma\rangle$ has a simple structure in the high temperature limit. To use this as a systematic approximation to the state corresponding to finite-size wormholes, it is interesting to investigate finite-temperature corrections to this. In this section we will consider this first for the simple two-boundary case and then for three boundaries.

4.6.1 Two boundaries

In the two-boundary case, we want to understand and characterise the departure from the trivial network pictured in figure 16. The departure will be significant when we consider small regions, of order the thermal scale or smaller. For simplicity, we diagnose this by considering the mutual information between a subregion in one boundary and the whole of the other boundary.

The key finite temperature effect is that, for small regions, there is a competition between different possible minimal surfaces in the bulk homologous to A. For $S(A)$, we need the smaller of $l(\gamma_A)$, the length of the minimal (connected) geodesic γ_A homotopic to A, or $l(\gamma_{A^c}) + L$, where γ_{A^c} is the minimal (connected) geodesic homotopic to A^c and L is the length of the closed geodesic at the horizon. Similarly $S(A^c)$ is determined by either $l(\gamma_{A_c})$ or $l(\gamma_A) + L$, and there is an interesting competition between these two possibilities when A is nearly the whole boundary.

At high temperature the geodesics γ_A, γ_{A_c} behave as shown in figure 23. As a function of the angle ϕ, they drop quickly from the boundary to the horizon, hug the horizon while traversing an angle nearly $2\pi - \Delta\phi$, and then quickly return to the boundary. One thus finds

$$l(\gamma_A) = L\frac{\Delta\phi}{2\pi} + O(L^0), \quad l(\gamma_{A^c}) = L\left(1 - \frac{\Delta\phi}{2\pi}\right) + O(L^0), \tag{4.14}$$

which reproduces the behaviour in (4.12) found in [95].

At finite L, corrections to (4.14) are exponentially small in L when A and A^c are larger than the thermal scale, and the entropy remains close to linear in $\Delta\phi$. But for any finite L there is a

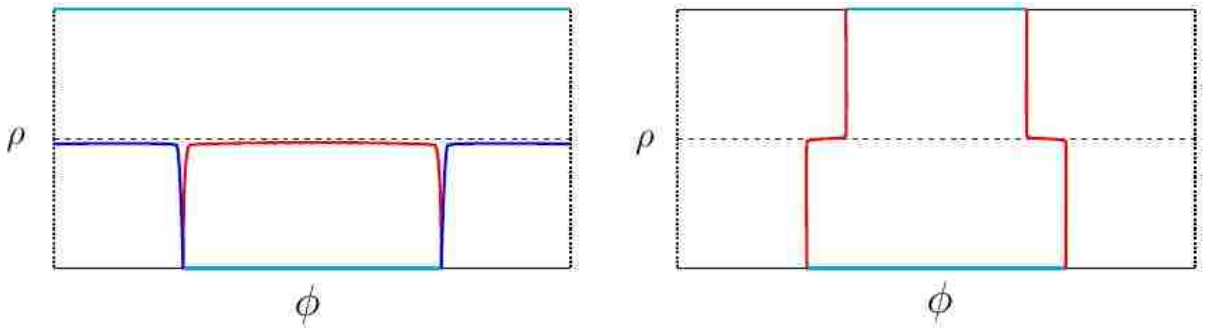

Figure 23: The geodesics giving, in the high-temperature limit, the phases of entanglement entropy of the union of a pair of intervals (cyan) lying on opposite boundaries, along with the event horizon added to satisfy the homology constraint, marked by the horizontal dashed line. When one of the intervals is a whole boundary, there are only two relevant phases (left), otherwise a third phase (right) may dominate, for which the corresponding geodesics cross the horizon and have endpoints lying on opposite boundaries.

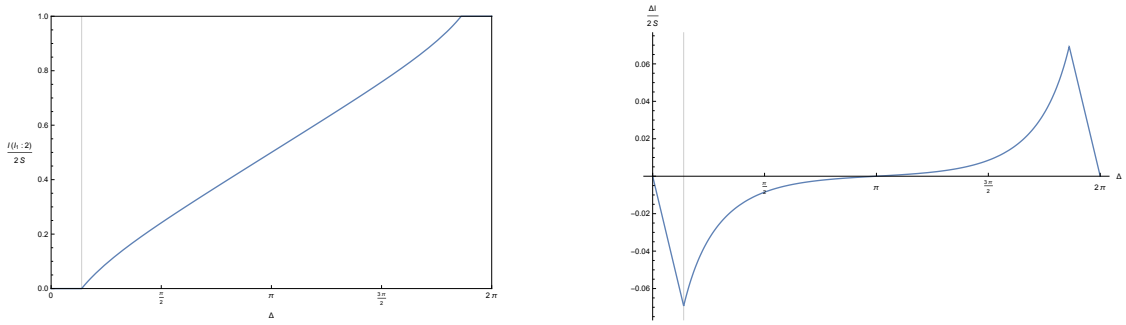

Figure 24: Left: Plot for $L = 10$ of the mutual information $I(I_1; 2)$ between an interval I_1 of size Δ in B_1 and all of B_2, as a function of Δ, scaled by the maximal value $2S$. The mutual information increases approximately linearly in Δ and becomes non-zero at the phase transition where $\Delta \sim l^{-1}$ (vertical line near left edge). Right: Plot of the deviation in the mutual information shown at left from the high-temperature estimate $2S\frac{\Delta}{2\pi}$. This deviation is very small; for readability the vertical scale has been magnified relative to the left-hand plot. The deviation is most significant for small and large values of Δ, and decays exponentially in L at intermediate values as expected.

Ryu-Takayanagi phase transition when either A or A^c becomes sufficiently small. In that regime the relevant entropy $S(A)$ or $S(A^c)$ becomes controlled by the disconnected geodesic. Thus, when the length of A falls below $2\pi \log 2/L + O(e^{-L}/L)$ one finds $I(A : B) = 0$. For A^c smaller than this threshold, one finds $I(A : B) = 2S(B) = \frac{L}{2G}$. Plotting the full $I(A : B)$ at large but finite T clearly shows these "plateaux" as in figure 24. These plateaux were studied in [110]; they can be characterised in terms of saturation of the Araki-Lieb inequality as discussed in [111].

The fact that small intervals do not capture the entanglement with boundary 2 indicates that this information is encoded in a way that is non-local on the thermal length scale. This is

not surprising, but it is useful to note that this correction to the large L picture has a natural expression in the language of [59]. It says that at finite temperature the information about the entanglement between the two boundaries is not encoded locally in degrees of freedom at individual spatial points, but rather in a code subspace in each boundary, which entangles individual spatial degrees of freedom on the thermal scale. The ability to recover all of the information from any sufficiently large spatial subset of the degrees of freedom is the characteristic signature of such encoding in a code subspace. In [59], the size of the region needed to access information in a code subspace was related to the radial location of the bulk region encoded. Similarly, in BTZ this size is related to the radial position of the horizon.

On a related note, the plateau at large $\Delta\phi$ appears precisely when the Ryu-Takayanagi surface for region A is $\gamma(A^c)$ plus the horizon. In other words, it occurs precisely when the so-called entanglement wedge [93] – the region inside this Ryu-Takayanagi surface – reaches all the way to the horizon. Indeed, in this case we see that it touches each and every point on the horizon and on A's side of the horizon it misses only a small part of the space near A^c. This suggests that the bulk near-horizon degrees of freedom are encoded non-locally in the CFT in such a way that they can be perfectly recovered from a large spatial subset A that remains slightly smaller than the entire boundary.

4.6.2 Pair of pants

For the pair of pants, we again study finite temperature corrections by considering the departure of the mutual information between a region in one boundary, say boundary 3, and the whole of another boundary, say boundary 1,

$$I(A_3 : 1) = S_{A_3} + S_1 - S_{A_3 \cup 1}, \tag{4.15}$$

from the approximation suggested by (4.13). As for the two boundary case, we expect the main departure to come near transitions between different phases, where different geodesics are exchanging dominance in the calculation of the holographic entanglement entropies. For this case, the phase transitions depend on two parameters: the size of A_3 and its location on boundary 3. The different possible phases for $S(A_3)$ and $S(A_3 \cup B_1)$ are illustrated in figures 25 and 26 respectively.

The calculation of the associated geodesic lengths can be easily automated using the description

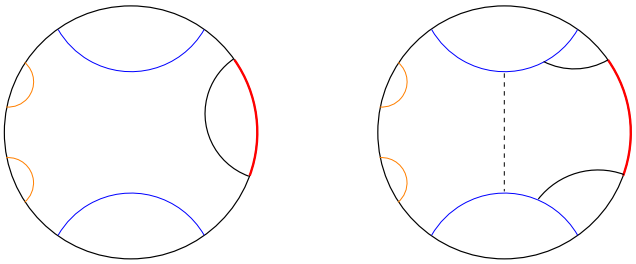

(a) Phase 1: 1 (b) Phase 2: g_1^{-1}

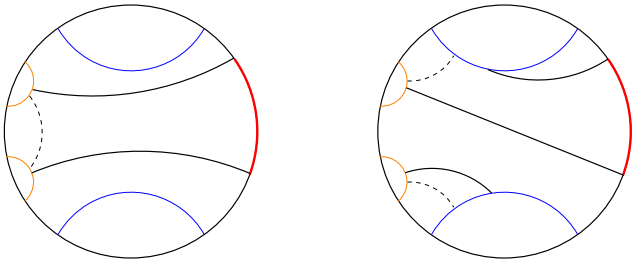

(c) Phase 3: g_2^{-1} (d) Phase 4: $g_2 g_1^{-1}$

Figure 25: The geodesics giving the four possible phases of entanglement entropy of a single interval, in red, along with the event horizons added to satisfy the homology constraint, marked by dashed lines.

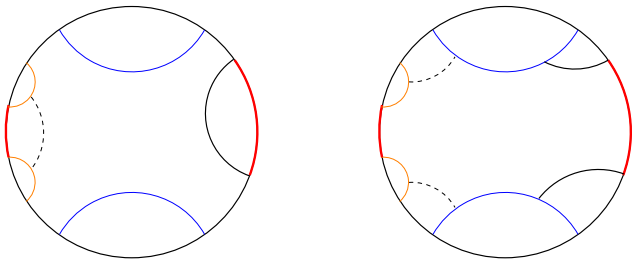

(a) Phase 1: 1 (b) Phase 2: g_1^{-1}

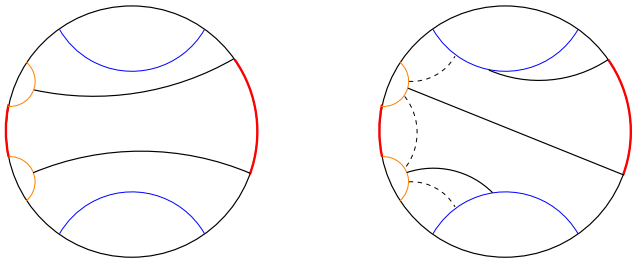

(c) Phase 3: g_2^{-1} (d) Phase 4: $g_2 g_1^{-1}$

Figure 26: The geodesics giving the four possible phases of entanglement entropy of the union of a single interval A_1 and the whole of boundary 2, in red, along with the event horizons added to satisfy the homology constraint, marked by dashed lines.

of the geodesic lengths as traces of corresponding $SL(2,\mathbb{R})$ group elements exploited in [109]. The lengths of the relevant geodesics can be found by computing the appropriate matrix products and traces. While the exact form of the answer is complicated and unilluminating, the general structure is fairly simple, being built mostly from polynomials in parameters encoding horizon

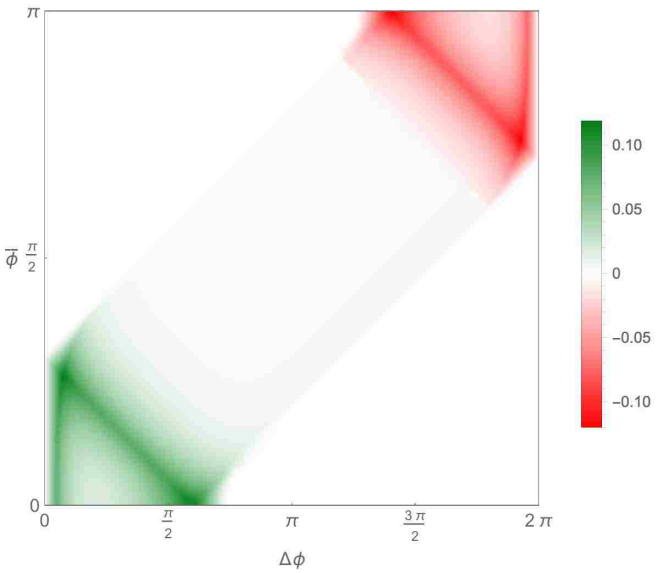

Figure 27: Deviation of the mutual information $I(A : B_1)$ between a region $A = \{\phi_3 \in [\bar{\phi} - \Delta\phi/2, \bar{\phi} + \Delta\phi/2]\}$ in B_3 and the whole of boundary 1 from the piecewise-linear form implied by figure 17 (lower right) for $L_1 = 9, L_2 = 15, L_3 = 30$. We plot the ratio between the error and the maximal mutual information (twice the entropy of B_1). Here $\phi_3 = 0$ is the leftmost point in figure 17 (lower right) and for comparison the inverse temperature β_3 is $\frac{(2\pi)^2}{30} \approx 1.3$. The error is exponentially small in L, except in a region of thermal scale around certain phase transitions, where the order L^0 terms in (4.13) contribute. The diagonal lines with largest error occur where an endpoint of A leaves the region of B_3 entangled with B_1. The vertical lines with similarly large error are along a plateau phase transition, as occurs in the two boundary case.

lengths and the position of the interval. With a list of all contributing monomials in hand, finding the length in the large L limit is equivalent to finding the maximum of a set of linear functions. This calculation is implemented in `Mathematica` by performing a truncated series expansion.

Of course, the full series can also be computed numerically. The results are summarized in figure 27, which shows numerical results at finite-temperature for deviations from the high-temperature approximation (4.13). The errors are indeed largest near the regions where nearby horizons are not exponentially close (i.e., where the causal shadows become large) and for intervals of size comparable to the thermal scale. Such regimes are close to phase transitions in the mutual information, where pairs of minimal curves exchange dominance.

In addition to the bipartite entanglement, at large but finite temperature one expects to find tripartite entanglement associated with the shadow region between the horizons. But as noted above the area of the pair-of-pants causal shadow is $A_{CS} = 2\pi$ in AdS units for all values of the moduli L_a. Chopping off the exponentially thin "arms," it can be useful to model this region as an AdS-scale disk. This is quite reminiscent of the picture obtained in the tensor network model

of the AdS vacuum in [105], where different spatial regions mostly had bipartite entanglement, with a residual multipartite component corresponding to an AdS-scale region.

4.7 Discussion

Our main result is that, in the limit of large black hole horizons, the pair-of-pants wormhole in 2+1 gravity is dual to a CFT state formed by sewing together thermofield doubles in one of the manners shown on the right of figure 17, or to the degenerate case that interpolates between them. We showed this by directly analyzing the CFT path integral defining the state $|\Sigma\rangle$, and used consistency with bulk holographic calculations of the mutual information to argue that the Σ-wormhole dominates the associated bulk Euclidean path integral. We focused on the pair of pants for simplicity but – as will be discussed further below – it is easy to extend the central aspects of our discussion to more complicated wormhole spacetimes.

We also focused on the case of circular boundaries, but the same conclusions apply to the planar case. In 2+1 bulk dimensions, such high-temperature n-boundary planar cases are just AdS_3 in non-standard coordinates corresponding to performing certain conformal transformations on the dual CFT vacuum that are singular at n points on the circle, with each segment running between two such singular points representing a distinct planar boundary. One may also consider wormholes having both planar and circular boundaries.

Let us now briefly describe the extension to more general Riemann surfaces. Recall that a general orientable Riemann surface Σ (other than the sphere or annulus) can be decomposed into pairs-of-pants. Let us think of Σ as the $t = 0$ slice of a wormhole spacetime with n boundaries each asymptotic to AdS_3. Then the surface contains geodesics H_i $(i = 1, 2, \ldots, n)$ that define bifurcation surfaces of the event horizons for each boundary. In addition, it contains a number of internal geodesics. Each pair-of-pants decomposition of Σ corresponds to cutting Σ into pair-of-pants pieces along some set of these internal geodesics. It will be convenient for us to also cut along the H_i so that we in fact decompose Σ into n cylinders C_i and some number of pair-of-pants pieces Σ_I. In a somewhat redundant notation, we will refer to the geodesics forming the three boundaries of Σ_I as H_{Ia} for $a = 1, 2, 3$. Note that the set of H_{Ia} includes the horizons H_i. In this decomposition, the moduli space of the Riemann surface is parametrised by the lengths L_{Ia} of the H_{Ia} and the twists θ_{Ia} specifying the relative rotation between the two pairs of pants on the internal geodesics where we are sewing pairs of pants together.

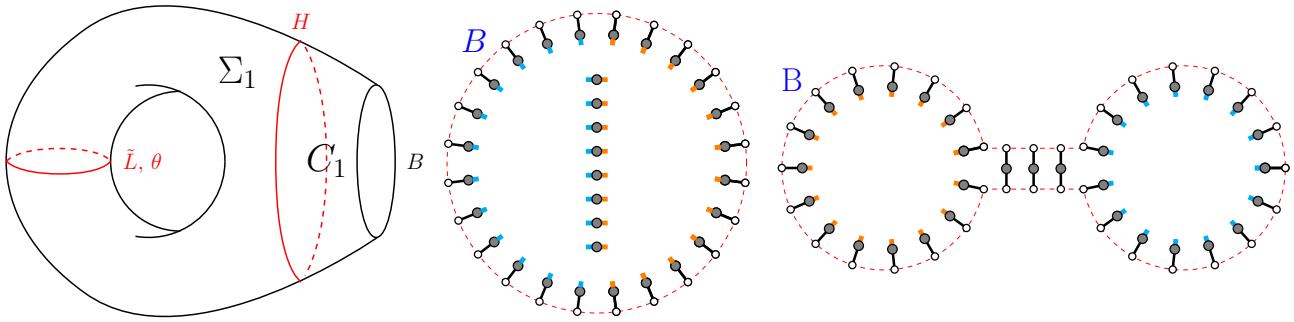

Figure 28: A decomposition of the torus wormhole (left) with one boundary B into a single pair of pants Σ_1 and a single cylinder C_1. Taking boundary 3 of Σ_1 to adjoin C_1, we see that there are three distinct moduli: the length L_3 of H, $L_1 = L_2 = \tilde{L}$, and a possible twist θ. Tensor networks for $\theta = 0$ dual CFT states with large $L_3, \tilde{L}$ are also shown for $L_3 < 2\tilde{L}$ (middle) and $L_3 > 2\tilde{L}$ (right). In both cases, corresponding cyan and orange links are to be identified as dictated by the twist angle θ. For $\theta = 0$, this identification is reflection about the vertical axis through the center of each diagram. (Without this reflection, the spacetime is a punctured Klein bottle instead of a torus.) The cyan and orange links should be viewed as exponentially short, while the black links have length $\beta/2$ set by the inverse effective temperature β of the black hole. So for $\theta = 0$ these identifications generate exponentially short closed loops which can be removed from the tensor without changing the state at leading order in large $L_3, \tilde{L}$ and central charge c. See discussion in main text below.

Each Σ_I has the same geometry as the causal shadow region lying between the three horizons in figure 21 as defined by the corresponding L_{Ia}. So each $\Sigma_\pm$ has area precisely 2π, independent of moduli. Any H_{Ia} which is long will lie exponentially close to another H_{Ia} (or another region of the same H_{Ia}) across the causal shadow region. As a result, a large number of such Σ_I can be sewn together without introducing an appreciable causal shadow or an appreciable reduction of the local energy density along each boundary. Away from the special points in each boundary corresponding to vertices in our previous discussion, the effective $|TFD\rangle$ temperature remains uniform in the round conformal frame specified by the cylinders C_i. Note that this is needed for consistency with the fact that the solution is precisely BTZ outside each horizon H_i, so that each boundary has constant energy density in our round frame[36]. Some simple examples are shown in figures 28 and 29, the former being a 1-boundary wormhole whose causal shadow at $t = 0$ has the topology of a punctured torus.

[36]When the number of such pieces becomes comparable to the lengths L_i of the horizons H_i, the qualitative effect on the CFT state $|\Sigma\rangle$ will depend on how these pieces of causal shadow are distributed along each boundary, and in particular on whether any regions of the boundaries do in fact remain far enough away to retain their $|TFD\rangle$ description.

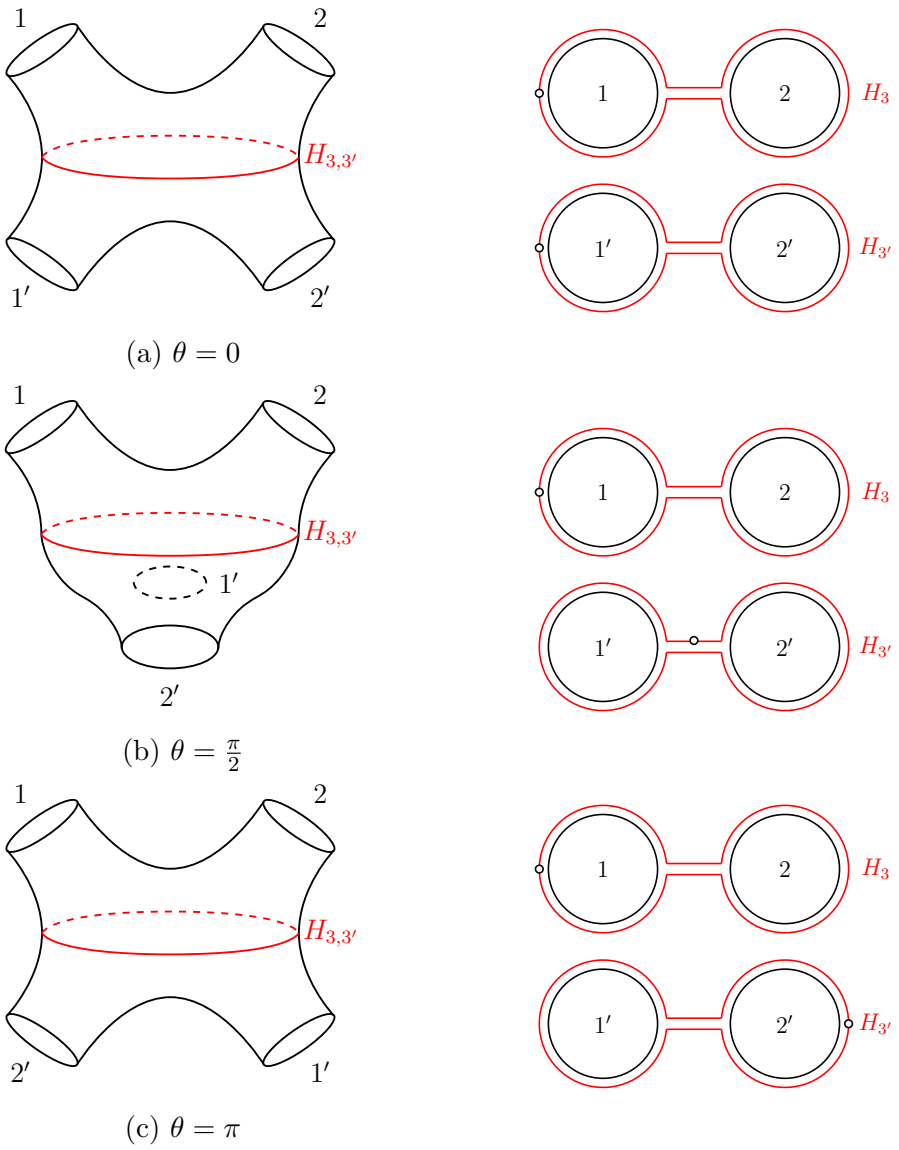

Figure 29: (Left diagrams) Two pairs-of-pants Σ and Σ' are each cut along $H_{3,3'}$ (red) and the pair of interior portions are sewn together along the cuts with twists $\theta = 0, \pi/2, \pi$ to form a four-boundary wormhole. Here we consider the case with $L_3 > L_1 + L_2$, $L_{3'} > L_{1'} + L_{2'}$. In (a,c left) each pair of pants is bisected by an additional closed geodesic (not shown) that runs vertically around the diagram. In the high-temperature limit, the corresponding entanglement structure is given by identifiying the outer boundaries $H_{3,3'}$ of a pair of "eyeglass" diagrams, shown in red on the right-hand figure. This identification entails a twist θ which is represented by the dot in each cut which are identified across the join in accordance with the twist. For $\theta = 0$ (top) we infer that boundaries 1 and 2 are each entangled only with $1'$ and $2'$ respectively. For $\theta = \frac{\pi}{2}$ (middle) and the chosen values of L_a intervals within any given boundary are entangled with intervals in each of the others. The pattern of such entanglements become chaotic at generic θ, though a twist in this setting never entangles two distinct intervals within the same boundary. For $\theta = \pi$ (bottom) boundaries 1 and 2 are each entangled only with $2'$ and $1'$ respectively.

Interesting new behaviour can arise as a function of the twists as we sew together pairs of pants with the structure of the lower panel in figure 17, as we illustrate by example in figure 29. Consider for example a four-boundary wormhole with external horizons H_1, H_2, H_1', H_2', and split it into two pairs of pants along an internal geodesic $H_3 = H_3'$ separating $H_{1,2}$ from $H_{1,2}'$. We take $L_3 \gg L_1 + L_2$, $L_3 \gg L_1' + L_2'$. If H_3 and H_3' are identified via some twist θ, a given region in say H_1 is entangled with a region in H_3, which is in turn identified with some region in H_3'. For generic θ at large L_3 this will be entangled with some other region in H_3', which is then identified back to H_3. For large L_3 we will cycle through the identification between H_3 and H_3' many times before finally identifying the region with one of the other horizons $(H_2, H_{1'}, H_{2'})$. In the limit where L_3 is much larger than the external horizons, the identifications resulting from a general twist are chaotic and appear to give a fractal entanglement structure. It would be interesting to characterize these structures in more detail, and to relate this behavior to the well-known chaotic dynamics of geodesics on compact hyperbolic spaces.

Another subtlety arises in cases like that shown in figure 29 *a*), where we consider the four-boundary system with zero twist, and take for simplicity $L_1 = L_1'$ and $L_2 = L_2'$ with L_3 again very large. Then sewing together the two copies of figure 17 (lower right) indicates that B_1 is entangled only with $B_{1'}$ and that B_2 is entangled only with $B_{2'}$. As a result, taking $A = B_1 \cup B_{1'}$ and $B = B_2 \cup B_{2'}$, the CFT state has $I(A:B) = 0$ (at leading order in large c and L). This result may seem is surprising from the bulk point of view, as Σ contains a closed geodesic that runs vertically around figure 29 (a), separating A from B. So HRT predicts $I(A:B) = L/2G$, where L is the length of this geodesic. This would be consistent with the above prediction as large L_3 makes this geodesic exponentially short so that its length can be ignored at leading order. Note that this geodesic is short only for zero twist: we saw that for small-but-nonzero twist θ a part of B_1 is instead entangled in a local $|TFD\rangle$ state with part of $B_{2'}$, so the mutual information is non-zero and grows as we scale up the L_a. Thus A and B can no longer be separated by a closed bulk geodesic of negligible length[37].

Despite the above consistency, the appearance of such a short geodesic also suggests that our Σ-wormhole may not in fact be the dominant bulk saddle for the CFT state $|\Sigma\rangle$. It seems natural to conjecture that – unless forbidden by global features like a choice of spin structure – when Σ contains such exponentially short geodesics there will be another bulk saddle of smaller

[37]This is also clear from the fact that the local bulk geometry of these regions is essentially that of a segment of BTZ, and any such separating geodesic must traverse part of this segment of BTZ and thus have non-negligible length

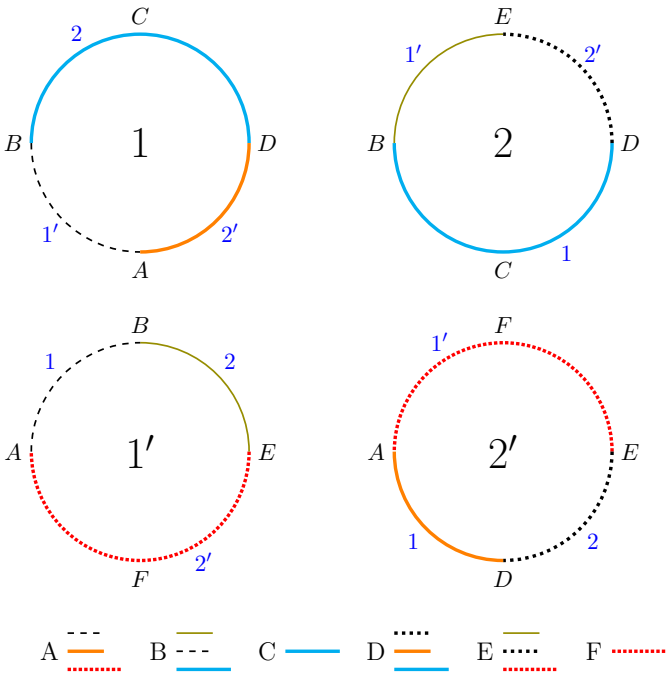

Figure 30: The entanglement structure of the 4-boundary wormhole (figure 29) with large $L_3 = L_{3'}$ for $L_1 = L_{1'} = L_2 = L_{2'} = \frac{1}{4}L_3$ and $\theta = \frac{11\pi}{8}$. The state is well-described by a tensor network analogous to figure 17 right. The state on any pair of boundary intervals formatted in the same way (color, dots/dashes/solid lines) is a local piece of $|TFD\rangle$; the labels $1, 1', 2, 2'$ indicate the boundaries connected to each TFD segment. The TFD intervals join at four vertices A, B, D, E located as shown. Each vertex connects the 3 local TFD states listed in the key below the diagram. C, F are not vertices, but are simply in the middle of the indicated (relatively long) TFD intervals. Some TFD strips connect oppositely-oriented intervals, while some preserve orientation.

action where the geometry is modified so that these geodesics are contractible when viewed as living on the boundary of the new saddle. That is, we conjecture that $|\Sigma\rangle$ in such cases is in fact dual to a bulk geometry with $t = 0$ surface Σ' built by cutting Σ along all exponentially small geodesics and capping off the resulting holes with small disks. This $\Sigma'-$ "wormhole" may not then connect all the boundaries. From the tensor network point of view, the point is that the network obtained by gluing together two copies of figure 17 with no twist breaks up into two disconnected components, one connecting B_1 and $B_{1'}$ and one connecting B_2 and $B_{2'}$. The remaining chains merely form closed loops. At leading order in large central charge c the properties of the state $|\Sigma\rangle$ are unchanged if we remove all chains that form closed loops rather than ending on boundaries. The resulting tensor network defines the manifold Σ'. The difference between $|\Sigma\rangle$ and $|\Sigma'\rangle$ is then exponentially small at large c, and we conjecture the Σ'-"wormhole" to be the leading bulk saddle describing both states. This feature also arises for the punctured torus shown in figure 28

for $L_3 < 2\tilde{L}$ (middle figure) with vanishing twist θ.

It is worth elaborating further on this last point. As noted in the caption for figure 17, the diagrams in this chapter include only a simple cartoon of the $|TFD\rangle$ tensor networks from e.g. [14]. The full tensor network for $|\Sigma\rangle$ obtained by sewing together $|TFD\rangle$ pieces as we describe will be correspondingly more complicated as well. In particular, returning to the simple example of two pairs of pants with very large L_3 sewn together along the corresponding boundary, this full tensor network will certainly not factorize into unentangled states on $B_1 B_{1'}$ and $B_2 B_{2'}$. Instead, it will merely imply that the mutual information between $B_1 B_{1'}$ and $B_2 B_{2'}$ remains of order 1 at large central charge c. This is analogous to $|TFD\rangle$ below the Hawking-page transition where it describes two entangled copies of a thermal gas on pure global AdS_3 backgrounds. Our conjecture is thus that the dominant bulk geometry at $t = 0$ is correctly predicted by removing parts of the full tensor network that fail to transmit mutual information of order c. We note that evaluating this criterion requires understanding the tensor structure of each node in the tensor network implied by the CFT dynamics; it is not apparent from the graph representation of the tensor network alone.

So far we have considered tensor networks constructed by sewing together pair of pants networks in the way suggested by bulk wormhole geometries. But it is possible to consider a more general class of states defined by sewing together high-temperature $|TFD\rangle$ states in arbitrary fashions. For example, one may sew a $|TFD\rangle$ to itself (or others) so as to introduce a 'bud' on the tensor network as shown in figure 31. Second, some pieces of some $|TFD\rangle$'s – or even entire such states – may now be entirely internal to the tensor network, lengthening some chains and thus lowering the local temperature. In general, the chain length can then be non-uniform across any boundary. Together, these two effects recover the freedom to make arbitrary conformal transformations relative to the round conformal frame used above. That is, these more general states must be related to the states considered above rewritten in a more general conformal frame.

Finally, one may also generate non-orientable Σ by performing antipodal identifications on some circle boundary. For example, doing so one one boundary of a cylinder shows that the CFT state dual to the high-temperature AdS_3 geon (see e.g. [112]) is given by the thermofield double tensor network on a Möbius strip.[38] The Möbius strip can of course be constructed by cutting

[38]This creates a local connection between antipodal points on the boundary. The fact that the bulk geodesic between antipodal points is short in the large temperature limit can be seen from the explicit formula for the geodesic lengths in [113], although it is incorrectly stated there that the length of the geodesic through the identification is always longer than the one outside the horizon.

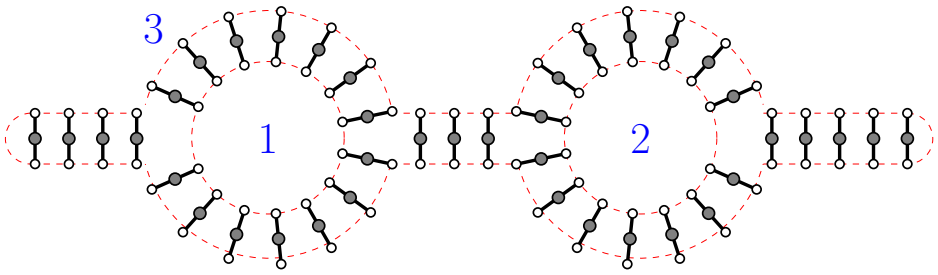

Figure 31: Another way to sew three $|TFD\rangle$ states together. Here the outer $|TFD\rangle$ has been sewn to itself at the ends as well as in the middle. The sewing at the ends creates features we call 'buds.' Such buds are removed if one transforms the result to the round conformal frame. One may construct similar buds from the vacuum by applying a smooth conformal transformation approximating over some region the singular one that gives the infinitely long planar thermofield double state.

open the cylinder along $\phi = 0$ and gluing the two ends back together with a half twist. It is an interesting question to what extent such gluing operations reproduce desired states when applied to particular e.g. MERA-like tensor network representations of states at finite temperature and finite central charge c. Results related to this issue will appear in [114].

While we have stressed the limit where all L_a become large, the discussion may be generalized to allow some L_a to remain small. The pair-of-pants CFT states $|\Sigma\rangle$ are then described by figure 17 (right) with the small-L boundaries contracted to points that merge with the vertices where the approximation by local TFDs breaks down. But regions of any large-L boundaries far from the new vertices remain well-described by the indicated local TFDs. One should be aware that, due to the possibility of bulk phase transitions like those described above, having some L_a small may make it less clear which bulk spacetime is in fact dual to $|\Sigma\rangle$. Nevertheless, the local TFD description of $|\Sigma\rangle$ remains valid. In particular, any entanglement of large-L boundaries with those having small-L will be confined to intervals no longer than the effective thermal scale. The tensor network issue dual to uncertainties regarding bulk connectivity is that some new vertices may now be trivial in the sense that they no longer lead to order-c mutual information with the small boundary. When this occurs and creates a 'bud' as in figure 31, the bud may again be absorbed into a neighboring vertex without changing the large-c structure of the state other than by acting with a conformal transformation[39]. Similar comments apply to Σ having more boundaries or more general topology when some of the L_{Ia} remain small.

Although we have discussed 2+1-dimensional bulk geometries above, but many of our

[39]It is then the diagram without the bud that describes the round conformal frame.

considerations clearly apply to the higher dimensional case as well. In particular, sewing together high-temperature $|TFD\rangle$'s defines a zoo of interesting states $|\Sigma\rangle$ and conformal geometries Σ. And it is again natural to conjecture the CFT states $|\Sigma\rangle$ defined by such sewing operations to be dual to Σ'-wormholes defined by having a moment of time-reflection symmetry on which the induced geometry differs from (planar) Schwarzschild-AdS only by small corrections outside a finite number of AdS-scale regions. But much remains to be understood and the details will prove interesting to explore. In particular, one would like to find an algorithm that takes the tensor network naturally associated with $|\Sigma\rangle$ defined by the above gluing procedure and turns it into one in which the geometry of Σ' is manifest – e.g., with the tensor network providing a cellular decomposition of Σ' in terms of AdS-scale cells [115–118]. One wonders if solving the Euclidean Einstein equations to construct Σ' from Σ can be related to a renormalization-group flow on tensor networks akin to those discussed in [119, 120].

5 Tensor Network Models of Multiboundary Wormholes

The work in this chapter is reproduced from a collaborative paper [4] with Prof. Simon Ross. In this chapter we consider the entanglement structure of states dual to multiboundary wormhole geometries using tensor network models. Perfect and random tensor networks tiling the hyperbolic plane have been shown to provide good models of the entanglement structure in holography. We extend this by quotienting the plane by discrete isometries to obtain models of the multiboundary states. We show that there are networks where the entanglement structure is purely bipartite, extending results obtained in the large temperature limit. We analyse the entanglement structure in a range of examples.

5.1 Introduction

Multiboundary wormhole geometries are a useful laboratory for studying the relation between the entanglement structure of CFT states and the bulk geometry. In [98], an investigation of the entanglement structure of a class of asymptotically AdS $2+1$ dimensional spacetimes with n asymptotic boundaries was initiated; these are dual to states in n copies of the CFT on $S^1 \times \mathbb{R}$. These solutions were introduced in [52–55], and their holographic study was initiated by [101–103]. The CFT states are given by a path integral on a Riemann surface Σ with n boundaries. The entanglement structure of these states has a complicated dependence on the moduli of the Riemann surface, exhibiting regions of multipartite entanglement but also regions where bipartite entanglement between different copies is dominant. In the previous chapter, the entanglement structure in a region of large moduli, where the CFT states involve highly excited states on each $S^1 \times \mathbb{R}$ factor, was explored in more detail. This is effectively a regime of high temperature, although the reduced density matrix in a single copy of the CFT is not necessarily thermal. The structure in this regime is dominated by local, bipartite entanglement between subregions on each boundary on a scale set by the effective temperature. There can be a multipartite component in this regime, but it is associated just with a single thermal volume, so it is a small part of the overall state.

It is difficult to gain more insight into the entanglement structure for more generic moduli from the full CFT path integral. This motivates the study of tensor network models, which share many of the entanglement and geometrical features of the full state.[40] Other approaches to multiboundary wormholes have recently been explored in [125, 126]; see also the interesting work on multipartite entanglement in tensor networks [127].

The models we consider were introduced in [105, 128, 129] to model the relation of the entanglement structure of the vacuum state to global AdS, explicitly exhibiting the ideas of code subspaces in [59]. They are based on tiling the hyperbolic plane with perfect or random tensors, and were shown to reproduce the Ryu-Takayanagi formula for entanglement entropies. Following [130], we consider discrete quotients of the tiled plane, and use the tensor network on the quotient space as a model of the CFT states dual to such multiboundary geometries. In these models,

[40] The most robust model of the holographic entanglement structure are MERA networks [96, 121], which provide a good description of the ground state in conformal field theories, and have been related to holographic descriptions of the state [115, 117, 122, 123]. A MERA version of the quotient giving BTZ was constructed in [124]. However, it appears difficult to extend this construction to the more general quotients we are interested in with multiple generators. We will therefore focus our attention on more phenomenological models.

we can explore intermediate regions in the moduli space of Riemann surfaces, and study the entanglement structure of the corresponding states.

Surprisingly, we find that even at generic values of the moduli, there can be tilings where the entanglement structure is purely bipartite. Although this result presumably reflects the limited resolution of the discrete tensor network models, it is interesting as it provides explicit illustration of the way in which a connected multiboundary state can be built up from purely bipartite entanglement. In these cases, the state is distillable to a state containing just Bell pairs. For other tilings, there is a residual multipartite component, and we attempt to characterise the multipartite structure in its entanglement using negativity of the reduced density matrices, comparing to a random state on the same Hilbert space. Further characterisation of this multipartite component is an interesting challenge for further work. Our computations are for low bond dimension, and it would also be interesting to see how they extend to higher bond dimension.

In the next section, we review previous work on multiboundary wormholes. In section 5.3, we construct tilings of the Riemann surface Σ for discrete values of the moduli by quotienting tilings of the hyperbolic plane by discrete isometries. We discuss the discrete analogue of horizons and the causal shadow region in these tilings, and show that in some cases there is no causal shadow region. In section 5.4, we review the tensor network models built on the tilings of the hyperbolic plane. In section 5.5, we apply these methods to the tilings of the Riemann surface Σ and analyse the entanglement structure of the resulting states.

5.2 Holographic Multiboundary Wormholes

The holographic description of multiboundary wormholes generalises the relation between the thermofield double state

$$|TFD\rangle = \sum_E e^{-\frac{\beta}{2}E} \, |E\rangle_1 \, |E\rangle_2 \tag{5.1}$$

in two copies of the CFT and the eternal black hole [30]. This state is obtained as the result of a Euclidean CFT path integral on a cylinder of length $\beta/2$ (taking the S^1 to have period 2π). The trace over one copy gives a thermal density matrix, at inverse temperature β. At sufficiently high temperatures (small β), the dominant bulk saddle for these boundary conditions is a Euclidean black hole. Analytically continuing to Lorentzian time, the two copies of the CFT live on the two boundaries of the black hole, and the entanglement of the state (5.1) is essential to account for

the connectedness of the bulk geometry.

In [98], this picture was extended to consider the role of the entanglement in the CFT in multiboundary wormhole geometries. In $2+1$ dimensions, such geometries can easily be constructed by considering quotients of vacuum AdS_3. The Euclidean quotients we are interested in are usefully described by writing the Euclidean AdS_3, equivalently H^3, in a coordinate system

$$\frac{ds^2}{l_{AdS}^2} = dt_E^2 + \cosh^2 t_E d\Sigma^2 \tag{5.2}$$

where t_E is Euclidean time and $d\Sigma^2$ is the unit-radius metric on H^2. The eternal BTZ black hole arises as a quotient by a discrete subgroup Γ of the $SL(2,\mathbb{R})$ isometry group of this H^2 generated by a single hyperbolic element [106]. This converts H^2 into a cylinder with two boundaries, with a hyperbolic metric. The more general quotients we are interested in correspond to considering discrete subgroups Γ generated by k hyperbolic elements. These geometries were introduced in [52–55]. The resulting surface $\Sigma = H^2/\Gamma$ is a smooth Riemann surface with genus g and n boundaries. This Riemann surface has $6g-6+3n$ moduli, which are encoded in the choice of discrete group Γ. Since the quotient acts on the surfaces of constant t_E, we can define a corresponding Lorentzian geometry by analytically continuing $t_E \to -it$. This has n asymptotically AdS regions, connected by a collapsing wormhole which generalises the Einstein-Rosen bridge in the eternal black hole. Topological censorship implies that associated to each boundary of the geometry is a horizon [107, 108]. The absence of local degrees of freedom implies that the geometry in the exterior regions outside the horizons is exactly the BTZ geometry exterior to a black hole.

We want to understand the structure of the dual CFT state which encodes this geometry, and specifically its entanglement. The holographic description of these geometries was initiated in [101–103]. The conformal boundary of this spacetime lies at $t_E \to \pm\infty$, and consists of two copies of the surface Σ. The CFT path integral over this surface has a rich phase structure [98, 131]. In a region of the moduli space, the dominant bulk contribution comes from the multiboundary wormhole (5.2), where the spatial slices are the Riemann surface Σ. Thus, in this region of moduli space the $t=0$ bulk geometry Σ corresponds to a CFT state on the n boundaries obtained by a path integral on Σ.

For the BTZ black hole, the entanglement structure of the state (5.1) is purely bipartite. In the high temperature limit, this has a particularly simple structure: high temperature is small β, so the cylinder is short, and if we consider scales larger than the thermal scale β on the spatial

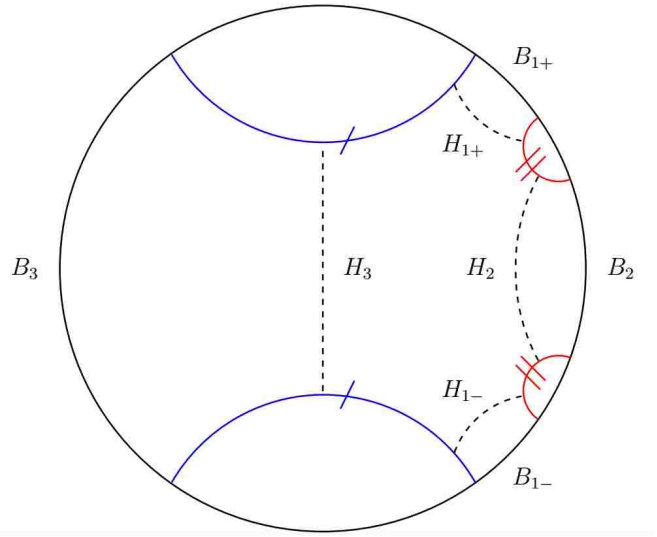

Figure 32: The surface Σ as a quotient of the Poincaré disc for the pair of pants. The pairs of labeled geodesics (blue and red in colour version) are identified by the action of Γ. The region of the Poincaré disc bounded by these geodesics provides a fundamental domain for the quotient. B_3, B_2 and $B_1 = B_{1+} \cup B_{1-}$ become the desired three circular boundaries. There are corresponding minimal closed geodesics H_3, H_2 and $H_1 = H_{1+} \cup H_{1-}$. The lengths L_a of these geodesics fully characterize the geometry of Σ.

circle, the path integral simply identifies states on the two boundaries. This local character of the entanglement was verified in [95] by considering mutual informations between subregions on the two boundaries.

The next simple example is the three-boundary wormhole or pair of pants, whose Euclidean geometry is obtained by quotienting by a group Γ generated by a pair of hyperbolic elements g_1, g_2. A fundamental domain of the identification on H^2 is the region bounded by a pair of geodesics identified by g_1 and a pair of geodesics bounded by g_2, as depicted in figure 32. This surface has three moduli, corresponding to the lengths of the three minimal closed geodesics shown in the figure. In the Lorentzian spacetime, these geodesics become the bifurcation surfaces of the event horizons in each asymptotic region. The CFT path integral on the pair of pants is hard to do analytically, but it simplifies in limits of the moduli space. In [98] the entanglement properties of the dual state were studied in the "puncture limit", where the minimal geodesics are short.

In chapter 4, the structure in the "high-temperature" limit, where the geodesics are long, was studied. This leads to particular simplifications. For the three-boundary wormhole, the "high-temperature" limit is defined by scaling the sizes of all of the horizons to infinity, whilst

fixing their ratios, which then characterise the high temperature geometry. The geometry outside the horizons are high-temperature BTZ solutions, which justifies the name, although the CFT state on the boundaries is not thermal. Since the exterior cylinders are BTZ, they behave in the same way as before: considering scales above the thermal scale, the state on the boundary is identified with the state on the horizon. There is a causal shadow region between the horizons, but its volume is fixed in AdS units by the Gauss-Bonnet theorem, so as the horizons become long, the distance between them shrinks over almost all of the horizon. The causal shadow region is thus effectively a seam which connects the horizons of the exterior regions and whose shape is determined by the ratios of the moduli. Thus, in the high-temperature limit we infer that the path-integral just identifies states across this seam, so that intervals in different boundaries which are opposite each other across the shadow region are maximally entangled, and again the resulting entanglement structure is almost *entirely* bipartite and local. This behaviour is depicted in figure 33. There could be some residual multipartite component, but this would only involve a subregion of order the thermal scale on each boundary.

Note the figure depicts the regime where the horizons are all roughly of the same length. If we take $L_1 \geq L_2 \geq L_3$, this is the regime $L_1 < L_2 + L_3$, referred to in the previous chapter as the "wheel" regime, after the figure on the right side of figure 33. The alternative regime $L_1 \geq L_2 + L_3$ is referred to as the "eyeglass" regime. The entanglement remains primarily bipartite in this regime, but there are regions of boundary 1 which are entangled with other regions of boundary 1, rather than with one of the other boundaries.

The result generalises easily to wormholes with more boundaries and topology behind the horizon. Any Riemann surface can be decomposed into pairs of pants, sewn together across minimal geodesics. There is a region of the moduli space where all the minimal geodesics involved in the sewing are long, and the individual pairs of pants are in the high-temperature configuration described above. The path-integral then identifies states across the regions between minimal geodesics, again generating a local bipartite entanglement structure which can be characterised by appropriate compositions of the diagrams of which figure 33 *c*) is an example.

5.3 Hyperbolic Tilings & Quotients

The tensor network models of [105, 129] are based on tiling the hyperbolic plane with perfect or random tensors. We want to take a quotient of these networks by a discrete isometry of

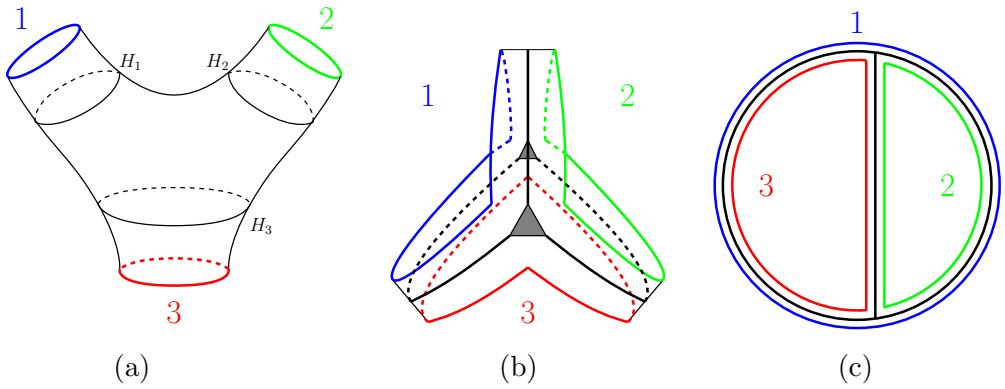

Figure 33: The geometry of the pair-of-pants in the high temperature limit and the resulting entanglement structure. a) the pair-of-pants geometry with the three coloured boundaries indicated and labelled 1-3, the black lines depict the horizons pertaining to each exterior region, and are labelled H_a, $a = 1, 2, 3$. The interior of the horizons is the causal shadow region. b) Cartoon of a) in the high-temperature limit, with fixed ratios of the moduli. The exterior cylinders shrink (the strips should be thought of as being extremely thin, we've exaggerated them here) and the distance between the horizons across the causal shadow region is small almost everywhere. The black lines represent identifications between horizons, which is true to exponential accuracy away from the junctions. c) The resulting entanglement structure can be depicted with this "wheel" diagram: the path integral locally identifies the states in portions of the three boundaries. States localised in some boundary interval are purified by an interval of the same size on the opposite side of the seam, which may lie on any of the three boundaries, as the ratios of the moduli are varied. The resulting entanglement structure is almost entirely bipartite.

the network to obtain a model of the multiboundary wormholes. We can usefully seperate the geometrical aspects of choosing a tiling of the hyperbolic plane and its quotients by discrete isometries from the choice of tensors, so we will first discuss the geometric aspects in this section.

Introducing a regular tiling of the hyperbolic plane provides us with a natural discretization of H^2. A particular choice of tiling will preserve some discrete subgroup of the $SL(2,\mathbb{R})$ isometries of H^2, and we can quotient by some of these isometries of the tiling to obtain discretizations of the Riemann surface Σ for some discrete values of the moduli. In this section, we describe the tilings and quotients, and define analogues of the horizons in the tiling.

As in [130], we describe the tilings in terms of Coxeter groups [132–134]. A constant curvature connected Riemann surface can be tiled by repeated reflections of a seed triangle about its edges. If the interior angles of the seed triangle are given by $\frac{\pi}{r}$, $\frac{\pi}{p}$ and $\frac{\pi}{q}$ for $p, q, r \in \mathbb{Z}^+$ then the set of all reflections in its edges form a Coxeter group, denoted $[r, p, q]$. The triangulation of a space obtained by repeated reflection of a seed triangle in its edges is referred to as a Coxeter tiling,

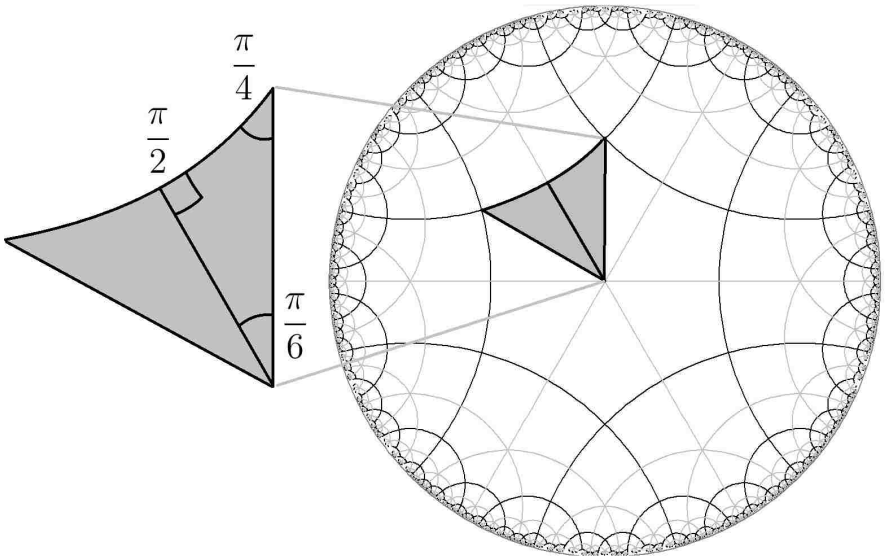

Figure 34: The [2,4,6] tiling of the hyperbolic plane H^2. One of the seed triangles is indicated, the whole tiling is covered by the action of reflecting the seed along its edges. The black, primary tiling lines divide the network into a regular array of hexagons.

and the Coxeter group forms the discrete isometries of the tiling. By the Gauss-Bonnet theorem, for hyperbolic spaces, the required seed triangle must have

$$\frac{1}{p} + \frac{1}{q} + \frac{1}{r} < 1. \tag{5.3}$$

The $[r, p, q]$ tilings satisfying (5.3) tile H^2 with a regular array of q-gons. These Coxeter tilings underly the tensor networks considered in [105, 129, 130]. An example hyperbolic tiling is illustrated in figure 34. The edges of the q-gons are geodesics in H^2, so the volume of each q-gon is of order the AdS scale.

The tensor networks considered in [105, 128, 129] are constructed by thinking of the tiling as a graph, and taking the tensor network to be the dual graph. That is, each q-gon face in the tiling is replaced by a vertex in the tensor network, which has q legs, connecting it to the tensors in the adjacent faces, across the edges of the tiling. There are uncontracted legs at the boundary of the hyperbolic plane.

The tiling is invariant under reflections in any of these edges, forming the Coxeter group associated with the tiling. We can quotient by any subgroup of this group. In the construction of the Riemann surface Σ in the previous section, we considered quotients by hyperbolic elements, which identified pairs of geodesics in the hyperbolic plane. We can obtain such hyperbolic elements by combining a pair of reflections in distinct geodesics [130]. We can see that this follows by

considering AdS_3 as the hyperboloid embedded in $\mathbb{R}_4$,

$$X_0^2 + X_3^3 - X_1^2 - X_2^2 = l^2 \tag{5.4}$$

the $t = 0$ slice corresponds to $X_3 = 0$. Now consider the two hyperplanes P_1 and P_2 with corresponding normals $n_1 = (0, 0, 1, 0)$, $n_2 = (\cosh(\frac{\eta}{2}), \sinh(\frac{\eta}{2}), 0, 0)$ respectively. Under a reflection in the hyperplane with normal n, a point X transforms as

$$\tilde{X} = X - 2(n \cdot X)n \tag{5.5}$$

So that under the pair of subsequent reflections, first in P_1 and then in P_2, the $t = 0$ slice is preserved whilst the X_0 and X_2 are Lorentz boosted, by

$$\begin{pmatrix} \tilde{X_0} \\ \tilde{X_2} \end{pmatrix} = \begin{pmatrix} -\cosh(\eta) & \sinh(\eta) \\ \cosh(\eta) & -\sinh(\eta) \end{pmatrix} \begin{pmatrix} X_0 \\ X_2 \end{pmatrix}. \tag{5.6}$$

Thus, the hyperbolic element identifying any pair of geodesics which form edges of the tiles will be an isometry of the tiling. We can thus quotient by discrete groups Γ composed of such hyperbolic elements to obtain a tiling of a Riemann surface $\Sigma = H^2/\Gamma$, and hence (considering the dual graph) a tensor network with the topological structure of Σ. We can construct this tiling only for some discrete choices of the moduli of the Riemann surface, as given a tiling, the area of the tiles, and hence the distance between the geodesics to be identified, is fixed by the Gauss-Bonnet theorem. In [130], this approach was used to obtain tilings and hence tensor networks corresponding to the BTZ geometry. We now want to generalize this to multiboundary wormholes. Our detailed analysis will focus mainly on the pair of pants. An illustrative example of the construction is given in figure 35.

Despite the discretization of the moduli of Σ, the minimal geodesics will not generally lie along edges of the tiling. Thus, it is important to identify the analogues in the tiling of these minimal geodesics. We will take this to be the minimal closed path along the edges of the tiling homologous to each boundary. This is natural because once we introduce the tensors in each tiling, this path will cut across the links between tensors.[41] This will lead to degeneracy in some

[41] Note that this is slightly different from the prescription in [130], where the BTZ horizon in the example in figure 35 was identified with a tensor in the network, as the actual minimal geodesic runs along the middle of the tile. For the more general case we consider, it is more natural to take the definition above, even though this leads to an artificial degeneracy in the BTZ case.

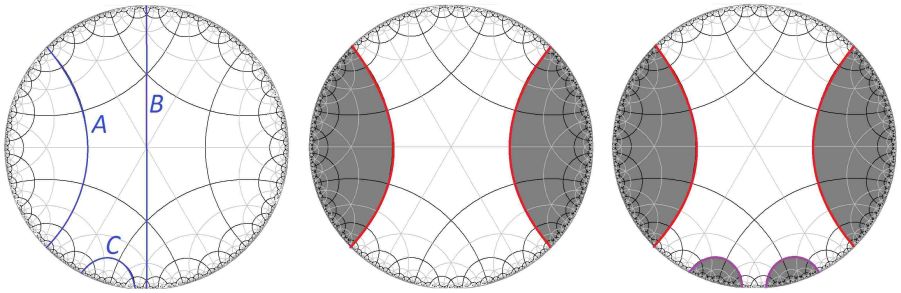

Figure 35: An illustration of the quotient operation in the [2,4,6] tiling. We take r_A, r_B, r_C to be the reflections in the geodesics labelled in the left-hand diagram. Quotienting by Γ generated by $g_1 = r_A r_B$ gives the tiling of BTZ shown in the middle diagram. Quotienting by Γ generated by $g_1 = r_A r_B$ and $g_2 = r_B r_C$ gives the tiling of the pair of pants shown in the right-hand diagram. The unshaded region is a fundamental region for the identification in both cases.

cases, where there can be multiple paths of the same length along the edges. Some examples are illustrated in figure 36.

An interesting feature is that in some cases there is then *no* causal shadow region in the tiling; the minimal length paths in the network can coincide. We will see below that this leads to tensor networks where the entanglement is entirely bipartite. In the continuum, there is of course still a causal shadow for these choices of Σ, which partially covers some tiles, so this could be viewed as just a discretization error, but we argue that it is actually an interesting feature. It implies that in the context of the tensor network models, it is possible to have a network on the pair of pants that gives rise to a state with only bipartite entanglement, providing further evidence that multipartite entanglement is not an essential component in obtaining multiply connected geometries. These explicit examples help us to understand how the geometry arises from purely bipartite entanglement.

5.4 Tensor Networks & Holography

We now turn to the specific tensor network models we use, following [105, 129]. We obtain a network from the tiling by considering the dual graph, with a network vertex in each tile and legs connecting the vertices in adjacent tiles. In general, a network is used to define a quantum state by first associating a tensor $T_{i_1 \ldots i_n}$ to each vertex in the network, with the rank of the tensor equal to the number of legs at the vertex. We then associate a state $|T\rangle$ in a tensor product

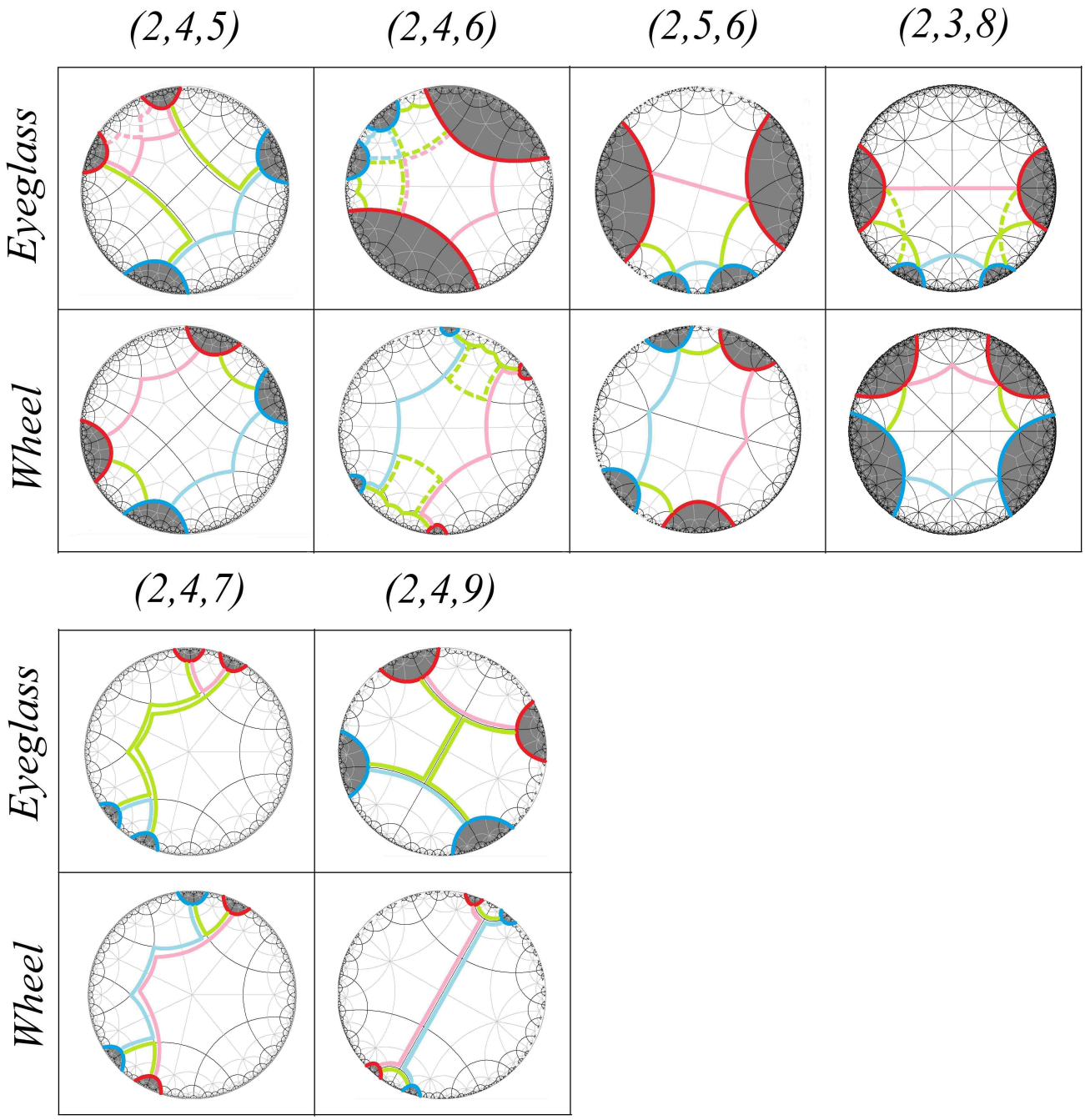

Figure 36: Illustrations of three-boundary tilings obtained by quotienting the tilings of the hyperbolic plane indicated by each column, and with discrete moduli in the regimes indicated by each row. The unshaded region is a fundamental region for the identification. The minimal closed paths along tile boundaries homologous to each conformal boundary are indicated. The cases with two paths of the same colour, where one is dashed, represent degeneracies in the choice of closed path. The second group of examples show cases where there is no causal shadow; the minimal closed paths coincide, so the entanglement between different regions is entirely bipartite.

Hilbert space $\mathcal{H} = \otimes_n \mathcal{H}_n$ with the tensor,

$$|T\rangle = \sum_{i_k} T_{i_1 \ldots i_n} |i_1\rangle_1 \otimes \ldots \otimes |i_n\rangle_n, \tag{5.7}$$

where $|i_k\rangle_k$ is a basis for the kth factor with $i_k = 1, \ldots, D_k$ where D_k is the dimension of $\mathcal{H}_k$, which we will take to be some constant χ for all legs, called the bond dimension. Taking the product over all the vertices defines a product state $|\{T\}\rangle = \otimes_V |T^V\rangle$. For each leg joining two vertices, we make a projection onto the maximally entangled state

$$|ij\rangle = \frac{1}{\sqrt{\chi}} \sum_{a=1}^{\chi} |a\rangle_i \otimes |a\rangle_j \tag{5.8}$$

in the associated Hilbert spaces. This defines a state in the Hilbert space associated to the uncontracted legs,

$$|\tilde{T}\rangle = \otimes_{\{ij\}} \langle ij| \, \{T\}\rangle, \tag{5.9}$$

where the product runs over all the contracted legs, which could include self-contractions in general.

If we take the network constructed from the dual graph of a Coxeter tiling of H^2, the remaining uncontracted legs are located at the boundary of the hyperbolic plane. Given a choice of tensor at each vertex, this defines a state on the boundary legs. This is referred to as a **holographic state**. In an alternative construction, a $q+1$ legged tensor is associated to each vertex, leaving one uncontracted leg at each vertex in the network, which are referred to as bulk legs, in addition to the uncontracted boundary legs. This network can be viewed as a map from the Hilbert space $\mathcal{H}_{\text{Bulk}}$ of the bulk legs to the Hilbert space $\mathcal{H}_{\text{Boundary}}$ of the boundary legs. This model can be used to study the encoding of local bulk operators in the boundary Hilbert space, so it is referred to as a **holographic code**.

Holographic states realise a discrete version of the Ryu-Takayanagi formula [12], relating the entanglement entropy of some subset of the boundary legs to the length of a cut in the bulk. Suppose we have two boundary regions A and A^C, and a cut γ_A in the bulk, which is a path in the bulk along edges of the tiling, which cuts through tensor legs, separating the network into two components, such that one component has boundary $\gamma_A \cup A$ and the other has boundary $\gamma_A \cup A^C$. Then the number of legs $|\gamma_A|$ along the cut provides an upper bound for the entanglement entropy of the reduced density matrix on A in the holographic state given by the network [105]:

$$S_A \leq |\gamma_A| \ln \chi, \tag{5.10}$$

where χ is the bond dimension. We obtain the tightest bound by considering the minimal cut,

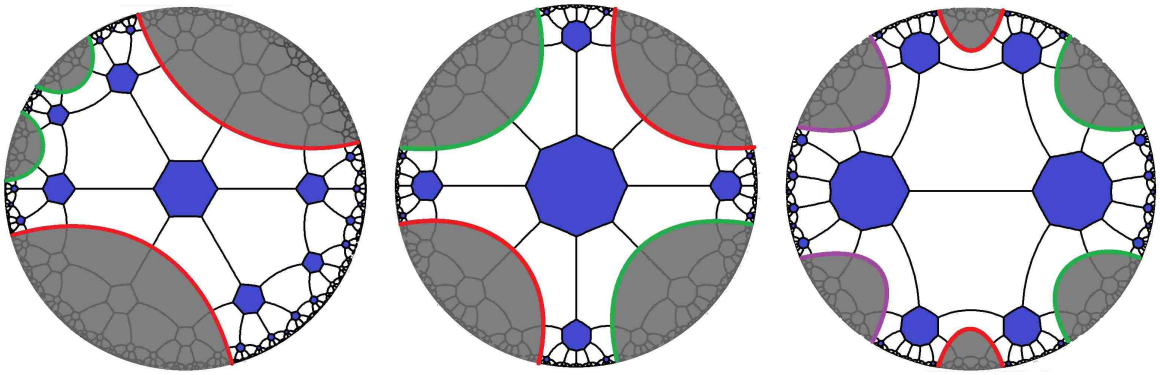

Figure 37: Some examples of topologically interesting holographic states constructed from quotients of various coxeter tilings. The fundamental domain between colour-coded pairs of identified cuts is the unshaded region in each case. These are holographic states representing the three-boundary wormhole (left), a torus wormhole (centre) and a four-boundary wormhole (right).

which we can think of as the network analogue of a minimal surface. This bound is saturated if the two components of the network are isometries from γ_A to A and from γ_A to A^C. This then realises a lattice version of Ryu-Takayanagi, relating the entropy to the length of the minimum cut. There can be degenerate minimal cuts in the networks, though this does not alter the bound 5.10 as in such cases, the minimal cuts are of equal length.

Applying the same prescription to the quotient tilings, we can build tensor networks on a Riemann surface Σ, giving states and codes for multiboundary geometries. A selection of examples are illustrated in figure 37.

5.4.1 Perfect Tensors

In [105], the tensors at each vertex were taken to be perfect tensors. A perfect tensor is a $2n$ index tensor T such that for any division of its indices into a set A and its complement A^C such that $Dim(\mathcal{H}_A) < Dim(\mathcal{H}_{A^C})$, T is proportional to an isometry from $\mathcal{H}_A$ to $\mathcal{H}_{A^C}$. That is, the map from $\mathcal{H}_A$ to $\mathcal{H}_{A^C}$ preserves the inner product up to an overall factor. If we denote the indices in A by a collective index a, and the indices in A^C by b', the condition is

$$\sum_{b'} T^{\dagger}_{ab'} T_{b'c} = C\delta_{ac} \tag{5.11}$$

for some constant C. A visual depiction of isometric tensors is given in figure 38,

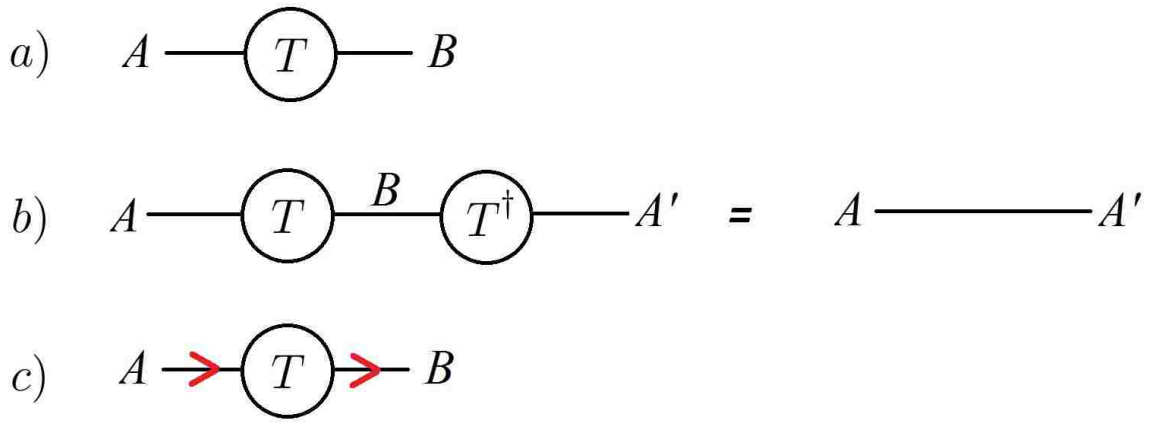

Figure 38: Cartoon illustrating the property of isometric tensors. a) The tensor T has two legs A and B, so it describes a state in the Hilbert space $\mathcal{H}_A \otimes \mathcal{H}_B$. Equivalently, T defines a linear map from a state in $\mathcal{H}_A$ to a corresponding state in $\mathcal{H}_B$. b) The property that T is an isometry from $\mathcal{H}_A$ to $\mathcal{H}_B$ (or equivalently from the leg A to B) implies that contracting T with its conjugate on leg B, as depicted, resolves the identity map on leg A. c) the isometry property b) is usefully depicted using arrow assignments, as shown. In this case, the fact that one arrow is incoming on leg A and another is outgoing on B represents the fact that T is an isometry from A to B.

The isometry property implies that we can convert an operator acting on $\mathcal{H}_A$ into an operator acting on $\mathcal{H}_{A^C}$; given an operator $\mathcal{O}$ acting in $\mathcal{H}_A$, we define

$$\tilde{\mathcal{O}} = \frac{1}{C} T \mathcal{O} T^\dagger \tag{5.12}$$

acting in $\mathcal{H}_{A^C}$, so that $T\mathcal{O} = \tilde{\mathcal{O}}T$. In a holographic code, this enables us to rewrite an operator acting on a bulk leg as an operator acting on some subspace of the boundary Hilbert space, by using the perfect tensors in the network to push the operator outwards, as illustrated in figure 39. An example depicting how operator pushing can be used to reconstruct bulk legs from portions of the boundary of a holographic code is illustrated in figure 40. This provides a tensor network realisation of bulk reconstruction. Since we can use the perfect tensor property to map the bulk leg to different subsets of the boundary legs, it can be mapped to operators acting on different subspaces of the boundary Hilbert space, realising the ideas of [59].

In [105], a greedy algorithm was introduced to identify the portion of the bulk that can be reconstructed from a given region A of the boundary, not necessarily connected. This proceeds by taking some initial region that can be reconstructed from the boundary region (consisting of tensors in the asymptotic region) and iteratively adding to this region a tensor with more than

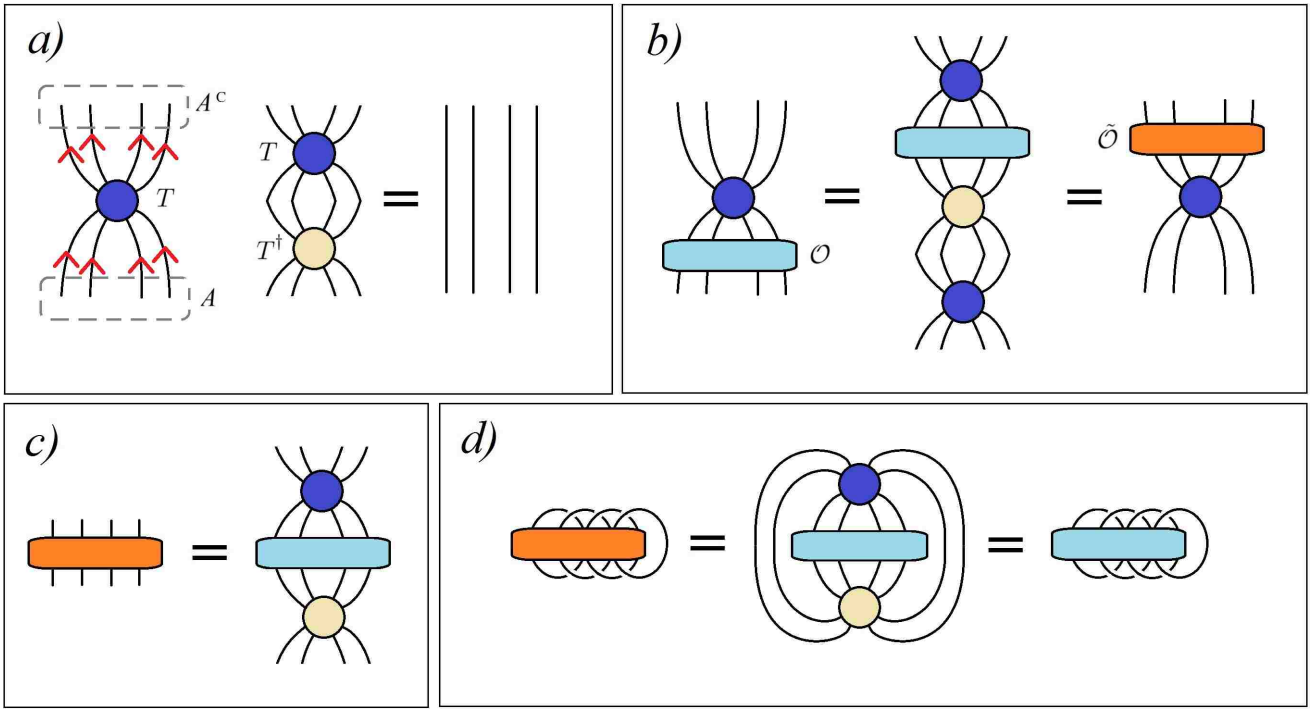

Figure 39: Cartoon depicting operator pushing through isometric tensors. a) The tensor T is an isometry from leg A to leg A^C, as represented by the arrow assignments. b) Because T is an isometry, the light blue operator $\mathcal{O}$ acting on the legs A of T is equivalent to the orange operator $\tilde{\mathcal{O}}$ acting on the legs A^C of T, where $\tilde{\mathcal{O}} = T^\dagger \mathcal{O} T$ is depicted in c). We say that because T is an isometry from A to A^C, then the operator $\mathcal{O}$ acting on A can be "pushed through" T onto the legs A^C (becoming $\tilde{\mathcal{O}}$), according to the arrow assignment. d) The spectrum of $\tilde{\mathcal{O}}$ on the legs A^C is the same as the spectrum of $\mathcal{O}$ on the legs A, as depicted, due to the isometry property of T shown in a). Consequently, the fact that $\mathcal{O}$ can be pushed through T means that we can reconstruct the action of $\mathcal{O}$ on legs A from the action of $\tilde{\mathcal{O}}$ on legs A^C.

half of its legs connected to tensors already in the region, until there are no more such tensors. The boundary of this region is a cut of the network referred to as the greedy geodesic γ_A. In the case of the holographic state, the collection of tensors $\mathcal{G}_A$ lying between A and γ_A define an isometry from γ_A to A. For holographic codes, we have an isometry from γ_A and the bulk Hilbert space in $\mathcal{G}_A$ to A. This gives a tensor network realisation of the idea of the bulk wedge associated with a given boundary region. Since $\mathcal{G}_A$ defines an isometry, we can view moving from the boundary region A to γ_A as a process of distillation, extracting the degrees of freedom in A which are entangled with A^C.

If we divide the boundary into several different regions, there will be a greedy geodesic associated to each of them, and the union of the different wedges $\mathcal{G}_A$ may not cover the whole network. The remaining portion was called in [105] the residual multipartite region, and can be

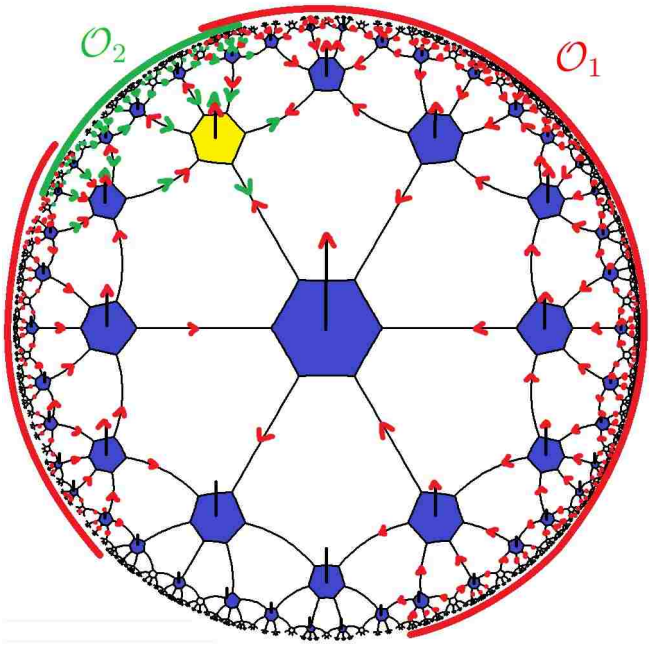

Figure 40: Bulk reconstruction for the holographic heptagon code. Due to the fact that each tensor is perfect, the local bulk operator $\mathcal{O}$ acting on the bulk leg of the yellow-highlighted tensor can be pushed to a non-local boundary operator in multiple ways, corresponding to different arrow assigments that describe isometric maps from a given bulk leg to different (not-necessarily connected) boundary subregions. Two examples of such isometric maps are indicated by the red and green arrow assignments. The green arrow assignment defines an isometry from the bulk leg of the yellow-highlighted tensor to the operator $\mathcal{O}_2$ acting on the connected interval shown in green, while the red arrow assignment defines an isometry from this site to an operator $\mathcal{O}_1$ acting on the disconnected interval shown in red. For the maps defined by the arrow assignments to be an isometry, we require that for each tensor with outgoing arrows, that the number of ingoing arrows is more than half of the total number of legs. For this heptagon code, this requires that every tensor with outgoing arrows must have at least four ingoing arrows assigned to its legs. This is indeed the case for the arrow assignments depicted.

thought of as encoding the entanglement between the different boundary regions. We expect the causal shadow region in our quotient networks to play a similar role.

It was also shown in [105] that for holographic states, for any connected region A on the boundary of a simply-connected perfect tensor network of non-positive curvature, the lower bound in (5.10) is saturated, so that the lattice Ryu-Takayanagi formula holds.

5.4.2 Random Tensors

In [129], a different approach was taken based on selecting the individual tensors in the network independently at random from a suitable distribution. This corresponds to taking the state at the individual vertices (5.7) to be a Haar random state.

In the limit of large bond dimension χ, the calculation of the second Renyi entropy averaged over the randomness was mapped to a partition function of an Ising spin system. This was used to show that these random tensor networks also satisfy a lattice Ryu-Takayanagi formula.

Random tensors are not perfect tensors, but it was shown that in the limit of large bond dimension, they are approximately perfect tensors. This is essentially because the Page theorem [135] says that a random tensor is *approximately* an isometry from any subset of *less* than half of its indices to the remaining set. The maximum entanglement entropy of the reduced density matrix on an n-dimensional share of a state in an $(m+n)$-dimensional Hilbert space is

$$S_{\max} = Log(m) - \frac{m}{2n} + ... \tag{5.13}$$

where the "..." terms refer to terms subleading in $\frac{m}{n}$. For a Haar random state of dimension $n = \chi N$, defined by an N-legged tensor T with bond dimension χ, (5.13) implies that the reduced density matrix on any subset of $M < \frac{N}{2}$ legs is approximately maximally mixed and hence the map from the M legs to the remaining $(N-M)$ legs is an approximate isometry. This approximate isometry is sufficient for results similar to the perfect tensors to apply; we can map local bulk operators in a holographic code to operators acting on subspaces of the boundary, and given a boundary region there is a corresponding bulk region which is reconstructable.

5.5 Multiboundary Networks

5.5.1 BTZ

We now apply these tensor network constructions to the tilings obtained for multiboundary geometries in section 5.3. If we consider first the BTZ black hole, there is a single identification. Asymptotically far from the black hole, the network will look like the network for H^2. The region outside a large black hole was already analysed qualitatively in [105]. For holographic states, the network lying between the minimal closed path and the boundary will be an (approximate)

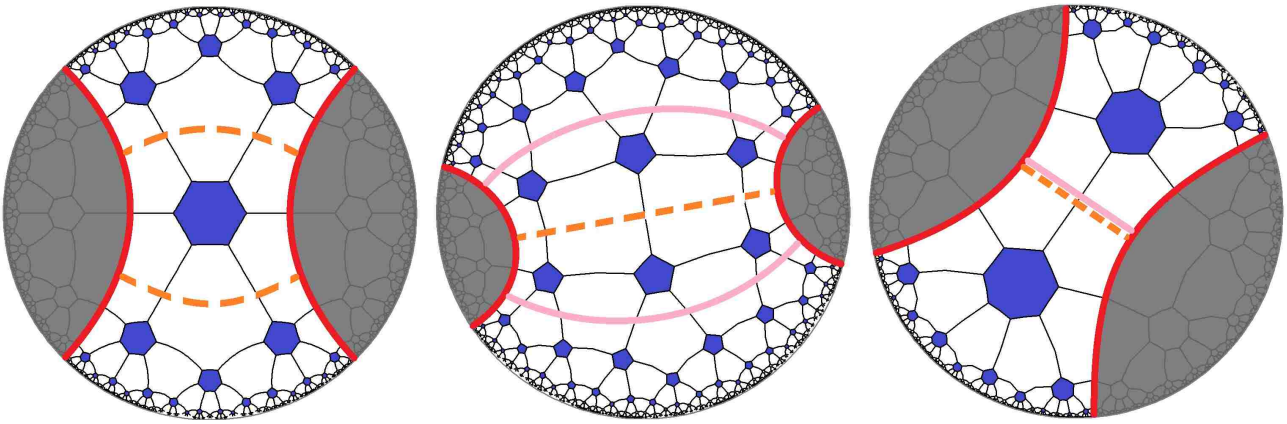

Figure 41: BTZ networks exhibiting tiling artifacts. The network shown on the left has two equal-length minimal cuts, being *either* of the orange, dashed cuts. The continuum horizon is not a mirror of the tiling underlying this network. The network in the centre has a unique minimal cut, but has a bipartite residual region consisting of the 6 tensors lying inbetween the pink greedy geodesic (being a pair of disconnected cuts). Due to the identification, there are too few legs crossing the greedy geodesic to be able to push it to the minimal cut. The network on the right exhibits the behaviour we expect; there is a unique minimal cut that is reached by the greedy geodesic so that we can distill all of the entanglement between the two boundaries to Bell pairs crossing the minimal cut.

isometry, so we can think of the network legs lying across the minimal closed path as representing the distilled entanglement between the two asymptotic regions. This minimal closed path provides a minimal cut in the network, where we take the region A to be the whole of one of the boundaries. In this case the entanglement is entirely bipartite, with each leg across the cut corresponding to a pair of Hilbert spaces in the maximally entangled state (5.8) - the analogue of a Bell pair for systems of dimension χ.

Our choice of a minimal closed path as the analogue of the horizon introduces some minor differences from the analysis of [130]. As previously noted, some choices of BTZ tiling lead to degenerate minimal closed paths, as in the left example in figure 41. This is just a failure of the discretization; the actual minimal geodesic does not lie along the tile boundaries, so there are degenerate approximations to it.

The greedy algorithm can also fail to reach all the way to the minimal closed path, so the greedy geodesic associated to one boundary may be different from the minimal closed path, leading to the appearance of a non-trivial bipartite residual region, as depicted in the central example in figure 41. The failure of the greedy geodesic to reach the minimal closed path arises because of closed loops in the network, where the number of legs pointing "out" towards the

boundary is smaller than the number of other legs. Since we have not yet reached the minimal closed path, the number of legs pointing "out" must overall be less than the number of legs pointing "in", but the legs around the identification can lead to situations where the exterior legs do not contain enough information to reconstruct the tensors in the shadow region.

Self-contractions of tensors within the network are an interesting special case which are a new feature of the quotient networks. For the perfect tensors, the self-contracted tensor is no longer an isometry from a subset of the remaining legs to the other legs. For sufficiently generic perfect tensors, it is however still an approximate isometry from less than half the remaining legs to the other subset of remaining legs. This feature can inhibit bulk reconstruction by preventing greedy geodesics from crossing loops in order to reach a minimal cut, as depicted in figure 42.

For closed loops, each tensor remains a perfect tensor, but if there are the same number of legs below and above a loop, there will not be enough information in the legs below the loop to be able to push onto the loop itself and subsequently be able to reconstruct the outgoing legs, as depicted in figure 42 a). If there are more legs below, we can push onto the loop and push past it, as in figure 42 b).

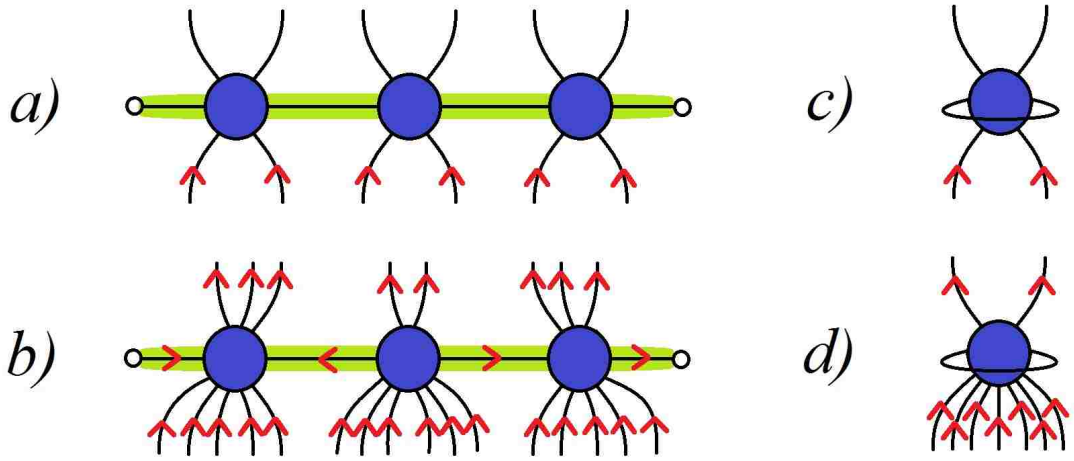

Figure 42: Reconstruction with loops and self-contractions within tensor networks. for a) there is not enough information on the lower legs for the greedy algorithm to push across the loop (green), in either the random or perfect tensor case. b) There is enough information on the lower legs of the central tensor for the greedy algorithm to push onto the loop using the arrow assignment depicted. c) The self-contracted tensor is not an isometry from the upper to the lower legs. d) there are sufficiently many legs below for the self-contracted tensor to be an approximate isometry from the upper to the lower legs in the large χ limit.

5.5.2 Multiboundary wormholes

Considering a more general Riemann surface Σ, the portion of the network between a given boundary and the minimal cut homologous to this boundary is the same as for BTZ; thus, this defines an isometry from the minimal cut to the boundary, and we can distill the state on the boundary to a state on the legs crossing the cut, which describes the entanglement with the other regions. Hence, the causal shadow region lying between these minimal cuts encodes the entanglement between the different boundaries. For the three boundary case, this causal shadow region will encode the residual tripartite entanglement between the three boundaries.

As noted in section 5.3, we can have examples where there is no causal shadow region. In this case, we can now see that the entanglement in the holographic state is entirely bipartite, encoded in the maximally entangled states (5.8) on each leg crossing the cuts. This is similar to the entanglement structure seen in the high temperature limit of the CFT path integral, but it is surprising that we can find cases where the entanglement is *entirely* bipartite, and that this can occur even for generic moduli. Examples of this behaviour for the wheel and eyeglass regimes are illustrated in figure 43.

In other cases, there will be a tripartite residual region, and we can ask about the importance

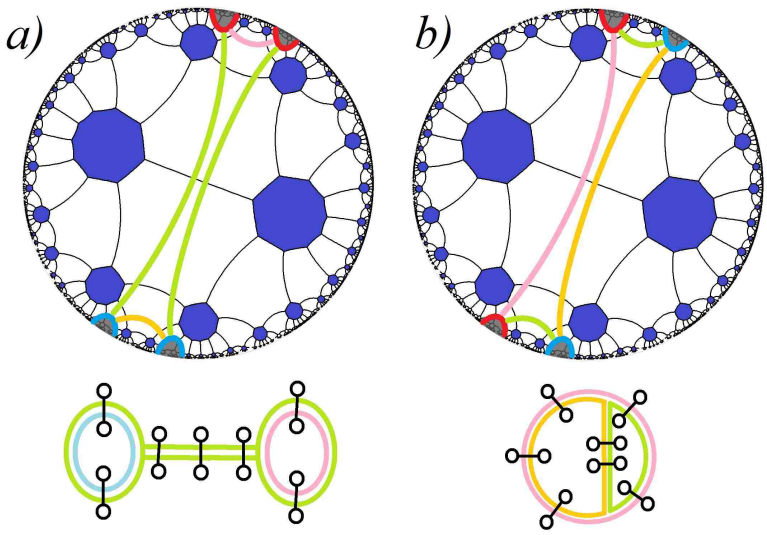

Figure 43: Purely bipartite tensor network states for low-T three-boundary wormholes. The fundamental domain is the unshaded region, and the minimal cuts homologous to each region are colour-coded. In each case, there is no multiparty residual region, and states across the minimal cuts are identified. The set of Bell pairs corresponding to states identified across each cut are depicted below each network; coloured lines guide the eye to recognise across which minimal cuts states are identified. These reproduce, schematically, the known structure of the high-T entanglement.

of this region and the nature of its entanglement. It is interesting to first make contact with our previous work in the high-temperature limit. We can do so by carefully choosing a low-T network and then letting the quotient mirrors retreat to produce a high-T network with large horizons. What we expect to find in this limit is that the minimal cuts associated to each of the three boundaries become identified for most of their length up to an AdS scale tripartite residual region consisting of only a small number of tensors, whose size remains fixed in this limit. One example of this behaviour is illustrated in figure 44. Note however that it requires a choice of network to realise these expected features; in other cases the causal shadow grows (or disappears altogether) due to the tiling artefacts illustrated in figure 41.

The main interest in studying the tripartite residual region in these tensor network models, however, is that we can study the structure for small values of the discrete moduli, where the network in the causal shadow region is of modest size, and we can hope to analyse the resulting state on the legs crossing the horizon, and directly address questions about the nature of the entanglement. An example is shown in figure 45. However, even for the smallest values of the moduli we are in a regime where there is no full classification of multipartite entanglement structures, so there is a shortage of general expectations to compare to. In [98], the entanglement

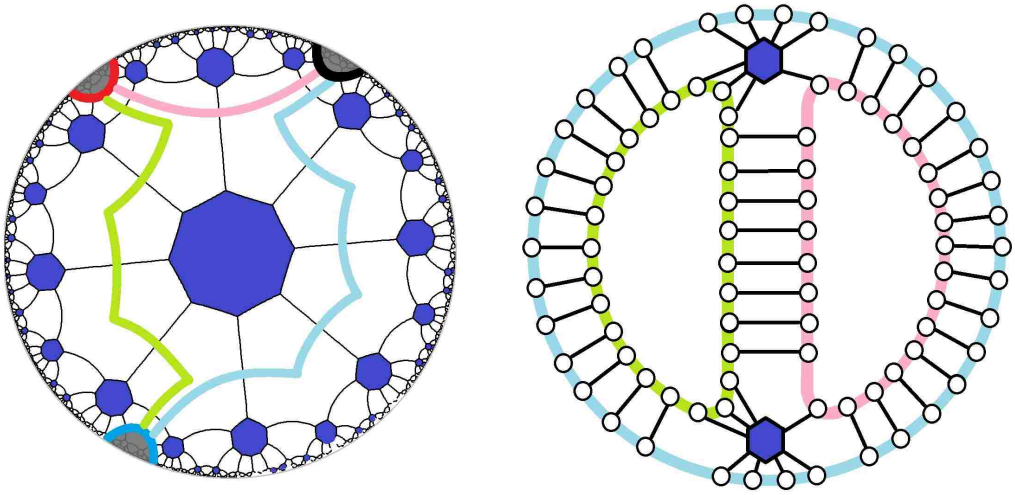

Figure 44: Taking the high-T limit of a low-T three-boundary network. For convenience, only half of the tiling (left) is displayed, the non-visible half (the mirror image of what is depicted) is located on the opposite side of the black mirror. We can take a high-T limit by letting the red, blue and black mirrors retreat, increasing the length of each horizon by the same amount. This produces a wheel network in which the horizons have approximately equal lengths. Notably, the tripartite residual region representing the causal shadow, being the central tensor (along with it's unseen reflection) between the coloured cuts, is invariant in the limit. This accords with our intuition that the size of the causal shadow is fixed due to the Gauss-Bonnet theorem. As the minimal cuts become larger, they become identified for most of their length, giving rise to the entanglement structure depicted in the cartoon (right). Bell pairs are identified across the minimal cuts, up to the pair tensors depicted, inhabiting the tripartite residual region.

entropies obtained from holographic calculations were found to be consistent with those expected for random states in a reduced Hilbert space. This motivates us to compare the results obtained for the network in the causal shadow region to those for a Haar-random state on the legs crossing the minimal cuts, drawn as a blob in the right panel of figure 45.

We characterise the states by considering the entanglement entropy associated to each of the asymptotic regions, and by considering the logarithmic negativity for pairs of regions [136, 137]. The logarithmic negativity for a density matrix ρ on a Hilbert space $\mathcal{H}_A \otimes \mathcal{H}_{A^C}$ is defined as [138]

$$L = \log(2\mathcal{N} + 1) \tag{5.14}$$

where $\mathcal{N}$ is the entanglement negativity defined to be,

$$\mathcal{N}_A = \frac{\|\rho^{T_A}\| - 1}{2} \tag{5.15}$$

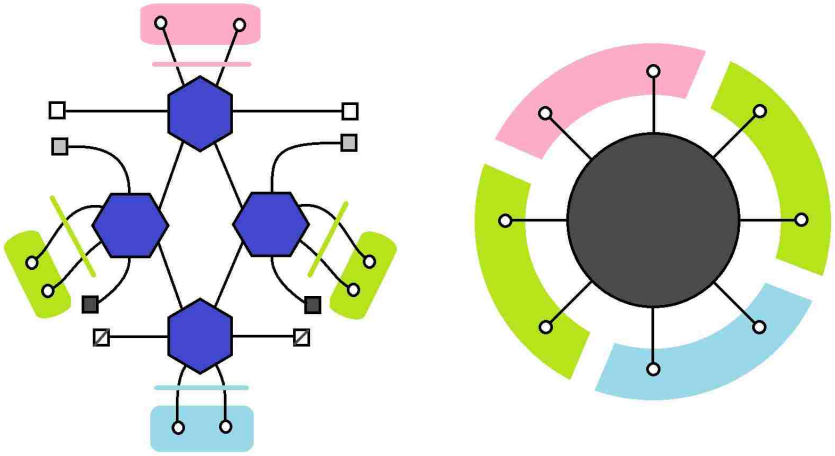

Figure 45: (Left) The tripartite residual region of a network representing a very low temperature three-boundary wormhole. The coloured region containing circular boundary nodes depict the three different boundaries, and the cuts of the same colour indicate the horizon corresponding to each boundary. We compare the entanglement structures of the tensor network state and a state in the same Hilbert space defined by a Haar random state (right).

and where ρ^{T_A} is the partial transpose of the density matrix ρ on the factor A. If ρ has components $\rho_{ab\,a'b'}$, The components of the partially transposed density matrix are $(\rho^{T_A})_{ab\,a'b'} = (\rho^{T_A})_{a'b\,ab'}$. The logarithmic negativity (5.14) provides an upper bound for the distillable entanglement, or the number of Bell pairs that can be distilled between the factor A and its complement [139]. Consider a Hilbert space of dimension χ^N (such as the state defined by an N-legged tensor with bond-dimension χ), the maximum number of Bell pairs that could be ideally distilled from this state is $N_{\text{Bell}} = N \log_2(\chi)$. When we have $L < N_{\text{Bell}}$ it indicates that there can be some component of the entanglement between A and A^C which is intrinsically multipartite.

Results comparing the entanglement structure of tripartite residual regions for low-temperature wormholes built from a selection of tilings are shown in figure 46. We find that the distinction between these networks and random blobs depends strongly on the tiling. Not surprisingly, for choices of tilings where the causal shadow contains a single tensor, the results are as for a Haar random state, as is the case for the examples shown in figure 47. In contrast, networks for which the causal shadow region contains multiple tensors generically exhibit distinct entanglement structure, as with the networks shown in figure 46. The right-hand plots of figure 46 correspond to non-vanishing logarithmic negativities on a single boundary factor. This is qualitatively unlike the GHZ state, for which the logarithmic negativity on any single factor vanishes, and suggests the presence of some bipartite entanglement even in the state in this tripartite residual region.

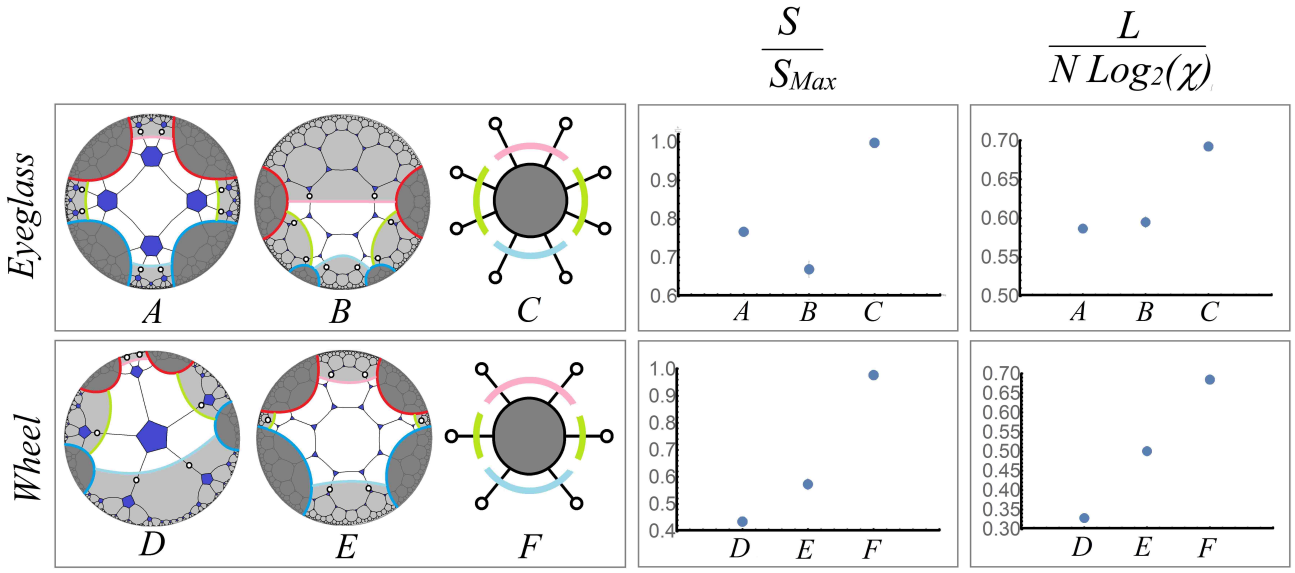

Figure 46: Results comparing the entanglement structures of tripartite residual regions (highlighted regions of each network) of very low-temperature networks built out of Haar random tensors. We compare a pair of networks in each of the eyeglass (A and B) and wheel (D and E) regimes with a corresponding random states (C and F respectively) with the same dimensions. We compare the resulting entropy and logarithmic negativity on the light-blue factor in each case and compare the result with an appropriate random state, as shown in the plots on the right; error bars are barely perceptible. In the cases illustrated, the entanglement structure is quantitatively distinct to a random state. Here we take $\chi = 3$.

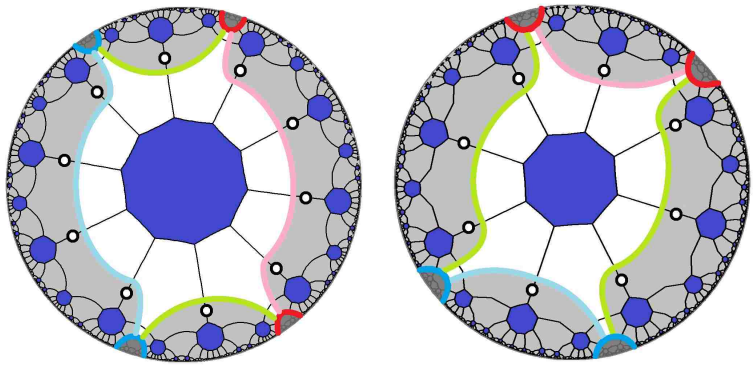

Figure 47: Networks for low-T three-boundary wormholes for which the causal shadow (unshaded) is presicely a Haar random state, in the eyeglass (left) and wheel (right) regimes.

The fact that the logarithmic negativities do not reach their maximum value however implies a degree of intrinsically multipartite entanglement, as we expect. Though our results correspond only to relatively low bond-dimension, we expect the results for high bond-dimension should be at least qualitatively similar insofar as the entanglement structure of tensor network states is primarily dependent on the set of contractions within it.

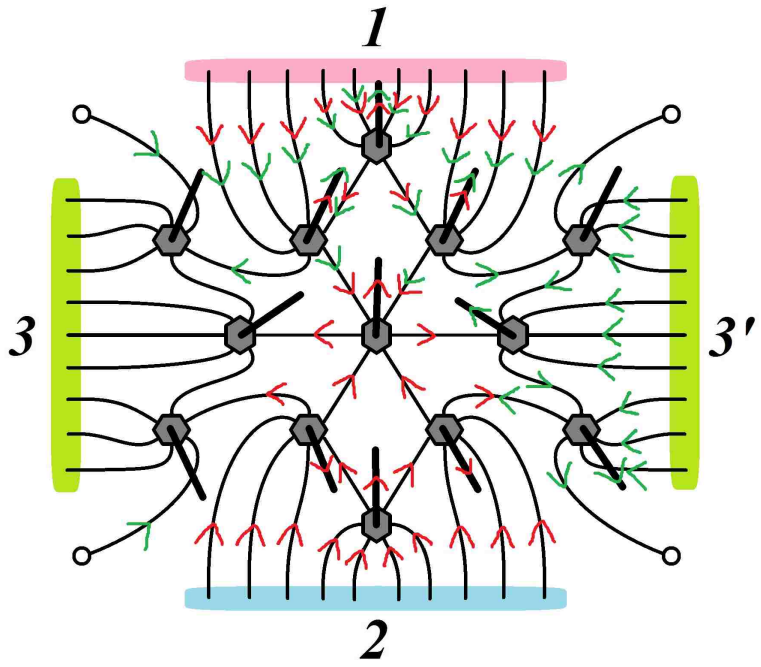

Figure 48: A holographic septagon code for three-boundary wormhole in the wheel regime. Dangling bulk legs are indicated by thicker lines. The red and green arrow assignments depict our attempts to reconstruct the operator bulk site at the centre. The red arrow assignment corresponds to choosing the 1 and 2 for which we can reconstruct the central site. The green arrow assignment attempts to reconstruct the central site from just boundary 1 and 3' (half of boundary 3) and fails. The code thus behaves like a quantum secret sharing scheme, for which access to information, here pertaining to local bulk information, is only accessible with a sufficiently large share in hand; in this case being a sufficiently large portion of the boundary.

It is also interesting to take a holographic code network, and consider the reconstruction of operators in the causal shadow region in terms of boundary operators. This requires us to push the operator back to the boundary through the tensors in the network. If there are self-contractions on the tensors this can lead to obstructions, but in general we find results that are consistent with the expectation that we can reconstruct an operator in this region from a subset of the boundary including more than half the legs along the boundary of the causal shadow region. An example is given in figure 48.

We can also consider cases with more boundaries. These will then contain internal cycles, which can lead to important differences from the Haar random blob structure for the multipartite residual region. Short internal cycles constrain the maximum value of the entropy associated to a given subregion to *less* than the typical maximal value. One example is the four-boundary wormhole with a short internal cycle. In the continuous case it is easy to see that sufficiently short

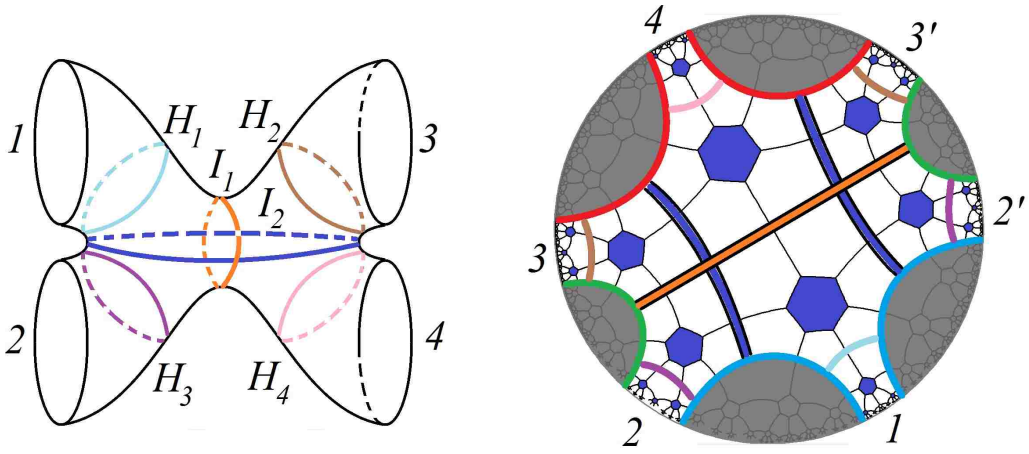

Figure 49: A four boundary wormhole with horizons H_a, $a = 1, ...4$ (cyan, brown, pink, purple) and internal cycles I_b, $b = 1, 2$ (orange,blue) depicted. Here, $I_1 < H_1 + H_2, H_3 + H_4$ and so I_1 is the RT surface for regions 1 & 2 and regions 3 & 4. A corresponding holographic state (right) is depicted, with colour-coded horizons and emphasised internal cycles indicated. Having $|I_1| < |H_1| + |H_3|$ constrains $S(1 \cup 2) \leq |I_1| \ln \chi = 3 \ln \chi$. In contrast, for a Haar random blob we would have $S(1 \cup 2) \leq \ln(dim(\mathcal{H}_1 \otimes \mathcal{H}_2)) = 5 \ln \chi$.

internal cycles are dominant RT surfaces, as illustrated in figure 49 (left). In a corresponding network this amounts to a constraint on the maximum entropy of the state on a set of boundaries for which the internal cycle is shorter than it's corresponding greedy geodesic, as illustrated in figure 49 (right).

Another example with internal topology is the torus wormhole. We find that networks constructed on tilings of the torus wormhole exhibit the expected features of their continuum analogues, up to tiling artefacts like those shown in figure 41. In particular, we expect the torus networks to have a minimal cut homologous to the boundary that wraps the throat of the torus. Behind this region is the causal shadow with the topology of a torus. We expect that for low-temperature torus wormholes, the causal shadow region is reconstructible only with the entire boundary, whereas for higher temperatures we expect to be able to reconstruct information in the causal shadow with only subsets of the boundary. Examples of this behaviour are illustrated in figure 50 a) and b).

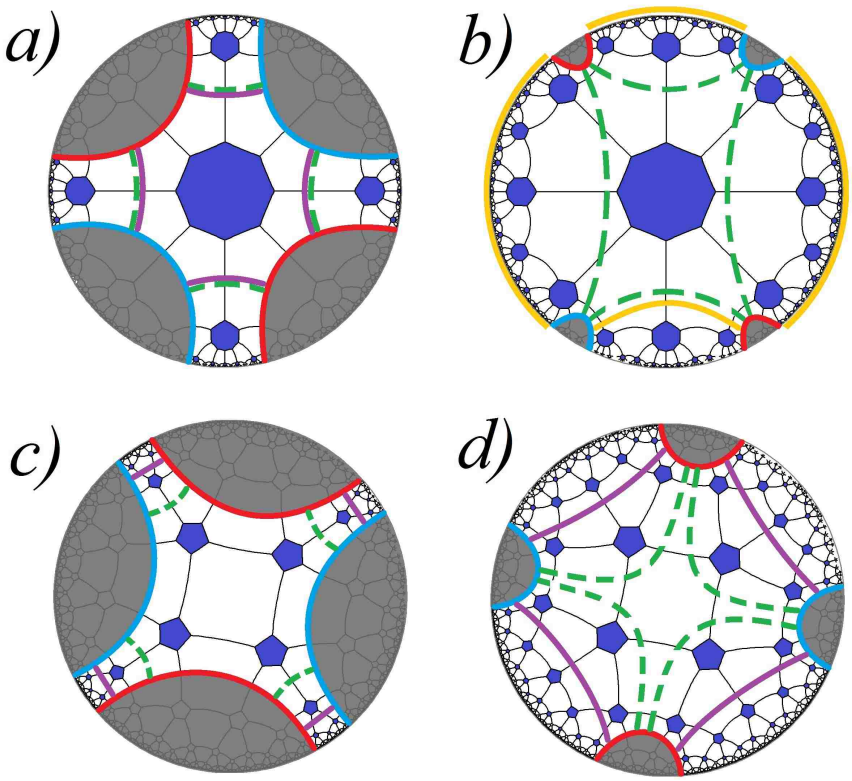

Figure 50: low-T torus wormhole networks. a) A very low-T octagon state for which the minimal cut (dashed, green) wrapping the throat coincides with the greedy geodesic for the whole boundary (purple). Here we cannot reconstruct the central tensor encoding the causal shadow. b) A higher-T octagon state for which the greedy geodesic is trivial meaning we can construct the central tensor lying behind the minimal cut from the whole boundary as we expect. In fact, we can reconstruct the tensor at the centre from only a subset of the boundary, as depicted by the yellow greedy geodesic associated to the portion of the boundary highlighted in the same colour, which passes through the central tensor. This mimics the anticipated high-T behaviour. c) A very low-T pentagon state with tiling artifacts in which the residual region does not reach the minimal cut. d) A higher-T pentagon state with the same tiling artifacts wherein we cannot reconstruct the region behind the minimal cut even with the whole boundary, because its corresponding greedy geodesic cannot penetrate the identifcation.

Outlook

The work in this thesis invariably presents outstanding issues that are sources for further questions; here I outline some of these questions, as well as some approaches that have generated results in related directions.

In chapters 2 and 3 we established the existence of a good holographic dictionary for asymptotically locally Schrödinger spacetimes. One issue with this work is that we remain agnostic to the existence of a dual field theory; it's assumed to be the dual Schrödinger field theory of the asymptotically locally Schrodinger bulk massive vector theory. From the condensed matter point-of-view finding a holographic Schrödinger field theory to proxy systems seen in nature (such as cold atoms at unitarity) would be extremely desirable. In this case the generalised holographic machinery that we've developed can be brought to bear. A top-down approach which derives the Schrödinger geometry in the context of string theory via a so-called null Melvin twist is discussed in [140]. Related top-down approaches to non-relativistic holography may identify explicit NRFT constructions applicable to condensed matter systems seen in nature. We compare our results with the related approach [35–38] which treats Schrödinger field theory as a perturbation of a relativistic CFT by an irrelevant vector operator. Our construction, in contrast, is non-perturbative owing to the identification of boundary data as sources and vevs for boundary operators with definite scaling dimensions with respect to the non-relativistic, anisotropic scaling symmetry. Another approach that could provide valuable hints in this direction is non-relativistic holography for $3D$ higher-spin theories [141, 142]. There, the huge amount of redundancy deriving from the higher-spin gauge transformations leads to very large asymptotic symmetry groups. The naturally constraining nature of symmetries may lead to the successful identification of a Schrodinger field theory with these corresponding, large symmetry groups. For $z > 2$ we do not know if a sensible holographic dictionary is possible, since as we've stated, the leading asymptotics no longer carry leading r dependence. There's then no immediately obvious way to interpret boundary data as boundary sources in the usual sense, nonetheless this by itself does not rule out the possibility that there is a tenable holographic interpretation; this is an interesting question for future work. An interesting problem for Schrodinger holography and for non-AdS holography in general is whether or not the RT formula holds unchanged in these cases. The result [143] would seem to suggest, as least for the asymptotically Lifshitz case, that naive application of the usual holographic entropy calculations may be fraught with additional subtleties. A similar story

may persist for the asymptotically locally Schrödinger geometries.

One of the main open questions of chapter 4 is the extent to which the results there generalise suitably to regions of smaller moduli. There we had some discussion as to what can happen when not all of the moduli are large, where the identifications of boundary states persist away from the smaller boundaries. In general the work in chapter 5 is an attempt to provide an answer to this question using the formalism of holographic tensor networks. In the latter case we unearthed the interesting suggestion that the main result of chapter 4 does generalise even to cases of very small moduli. It would be interesting to explore how the results of chapter 5 generalise to large bond-dimensions, where the random tensors should more closely resemble perfect tensors. Exploring this regime presently entails a computationally expensive barrier. Another issue is that the tensor network models considered in chapter 5 are highly heuristic, they merely serve as proxies for the path-integrals on Riemann surfaces and do not pertain to any particular dynamics. A more robust approach could entail looking for an appropriate generalisation of the $MERA$ network to multiboundary states. It was shown in [124] that one can obtain thermal states as quotients of $MERA$. This naturally suggests that one can take similar quotients to obtain network models for the pair-of-pants geometry, for example. One can indeed show that an appropriate quotient construction for the pair of pants geometry exists [144], but what is far less obvious is a sensible choice of cut-off that respects the symmetries of the quotient. In a related approach [119] it was shown that through a prescribed series of local replacements called tensor network renormalisation (TNR) that one can coarse-grain the tensor network representation of the Euclidean path-integral on the infinite strip to generate precisely the $MERA$ for the CFT ground state. This suggests that one might be able to apply a similar tensor network replacement algorithm to a lattice network on the pair-of-pants geometry in order to obtain a $MERA$ for the corresponding boundary state. It's not clear that there's a way to apply TNR to such a network without leading to inconsistencies. We can choose to start from the networks obtained in chapter 5, but then it seems that one cannot implement local replacements in a scale-invariant way. The results of chapters 4 and 5 also play a part in shedding light on ideas of bulk reconstruction, particularly the idea of entanglement vs. causal wedge reconstruction and whether or not information pertaining to boundary regions is sufficient to reconstruct bulk information localised beyond the horizons, which in turn is related to the hotly debated story of firewalls and the black hole information paradoxes [145–150]. The general intuition, especially in relation to the QEC proposals [59], is that reconstruction of local bulk operators located beyond

the horizon is possible due to the quantum secret-sharing character of holographic states. In the multiboundary holographic states considered in chapter 5 we find that boundary regions of sufficient size may be used to reconstruct operators located within the causal shadow region in accordance with these proposals.

Since its inception almost 20 years ago, interest in the AdS/CFT correspondence has bloomed. The correspondence continues to generate vast bodies of powerful and far-reaching results in our attempts to understand quantum gravity, strongly-coupled condensed matter systems and beyond. In time, the significance of the relation between bulk geometry and boundary entanglement has been explicated in many different examples and while many exciting open questions abound, it seems that in this regard we are drawing surely closer to an understanding of the inner workings of the correspondence. The great expectation is that it's only a matter of time before this fruitful story inspires the next great step that will lead to the formulation of a successful theory of quantum gravity.

Appendices

A Spatially dependent modes for $z = 2$

We consider here for completeness the linearised equations for $d_s = 2$ with dependence on the spatial directions $\vec{x}$ included. The equations are the $z \to 2$ limit of the analysis in chapter 2. Considering a single Fourier mode in all boundary directions, we can use the rotation symmetry to orient the spatial coordinates so that the spatial momentum is along the x direction, so the coordinate dependence in all modes is $e^{i\omega t + ik_\xi \xi + ik_x x}$. Then the modes split up into the scalar modes H_{tt}, $H_{t\xi}$, $H_{\xi\xi}$, H_{tx}, $H_{\xi x}$, H_{xx}, H_{yy} s_t, s_x, s_r and the vector modes H_{ty}, $H_{\xi y}$, H_{xy}, s_y. As in the discussion with no spatial dependence, these all have an expansion in powers of $k_\xi \omega r^2$ and $k_x^2 r^2$. The leading terms take the same form as for the constant modes above.

The equations of motion in the vector sector are

$$0 = rk_x[r^2\omega H_{\xi y} + k_\xi(H_{ty} + H_{\xi y})] - (k_\xi^2 + 2k_\xi\omega r^2)H_{xy} - 3rH'_{xy} + r^2 H''_{xy}, \tag{A.1}$$

$$0 = 2H_{\xi y} - k_x^2 r^2 s_y - (k_\xi^2 + 2k_\xi\omega r^2 + 5)s_y + r(2H'_{\xi y} - 3s'_y + rs''_y), \tag{A.2}$$

$$0 = k_x(k_\xi r H_{xy} - k_x r^2 H_{\xi y}) + k_\xi^2 H_{ty} - (3 + k_\xi\omega r^2)H_{\xi y} + r(-H'_{\xi y} + rH''_{\xi y}), \tag{A.3}$$

$$\begin{aligned} 0 = {} & k_x r(r^2\omega H_{xy} - k_x r H_{ty}) + (k_\xi\omega r^2 - k_\xi^2 - 5)H_{ty} + 10s_y + (k_\xi\omega r^2 + \omega^2 r^4 - 2)H_{\xi y} \\ & + r(rH''_{ty} - 2(H_{\xi y} + s_y)' - 5H'_{ty}), \end{aligned} \tag{A.4}$$

and additionally,

$$0 = k_\xi[(H_{ty} - H_{\xi y} + 2s_y) - r(H_{ty} + H_{\xi y})'] - \omega r^2[H_{\xi y} + rH'_{\xi y}] - k_x r^2 H'_{xy}. \tag{A.5}$$

We can solve these equations order by order in $k_\xi\omega$ and k_x^2. The subleading components determine the subleading terms in the expansion of the fields. But there are also additional constraints on the leading terms, corresponding to the expected Ward identities. Equation (A.5) gives at leading order

$$k_\xi[2H^{(+)}_{ty} - s^{(+)}_y] + 2\omega H^{(+)}_{\xi y} + 2k_x \bar{H}^{(4)}_{xy} = 0. \tag{A.6}$$

At $k_\xi = 0$, this corresponds to the Ward identity

$$\partial_t \mathcal{P}_y + \partial_x \Pi^x_y = 0. \tag{A.7}$$

In the scalar sector, the equations of motion are

$$0 = 2k_x r(k_\xi + \omega r^2)(H_{tx} + H_{\xi x}) + k_x^2 r^2\Big(\frac{1}{2}H_{tt} - \frac{1}{2}H_{\xi\xi} - H_{t\xi} - k\Big) + 6H_{tt} - (k_\xi + \omega r^2)^2 k$$
$$+ i(k_\xi + 2\omega r^2)s_r + 12s_t + 4s_\xi - 4rH'_{t\xi} - \frac{1}{2}rH'_{\xi\xi} - 2rk' - rs'_\xi - r[7H'_{tt} + 2s'_t] + \frac{1}{2}r^2H''_{tt}$$
$$+ r^2H''_{t\xi} + \frac{1}{2}r^2H''_{\xi\xi} + r^2k'', \tag{A.8}$$

$$0 = k_x r\Big(k_\xi H_{tx} + (2k_\xi + \omega r^2)H_{\xi x}\Big) - k_x^2 r^2(H_{t\xi} + H_{\xi\xi} + k) - 2(k_\xi^2 + \omega k_\xi r^2)k$$
$$- 3r\Big(H'_{t\xi} + 2k'\Big) + r^2H''_{t\xi} + r^2H''_{\xi\xi} + 2r^2k'', \tag{A.9}$$

$$0 = rk_x[\omega r^2(H_{\xi\xi} + k) - 2is_r - k_\xi H_{tt} + (\omega r^2 - k_\xi)H_{t\xi}] + (k_\xi^2 + k_\xi\omega r^2 - 5)H_{tx}$$
$$- (k_\xi\omega r^2 + \omega^2 r^4 - 2)H_{\xi x} - 10s_x + 5rH'_{tx} + 2r(H'_{\xi x} + s'_x) - r^2H''_{tx}, \tag{A.10}$$

$$0 = -2k_xk_\xi rH_{\xi x} + k_x^2r^2H_{\xi\xi} + 4H_{\xi\xi} + 2k_\xi^2k - rH'_{\xi\xi} - r^2H''_{\xi\xi}, \tag{A.11}$$

$$0 = k_x r\Big(k_\xi(H_{t\xi} + k) - \omega r^2H_{\xi\xi}\Big) - k_\xi^2H_{tx} + \Big(k_\xi\omega r^2 + 3\Big)H_{\xi x} + rH'_{\xi x} - r^2H''_{\xi x}, \tag{A.12}$$

$$0 = r^2k'' + r^2H''_{\xi\xi} + 2r^2H''_{t\xi} - rs'_\xi - 3rk' - 2rH'_{\xi\xi} - 6rH'_{t\xi} + 8s_\xi + 2ik_\xi s_r - (k_\xi^2 + 2\omega k_\xi r^2)k$$
$$+ \Big(-4 + \omega^2r^{2z}\Big)H_{\xi\xi} - 2k_\xi\omega r^2H_{t\xi} + k_\xi^2H_{tt}, \tag{A.13}$$

$$0 = 2k_x r\Big(k_\xi(H_{tx} + 2H_{\xi x}) + \omega r^2H_{\xi x}\Big) - r^2k_x^2(2H_{tx} + H_{\xi\xi}) + r^2k'' + r^2H''_{\xi\xi} - 2rs'_\xi - 3rk'$$
$$- 2rH'_{\xi\xi} - 6rH'_{t\xi} + 8s_\xi + 2ik_\xi s_r - (k_\xi^2 + 2\omega k_\xi r^2)k + \Big(-4 + \omega^2r^4\Big)H_{\xi\xi} - 2k_\xi\omega r^2H_{t\xi}$$
$$+ k_\xi^2H_{tt}, \tag{A.14}$$

$$0 = k_xk_\xi rs_x - k_x^2r^2s_\xi + 4H_{\xi\xi} + 2ik_\xi s_r + k_\xi^2s_t - \Big(8 + k_\xi\omega r^2\Big)s_\xi + 2rH'_{\xi\xi} - ik_\xi rs'_r - rs'_\xi$$
$$+ r^2s''_\xi, \tag{A.15}$$

$$0 = k_x r(k_\xi + \omega r^2)s_x - 2k_x^2r^2(s_\xi + s_t) + 4i(2k_\xi + \omega r^2)s_r + 2\Big(\omega^2r^4 - 8\Big)s_\xi + 2rH'_{\xi\xi} - 4rk'$$
$$- 2i(k_\xi + \omega r^2)rs'_r - 6rs'_\xi - 2k_\xi\omega r^2s_t - 10rs'_t + 2r^2s''_t + 2r^2s''_\xi, \tag{A.16}$$

$$0 = k_x r\Big(2is_r + k_\xi s_t + (k_\xi + r^2\omega)s_\xi - irs'_r\Big) + 2H_{\xi x} - \Big(k_\xi^2 + 2k_\xi\omega r^2 + 5\Big)s_x + 2rH'_{\xi x}$$
$$- 3rs'_x + r^2s''_x, \tag{A.17}$$

and additionally,

$$0 = k_\xi^2 H_{tt} + 2k_\xi k_x r H_{tx} - 2(k_x^2 + k_\xi\omega)r^2 H_{t\xi} + 2rk_x(k_\xi + \omega r^2)H_{\xi x} - \Big(k_x^2 r^2 + 4 + \omega^2 r^2\Big)H_{\xi\xi}$$
$$- \Big(2k_\xi^2 + r^2(k_x^2 + 4k_\xi\omega)\Big)k - 2ik_\xi s_r + 8s_\xi - 6rH'_{t\xi} - 4rH'_{\xi\xi} - 6rk' + 2rs'_\xi, \tag{A.18}$$

$$0 = k_x r\Big((H_{tx} + H_{\xi x}) - rH'_{tx}\Big) + (k_\xi + 3\omega r^2)H_{\xi\xi} - 2k_\xi k - 8is_r - 2\omega r^2 s_\xi$$
$$+ k_\xi\Big(2(H_{tt} + s_t) - rH'_{tt}\Big) + (-k_\xi r^{2-z} + \omega r^z)rH'_{t\xi} + \omega r^{z+1}(H'_{\xi\xi} + k'), \tag{A.19}$$

$$0 = -k_x r\Big(H_{\xi x} + rH'_{\xi x}\Big) - (k_\xi + 2\omega r^2)H_{\xi\xi} + k_\xi rH'_{t\xi} - r\omega r^2 H'_{\xi\xi} + 2k_\xi rk', \tag{A.20}$$

$$0 = k_\xi(H_{tx} - H_{\xi x} + 2s_x) - \omega r^2 H_{\xi x} - k_\xi rH'_{tx} - (k_\xi + \omega r^2)rH'_{\xi x}$$
$$+ k_x r\Big((H_{\xi\xi} + 2s_\xi) + 2r(H'_{t\xi} + H'_{\xi\xi} + k')\Big), \tag{A.21}$$

$$0 = k_x r(4H_{\xi x} + 2s_x + rs'_x) - 2ik_x^2 r^2 s_r + 2(k_\xi + 2\omega r^2)H_{\xi\xi} - 4k_\xi k - 2i\Big(k_\xi^2 + 8 + 2k_\xi\omega r^2\Big)s_r$$
$$+ 2k_\xi(-2s_t + rs'_t) + 2(k_\xi + \omega r^2)s'_\xi. \tag{A.22}$$

Again, the constraints corresponding to the Ward identities are modified. Equation (A.21) gives at leading order

$$k_\xi[2H^{(+)}_{tx} - s^{(+)}_x] + 2\omega H^{(+)}_{\xi x} + k_x[2k^{(4)} - \frac{5}{3}s^{(4)}_\xi] = 0. \tag{A.23}$$

At $k_\xi = 0$, this corresponds to the Ward identity

$$\partial_t \mathcal{P}_x + \partial_x \Pi^x_x = 0. \tag{A.24}$$

Equation (A.20) gives

$$k_\xi\Big(k^{(4)} + \frac{2}{3}s^{(4)}_\xi\Big) - \omega H^{(+)}_{\xi\xi} - k_x H^{(+)}_{\xi x} = 0. \tag{A.25}$$

At $k_\xi = 0$, this corresponds to the Ward Identity

$$\partial_t \rho + \partial_x \rho^x = 0. \tag{A.26}$$

Finally, there is a linear combination of equations (A.22) and (A.19) which eliminates s_r giving,

$$k_\xi\Big(2H^{(+)}_{tt} + s^{(+)}_t\Big) - \omega\Big(2k^{(4)} - \frac{5}{3}s^{(4)}_\xi\Big) + k_x\Big(2H^{(+)}_{tx} + 2s^{(+)}_x\Big) = 0. \tag{A.27}$$

At $k_\xi = 0$, this corresponds to the Ward Identity

$$\partial_t \mathcal{E} + \partial_x \mathcal{E}^x = 0. \tag{A.28}$$

Thus the full linearised perturbations behave as we expect.

B The horizons H_1, H_2 in BTZ coordinates

We now compute the parameters characterising the region Σ_+, corresponding to half of the $t = 0$ slice of the three-boundary wormhole with horizons H_1, H_2, H_3, of respective lengths L_1, L_2, L_3. In chapter 4 we ordered the lengths so that $L_3 > L_1, L_2$; this assumption is relaxed here. The region Σ_+ is bounded by three geodesics G_{ab}, running between the boundary components labelled by a and b, and meeting horizons H_a, H_b orthogonally.

We use the metric (4.7) with H_3 lying at $\rho = 0$ and G_{13}, G_{23} lying at $x = \pm\frac{L_3}{4}$. Thus $x \in [-\frac{L_3}{4}, \frac{L_3}{4}]$. Consider a geodesic parameterised by arclength s, using a dot to denote differentiation with respect to s. From translation invariance, there is a conserved quantity $(1+\rho^2)\dot{x}$, which for geodesics with both endpoints at $\rho = \infty$ is given by $\sqrt{1+\rho_0^2}$, where $\rho_0 > 0$ is the minimal value of ρ. The geodesic is then given by

$$\rho = \rho_0 \cosh s, \quad x = x_0 + \tanh^{-1}\left(\frac{\tanh s}{\sqrt{1+\rho_0^2}}\right). \tag{B.1}$$

Consider first the geodesics G_{12} and that corresponding to H_{1+} (see fig. 51 for the various relevant geodesics and quantities). The endpoints of G_{12} lie at $x = x_1, x_2$, and it will be convenient to parametrise these by the centre $\bar{x} = \frac{x_1+x_2}{2}$ and the half-width $\Delta x = \frac{x_2-x_1}{2}$. We intend to find L_1 in terms of these parameters, and along the way will also obtain the minimal distance d_{13} between H_{1+} and H_{3+}, as well as the position at which G_{12} and H_{1+} intersect.

The geodesics are given by

$$G_{12} : \rho = \frac{\cosh s}{\sinh \Delta x}, \quad x = \bar{x} + \tanh^{-1}(\tanh \Delta x \tanh s), \quad s \in \mathbb{R}, \tag{B.2}$$

$$H_{1+} : \rho = \sinh d_{13} \cosh s, \quad x = -\frac{L_3}{4} + \tanh^{-1}\left(\frac{\tanh s}{\cosh d_{13}}\right), \quad 0 \le s \le \frac{L_1}{2}, \tag{B.3}$$

with the constraint that they intersect at right angles at the endpoint of H_{1+}, where the arclength along H_{1+} is $s = \frac{L_1}{2}$, and along G_{12} is $s = s_1$, say, where $s_1 < 0$.

The condition that two geodesics intersect orthogonally determines the value of ρ at which they meet in terms of the conserved quantities for the two geodesics; for H_{1+} and G_{12} it gives

$$\rho^2 = \sinh^2 d_{13} + \coth^2 \Delta x = \cosh^2 d_{13} + \operatorname{csch}^2 \Delta x \text{ at intersection.} \tag{B.4}$$

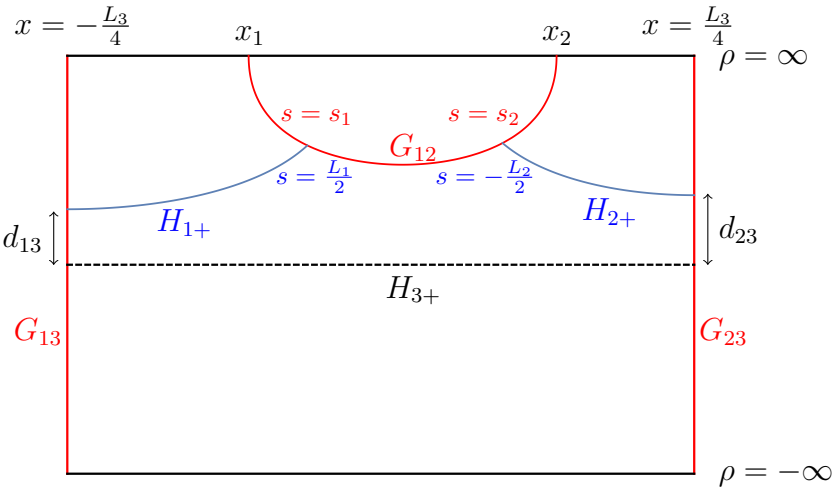

Figure 51: The geodesics G_{ab} bounding the patch Σ_+ in BTZ coordinates. The horizons H_{a+} are also shown. The ρ direction runs vertically, and x horizontally. The positions where the geodesics intersect are labelled with the arclength along each curve, measured from the deepest point (minimal ρ), and d_{13}, d_{23} mark the minimal distances between the horizons.

We now get two equations from identifying the value of ρ at intersection with the values of ρ for G_{12} at $s = s_1$, and for H_{1+} at $s = \frac{L_1}{2}$. A third comes from identifying the x coordinates at these same arclengths:

$$\coth \Delta x = \sinh d_{13} \sinh \frac{L_1}{2}, \tag{B.5}$$

$$\sinh s_1 = -\sinh \Delta x \cosh d_{13}, \tag{B.6}$$

$$\bar{x} + \tanh^{-1}(\tanh \Delta x \tanh s_1) = -\frac{L_3}{4} + \tanh^{-1}\left(\frac{\tanh \frac{L_1}{2}}{\cosh d_{13}}\right). \tag{B.7}$$

We then solve for L_1, d_{13}, s_1 in terms of $\bar{x}, \Delta x$ to obtain

$$\cosh \frac{L_1}{2} = \frac{\sinh\left(\frac{L_3}{4} + \bar{x}\right)}{\sinh \Delta x}, \quad \tanh d_{13} = \frac{\cosh \Delta x}{\cosh\left(\frac{L_3}{4} + \bar{x}\right)}, \quad \tanh s_1 = -\frac{\tanh \Delta x}{\tanh\left(\frac{L_3}{4} + \bar{x}\right)}. \tag{B.8}$$

It is straightforward to translate these results into expressions for L_2, the distance d_{23} between horizons H_{2+} and H_{3+}, and s_2, the arclength along G_{12} at which it intersects H_{2+}:

$$\cosh \frac{L_2}{2} = \frac{\sinh\left(\frac{L_3}{4} - \bar{x}\right)}{\sinh \Delta x}, \quad \tanh d_{23} = \frac{\cosh \Delta x}{\cosh\left(\frac{L_3}{4} - \bar{x}\right)}, \quad \tanh s_2 = \frac{\tanh \Delta x}{\tanh\left(\frac{L_3}{4} - \bar{x}\right)} \tag{B.9}$$

Finally, the above can be inverted to find $\bar{x}$, Δx, and d_{ab} (where, in particular, $d_{12} = s_2 - s_1$

is the minimal distance between H_{1+}, H_{2+}) in terms of L_1, L_2, L_3.

$$\sinh \bar{x} = \frac{\left(\cosh \frac{L_1}{2} - \cosh \frac{L_2}{2}\right) \sinh \frac{L_3}{4}}{\sqrt{\cosh^2 \frac{L_1}{2} + \cosh^2 \frac{L_2}{2} + 2 \cosh \frac{L_1}{2} \cosh \frac{L_2}{2} \cosh \frac{L_3}{2}}}, \tag{B.10}$$

$$\sinh \Delta x = \frac{\sinh \frac{L_3}{2}}{\sqrt{\cosh^2 \frac{L_1}{2} + \cosh^2 \frac{L_2}{2} + 2 \cosh \frac{L_1}{2} \cosh \frac{L_2}{2} \cosh \frac{L_3}{2}}}, \tag{B.11}$$

$$\cosh d_{12} = \frac{\cosh \frac{L_1}{2} \cosh \frac{L_2}{2} + \cosh \frac{L_3}{2}}{\sinh \frac{L_1}{2} \sinh \frac{L_2}{2}} \quad \text{(and permutations)} \tag{B.12}$$

In particular, the explicit inversion shows that the mapping between (x_1, x_2) and (L_1, L_2) is bijective and smooth.

We may now work out the asymptotic values of these quantities in the limit where all lengths L_a are large. The typical expressions reduce to sums of exponentials of linear combinations of L_a, so there are separate regimes depending on the relative sizes of the exponents; these turn out to be three regimes where one horizon is longer than the sum of the others ($L_1 > L_2 + L_3$ and permutations), and the regime where no horizon is dominant in this way.

$$\bar{x} \sim \begin{cases} \frac{L_3}{4} - \frac{1}{2} \exp\left(-\frac{L_1 - L_2 - L_3}{2}\right) & L_1 > L_2 + L_3 \\ -\frac{L_3}{4} + \frac{1}{2} \exp\left(-\frac{L_2 - L_1 - L_3}{2}\right) & L_2 > L_1 + L_3 \\ \frac{L_1 - L_2}{4} & \text{otherwise} \end{cases} \tag{B.13}$$

$$\Delta x \sim \begin{cases} \exp\left(-\frac{L_1 - L_3}{2}\right) & L_1 > L_2 + L_3 \\ \exp\left(-\frac{L_2 - L_3}{2}\right) & L_2 > L_1 + L_3 \\ \frac{L_3 - L_1 - L_2}{4} + \log 2 & L_3 > L_1 + L_2 \\ \exp\left(-\frac{L_1 + L_2 - L_3}{4}\right) & \text{otherwise} \end{cases} \tag{B.14}$$

$$d_{12} \sim \begin{cases} \frac{L_3 - L_1 - L_2}{2} + 2 \log 2 & L_3 > L_1 + L_2 \\ 2 \exp\left(-\frac{L_2}{2}\right) & L_1 > L_2 + L_3 \\ 2 \exp\left(-\frac{L_1}{2}\right) & L_2 > L_1 + L_3 \\ 2 \exp\left(-\frac{L_1 + L_2 - L_3}{2}\right) & \text{otherwise} \end{cases} \tag{B.15}$$

The corrections in each case are exponentially small in the L_a, except when $L_3 - L_1 - L_2$ is order

one, for example.

The interval $[x_1, x_2]$ looks qualitatively different in each of the four regimes. When $L_3 > L_1 + L_2$, it is long (the same order as the horizon lengths), and at a generic position. When $L_1 > L_2 + L_3$, it is exponentially short, and also close to the right end of the strip; it is similarly short and close to the left end when $L_2 > L_1 + L_3$. In the remaining regime, it is again exponentially short, but in a generic position.

References

[1] T. Andrade, C. Keeler, A. Peach, and S. F. Ross, *Schrdinger holography for z ¡ 2*, *Classical and Quantum Gravity* **32** (2015), no. 3 035015.

[2] T. Andrade, C. Keeler, A. Peach, and S. F. Ross, *Schrdinger holography with z = 2*, *Classical and Quantum Gravity* **32** (2015), no. 8 085006.

[3] D. Marolf, H. Maxfield, A. Peach, and S. Ross, *Hot multiboundary wormholes from bipartite entanglement*, *Classical and Quantum Gravity* **32** (2015), no. 21 215006.

[4] A. Peach and S. F. Ross, *Tensor Network Models of Multiboundary Wormholes*, arXiv:1702.0598.

[5] J. M. Maldacena, *The Large N limit of superconformal field theories and supergravity*, *Int. J. Theor. Phys.* **38** (1999) 1113–1133, [hep-th/9711200]. [Adv. Theor. Math. Phys.2,231(1998)].

[6] E. Witten, *Anti-de Sitter space and holography*, *Adv. Theor. Math. Phys.* **2** (1998) 253–291, [hep-th/9802150].

[7] I. R. Klebanov, *TASI lectures: Introduction to the AdS / CFT correspondence*, in *Strings, branes and gravity. Proceedings, Theoretical Advanced Study Institute, TASI'99, Boulder, USA, May 31-June 25, 1999*, pp. 615–650, 2000. hep-th/0009139.

[8] H. Nastase, D. Vaman, and P. van Nieuwenhuizen, *Consistent nonlinear K K reduction of 11-d supergravity on AdS(7) x S(4) and selfduality in odd dimensions*, *Phys. Lett.* **B469** (1999) 96–102, [hep-th/9905075].

[9] E. D'Hoker and D. Z. Freedman, *Supersymmetric gauge theories and the AdS / CFT correspondence*, in *Strings, Branes and Extra Dimensions: TASI 2001: Proceedings*, pp. 3–158, 2002. hep-th/0201253.

[10] S. A. Hartnoll, *Lectures on holographic methods for condensed matter physics*, *Class. Quant. Grav.* **26** (2009) 224002, [arXiv:0903.3246].

[11] U. Gursoy, *Improved Holographic QCD and the Quark-gluon Plasma*, *Acta Phys. Polon.* **B47** (2016) 2509, [arXiv:1612.0089].

[12] S. Ryu and T. Takayanagi, *Holographic derivation of entanglement entropy from AdS/CFT*, *Phys.Rev.Lett.* **96** (2006) 181602, [hep-th/0603001].

[13] M. Van Raamsdonk, *Building up spacetime with quantum entanglement*, *General Relativity and Gravitation* **42** (2010), no. 10 2323–2329, [arXiv:1005.3035].

[14] J. Maldacena and L. Susskind, *Cool horizons for entangled black holes*, *Fortschritte der Physik* **61** (2013), no. 9 781–811, [arXiv:1306.0533].

[15] A. Lewkowycz and J. Maldacena, *Generalized gravitational entropy*, *Journal of High Energy Physics* **2013** (2013), no. 8 1–29, [arXiv:1304.4926].

[16] M. Rangamani and T. Takayanagi, *Holographic Entanglement Entropy*, arXiv:1609.0128.

[17] S. W. Hawking, *Gravitational radiation from colliding black holes*, *Phys. Rev. Lett.* **26** (1971) 1344–1346.

[18] J. D. Bekenstein, *Black holes and entropy*, *Phys. Rev. D* **7** (Apr, 1973) 2333–2346.

[19] R. Bousso, *A Covariant entropy conjecture*, *JHEP* **07** (1999) 004, [hep-th/9905177].

[20] G. 't Hooft, *Dimensional reduction in quantum gravity*, in *Salamfest 1993:0284-296*, pp. 0284–296, 1993. gr-qc/9310026.

[21] L. Susskind, *The World as a hologram*, *J. Math. Phys.* **36** (1995) 6377–6396, [hep-th/9409089].

[22] S. W. Hawking, *Particle creation by black holes*, *Communications in Mathematical Physics* **43** (1975), no. 3 199–220.

[23] G. 't Hooft, *The Quantum Black Hole as a Hydrogen Atom: Microstates Without Strings Attached*, arXiv:1605.0511.

[24] A. Strominger and C. Vafa, *Microscopic origin of the Bekenstein-Hawking entropy*, *Phys. Lett.* **B379** (1996) 99–104, [hep-th/9601029].

[25] G. 't Hooft, S. B. Giddings, C. Rovelli, P. Nicolini, J. Mureika, M. Kaminski, and M. Bleicher, *The Good, the Bad, and the Ugly of Gravity and Information*, in *2nd Karl Schwarzschild Meeting on Gravitational Physics (KSM 2015) Frankfurt am Main, Germany, July 20-24, 2015*, 2016. arXiv:1609.0172.

[26] N. Itzhaki, J. M. Maldacena, J. Sonnenschein, and S. Yankielowicz, *Supergravity and the large N limit of theories with sixteen supercharges*, *Phys. Rev.* **D58** (1998) 046004, [hep-th/9802042].

[27] H. J. Boonstra, K. Skenderis, and P. K. Townsend, *The domain wall / QFT correspondence*, *JHEP* **01** (1999) 003, [hep-th/9807137].

[28] S. S. Gubser, I. R. Klebanov, and A. M. Polyakov, *Gauge theory correlators from noncritical string theory*, *Phys. Lett.* **B428** (1998) 105–114, [hep-th/9802109].

[29] S. Carlip, D.-W. Chiou, W.-T. Ni, and R. Woodard, *Quantum Gravity: A Brief History of Ideas and Some Prospects*, *Int. J. Mod. Phys.* **D24** (2015), no. 11 1530028, [arXiv:1507.0819].

[30] J. M. Maldacena, *Eternal black holes in anti-de Sitter*, *JHEP* **0304** (2003) 021, [hep-th/0106112].

[31] S. de Haro, S. N. Solodukhin, and K. Skenderis, *Holographic reconstruction of space-time and renormalization in the AdS / CFT correspondence*, *Commun. Math. Phys.* **217** (2001) 595–622, [hep-th/0002230].

[32] J. de Boer, E. P. Verlinde, and H. L. Verlinde, *On the holographic renormalization group*, *JHEP* **08** (2000) 003, [hep-th/9912012].

[33] I. Heemskerk, J. Penedones, J. Polchinski, and J. Sully, *Holography from Conformal Field Theory*, *JHEP* **10** (2009) 079, [arXiv:0907.0151].

[34] J. D. Brown and M. Henneaux, *Central charges in the canonical realization of asymptotic symmetries: an example from three-dimensional gravity*, *Comm. Math. Phys.* **104** (1986), no. 2 207–226.

[35] M. Guica, K. Skenderis, M. Taylor, and B. C. van Rees, *Holography for Schrodinger backgrounds*, *JHEP* **1102** (2011) 056, [arXiv:1008.1991].

[36] R. Caldeira Costa and M. Taylor, *Holography for chiral scale-invariant models*, *JHEP* **1102** (2011) 082, [arXiv:1010.4800].

[37] M. Guica, *A Fefferman-Graham-Like Expansion for Null Warped AdS(3)*, arXiv:1111.6978.

[38] B. C. van Rees, *Correlation functions for Schrodinger backgrounds*, arXiv:1206.6507.

[39] J. McGreevy, *Holographic duality with a view toward many-body physics*, *Adv. High Energy Phys.* **2010** (2010) 723105, [arXiv:0909.0518].

[40] M. Taylor, *Non-relativistic holography*, arXiv:0812.0530.

[41] S. F. Ross and O. Saremi, *Holographic stress tensor for non-relativistic theories*, *JHEP* **0909** (2009) 009, [arXiv:0907.1846].

[42] D. Son, *Toward an AdS/cold atoms correspondence: A Geometric realization of the Schrodinger symmetry*, *Phys.Rev.* **D78** (2008) 046003, [arXiv:0804.3972].

[43] P. Nozières and S. Schmitt-Rink, *Bose condensation in an attractive fermion gas: From weak to strong coupling superconductivity*, *Journal of Low Temperature Physics* **59** (1985), no. 3 195–211.

[44] D. M. Eagles, *Possible pairing without superconductivity at low carrier concentrations in bulk and thin-film superconducting semiconductors*, *Phys. Rev.* **186** (Oct, 1969) 456–463.

[45] S. F. Ross, *Holography for asymptotically locally Lifshitz spacetimes*, *Class.Quant.Grav.* **28** (2011) 215019, [arXiv:1107.4451].

[46] P. Calabrese and J. L. Cardy, *Entanglement entropy and quantum field theory*, *J. Stat. Mech.* **0406** (2004) P06002, [hep-th/0405152].

[47] T. Nishioka, S. Ryu, and T. Takayanagi, *Holographic Entanglement Entropy: An Overview*, *J. Phys.* **A42** (2009) 504008, [arXiv:0905.0932].

[48] V. E. Hubeny, M. Rangamani, and T. Takayanagi, *A covariant holographic entanglement entropy proposal*, *Journal of High Energy Physics* **2007** (2007), no. 07 062, [hep-th/0705.0016].

[49] "Lecture Notes on Quantum Gravity and Black Holes, http://www.hartmanhep.net/topics2015/, Accessed: 2017-03-08."

[50] M. Banados, C. Teitelboim, and J. Zanelli, *The Black hole in three-dimensional space-time*, *Phys. Rev. Lett.* **69** (1992) 1849–1851, [hep-th/9204099].

[51] L. Susskind, *Copenhagen vs Everett, Teleportation, and ER=EPR*, *Fortsch. Phys.* **64** (2016), no. 6-7 551–564, [arXiv:1604.0258].

[52] D. R. Brill, *Multi - black hole geometries in (2+1)-dimensional gravity*, *Phys.Rev.* **D53** (1996) 4133–4176, [gr-qc/9511022].

[53] S. Aminneborg, I. Bengtsson, D. Brill, S. Holst, and P. Peldan, *Black holes and wormholes in (2+1)-dimensions*, *Class.Quant.Grav.* **15** (1998) 627–644, [gr-qc/9707036].

[54] D. Brill, *Black holes and wormholes in (2+1)-dimensions*, *Lect.Notes Phys.* **537** (2000) 143, [gr-qc/9904083].

[55] S. Aminneborg, I. Bengtsson, and S. Holst, *A Spinning anti-de Sitter wormhole*, *Class.Quant.Grav.* **16** (1999) 363–382, [gr-qc/9805028].

[56] A. Hamilton, D. N. Kabat, G. Lifschytz, and D. A. Lowe, *Holographic representation of local bulk operators*, *Phys. Rev.* **D74** (2006) 066009, [hep-th/0606141].

[57] A. Hamilton, D. N. Kabat, G. Lifschytz, and D. A. Lowe, *Local bulk operators in AdS/CFT: A Boundary view of horizons and locality*, *Phys. Rev.* **D73** (2006) 086003, [hep-th/0506118].

[58] T. Banks, M. R. Douglas, G. T. Horowitz, and E. J. Martinec, *AdS dynamics from conformal field theory*, hep-th/9808016.

[59] A. Almheiri, X. Dong, and D. Harlow, *Bulk Locality and Quantum Error Correction in AdS/CFT*, arXiv:1411.7041.

[60] J.-W. Kim, *Explicit reconstruction of the entanglement wedge*, *JHEP* **01** (2017) 131, [arXiv:1607.0360].

[61] X. Dong, D. Harlow, and A. C. Wall, *Reconstruction of Bulk Operators within the Entanglement Wedge in Gauge-Gravity Duality*, *Phys. Rev. Lett.* **117** (2016), no. 2 021601, [arXiv:1601.0541].

[62] E. Mintun, J. Polchinski, and V. Rosenhaus, *Bulk-Boundary Duality, Gauge Invariance, and Quantum Error Correction*, arXiv:1501.0657.

[63] B. Freivogel, R. A. Jefferson, and L. Kabir, *Precursors, Gauge Invariance, and Quantum Error Correction in AdS/CFT*, *JHEP* **04** (2016) 119, [arXiv:1602.0481].

[64] D. Harlow, *The Ryu-Takayanagi Formula from Quantum Error Correction*, arXiv:1607.0390.

[65] N. Engelhardt and S. Fischetti, *Causal Density Matrices*, arXiv:1703.0532.

[66] K. Balasubramanian and J. McGreevy, *Gravity duals for non-relativistic CFTs*, *Phys.Rev.Lett.* **101** (2008) 061601, [arXiv:0804.4053].

[67] S. Kachru, X. Liu, and M. Mulligan, *Gravity duals of Lifshitz-like fixed points*, *Phys.Rev.* **D78** (2008) 106005, [arXiv:0808.1725].

[68] M. Baggio, J. de Boer, and K. Holsheimer, *Hamilton-Jacobi Renormalization for Lifshitz Spacetime*, *JHEP* **1201** (2012) 058, [arXiv:1107.5562].

[69] R. B. Mann and R. McNees, *Holographic Renormalization for Asymptotically Lifshitz Spacetimes*, *JHEP* **1110** (2011) 129, [arXiv:1107.5792].

[70] W. Chemissany, D. Geissbuhler, J. Hartong, and B. Rollier, *Holographic Renormalization for z=2 Lifshitz Space-Times from AdS*, *Class.Quant.Grav.* **29** (2012) 235017, [arXiv:1205.5777].

[71] M. H. Christensen, J. Hartong, N. A. Obers, and B. Rollier, *Torsional Newton-Cartan Geometry and Lifshitz Holography*, *Phys.Rev.* **D89** (2014) 061901, [arXiv:1311.4794].

[72] M. H. Christensen, J. Hartong, N. A. Obers, and B. Rollier, *Boundary Stress-Energy Tensor and Newton-Cartan Geometry in Lifshitz Holography*, *JHEP* **1401** (2014) 057, [arXiv:1311.6471].

[73] Y. Korovin, K. Skenderis, and M. Taylor, *Lifshitz from AdS at finite temperature and top down models*, *JHEP* **1311** (2013) 127, [arXiv:1306.3344].

[74] Y. Korovin, K. Skenderis, and M. Taylor, *Lifshitz as a deformation of Anti-de Sitter*, *JHEP* **08** (2013) 026, [arXiv:1304.7776].

[75] Y. Nishida and D. T. Son, *Nonrelativistic conformal field theories*, *Phys.Rev.* **D76** (2007) 086004, [arXiv:0706.3746].

[76] J. Hartong and B. Rollier, *Particle Number and 3D Schroedinger Holography*, arXiv:1305.3653.

[77] M. Rangamani, S. F. Ross, D. Son, and E. G. Thompson, *Conformal non-relativistic hydrodynamics from gravity*, *JHEP* **0901** (2009) 075, [arXiv:0811.2049].

[78] I. Papadimitriou, *Holographic renormalization as a canonical transformation*, *JHEP* **1011** (2010) 014, [arXiv:1007.4592].

[79] T. Andrade and S. F. Ross, *Boundary conditions for metric fluctuations in Lifshitz*, *Class.Quant.Grav.* **30** (2013) 195017, [arXiv:1305.3539].

[80] I. Papadimitriou and K. Skenderis, *AdS / CFT correspondence and geometry*, hep-th/0404176.

[81] I. Papadimitriou and K. Skenderis, *Correlation functions in holographic RG flows*, *JHEP* **0410** (2004) 075, [hep-th/0407071].

[82] W. Chemissany and I. Papadimitriou, *Generalized dilatation operator method for non-relativistic holography*, arXiv:1405.3965.

[83] W. Chemissany and I. Papadimitriou, *Lifshitz holography: The whole shebang*, arXiv:1408.0795.

[84] M. Baggio, J. de Boer, and K. Holsheimer, *Anomalous Breaking of Anisotropic Scaling Symmetry in the Quantum Lifshitz Model*, *JHEP* **1207** (2012) 099, [arXiv:1112.6416].

[85] T. Zingg, *Logarithmic two-point correlation functions from a z =2 Lifshitz model*, *JHEP* **1401** (2014) 108, [arXiv:1310.4778].

[86] T. Faulkner, H. Liu, J. McGreevy, and D. Vegh, *Emergent quantum criticality, Fermi surfaces, and AdS(2)*, *Phys.Rev.* **D83** (2011) 125002, [arXiv:0907.2694].

[87] M. Henningson and K. Skenderis, *The Holographic Weyl anomaly*, *JHEP* **07** (1998) 023, [hep-th/9806087].

[88] S. de Haro, S. N. Solodukhin, and K. Skenderis, *Holographic reconstruction of space-time and renormalization in the AdS / CFT correspondence*, *Commun.Math.Phys.* **217** (2001) 595–622, [hep-th/0002230].

[89] E. Witten, *Multitrace operators, boundary conditions, and AdS / CFT correspondence*, hep-th/0112258.

[90] D. Anninos, G. Compere, S. de Buyl, S. Detournay, and M. Guica, *The Curious Case of Null Warped Space*, *JHEP* **1011** (2010) 119, [arXiv:1005.4072].

[91] J. Hartong, E. Kiritsis, and N. A. Obers, *Schrdinger Invariance from Lifshitz Isometries in Holography and Field Theory*, *Phys. Rev.* **D92** (2015) 066003, [arXiv:1409.1522].

[92] J. Hartong, E. Kiritsis, and N. A. Obers, *Lifshitz spacetimes for Schrdinger holography*, *Phys. Lett.* **B746** (2015) 318–324, [arXiv:1409.1519].

[93] B. Czech, J. L. Karczmarek, F. Nogueira, and M. Van Raamsdonk, *Rindler quantum gravity*, *Classical and Quantum Gravity* **29** (2012), no. 23 235025, [arXiv:1206.1323].

[94] D. Marolf and A. C. Wall, *Eternal Black Holes and Superselection in AdS/CFT*, *Class.Quant.Grav.* **30** (2013) 025001, [arXiv:1210.3590].

[95] I. A. Morrison and M. M. Roberts, *Mutual information between thermo-field doubles and disconnected holographic boundaries*, *JHEP* **1307** (2013) 081, [arXiv:1211.2887].

[96] G. Vidal, *Entanglement Renormalization: an introduction*, *ArXiv e-prints* (Dec., 2009) [arXiv:0912.1651].

[97] L. Susskind, *Computational Complexity and Black Hole Horizons*, arXiv:1403.5695.

[98] V. Balasubramanian, P. Hayden, A. Maloney, D. Marolf, and S. F. Ross, *Multiboundary Wormholes and Holographic Entanglement*, *Class.Quant.Grav.* **31** (2014) 185015, [arXiv:1406.2663].

[99] L. Susskind, *ER=EPR, GHZ, and the Consistency of Quantum Measurements*, arXiv:1412.8483.

[100] P. Hayden, M. Headrick, and A. Maloney, *Holographic Mutual Information is Monogamous*, *Phys.Rev.* **D87** (2013), no. 4 046003, [arXiv:1107.2940].

[101] K. Krasnov, *Holography and Riemann surfaces*, *Adv.Theor.Math.Phys.* **4** (2000) 929–979, [hep-th/0005106].

[102] K. Krasnov, *Black hole thermodynamics and Riemann surfaces*, *Class.Quant.Grav.* **20** (2003) 2235–2250, [gr-qc/0302073].

[103] K. Skenderis and B. C. van Rees, *Holography and wormholes in 2+1 dimensions*, *Commun.Math.Phys.* **301** (2011) 583–626, [arXiv:0912.2090].

[104] N. Bao, S. Nezami, H. Ooguri, B. Stoica, J. Sully, et al., *The Holographic Entropy Cone*, arXiv:1505.0783.

[105] F. Pastawski, B. Yoshida, D. Harlow, and J. Preskill, *Holographic quantum error-correcting codes: Toy models for the bulk/boundary correspondence*, arXiv:1503.0623.

[106] M. Banados, M. Henneaux, C. Teitelboim, and J. Zanelli, *Geometry of the (2+1) black hole*, *Phys.Rev.* **D48** (1993), no. 6 1506–1525, [gr-qc/9302012].

[107] J. L. Friedman, K. Schleich, and D. M. Witt, *Topological censorship*, *Phys.Rev.Lett.* **71** (1993) 1486–1489, [gr-qc/9305017].

[108] G. Galloway, K. Schleich, D. Witt, and E. Woolgar, *Topological censorship and higher genus black holes*, *Phys.Rev.* **D60** (1999) 104039, [gr-qc/9902061].

[109] H. Maxfield, *Entanglement entropy in three dimensional gravity*, arXiv:1412.0687.

[110] V. E. Hubeny, H. Maxfield, M. Rangamani, and E. Tonni, *Holographic entanglement plateaux*, *JHEP* **1308** (2013) 092, [arXiv:1306.4004].

[111] M. Headrick, *General properties of holographic entanglement entropy*, *JHEP* **1403** (2014) 085, [arXiv:1312.6717].

[112] J. Louko and D. Marolf, *Single exterior black holes and the AdS / CFT conjecture*, *Phys.Rev.* **D59** (1999) 066002, [hep-th/9808081].

[113] J. Louko, D. Marolf, and S. F. Ross, *On geodesic propagators and black hole holography*, *Phys.Rev.* **D62** (2000) 044041, [hep-th/0002111].

[114] B. Czech, G. Evenbly, L. Lamprou, S. McCandlish, X. Qi, J. Sully, and G. Vidal To appear.

[115] B. Swingle, *Entanglement Renormalization and Holography*, *Phys.Rev.* **D86** (2012) 065007, [arXiv:0905.1317].

[116] G. Evenbly and G. Vidal, *Tensor Network States and Geometry*, *Journal of Statistical Physics* **145** (Nov., 2011) 891–918, [arXiv:1106.1082].

[117] B. Swingle, *Constructing holographic spacetimes using entanglement renormalization*, arXiv:1209.3304.

[118] T. Hartman and J. Maldacena, *Time Evolution of Entanglement Entropy from Black Hole Interiors*, *JHEP* **1305** (2013) 014, [arXiv:1303.1080].

[119] G. Evenbly and G. Vidal, *Tensor Network Renormalization*, *ArXiv e-prints* (Dec., 2014) [arXiv:1412.0732].

[120] G. Evenbly and G. Vidal, *Tensor network renormalization yields the multi-scale entanglement renormalization ansatz*, *ArXiv e-prints* (Feb., 2015) [arXiv:1502.0538].

[121] G. Evenbly and G. Vidal, *Tensor Network States and Geometry*, *Journal of Statistical Physics* **145** (Nov., 2011) 891–918, [arXiv:1106.1082].

[122] B. Czech, L. Lamprou, S. McCandlish, and J. Sully, *Integral Geometry and Holography*, *JHEP* **10** (2015) 175, [arXiv:1505.0551].

[123] B. Czech, L. Lamprou, S. McCandlish, and J. Sully, *Tensor Networks from Kinematic Space*, arXiv:1512.0154.

[124] B. Czech, G. Evenbly, L. Lamprou, S. McCandlish, X.-L. Qi, J. Sully, and G. Vidal, *A tensor network quotient takes the vacuum to the thermal state*, arXiv:1510.0763.

[125] G. Salton, B. Swingle, and M. Walter, *Entanglement from Topology in Chern-Simons Theory*, arXiv:1611.0151.

[126] V. Balasubramanian, J. R. Fliss, R. G. Leigh, and O. Parrikar, *Multi-Boundary Entanglement in Chern-Simons Theory and Link Invariants*, arXiv:1611.0546.

[127] S. Nezami and M. Walter, *Multipartite Entanglement in Stabilizer Tensor Networks*, arXiv:1608.0259.

[128] Z. Yang, P. Hayden, and X.-L. Qi, *Bidirectional holographic codes and sub-AdS locality*, *JHEP* **01** (2016) 175, [arXiv:1510.0378].

[129] P. Hayden, S. Nezami, X.-L. Qi, N. Thomas, M. Walter, and Z. Yang, *Holographic duality from random tensor networks*, *JHEP* **11** (2016) 009, [arXiv:1601.0169].

[130] A. Bhattacharyya, Z.-S. Gao, L.-Y. Hung, and S.-N. Liu, *Exploring the Tensor Networks/AdS Correspondence*, *JHEP* **08** (2016) 086, [arXiv:1606.0062].

[131] H. Maxfield, S. Ross, and B. Way, *Holographic partition functions and phases for higher genus Riemann surfaces*, *Class. Quant. Grav.* **33** (2016), no. 12 125018, [arXiv:1601.0098].

[132] H. Coxeter, *Discrete groups generated by reflections*, *Ann. of Math* **35** (1934), no. 9 588.

[133] M. Murray, *Hyperbolic Geometry and Coxeter Groups*, *Masters Thesis (Graduate College of Bowling Green State University)* (2012).

[134] "Coxeter group." In Wikipedia, retrieved 15 February 2017 https://en.wikipedia.org/wiki/Coxeter_group.

[135] D. N. Page, *Average entropy of a subsystem*, *Physical Review Letters* **71** (1993), no. 9 1291.

[136] K. Zyczhowski, P. Horodecki, A. Sanpera, and M. Lewenstein, *Volume of the set of separable states*, *Phy. Rev. A* **58** (1998), no. 2 883.

[137] J. Eisert, V. Eisler, and Z. Zimborás, *Entanglement negativity bounds for fermionic Gaussian states*, *ArXiv e-prints* (Nov., 2016) [arXiv:1611.0800].

[138] M. B. Plenio, *Logarithmic Negativity: A Full Entanglement Monotone That is not Convex*, *Phys. Rev. Lett.* **95** (2005), no. 9 090503, [quant-ph/0505071].

[139] G. Vidal and F. Werner, *Computable measure of entanglement*, *Phy. Rev. A* **65** (2002), no. 3 032314.

[140] C. P. Herzog, M. Rangamani, and S. F. Ross, *Heating up Galilean holography*, *JHEP* **11** (2008) 080, [arXiv:0807.1099].

[141] M. Gary, D. Grumiller, and R. Rashkov, *Towards non-AdS holography in 3-dimensional higher spin gravity*, *JHEP* **03** (2012) 022, [arXiv:1201.0013].

[142] H. Afshar, M. Gary, D. Grumiller, R. Rashkov, and M. Riegler, *Non-AdS holography in 3-dimensional higher spin gravity - General recipe and example*, *JHEP* **11** (2012) 099, [arXiv:1209.2860].

[143] S. A. Gentle and C. Keeler, *On the reconstruction of Lifshitz spacetimes*, *JHEP* **03** (2016) 195, [arXiv:1512.0453].

[144] J.-d. Zhang and B. Chen, *Kinematic Space and Wormholes*, *JHEP* **01** (2017) 092, [arXiv:1610.0713].

[145] L. Susskind, *Singularities, Firewalls, and Complementarity*, arXiv:1208.3445.

[146] K. Papadodimas and S. Raju, *An Infalling Observer in AdS/CFT*, *JHEP* **10** (2013) 212, [arXiv:1211.6767].

[147] A. Almheiri, D. Marolf, J. Polchinski, and J. Sully, *Black Holes: Complementarity or Firewalls?*, *JHEP* **02** (2013) 062, [arXiv:1207.3123].

[148] A. Almheiri, D. Marolf, J. Polchinski, D. Stanford, and J. Sully, *An Apologia for Firewalls*, *JHEP* **09** (2013) 018, [arXiv:1304.6483].

[149] K. Papadodimas and S. Raju, *Black Hole Interior in the Holographic Correspondence and the Information Paradox*, *Phys. Rev. Lett.* **112** (2014), no. 5 051301, [arXiv:1310.6334].

[150] K. Papadodimas and S. Raju, *State-Dependent Bulk-Boundary Maps and Black Hole Complementarity*, *Phys. Rev.* **D89** (2014), no. 8 086010, [arXiv:1310.6335].